Tectonic evolution of the Late Archean Pontiac Subprovince, Superior Province, Canada: Structural, metamorphic, and geochronological studies

by

Mohammad Reza Ghassemi, B.Sc., M.Sc.

A thesis submitted to the School of Graduate Studies and Research

in partial fulfillment of

the requirements for the degree of

Doctor of Philosophy

Ottawa-Carleton Geoscience Centre

and

Department of Geology

University of Ottawa

Ottawa, Ontario

June 1996

ISBN 0-612-19962-2

In The Name of God

To My Brave Son Ali
and
To My Wife, Katayoun, Who Taught Me Love

If there is no love, no one is ever able to stand a trek like this

A. Shamloo

ABSTRACT

The Pontiac Subprovince is a Late Archean (*ca.* 2.7 Ga) metasedimentary-metavolcanic-granitoid-gneiss terrane situated along the southeastern margin of the Superior Province in Québec. Detailed structural study of the northwestern part of this amphibolite facies metasedimentary belt has revealed a protracted history of deformation in Late Archean and Early Proterozoic time. An early contractional event (D_1) resulted in development of steep foliations now preserved as folded or straight relics within microlithons of S_2 foliation. During this stage, the Cadillac-Larder Lake fault zone acted as a major fault zone along which greenstones of the Abitibi Subprovince were thrust over the Pontiac Subprovince. Regional metamorphism resulted from both thickening of the crust, and intrusion of voluminous I-type granites. D_2 structures record peak metamorphic high-temperature deformation of the crustal rocks during which large-scale D_2 nappes moved towards the south-southeast. The basal thrust faults of these nappes are preserved as high-strain shear zones within the study area. Second order east-trending recumbent F_2 folds, a penetrative S_2 crenulation foliation, and a north-northwest-trending L_2 elongation lineation are other important structures of this deformational event. A later D_3 contractional event superimposed east-trending upright folds on all earlier structures. Extensional D_4 structures are associated with reactivation of the Cadillac-Larder Lake fault zone as a normal fault zone, and are only recorded in or close to normal faults within this fault zone. Finally, brittle D_5 thrust faults and kink structures are superimposed on all older structures in the northwestern Pontiac Subprovince. Gneisses of the Lac Opasatica area record pre-D_1 penetrative structures that are not present within the other rock types of the study area.

Increasing metamorphic grade from biotite zone to sillimanite zone is evident from north (the Cadillac-Larder Lake fault zone) to south in the study area, close to outcrops of the S-type granites. Thermobarometry of samples from the study area indicates that regional metamorphism of the rocks in the northwestern Pontiac Subprovince occurred at about 590°C

and 6.2 kbar. Investigation of the metamorphic and structural history of these Late Archean rocks suggests a clockwise PT path similar to that of Phanerozoic collisional belts.

$^{40}Ar/^{39}Ar$ age constraints from this study combined with other geochronologic data indicate a slow cooling rate of about 2° to 6°C/Ma, and reveal that temperatures as high as 350°C and 280°C were persistent in crustal rocks of the area until *ca.* 150 Ma after attainment of peak metamorphic conditions.

Based on the present study, the tectonic history of the Pontiac Subprovince may be summarized as follows:

Rifting of the Abitibi arc system above a north-dipping subduction zone resulted in development of a backarc basin (*ca.* 2700-2690 Ma). The geometry and plate tectonic setting of this backarc basin are compared to those of backarc basins in the Indonesian region. Turbiditic graywackes of the Pontiac Group interlayered with mafic lavas were deposited within the spreading backarc basin. Collision of a suspect terrane to the south with the arc system is interpreted to have resulted in backarc basin inversion, and its closure at about 2680 Ma. Abitibi greenstones at this stage overthrust the sedimentary pile of the backarc basin. The coarse-grained detrital sequence of the Timiskaming Group was deposited in the foreland of the resulting thrust belt. The thickened crustal collision zone was intruded by widespread I-type granitoids emanating from an oceanic lithospheric slab left over from the subducting plate. Nappe structures started to develop at about 2670 Ma, when S-type granites, resulting from melting of the metasedimentary rocks, were emplaced into upper crustal levels. Extension of the crust, synchronous with development of a passive continental margin to the south of the Superior Province (before *ca.* 2500 Ma) reactivated old structures (including the Cadillac-Larder Lake fault zone) and produced half-grabens in which Early Proterozoic sedimentary rocks of the Cobalt Group were deposited. The latest record of a north-south contractional event within the study area may be correlated with the Penokean orogeny (*ca.* 1.9-1.7 Ma).

ACKNOWLEDGMENTS

I would like to thank my supervisor, Keith Benn, for his guidance, advice, and consistent support throughout the course of this work. To a great amount I have benefited from his stimulating and constructive discussions on structural geology, and other different aspects of my study. I thank him also for providing me with his data and sample collection from the Pontiac Subprovince. I had the opportunity to benefit from the vast knowledge of Ralph Kretz on metamorphic petrology. He is also thanked for his thoughtful reviews of earlier drafts. I would like to thank Allan Donaldson for his helpful discussions on sedimentary rocks of the study area. To a great amount the writing and organization of this thesis was improved by Allan Donaldson. Anthony Fowler and Andrew Hynes are thanked for their useful and constructive comments.

I am grateful to Hamish Sandeman for providing me with the information on the analytical procedures for the $^{40}Ar/^{39}Ar$ experiments that were carried out at the Queen's University and at the University of Waterloo. Amabel Ortega-Rivera is thanked for performing the $^{40}Ar/^{39}Ar$ analyses of the samples. Rob Berman provided the TWEEQU software, and guidance on different aspects of thermobarometry analyses. I would like to thank Mark Shore for providing me with geochemical data on a komatiitic sample from my study area. I am grateful to John Gillett and Davin Ala for sampling and reconnaissance field study in my thesis area. Pascal Gervais is thanked for assisting me during my field work. Peter Jones helped with the microprobe analyses, and John Loop helped with the wet chemical analyses, mineral separations, and mineral staining procedures. George Mrazek is thanked for preparing the standard and polished thin sections. Saeed Alirezai and Paul Waqué are thanked for their great help on study of opaque minerals. I would like to thank Hélène De Gouffe for supplying excellent administrative support.

This research was founded by a Lithoprobe grant to Keith Benn.

Many thanks to my wife, Katayoun Samii-Saket, for her unique companionship, patience and dedication throughout my graduate studies. She is also thanked for her help on preparing the data spreadsheets for my studies.

During my studies I suffered the very tragic loss of my beloved wife, who was among the most valuable graces that god granted me. Continuing my studies after this loss was not possible without help and support of persons that are thanked here:

My dear son Ali, from whom I learned my patience.

My mother-in-law Tahereh Samii-Saket who represents my wife's family as whole.

My mother Khadijeh Ghassemi who represents my own family as whole.

André Lalonde, director of graduate studies in Department of Geology for his unique support, encouragement and sympathy.

Dr. J. M. De Koninck, Dean of the School of Graduate Studies and Research, and Dr. Jean-Michel Beillard, Vice-Rector, University Relations and Development, for their moral and financial support for continuing my studies.

Last but not the least, I would like to thank people of my country, Iran, who provided me with the scholarship for my studies.

TABLE OF CONTENTS

List of Figures

CHAPTER 1 **Page**

CHAPTER 2

CHAPTER 3

CHAPTER 4

CHAPTER 5

CHAPTER 6

List of Tables

1. Introduction

The Superior Province of the Canadian Shield is the largest exposed Archean block in the world. Because of the occurrence of important deposits of gold and other precious and base metals, the Superior Province has been subjected to numerous comprehensive geologic studies. Archean greenstone belts and associated plutons are the major constituents of the Superior Province (Fig. 1.1). These greenschist to amphibolite facies volcanic-plutonic terranes are separated by elongate metasedimentary belts. High-grade (granulite facies) gneiss complexes represent the third important type of terrane within the province. The Superior Province contains small areas of pre-3.5 Ga crust (e.g. Minnesota foreland) but is largely composed of crust formed at 2.8 to 2.7 Ga (Hoffman 1989).

In recent years, application of different modern geologic research methods to the study of Archean terranes has revealed that most tectonic and other geologic processes operative in the Late Archean were similar to Phanerozoic processes. Studies of Archean terranes are especially important for learning about geologic processes of the early Earth, and allow their comparisons to those of Phanerozoic time. The economic importance of greenstone belts within the Superior Province has led to most of geologic investigations being largely concentrated within this type of belt. Recent studies, however, indicate that high-grade gneiss terranes and metasedimentary belts are very important for our understanding of Archean tectonics. They usually show higher grade metamorphism and represent deeper crustal levels compared to greenstone and plutonic belts, and hence provide more information on thermal and structural features of Archean terranes. Ductile deformation histories deduced from these terranes are much more complicated than those of the greenstone and plutonic belts, and may record more structural events. Many important gold camps within the Superior Province are concentrated along the tectonic boundaries between the metasedimentary and greenstone belts, or are associated with metasedimentary packages within the greenstone belts (e.g. Porcupine, Kirkland Lake, Val d'Or, and Red Lake camps). Integration of geological analyses from all

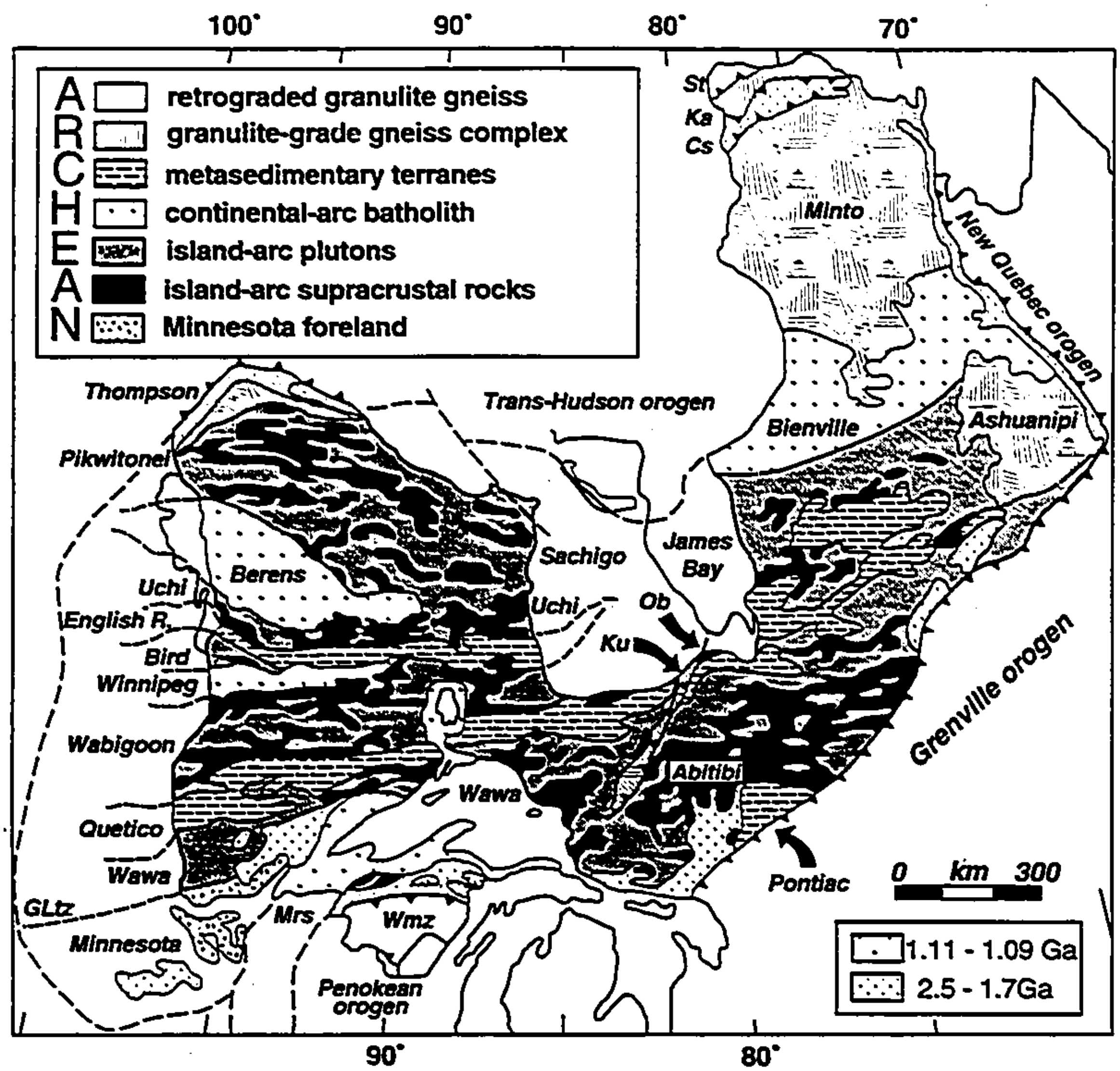

Fig. 1.1. Geology of the Superior province (after Hoffman 1989)

Cs	Cape Smith belt
GLtz	Great Lakes tectonic zone
Ka	Kovic antiform
Ku	Kapuskasing uplift
Mrs	Midcontinent rift system
Ob	Opatica belt
St	Sugluk terrane
Wmz	Wisconsin magmatic zones of Penokean orogen

kinds of Archean terranes, should therefore, result in a better understanding of the Archean provinces, their tectonic setting, and their metallogeny.

1.1. Statement of the problem

Studies carried out by Goulet (1978) in the northwestern part of the Pontiac Subprovince were confined to an small area close to the Cadillac-Larder Lake fault zone (Fig. 1.2), and although his research involved structural and metamorphic studies, it was basically oriented towards an understanding of stratigraphy of that area. Van de Walle's work (1978) in an area including the western part of the present study area did not involve detailed structural and metamorphic studies. Present study was carried out in the same area that was studied by Camiré and her coworkers (Camiré 1992, Camiré *et al.* 1993, Camiré and Burg 1993). However, preliminary field work by Keith Benn, and microscopic studies (by the author) of samples collected during the field work revealed many interesting structural and metamorphic features that were not studied and/or discussed by Camiré and her coworkers. In other words, their studies were not comprehensive in terms of mapping, sampling, and microscopic and analytical studies of samples. For example, their sampling and structural measurements were done along two lakes in eastern and western parts of the study area, and hence almost all resultant conclusions on metamorphism and structural geology of the area is an interpolation of data between these two lakes. Moreover, neither structure nor metamorphism of the samples were dealt with in detail by Camiré and her coworkers. Some shortcomings of the studies by Camiré and her coworkers are discussed in Chapter 3.

Structural, metamorphic, and geochronologic studies were planned for a better understanding of the geological entities within the Pontiac Subprovince, and their relationships to the Abitibi Subprovince. Initial reconnaissance studies during planning of the present study revealed that the Pontiac Subprovince is an amphibolite facies terrane that has undergone multiple stages of deformation. Research for this study has addressed questions about the

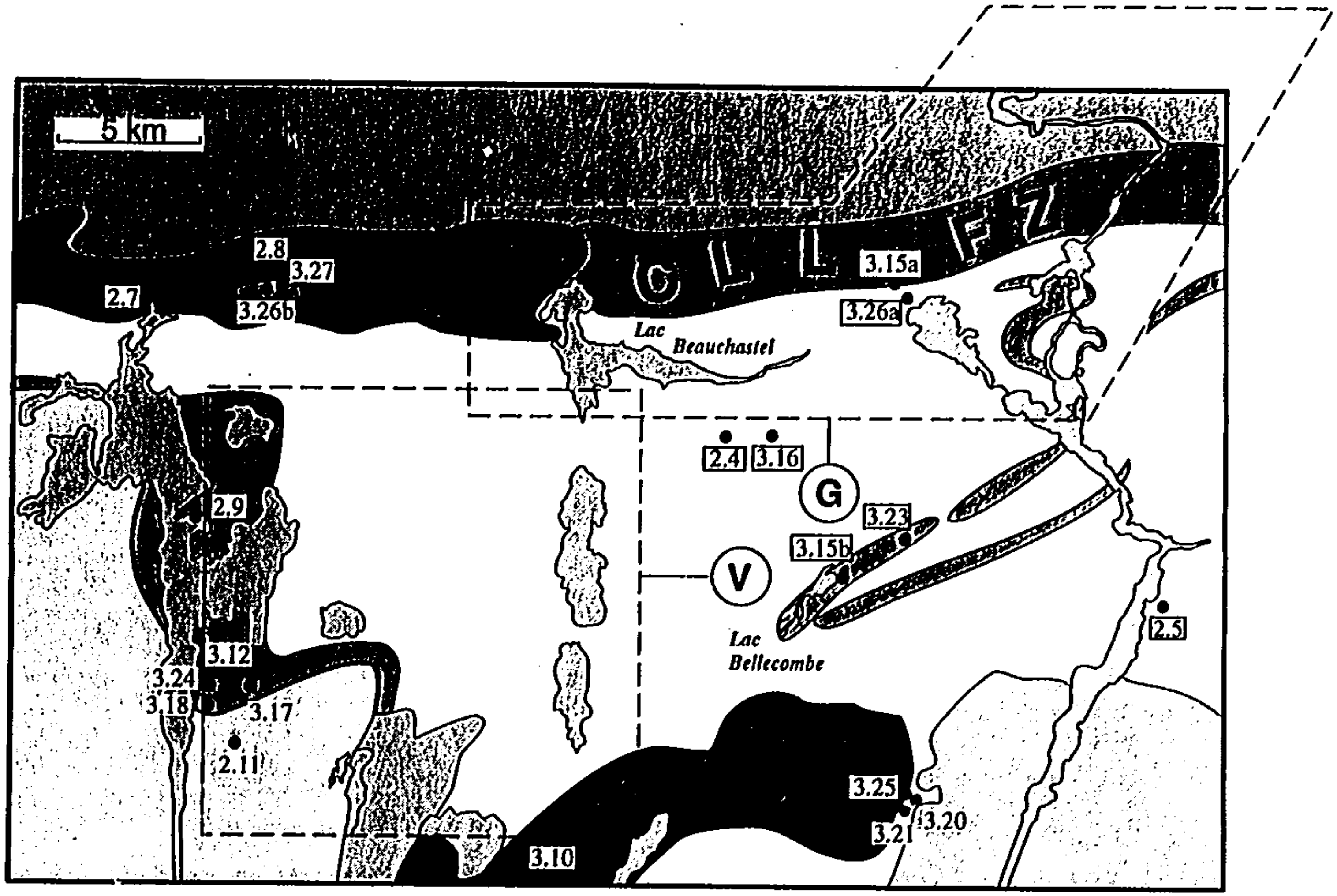

Fig. 1.2. Map illustrating areas studied by (G) Goulet (1978) and (V) van de Walle (1978). Shown also on this map are photograph numbers, and localities where the photographs of the present study are taken.

structural, metamorphic and tectonic evolution of the Pontiac Subprovince in Late Archean and Early Proterozoic time. The questions may be summarized as follows:

1) What was the nature and sequence of deformational events that have affected the rock suites within the study area?

2) What was the nature of metamorphic events that affected the rocks within the Pontiac Subprovince, and what was their relationship to these structural events.

3) Being a relatively high-grade terrane bordered by lower grade greenstones of the Abitibi Subprovince, does the Pontiac Subprovince represent an Archean metamorphic core complex?

4) What is the nature of structural and/or stratigraphic relationships of the Pontiac metasedimentary rocks to the Timiskaming Group clastic strata, Pontiac Group metavolcanic rocks, I-type and S-type granitoids, gneissic domains in the western part of the subprovince, and finally the Abitibi greenstones to the north and west?

5) What was the tectonic setting of the basin within which the Pontiac sedimentary rocks were deposited? Is the Pontiac metasedimentary belt an accretionary prism that faced an Archean magmatic arc system, as it is suggested (Card, 1989) for most other sedimentary belts within the Superior Province?

6) What were the tectonic events that resulted in sequential deformation of the Pontiac Subprovince?

The thesis study involved detailed structural and microstructural analyses of the northwestern part of the Pontiac Subprovince. The structural analysis was complemented by investigation of the P-T history of the region and interpretation of the geochronological data. The results provide new insights into the tectonic relationships between the Pontiac and Abitibi Subprovinces, and also provide a new framework for interpreting the tectonic evolution of this part of the Archean Superior Province.

1.2. Previous studies

Regional geologic investigations of what are now classified as the Abitibi and Pontiac Subprovinces began early in the century (Wilson, 1909), and although many investigations have since been undertaken, most of the work, recent as well as early, have been mainly directed towards the discovery and understanding of the economic mineral deposits in the region.

The geology and structure of the Abitibi greenstones have been extensively studied in both Québec (Dimroth *et al.* 1982, 1983a, b, Hubert *et al.* 1984, Ludden *et al.* 1986, Chown *et al.* 1992) and Ontario (review in Jackson and Fyon 1991). In contrast, little work has been published concerning the geology of the Pontiac Subprovince, even though, because of its lithologic and deformational characteristics, it appears to have a great potential for provision of a better understanding of the tectonic history of the adjacent Abitibi greenstone belt and the southern Superior Province. Geochemical, geochronological, structural, seismic, and petrological studies through the Abitibi and Pontiac Subprovinces within the last few decades have provided a good basis for tectonic interpretations of these regions (Camiré *et al.* 1993, Camiré and Burg 1993, Chown *et al.* 1992, Corfu 1993, Davis 1991, Dimroth *et al.* 1982, 1983a, b, Feng and Kerrich 1990, 1991, 1992, Feng *et al.* 1992, 1993a, b, Jolly 1978, Kerrich and Feng 1992, Kerrich and Kyser 1994, Kimura *et al.* 1992, Ludden *et al.* 1986, Mortensen and Card 1993, Sawyer and Barnes 1994, Benn *et al.* 1994).

Van de Walle (1978) completed detailed geological mapping and a geological report for the 'Canton de Montbeillard', which covers the western part of present study area (Fig. 1.2). Rive *et al.* (1989) compiled geological maps of the southern Abitibi and Pontiac Subprovinces at 1:125,000 scale. Structural studies of parts of the Pontiac and adjacent Abitibi Subprovinces have been carried out in different areas (Goulet 1978, Hubert and Trudel 1984, Robert 1989, Camiré and Burg 1993, Sawyer and Barnes 1994). More details on studies related to structural geology, metamorphism, geochronology and tectonics are provided within the introductory sections of related chapters.

1.3. Methodology

Preliminary field studies and sampling were done by Keith Benn, John Gillett and Davin Ala during the summers of 1991 and 1992, yielding a good structural data base and field observation, and about 50 samples from the study area. Magnetic and gravity profiles were established in the study area by Keith Benn and Warner Miles during the both field seasons (Benn *et al.* 1994).

Structural mapping and sampling were carried out by the author during the summer of 1993, during which about 425 outcrops were examined and about 170 hand samples were collected. A large part of the field work was done by motor-boat on lake shores of the area, where most of the best outcrops are found. Detailed mapping was also carried out along access roads and in off-road areas that contain exceptionally good outcrops. Topographic maps at a scale of 1:50,000 were used as a base for plotting the field data. A few short trips later allowed revisits to some outcrops, and additional sampling. A *Brunton* compass was used to measure the planar and linear structures, and all samples were oriented for use in structural and microfabric analyses.

Laboratory procedures included:

Standard and polished thin-section preparation.

Production of structural maps, cross sections and block diagrams.

Statistical analyses of the structural and microfabric data through stereographic projection, using the *Stereonet* (Allmendinger 1988) and *Spheristat* (Stesky 1995) computer software.

A total of 184 thin-sections were studied for microstructure, micro-fabric, mineralogic, petrographic, and modal analyses. Modal analyses were carried out applying the method described by Lewis and McConchie (1994) to 100 counts per thin-section. Apparent mean detrital grain size of quartz and feldspars were calculated for 40 grain size measurements per thin-section. Microstructures were studied using a *Wild M420 Makroscop*. The macroscope was equipped with a *Leica Wild MPS52* camera for taking photomicrographs. Mineralogic, petrographic and modal analyses were carried out using a polarizing *Leitz Laborlux 12 POL S* microscope. Quartz *c*-axis fabric measurements were done with a five axes *Leitz* universal stage (provided by R. L. Brown of Carleton University) mounted on the polarizing microscope.

A few chips from metasedimentary, metavolcanic, and igneous rock samples were stained to determine the presence and abundance of K-feldspar. The chips were first etched for about two seconds in a concentrated hydrofluoric acid; then they were rinsed, dried, and left in a 30% solution of sodium cobaltinitrate for about five minutes for staining.

Quartz-rich samples from the Lac Opasatica gneiss were studied to determine the quartz *c*-axes fabric and sense of shear. Two orthogonal thin-sections were produced from each sample, one including the lineation and the other one normal to it (both normal to the foliation in the rock). The thin-section coordinate system was selected using the right hand rule, with +Y parallel to the foliation and pointed as the arrow marked on the thin-section, +X perpendicular to the foliation, and +Z normal to the thin-section. The thin-section coordinate system was used for transformation of the measurements into the coordinate system of other thin-sections, and plotting the measurement data on stereonet. Both thin-sections from each rock sample were analyzed for *c*-axis orientation, and the results were transformed to the reference frame for the thin-section containing the lineation. A *Matlab* program was written and used for the related analysis and coordinate transformations (see Appendix A).

Electron microprobe qualitative analyses of minerals from representative samples were obtained on polished, carbon-coated thin-sections in the Electron Microprobe Laboratory at Department of Earth Sciences, Carleton University. The samples were analyzed by the energy-dispersive X-ray spectrometry method (EDX) using a *Cambridge Microscan 5* electron probe interfaced to an *Ortec Si* detector. Analytical conditions were: 20 kV accelerating potential, 75° take-off angle, and a beam current of 3.5 nA measured on a *Faraday* cup. A combination of well-characterized natural and synthetic mineral standards was used for calibration. Raw x-ray spectra were converted to elemental weight percentages by the program *EDDI* (Pringle 1989).

P-T values for the samples were estimated by means of the TWQ software of Berman (1991) on an *IBM* personal computer.

In order to evaluate the ferrous iron content of biotite crystals from samples that were used for microprobe analyses, and compare the results with the total iron analyses of microprobe method, five metasedimentary samples were analyzed by the redox titration method at the Geochemistry Laboratory of the Department of Geology, University of Ottawa. Fresh whole-rock samples were first broken into small pieces, and then pulverized by use of a pestle and mortar, and sieved to obtain a grain size close to the size of the biotite crystals within the samples. A horseshoe magnet was used to separate magnetite from the powder. Biotite was then separated from the non-magnetic minerals in a *Frantz* isodynamic separator (model *L-1*). For further purity, methylene iodine was used to gravitationally separate biotite garnet and amphibole. The final product was used for redox titration. The following is a description of the method (John Loop, personal communication): add 5 ml of vanadate solution to 0.2g of each sample, and dissolve the sample by 10 ml of cold (room temperature) hydrofluoric acid over a 24 hour period; add 50 ml of boric acid solution to a clean 250 ml Pyrex beaker; pour an additional 50 ml aliquot in into a reaction flask containing the dissolved sample, and transfer contents of the reaction flask to a beaker; add an additional 50 ml aliquot to the flask, rinse and transfer contents to the beaker; add a magnetic stirring bar; add 10 ml of phosphoric/sulfuric solution and 10 ml (accurately measured) of ferrous ammonium sulfate solution to the beaker; add 3 to 4 drops of indicator, and while stirring on a magnetic plate, titrate to a purple endpoint with dichromate solution. One blank and one standard were used along with the natural samples.

Calculations:

$$\%FeO = [(Vs - Vb)Ws] \times N \times 7.185$$

$$\%Fe_2O_3(ferric) = \%Fe_2O_3(total) - (\%FeO \times 1.111)$$

where N is normality of the dichromate solution, Vs is volume of the titrant for each sample (ml), Vb is volume of titrant for the blank (ml), and Ws is weight of the sample (g). Calculated and expected values for the standards are tabulated in Appendix B.

Mineral separations for $^{40}Ar/^{39}Ar$ age determinations were prepared as follows. Fresh whole-rock samples, initially crushed in a jaw crusher (manufactured by *TM Engineering LTD*), were further crushed to about 1.0 mm and smaller size using a *Bico* pulverizer. The crushed samples were sieved to obtain a grain size of about 200 µm, close to the grain size of the minerals. Magnetite was first separated from the samples with a horseshoe magnet, biotites and hornblende was then separated from the nonmagnetic fraction using a *Frantz* isodynamic separator (model *L-1*). Different positions of the magnetic separator (side and back tilt) were adjusted to obtain optimum purity. The operating current was kept at about 0.5A. Hornblende and garnet were separated from biotite grains in a density separation funnel using variably adjusted methylene iodine (M1). The separates were washed repeatedly in acetone. All mineral separates were then hand picked under a binocular microscope to ensure high purity.

The mineral separates were placed in labeled glass containers, and sent for $^{40}Ar/^{39}Ar$ age determination to the Queen's University at Kingston, Ontario. Following is a description of further procedures for sample preparation and $^{40}Ar/^{39}Ar$ analyses (Hamish Sandeman, personal communication):

Mineral separates and neutron flux monitors were wrapped in aluminum foil and sequentially stacked in an aluminum tube. Flux monitors included two reference materials of known age, HB3gr (1072 Ma: Roddick, 1983) and G-14 (1007 Ma: J. Hanes, unpublished data). These were evenly spaced with the unknowns, to enable precise determination of the irradiation parameter, "J", throughout the tube. Unknowns and flux monitors were sent to the McMaster University Reactor, McMaster University, Hamilton, Ontario, and were irradiated in fast neutrons for 10 days.

After irradiation, the canister and its contents were left to "cool" for approximately 1 to 2 months. The irradiation monitors and unknowns were then transferred to degassed Nb crucibles and stored in a lead-lined box. The monitors were analyzed first, and the J-values of individual flux monitors were calculated by means of the equation:

$$J = (e^{\lambda t} - 1)/(^{40}Ar^{*}/^{39}Ar_k),$$

where: λ = the decay constant of $^{40}K = 5.543 \times 10^{-10}\ yr^{-1}$

t = the K-Ar age of the flux monitor (Hb3gr or G-14)

$(^{40}Ar^{*}/^{39}Ar_k)$ = the measured ratio of radiogenic ^{40}Ar to irradiation-induced ^{39}Ar.

Irradiated samples were incrementally heated in a quartz tube using a *Lindburgh* furnace and temperature calibrated with an optical pyrometer. The quartz tube was connected to a stainless steel, gas extraction system, on-line with a substantially modified *AEI* MS-10 mass spectrometer run in the static mode. Measured isotopic ratios were extrapolated to zero-time and corrected to an $^{40}Ar/^{36}Ar$ atmospheric ratio of 295.5. The $^{40}Ar/^{39}Ar$ analyses were corrected for neutron induced ^{40}Ar from potassium and ^{39}Ar and ^{36}Ar from calcium.

Ages and their errors were calculated according to the methods of Dalrymple *et al.* (1981) using the decay constants recommended by Steiger and Jäger (1977). Errors represent the analytical precision at 2σ assuming no error in the J-values.

1.4. Statement of original contribution and funding

This thesis represents the most comprehensive study to date of the geological structure in the Pontiac Subprovince. Contrary to earlier structural studies (Goulet 1978, Camiré 1992, Camiré and Burg 1993, Sawyer and Barnes 1994), this work includes a very detailed investigation of microstructures, and demonstrates relationships between the microscopic structures and regional scale structures. The thesis also investigates relationships between sequential deformational events and metamorphic events.

Metamorphic isograd maps proposed by previous workers (Jolly 1978, van de Walle 1978, Goulet 1978, Camiré and Burg 1993) have been improved through a detailed sampling and study of thin-sections. A thermal history of the Pontiac Subprovince, based on $^{40}Ar/^{39}Ar$ data, is suggested for the first time. $^{40}Ar/^{39}Ar$ data from this study and U/Pb and Pb/Pb absolute ages from different sources are compiled to provide time constraints on different geological events including structural and metamorphic episodes. A P-T path, constructed on the basis of structural, metamorphic and geochronological data, represents the first attempt to constrain the tectonic-metamorphic evolution of the Late Archean orogeny that involved both the Pontiac and Abitibi Subprovinces.

A new model, compatible with results of the present and previous studies, is proposed for the tectonic evolution of the Pontiac Subprovince during Late Archean and Early Proterozoic time. The model includes deposition of the Pontiac Group sedimentary rocks within a backarc basin setting; this is a new interpretation for the geodynamic setting of a metasedimentary terrane within the Superior Province. The model also suggests a different tectonic setting for deposition of the Timiskaming Group as compared to previous models.

The proposal for this research and the methods of approach were decided by the author and his thesis supervisor. Funding for the research was mostly provided through a Lithoprobe research grant to Dr. Keith Benn. The early field work was carried out by Dr. Keith Benn, John Gillett and Davin Ala during the summers of 1991 and 1992. More extensive field work was completed by the author during the summer of 1993, with the assistance of Pascal Gervais. The author was responsible for synthesizing all of the structural and microstructural data, and measured and interpreted the quartz *c*-axis petrofabrics.

All P-T data and $^{40}Ar/^{39}Ar$ data are new and original to this thesis. Geochronological data from different sources on the Pontiac and Abitibi Subprovinces were compiled and synthesized by the author. The tectonic interpretations (Chapter 6) are those of the author. They are for the most part based on geochronological, geochemical, petrological, and stratigraphic studies of previous workers (cited throughout the thesis).

Standard thin-sections and polished thin-sections were produced by George Mrazek, Department of Geology, University of Ottawa. Microstructural, petrologic and petrofabric studies of the thin-sections, and related analyses, were done by the author. Electron microprobe analyses of the samples were done by the author at Carleton University, where Peter Jones carbon-coated the thin-sections, prepared the microprobe unit and ran the standards for different minerals. Redox titration of the biotite samples for determination of Fe^{2+}/Fe-total ratio, and K-feldspar staining were done by the author under the supervision of John Loop at the Geochemistry laboratory, Department of Geology, University of Ottawa. Mineral separates for titration and $^{40}Ar/^{39}Ar$ dating analyses were prepared by the author. The biotite, muscovite and amphibole separates were sent to the Department of Geological Sciences, Queen's University, for the $^{40}Ar/^{39}Ar$ analyses. The samples were prepared for irradiation, step-heated and analyzed by Amabel Ortega-Rivera. Prepared samples were irradiated in the McMaster University Reactor, McMaster University.

2. Geological setting

The Pontiac Subprovince is a Late Archean metasedimentary-metavolcanic-granitoid-gneiss terrane situated along the southeastern margin of the Superior Province in Québec (Fig. 1.1). It is limited to the south by the Proterozoic Grenville Province, to the west by Proterozoic Huronian sedimentary rocks of the Cobalt embayment, and to the north by the Cadillac-Larder Lake fault zone which separates the Pontiac Subprovince from the Southern Volcanic Zone (Ludden *et al.* 1986) of the Abitibi Subprovince (Fig. 2.1).

The study area is in the northwestern part of the Pontiac Subprovince (Fig. 2.2). This area was selected for detailed structural and metamorphic studies because of its better outcrops and access roads compared to other parts of the subprovince, the presence of distinct boundary relationships with southern Abitibi Subprovince to the north, presence of relatively well-defined metamorphic isograds, and the availability of two seismic profiles which cover part of the study area.

The Abitibi Subprovince, situated to the north and west of the Pontiac Subprovince, is a Late Archean greenstone belt that comprises thick greenschist facies volcanic sequences pierced by several granitoid plutons. Absolute ages of the greenstones and granitoids within the Abitibi Subprovince ranges from 2760 to 2670 Ma (Mortensen 1993a, Corfu 1993).

Dimroth *et al.* (1982, 1983a, b) proposed that the Pontiac Subprovince represents the fore-arc accretionary prism of an ensimatic magmatic arc (Southern Volcanic Zone of the Abitibi Subprovince, Ludden *et al.* 1986), intruded by syn-tectonic plutons during collision with a crustal block farther to the south. Kerrich and Feng (1992) proposed an alternative model in which the Pontiac Subprovince would be an exotic crustal block (micro-continent) having collided with and underthrust the Southern Volcanic Zone. These models suggest that the Cadillac-Larder Lake fault zone represents a north-dipping thrust, but differ in placement of the suture zone to the north or to the south of the Pontiac Subprovince. Dimroth *et al.* (1982,

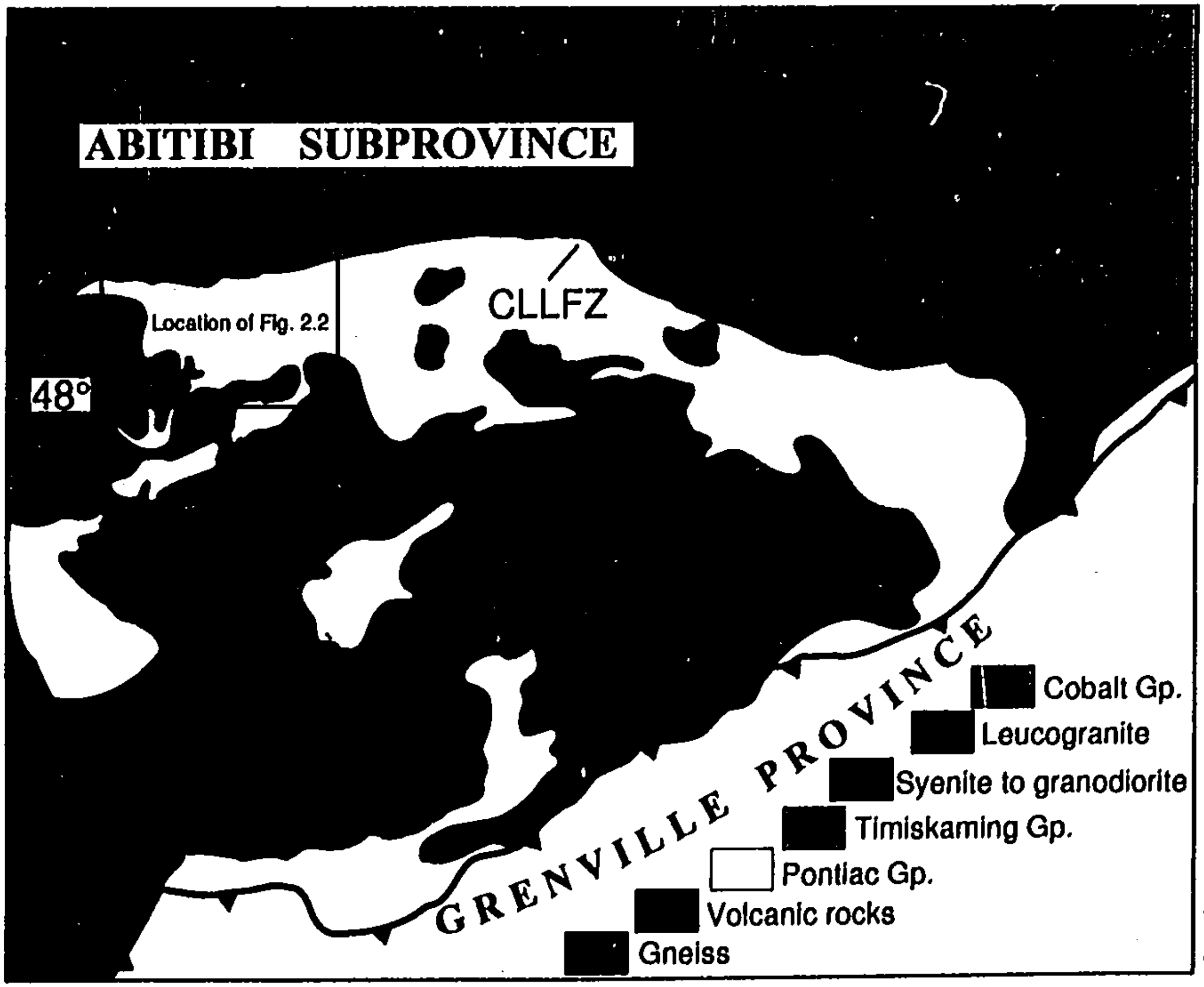

Abbreviations:

AG	Anglier volcanics
BB	Baby volcanics
BF	Belleterre-Fugerville tonalite
BL	Baie de Lys orthogneiss
BT	Belleterre volcanics
DC	Decelles granite
HL	Halle granite
LB	Lacorne Block
LF	Lac Frechette complex
LM	Lac Maple granite
LQ	Lac de Quinze gneiss
LR	Lac Remigny granite
LS	Lac Simard granite
OP	Opasatica gneiss
TB	Toure de Belleterre granite
CLLFZ	Cadillac-Larder Lake Fault Zone

Fig. 2.1. Geological map of the Pontiac Subprovince (from Hocq 1989).

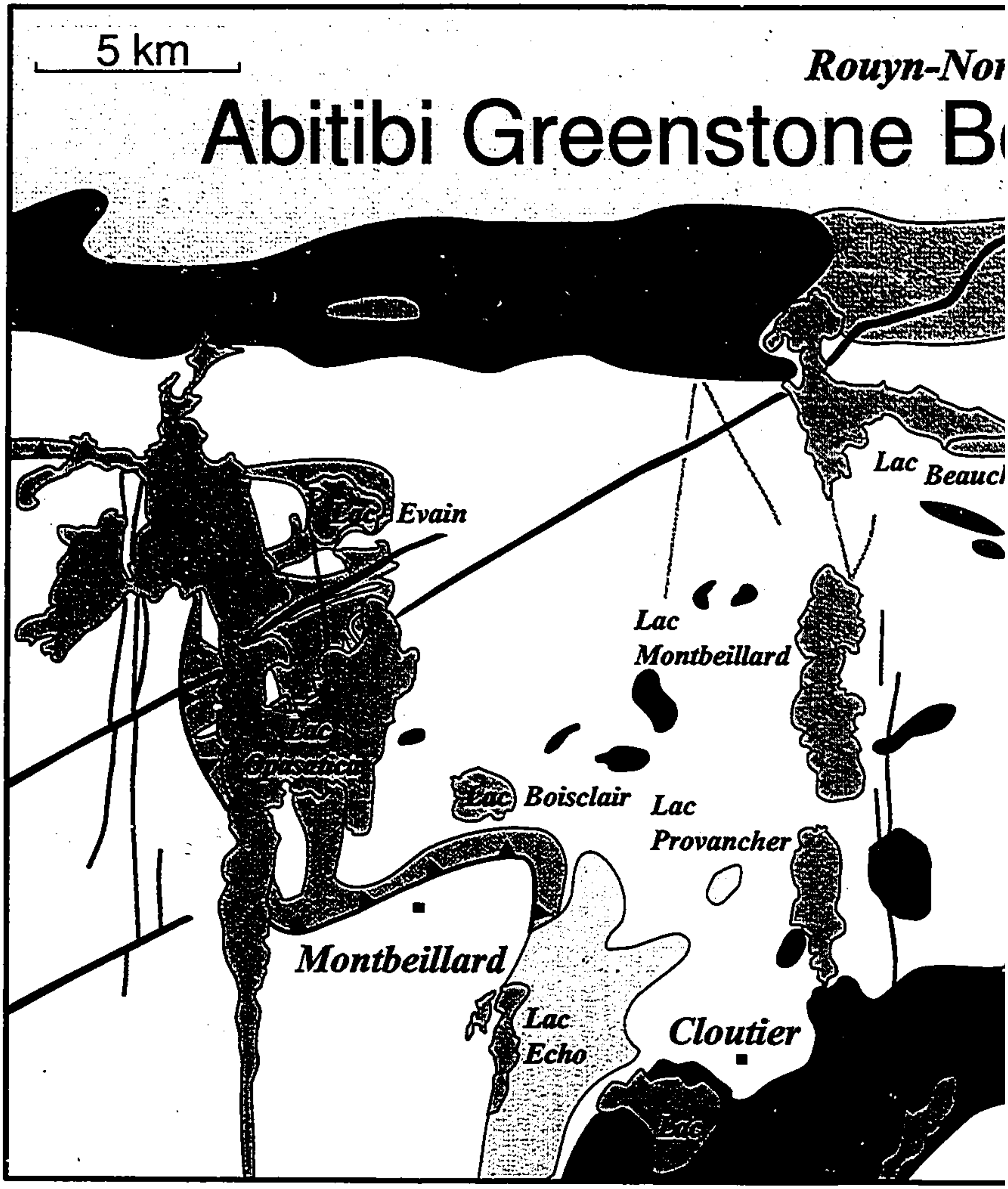

Fig. 2.2. Principal geological features of the study area. Geological maps by Rive (1989) and van de Walle

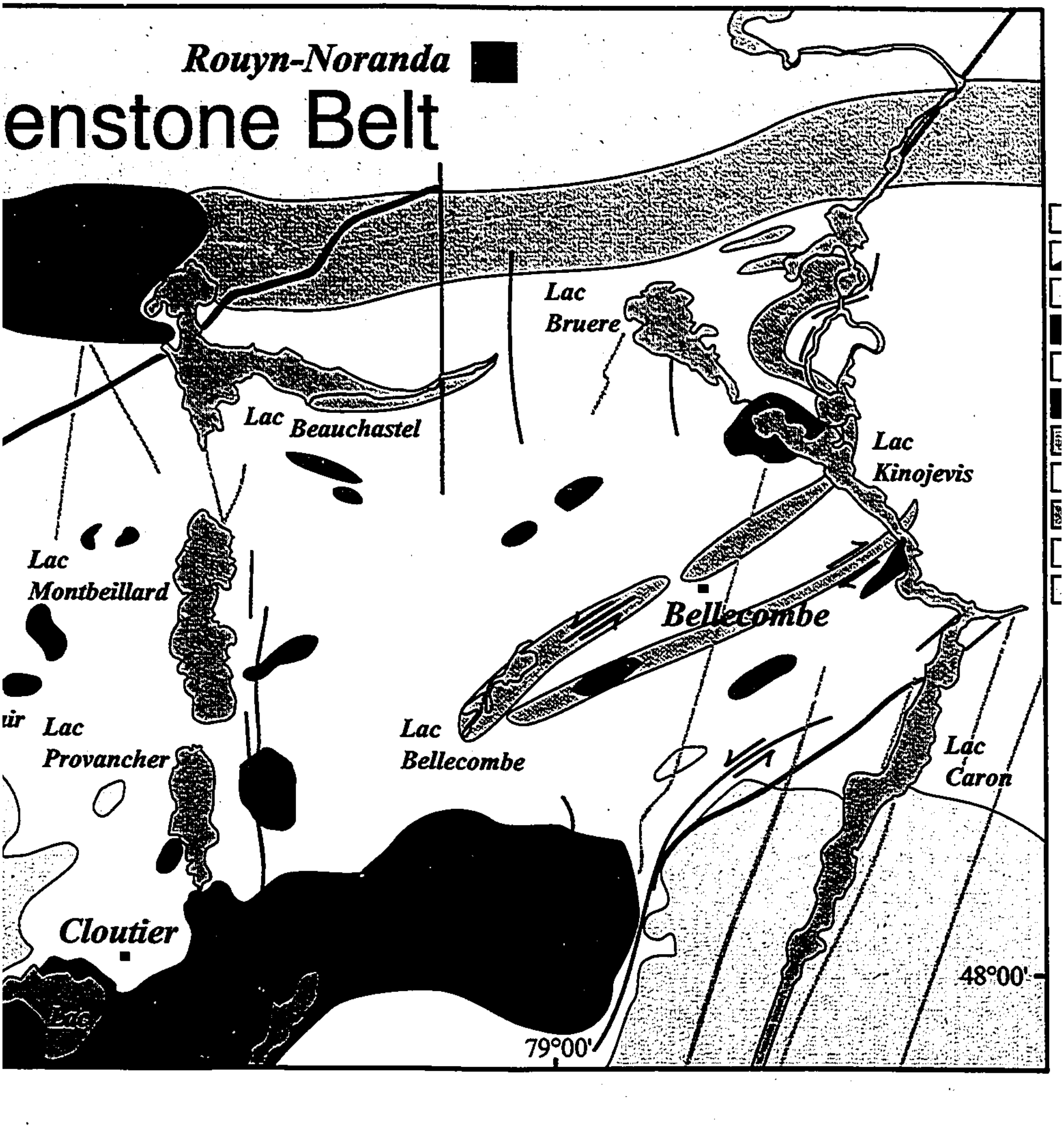

gical maps by Rive (1989) and van de Walle (1978) were used as bases.

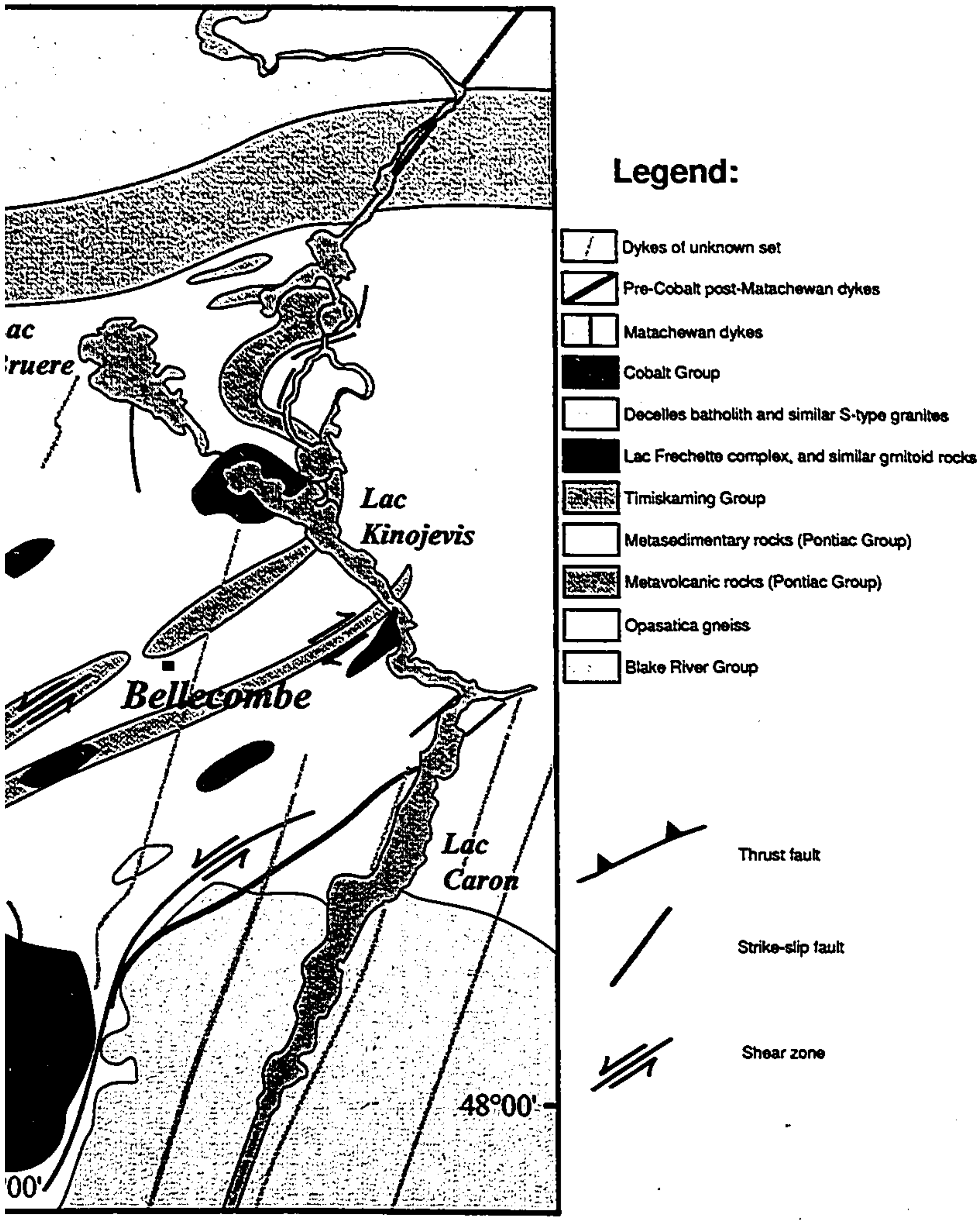
ac
ruere
Lac
Kinojevis
Bellecombe
Lac
Caron
48°00'
00'
Legend:
Dykes of unknown set
Pre-Cobalt post-Matachewan dykes
Matachewan dykes
Cobalt Group
Decelles batholith and similar S-type granites
Lac Frechette complex, and similar grnitoid rocks
Timiskaming Group
Metasedimentary rocks (Pontiac Group)
Metavolcanic rocks (Pontiac Group)
Opasatica gneiss
Blake River Group
Thrust fault
Strike-slip fault
Shear zone

es.

1983a, b) suggested that the fault zone was originally a (normal) growth fault that formed concurrently with volcanism in the Abitibi basin and sedimentation in the Pontiac basin.

The Lacorne block (Dawson 1966) is the only major metasedimentary terrane within the Abitibi Subprovince. Amphibolite facies rocks of the Lacorne block are intruded by both S-type and I-type granites. Due to its similarity to the Pontiac Subprovince, the Lacorne block has been interpreted as a tectonic window of this subprovince within the Abitibi Subprovince (Kerrich and Feng 1992).

2.1. Sedimentary rocks and stratigraphic relationships

Sedimentary rocks within the study area may be grouped in three different successions: Pontiac Group, Timiskaming Group, and Gowganda Formation. Figure 2.3 schematically represents the stratigraphic relationships between these and other units within the study area.

2.1.1. Pontiac Group

The Late Archean Pontiac Group (first described by Wilson 1909) in the northwestern Pontiac Subprovince includes a relatively thick succession of monotonous metasedimentary rocks. Dimroth *et al.* (1982) estimated a predeformation thickness of more than 1000 m for the sedimentary succession in the Pontiac Subprovince. A few thin (up to 2 m thick) and one thicker volcanic units (see geologic map, Fig. 2.2) are present within the Pontiac sedimentary succession, and hence are considered to be part of the Pontiac Group. A description of these volcanic rocks is presented in section 2.2.

The relative abundance of biotite and aluminum-rich metamorphic minerals compared to quartz and plagioclase, detected through modal analysis (Table 2.1), indicates that metasedimentary rocks of the Pontiac Group were originally graywackes. Bedding in these predominantly fine-grained sediments is well preserved and corresponds mostly to abrupt changes in detrital grain size. Bed thickness ranges from few centimetres to less than two metres.

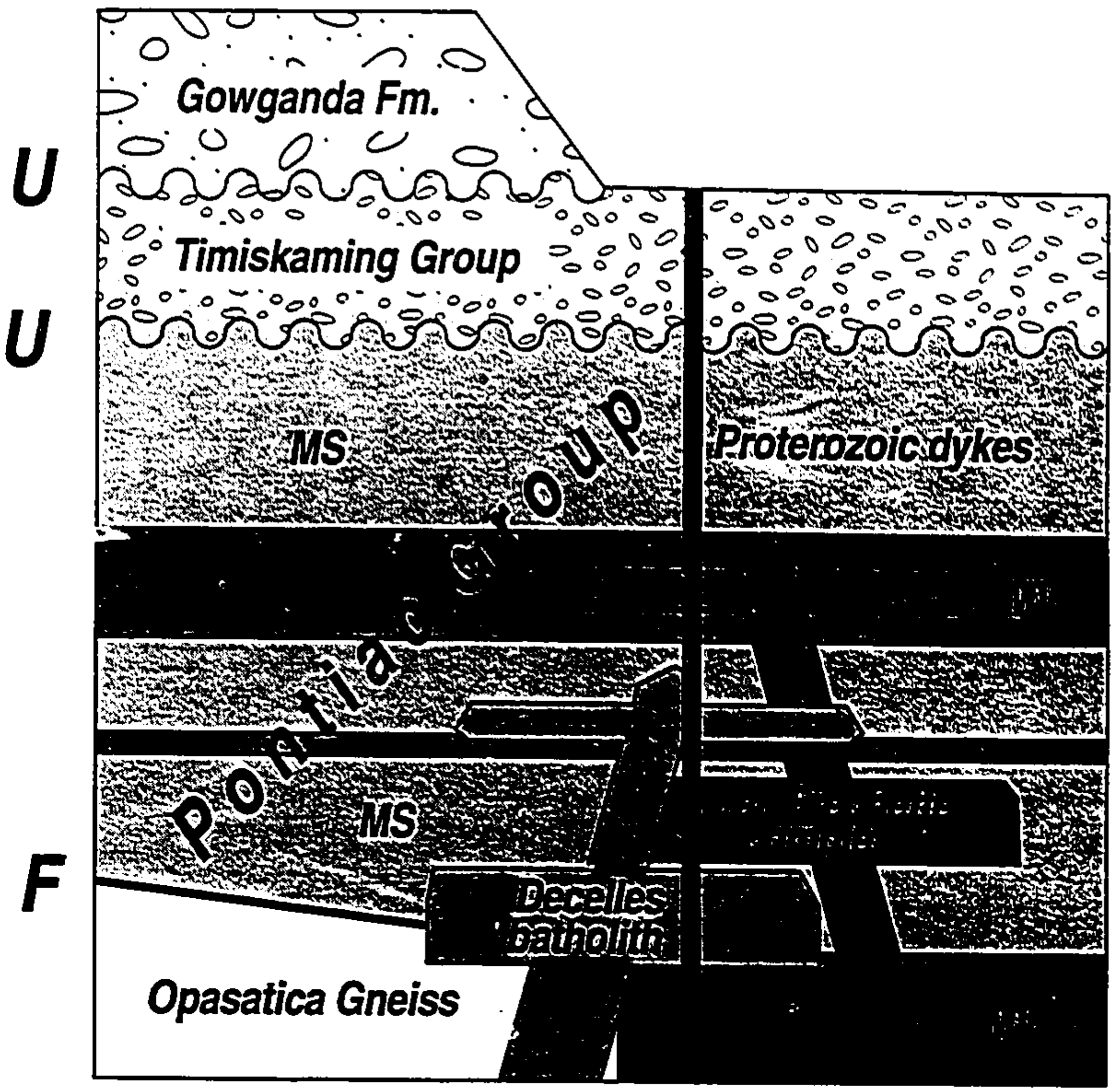

MS metasedimentary rocks

MV metavolcanic rocks

F faulted contact

U unconformity

Fig. 2.3. Stratigraphic relationships between different rock units within the study area.

Table 2.1. Modal analyses (based on point counting, 100 counts per thin-section) of the Pontiac metasedimentary rock samples.

Sample No.	Quartz	Plagioclase	Biotite	Muscovite	Chlorite	Garnet	Al-silicates*	Opaque
JL1B	60	12	24	0	0	0	0	4
JL2	49	27	10	0	13	0	0	1
JL3A	45	6	26	19	1	1	2	0
JL5	39	8	15	3	33	0	0	2
JL6	53	10	28	0	8	0	0	1
JL7	47	20	31	0	1	1	0	0
JL14A	54	18	22	4	0	0	2	0
JL25A	38	14	35	9	0	0	3	1
JL30	30	34	14	10	12	0	0	0
JL31	26	40	22	2	8	0	1	1
JL33A	26	16	16	32	9	1	0	0
JL34	44	19	23	9	0	1	4	0
JL35B	36	35	19	0	7	3	0	0
JL36	25	46	15	4	10	0	0	0
JL37	25	32	17	7	17	0	0	2
JL39	32	24	19	24	0	0	1	0
JL40	38	41	0	0	21	0	0	0
JL41	49	8	30	11	2	0	0	0
JL42A	38	17	24	13	2	1	5	0
JL43A	15	51	27	1	5	1	0	0
JL45	43	11	9	2	35	0	0	0
JL46	42	32	15	0	9	1	0	1
JL50	37	12	32	19	0	0	0	0
Average	38.7	23.2	20.6	7.3	8.4	0.4	0.8	0.6
Sd.	11.0	13.3	8.4	8.9	10.0	0.7	1.4	1.0

* The column for the Al-silicates (kyanite, sillimanite) also includes staurolite.

Tourmaline, zircon and apatite within the samples are usually less than 1%.

Despite undergoing amphibolite facies metamorphism and several deformational events, sedimentary structures such as graded bedding, cross lamination (Fig. 2.4), channels and cut-and-fill structures (Fig. 2.5) are clearly visible in many outcrops. Arenaceous balls within pelitic matrix are among other sedimentary structures that have resulted from dewatering of rapidly deposited sediments. Load casts and flame structures are reported by Goulet (1978) to be among other sedimentary structures. Most of these primary structures are good top indicators, and where detectable, were used to determine structural polarities.

Diagnostic features of Phanerozoic accretionary prism successions, such as tectonic melange, soft-sediment deformation (Williams *et al.* 1984), and intraformational unconformities have not been observed within the Pontiac Group.

Within the graded beds, increasing amounts of clay minerals before metamorphism may be inferred by the darker colour of the rock and higher content of biotite, staurolite, or aluminosilicates. Graded bedding is detectable in some thin-sections. Fresh surfaces of the Pontiac Group metagraywacke rocks are dark to pale gray, and weathered surfaces range from brownish gray to light beige gray.

A monomictic conglomerate unit, composed of graywacke pebbles and cobbles of the Pontiac Group within a graywacke matrix, is present in the northern part of the study area. Outcrops of this conglomeratic unit are best seen on the northern shores of Lac Beauchastel. This unit is considered by some workers to be situated in the upper part of the Pontiac sedimentary succession, close to the base of the Timiskaming Group (Goulet, 1978, Dimroth *et al.*, 1982); others (Podolsky 1950, Wilson 1962) have included them in the Timiskaming Group. As will be later discussed, this unit is best grouped within the Timiskaming sedimentary succession.

Detrital grain size of the metaturbidites ranges from 40 μm in pelitic siltstones to up to 15 mm in pebbly sandstones. Coarse-grained sediments are confined to a few outcrops in the eastern and northern parts of the study area, and in most cases are associated with cut-and-fill structures which separate them from the underlying fine-grained sediments (see Fig. 2.5).

Fig. 2.4. Cross-lamination within the metagraywackes of the Pontiac Group. Score and flame structures are visible left of coin. Dark areas, best visible on weathered surfaces such as this, indicate concentration of clay minerals that have been metamorphosed to produce micas. Photo oriented with top of metagraywacke to the left.

Fig. 2.5. Cut-and-fill structure in sedimentary rocks of the Pontiac Group on east shore of Baie Caron. Pebbly sandstone has filled the scoured channel on the graywacke layer. Photo oriented with top of sediments to the up.

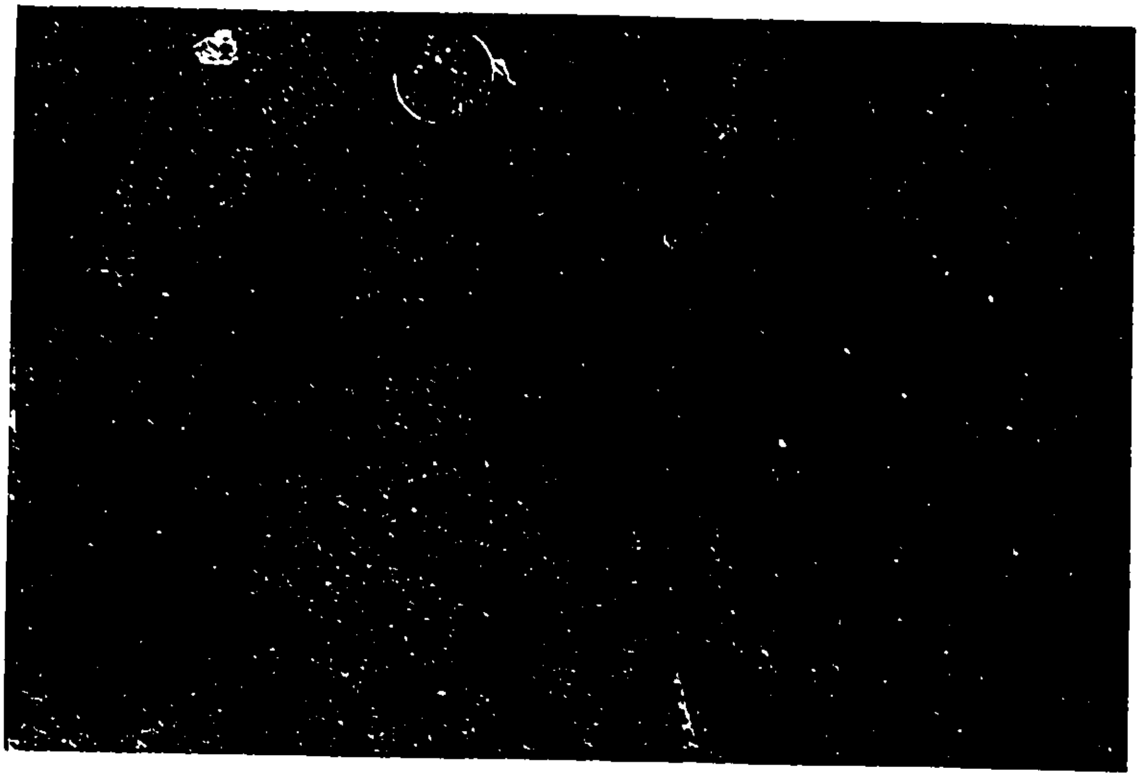

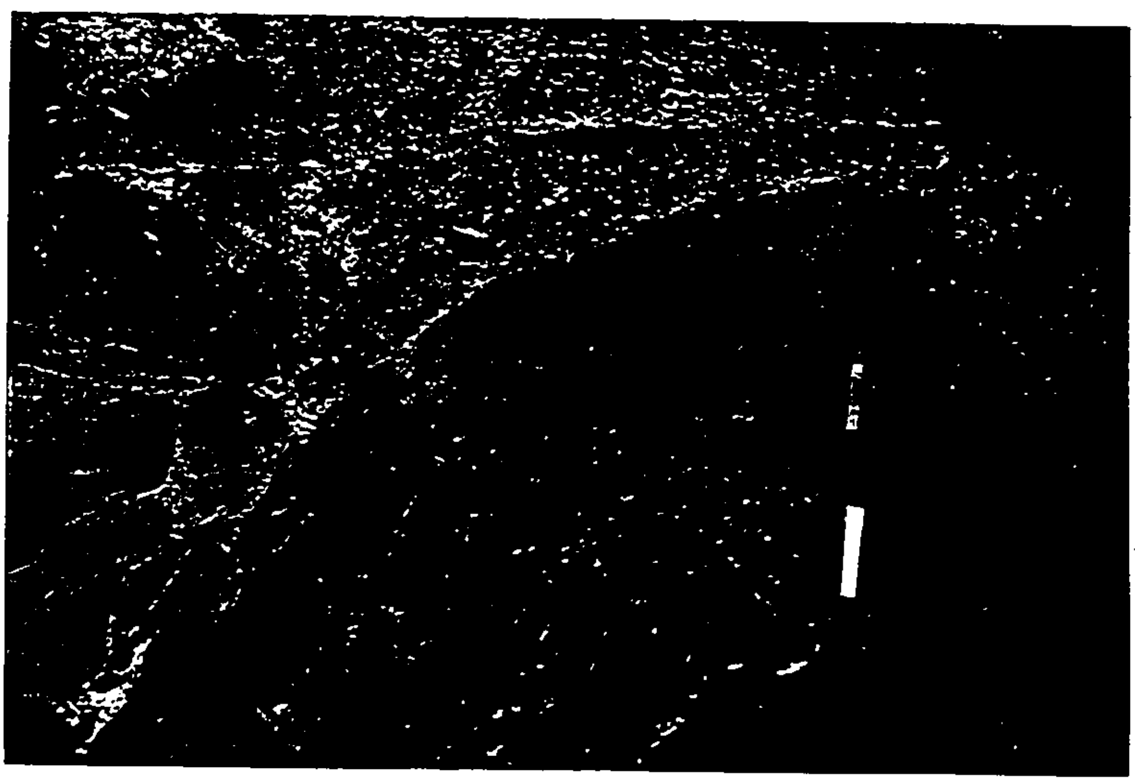

Lajoie and Ludden (1984) have documented a southward decrease in bed thickness, sand/shale ratio, and grain size of the Pontiac sedimentary rocks, on the basis of which they have postulated a southward-deepening basin. Microscopic investigation of quartz and feldspar grain-size during this study indicates that average grain-size increases towards the south (Fig. 2.6). This phenomenon is most likely a result of increase in metamorphic grade towards the south, which has caused an increase in size of the grains due to metamorphic recrystallization. Paleocurrent orientations were not analyzed systematically during this study, but a few observations of cross laminations indicate both westward and southward sediment transportation.

Modal analyses of the metasedimentary rocks (see Table 2.1) suggest that detrital grains of quartz and plagioclase were abundant in the sedimentary protoliths. Major mineral components of these metasediments from most to least abundant are: quartz, feldspar (predominantly plagioclase), biotite, chlorite, muscovite, garnet, staurolite, kyanite, sillimanite, magnetite, ilmenite, rutile and tourmaline. Small pebbles in a few pebbly sandstone beds are monomineralic plagioclase grains (one crystal per pebble). In less recrystallized rocks from northern part of study area, an abundance of detrital plagioclase crystals that do not show altered rims, and angular grains of quartz and feldspar, suggest the predominance of mechanical over chemical weathering in the source area. Geochemical and petrographic studies of the Pontiac Group turbidites suggest that the source rocks may have been tonalites, mafic and ultramafic rocks, and some older sedimentary rocks as evidenced by the presence of sandstone fragments (Dimroth *et al.* 1982, Lajoie and Ludden 1984, Camiré *et al.* 1993). The location of the source region is poorly constrained, and may have been to the north within the Abitibi Subprovince, or to the south and east within the reworked Archean rocks of the Grenville Province (Dimroth *et al.* 1982Camiré *et al.* 1993).

On the basis of stratigraphic relationships, the Pontiac Group is inferred to have been deposited after deposition of the Blake River Group in the Abitibi Subprovince (Goulet 1978, Dimroth *et al.* 1982). Geochronologic studies of the Pontiac metasedimentary rocks (see

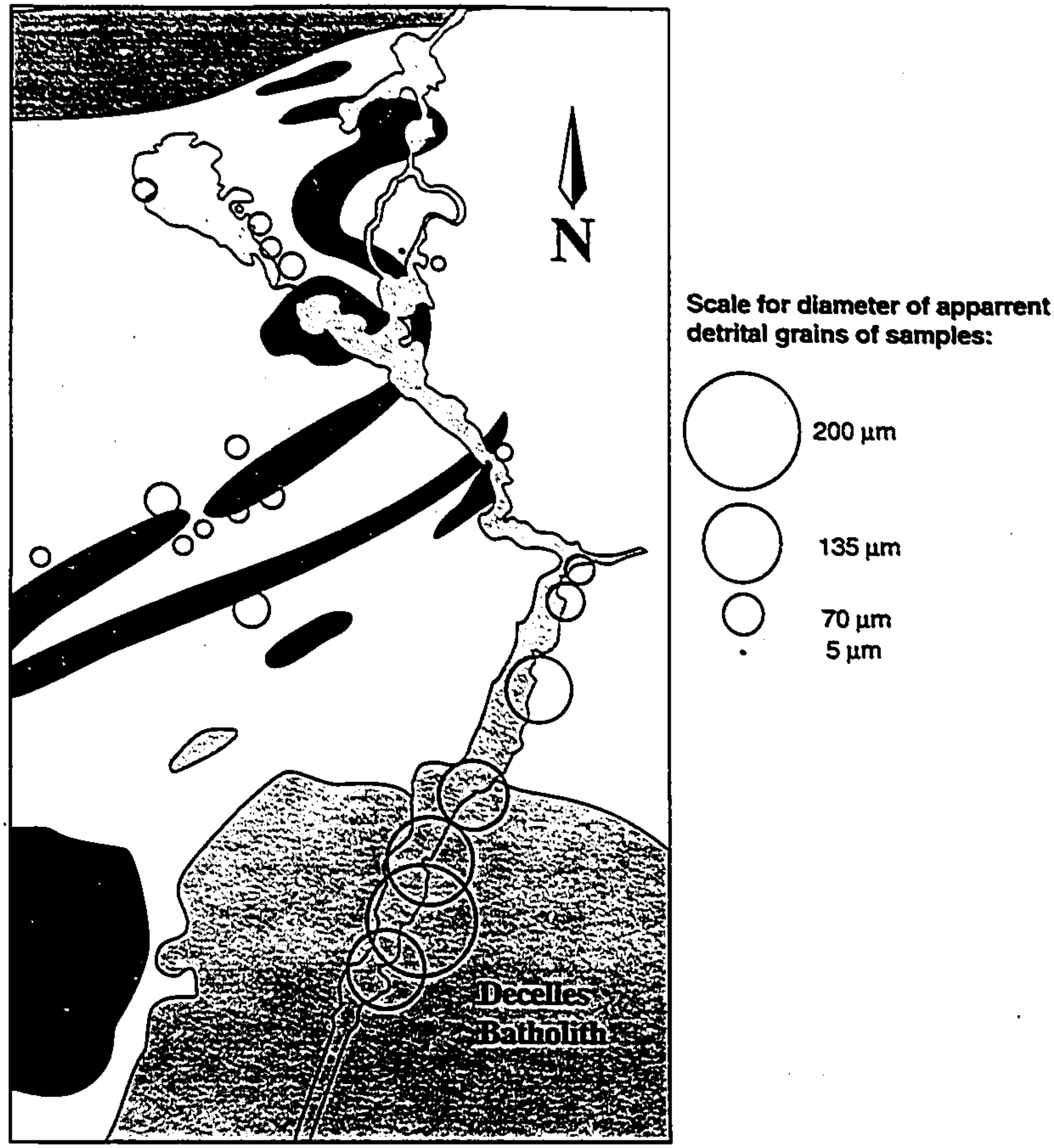

Fig. 2.6. Distribution of mean apparent detrital grain sizes (quartz and feldspar) within the metasedimentary rocks of the Pontiac Group. The measurements within the Decelles batholith are from metasedimentary enclaves.

Chapter 5) have yielded detrital zircon ages from 2940 Ma to 2683 Ma (Gariépy *et al.* 1984, Mortensen & Card 1993).

2.1.2. Timiskaming Group

Outcrops of Timiskaming Group rocks are limited to the northern part of the Pontiac Subprovince, where along the Cadillac-Larder Lake fault zone they separate the Pontiac metasedimentary rocks from the Blake River Group of the southern Abitibi Subprovince (Fig. 2.1). Matrix-supported to framework-supported polymictic conglomerates are the major components of this unit, although graywacke packages up to a few metres thick, are common. Within the study area, pebbles and cobbles in the Timiskaming Group range from 2 to 50 centimeters in diameter and in most cases are strongly deformed. Aspect ratio of the deformed pebbles in some places reaches up to 1:20. The clasts, in decreasing order of abundance, are felsic to intermediate intrusive rocks, felsic volcanic rocks, mafic to intermediate volcanic rocks, reworked sedimentary rocks, and magnetite. Deformation of the clasts happened simultaneously with the matrix, and no clast preserves evidence of a major deformational or metamorphic event prior to deposition. Geochemical and petrographic study of clasts from the Timiskaming Group (Legault and Hattori 1994) has indicated that these clasts were essentially derived from a volcanic arc environment. The most probable candidate for the source rock would, therefore, be the Abitibi greenstone belt.

Goulet (1978) reported an unconformity between the sedimentary rocks of the Pontiac and Timiskaming Groups. He introduced the name Granada Group, as a stratigraphic equivalent of the Timiskaming Group that unconformably overlies the Blake River Group north of the Cadillac-Larder Lake fault zone. Disagreement exists about whether the conglomeratic rocks of the Timiskaming Group represent a proximal facies of the Pontiac Group (Dimroth *et al.* 1982) or derivation from an entirely different source region (Lajoie and Ludden 1984). Mueller and Donaldson (1992) placed the Timiskaming Group rocks in Cycle 4 of their classification for sedimentary rocks of the Abitibi belt. They postulated this sedimentary cycle to have been deposited in an extensional basin comparable to modern pull-apart basins. Detrital zircons from the Timiskaming Group show absolute ages between *ca.* 2980 and 2679 Ma (Davis 1991).

The presence of an unconformity between the Pontiac Group and Timiskaming Group, presence of pebbles and cobbles of Pontiac Group rocks at the base of the Timiskaming sedimentary succession, and slightly younger detrital zircon ages within the Timiskaming Group rocks, suggest that the Timiskaming Group represents the end of deep-sea sedimentation within the Pontiac basin, emergence of the turbiditic sequence, and the start of a shallower succession in late Archean time. As will be shown in Chapter 3, the Timiskaming Group was deformed by the first deformational event (D_1) recognized within the study area, and its outcrops are confined to the footwall of the Cadillac-Larder Lake fault zone in which major thrusting occurred during the D_1 event. The most probable interpretation for the sedimentary environment of this succession is , therefore, a foreland basin.

2.1.3. Gowganda Formation

Sedimentary rocks of the Huronian Supergroup (Robertson *et al.* 1969) constitute the oldest Proterozoic sedimentary sequence that unconformably overlies the southern margins of the Archean Superior Province (see Fig. 1.1). This supergroup consists of four groups, which in ascending stratigraphic order are: the Elliot Lake, Hough Lake, Quirke Lake and Cobalt Groups (Robertson *et al.* 1969). The Cobalt Group (Miller 1913, Collins 1917) comprises four formations: the Gowganda, Lorrain, Gordon Lake and Bar River Formations (Bennett *et al.* 1991). The Early Proterozoic rocks within the study area appear to be part of the Gowganda Formation (Collins 1917, see also Powell and Hodgson 1992).

Clastic sedimentary rocks of the Gowganda Formation unconformably cover the metasedimentary rocks of the Pontiac and Timiskaming Groups, and volcanic rocks of the Blake River Group in the northwestern part of the study area. The unconformity surface is best exposed along the northernmost shores of Lac Opasatica. In this area, clast-bearing graywackes of the Gowganda Formation were deposited on a ragged surface of fractured Pontiac Group rocks (Fig. 2.7). Angular cobbles and boulders of the Pontiac metasedimentary rocks are present I in the lower part of the Gowganda sedimentary succession (Fig. 2.7).

The principal Lithologies of the Gowganda formation in the study area are graywackes and matrix-supported conglomerates. Greenish gray graywackes in Rouyn-Beauchastel area consist of angular to subangular grains of quartz, plagioclase and epidote (Wilson 1962). Clasts of the matrix-supported conglomerates reach diameters up to one meter, and are usually composed of amphibole and biotite granites, felsic volcanic rocks, and metagraywackes. Higher in the sequence, rounded cobbles and boulders predominate over the angular clasts, but they appear to be dropstones surrounded by a relatively uniform graywacke matrix (Fig. 2.8).

Sedimentary rocks of the Gowganda formation are considered to be glaciomarine deposits (Mustard and Donaldson 1987, and references therein). Deposition of the Huronian Supergroup is bracketed by a *ca.* 2454 Ma date on diabase dykes of the Matachewan swarm (Heaman 1988, U/Pb zircon), which it unconformably overlies, and a *ca.* 2219 Ma date on diabase dykes and sills of Nipissing swarm (Corfu and Andrews 1986, U/Pb baddeleyite), which are intruded into the Huronian sedimentary sequence.

2.2. Metavolcanic rocks

Volcanic rocks in the Pontiac Subprovince may be divided into three distinct groups. The first group, which is present in the northwestern part of the subprovince (the present study area), seems to have been deposited as several discrete units within the Pontiac sedimentary succession. The volcanic rocks of this group are predominantly composed of komatiitic, andesitic and basaltic flows showing pillow structure in some places. The thickest of these flows crop out along a folded belt occupying parts of the Lac Bruère, Lac Caron and Bellecombe areas (Fig. 2.2). Outcrops on Lac Beauchastel may be correlative with these volcanic rocks. Outcrops of mafic to ultramafic rocks in the eastern Lac Opasatica area, referred

Fig. 2.7. Irregular unconformity surface between the metasedimentary rocks of the Pontiac Group (beneath head of hammer) and sedimentary rocks of the Gowganda Formation; northern end of Lac Opasatica. Arrow indicates top direction. Photo oriented with top of sediments to the up.

Fig. 2.8. Granitic dropstone within the graywackes of the Gowganda Formation; roadside, highway 101. Arrow indicates top direction. Photo oriented with top of sediments to the up.

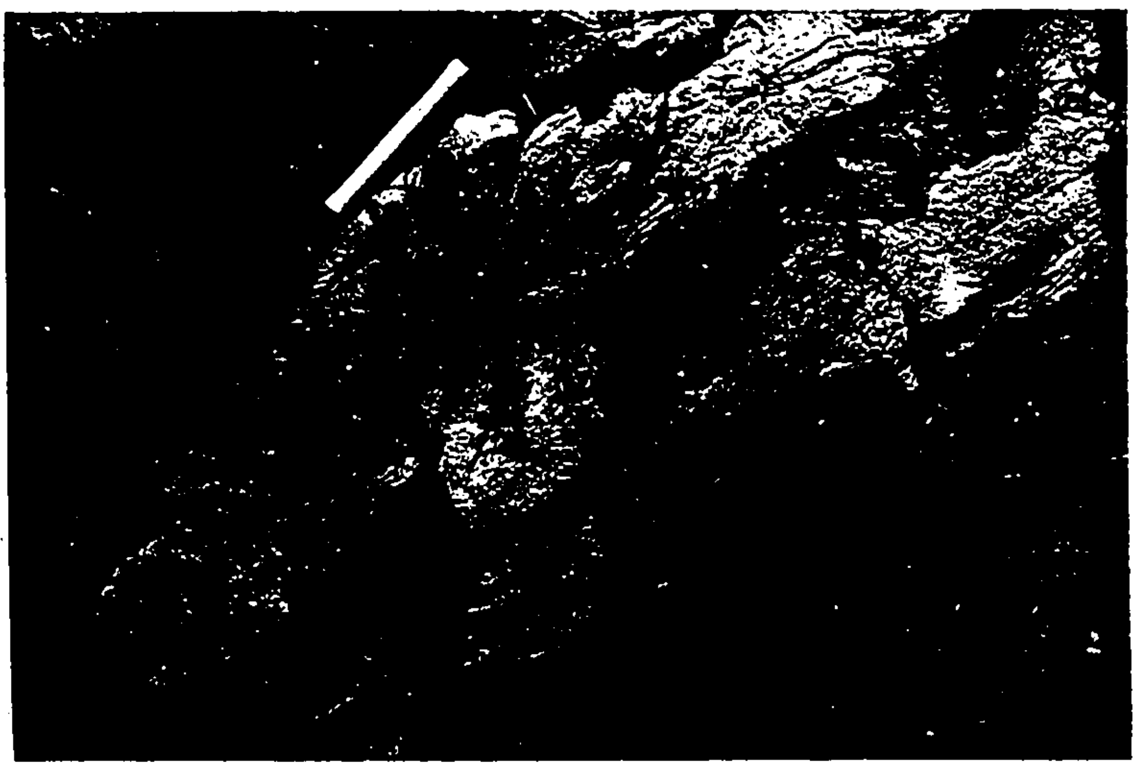

to as the Opasatica Formation by van de Walle (1978), may be correlative with rocks of the Bellecombe area.

Spinifex texture and polygonal structures are present here and there within the komatiitic rocks of this volcanic group, features that confirm their komatiitic character (Fig. 2.9). Chemical analysis done by Mark Shore (personal communication) on a sample from a hillside outcrop to the east of the Lac Opasatica, which lacks spinifex texture, indicates a komatiitic affinity based on its major and minor element composition (see Appendix C).

Another important group of volcanic rocks is present within the gneissic rocks of the Lac Opasatica area (Lac Opasatica gneiss, Fig. 2.2). The original composition of these rocks ranges from felsic to ultramafic, and they are associated with some iron-formations (Fig. 2.10). Variable compositions similar to the volcanic rocks of the Baby-Belleterre belt (described by Imreh 1973, Barnes *et al.* 1993, and Sawyer and Barnes 1994), and presence of the iron-formation (this study) suggest that they correlate to the Baby, Belleterre and Lac des Bois Groups in the south (the whole assemblage is known as the Belleterre-Angliers belt).

The third group of volcanic rocks occurs as three volcanic patches outside the study area, in the southwestern part of the subprovince (Fig. 2.1), and is known as the Belleterre-Angliers belt (Dimroth *et al.* 1982). These volcanic rocks are mainly composed of felsic to ultramafic components associated with iron-formation. The structural and stratigraphic position of these rocks relative to the Pontiac metasedimentary rocks is controversial. Imreh (1973) proposed that they concordantly overlie the Pontiac metasedimentary rocks, whereas other geologists have postulated these patches to be allochthonous (Sawyer and Barnes 1994). U/Pb zircon ages as old as *ca.* 2690 Ma from these rocks (Mortensen and Card 1993), indicate that the earlier viewpoint must be rejected, because these dates are older than the underlying Pontiac Group rocks (see Chapter 5).

Fig. 2.9. Spinifex texture within komatiitic volcanic rocks of the Lac Opasatica area. Diameter of coin is 26 mm.

Fig. 2.10. Photomicrograph of a deformed iron formation from metavolcanic rocks on the western shores of the Lac Opasatica. Minerals are quartz, amphibole, pyrite and magnetite. Because of intense deformation, field detection of top direction of the sample was not possible.

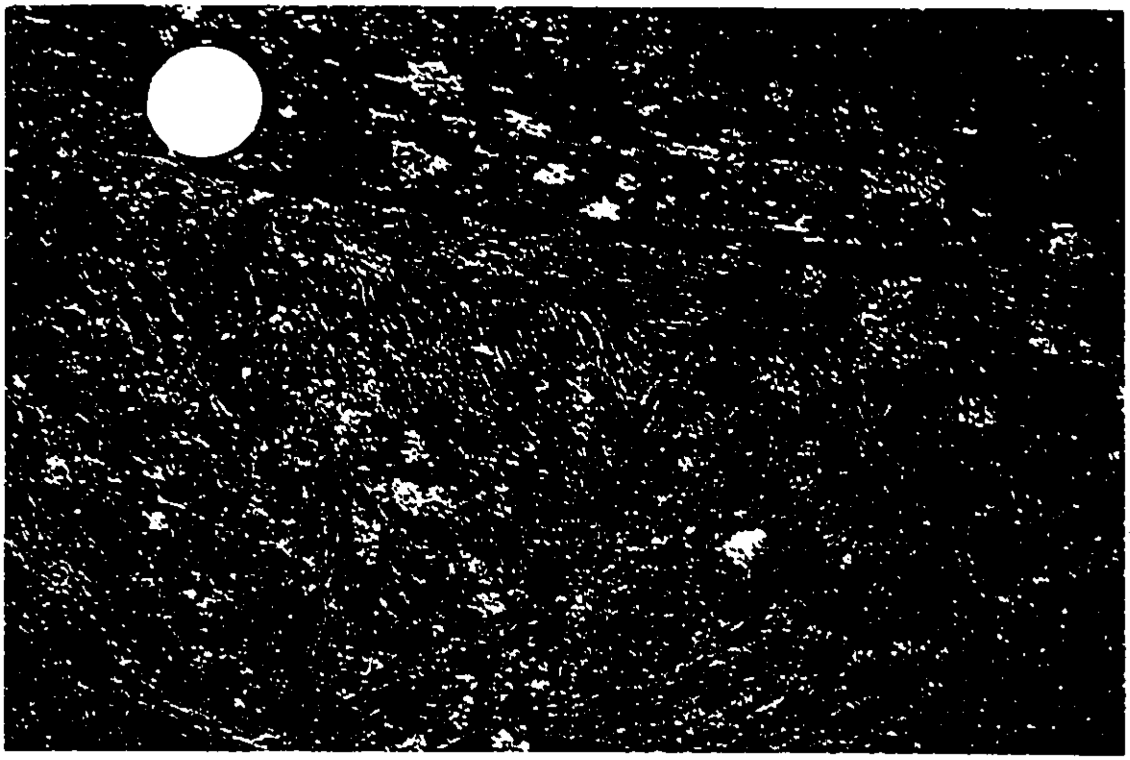


2 mm

2.3. Intrusive rocks

2.3.1. Granites, granitoids, and lamprophyres

On the basis of genetic relationships, intrusive bodies of the Pontiac Subprovince may be grouped into I-type and S-type classes. The I-type intrusions have an alkaline composition (van de Walle 1978), and compared to S-type granites, they have been intruded earlier through the sedimentary rocks of the subprovince (see Chapter 5). Minerals in these rocks include alkali feldspar (predominantly microcline), sodic plagioclase, hornblende, pyroxene (aegirine-augite), quartz, titanite, allanite, magnetite, and apatite. In some syenitic samples hornblende rims pyroxene, suggesting a reactive origin for the hornblende, although it is not clear whether the hornblende is of igneous or metamorphic origin. U/Pb age of zircons from these intrusions range from *ca.* 2686 to *ca.* 2669 Ma (Davis 1991, Mortensen and Card 1993, Machado *et al.* 1991).

The Lac Frechette complex (Fig. 2.2) is the largest unit of I-type granitoids mapped in the northwestern Pontiac Subprovince. Other smaller bodies with similar composition crop out here and there throughout Pontiac metasedimentary rocks, some of them concentrated along the Bellecombe shear zone. Chemical and modal analyses of these rocks indicate variable alkalic compositions from quartz-syenite (nordmarkite) to minette-type lamprophyres (van de Walle 1978). Scattered in these alkalic rocks are small and large inclusions of amphibolite which may be metamorphosed ultramafic xenoliths derived from volcanic rocks of the Pontiac Group, or from a different source at greater depths . Thin lamprophyric dykes associated with the I-type granitoid bodies are specially abundant in the Bellecombe shear zone. $^{40}Ar/^{39}Ar$ dating (see Chapter 5) has indicated the presence of lamprophyric dykes as young as *ca.* 1200 Ma in the western part of the study area.

In the southeastern part of the study area, south of Bellecombe village (Fig. 2.2), pegmatitic leucogranitic dykes have intruded metasedimentary and metavolcanic rocks of the Pontiac Group. The frequency and size of these dykes increases towards the south, and eventually in the Saint Roch area the main body of Decelles batholith outcrops (see map in Fig. 2.2). The batholith which is totally composed of peraluminous leucogranites with extensive cross-cutting pegmatitic dykes, includes the metamorphic minerals, sillimanite and garnet. Small and large xenoliths of Pontiac metasedimentary rocks are present within the batholith. Some of these xenoliths have mineralogy and textures that are intermediate between metasedimentary rocks of the Pontiac Group and the leucogranites. All of the above-defined characteristics suggest that the Decelles batholith is composed of S-type granites that have evolved from melting of Pontiac metasedimentary rocks during the peak metamorphic conditions. Oxygen isotope data and trace element analysis of these granitic rocks also supports their formation by melting of the prevalent Pontiac clastic sediments (Feng *et al.* 1993a). South of Cloutier village, the S-type granites are intruded into the I-type Lac Frechette complex.

No contact metamorphic aureole was observed within the metasedimentary rocks of the Pontiac Group close to the margins of the Lac Frechette complex and similar I-type plutons. However, such aureoles may have been overprinted by amphibolite facies regional metamorphism.

Outcrops of orthogneisses interlayered with mafic volcanic rocks are present to the western part of the study area (Fig. 2.11). Because of their widespread occurrence on the shores of Lac Opasatica, they hereafter are referred to as Lac Opasatica gneisses. The orthogneisses have a granodioritic composition, and are composed of quartz, feldspar (usually microcline and sodic plagioclase), biotite, hornblende and some magnetite. The quartz and feldspars are highly flat and elongated, and give the rocks their gneissic foliation. Composition and deformational style of these orthogneisses are very similar to Lac de Quinze gneisses that crop out in the southwestern part of the Pontiac Subprovince, south of the study area (Fig. 2.1, also see Carignan and Gariépy 1991).

The contact between the Lac Opasatica gneisses and volcanic and sedimentary rocks of the Pontiac Group is faulted and sheared (Montbeillard shear zone, see Chapter 3). Gneissose rocks of the Lac Opasatica area are cross-cut by I-type granites similar to those of the Lac

Fig. 2.11. A view of Lac Opasatica orthogneisses (light coloured) interlayered with metavolcanic rocks (dark) along highway 101, south of Montbeillard.

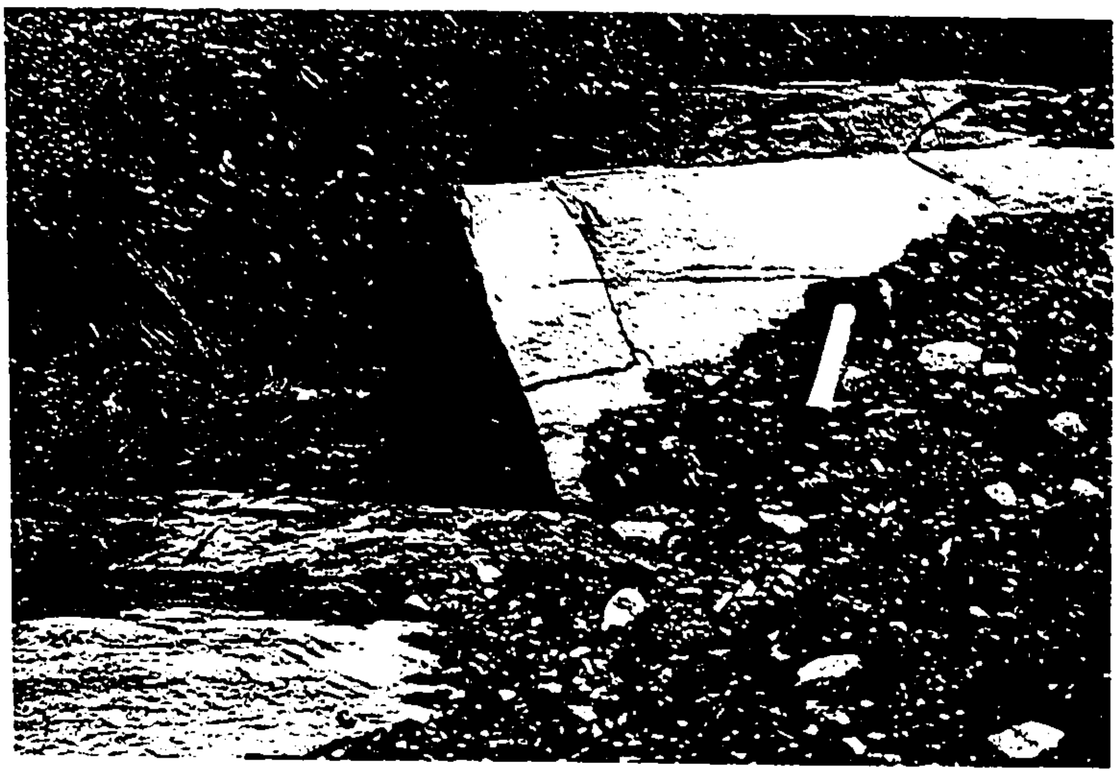

Frechette complex, where the granites show no sign of penetrative deformation. The gneisses therefore were deformed before intrusion of these I-type granitoids.

2.3.2. Albitite dyke

A small (less than 1 m thick) leucocratic dyke intrudes highly deformed metavolcanic rocks in an outcrop along highway 101. Microscopic examination of a sample from this dyke indicates that sodium-rich plagioclase constitutes almost 100% of the rock. Mechanical twinning is very common within these plagioclase crystals. This dyke may be grouped with the albitite dyke swarm in southwestern Abitibi Subprovince (Smith *et al.* 1990). No age has been reported for this dyke swarm; however, based on cross-cutting relationships, these dykes are considered to be partly contemporaneous with the main interval of gold mineralization in southwestern Abitibi Subprovince (Smith *et al.* 1990).

2.3.3. Mafic dyke swarms

Three sets of mafic dyke swarms intrude the northwestern Pontiac Subprovince (Fig. 2.2). The first set has a northward trend and is of pyroxenite and quartz diabase composition. The second set has a northeasterly trend and is composed of olivine diabase (van de Walle, 1978). On the basis of cross-cutting relationships (with other dykes and with Cobalt Group sedimentary rocks), and regional trend, Van de Walle (1978) classifies the first set with the Matachewan dyke swarm, and the dykes of the second set as part of a pre-Cobalt and post-Matachewan dyke swarm. The northeast-trending dyke north of Orignal Bay east of Lac Opasatica cross-cuts a north -trending dyke of the first set, and farther northeast disappears under the Cobalt Group sedimentary rocks. Dykes of the third set usually trend north-northeast and are abundant in southeastern part of the study area. These dykes usually have a diabasic composition, and because of parallelism with the conjugate set of faults related to the latest structural event, are considered to be younger than the two other dyke sets.

3. Structural geology

3.1. Introduction

Because of its importance as a precious-metal and base-metal mining region, the low-grade greenstones of the Abitibi Subprovince have been the subject of extensive geological and structural studies (Dimroth *et al.* 1982, 1983a and b, Hubert *et al.* 1984, Ludden *et al.* 1986, Chown *et al.* 1992, review in Jackson and Fyon 1991). In contrast, a relatively small number of studies have been concentrated in the high-grade metasedimentary and gneissic rocks of the neighboring Pontiac Subprovince. Nonetheless, some structural studies have been carried out in different parts of the Pontiac Subprovince, most in association with regional mapping, sedimentological or geochemical studies.

Goulet (1978) mapped the Pontiac and Timiskaming Groups close to the Cadillac-Larder Lake fault zone in the Rouyn-Beauchastel area (Fig. 1.2), and described two main sets of superposed folds as the dominant features of the structural geology. Both early north-trending and late east-trending superposed folds, mapped by Goulet, are upright and isoclinal, with associated steeply dipping axial planar foliations. According to Goulet, two other foliation sets strike northwest and northeast in the Rouyn-Beauchastel area. The northwest striking set is not associated with any major folds, but the northeast striking set is parallel to the axial surfaces of two broad antiforms that are superposed on older structures. Goulet suggested that faulting along the Cadillac-Larder Lake fault may have commenced with normal displacements during the formation of the Blake River volcanic complex to the north, and may have been reactivated several times later, including during deposition of the Timiskaming and Granada Groups. Goulet first defined the Granada Group as a lateral equivalent of the Timiskaming Group towards the north, and documented the unconformable relationship of the younger Granada and Timiskaming Groups to the Pontiac Group south of the Cadillac-Larder Lake fault zone, and to the Blake River Group north of the fault zone. On the basis of stratigraphic studies, he considered emerged volcanic islands, ancestral to the Abitibi greenstones, as the source area for the turbiditic sediments of the Pontiac, Timiskaming and Granada Groups. He also suggested that a regional fault system, equivalent to the Cadillac-Larder Lake fault zone, separated the volcanic chain to the north from the turbiditic basin to the south.

In his geological studies of Montbeillard township (Fig. 1.2), van de Walle (1978) described a series of tight eastward-plunging folds with north-dipping axial surfaces and southward diminishing amplitudes, that resulted from southward thrusting of the Pontiac Group rocks over a low-angle tectonic contact. This tectonic contact, that corresponds to the boundary of the Lac Opasatica gneiss domain, was first mapped by van de Walle. He also suggested that the presence of external tectonic breccias on the margins of the Lac Frechette complex indicates that the emplacement of these alkaline intrusions was carried out by buckling and extension of the country rocks.

In a study that included the same region as the present study, Camiré and Burg (1993) divided the northwestern part of the Pontiac Subprovince into two nappes, with the boundary between the two nappes defined by an abrupt change in structural style and metamorphic facies. They described two phases of tight to isoclinal folding in their upper nappe that were absent from the lower nappe. They suggested that nappe development, and associated south-verging inclined horizontal folds, and south-verging thrust faults were developed in response to regional north-south compression. The metavolcanic band exposed along the Kinojevis River (Fig. 2.2) is interpreted by Camiré (1992) as a folded klippe structure thrust onto the sedimentary rocks prior to peak metamorphism.

The present writer suggests that, despite the presence of small- and large-scale nappe-style folding, the presence of two distinct nappe structures in northwestern Pontiac Subprovince, as suggested by Camiré and Burg (1993), does not seem to be based on strong bases (see related discussion in section 3.8.1).

Geophysical studies, along with preliminary structural studies in the northwestern Pontiac Subprovince by Benn *et al.* (1994, see Appendix D) were used for interpretation of north-dipping superficial and subsurface structures related to south- to southeast-directed thrusting that resulted in a considerable amount of crustal thickening during a collisional event.

Sawyer and Barnes (1994) studied structural relationships between metavolcanic rocks of the Belleterre-Angliers greenstone belt (AG, BT and BB in Fig. 2.1) and metasedimentary rocks of the Pontiac Group in the southwestern part of the Pontiac Subprovince. They interpreted the Belleterre-Angliers belt as a thrust sheet above a mid-crustal duplex consisting of imbricating wedges of metasedimentary rocks and tonalite gneisses. The low-grade thrust sheet was postulated to be transported from north to south; however, derivation from the Abitibi Subprovince was ruled out. The sheared boundary between the Belleterre-Angliers greenstones and the underlying Pontiac Group was interpreted as an extensional shear zone developed during intraplating of tonalitic and granodioritic plutonic bodies within the Pontiac Subprovince.

One of the major regional structures in the area is the Cadillac-Larder Lake fault zone, which separates the low-grade southern Abitibi volcanic rocks from the relatively high-grade metasedimentary rocks of the Timiskaming and Pontiac Groups. In the present study area, the fault zone trends roughly east-west (though the map trace of the constituent faults is irregular), and at the surface it dips between 45° and 70° to the north. The fault zone, however, is suggested to dip steeply to the south both to the west in Ontario (Jackson *et al.* 1990), and to the east (Robert 1989) of the study area, near Val d'Or.

Because the Timiskaming Group outcrops immediately south of the Cadillac-Larder Lake fault zone, intense deformation due to movement along the shear zone is observed in these rocks. Some volcanic rocks of the Abitibi Subprovince, north of the fault zone are deformed in the immediate vicinity of the fault zone as well. Interpretations of the movement history along the fault zone differ, and include reactivation as a thrust fault of either an early normal fault (Dimroth *et al.* 1983) or an early sinistral transcurrent fault (Hubert *et al.* 1984, Hubert and Ludden 1986). Dextral transpression along the fault zone is inferred for the structures in the Val d'Or region (Robert 1989), east of the study area.

As revealed by the present study, the complex structure of rocks in the northwestern Pontiac Subprovince is the result of multiple deformational events that have developed sequentially under evolving metamorphic conditions. Figures 3.1 (map) and 3.2 (block diagram) illustrate the structural geology of the study area as interpreted by present study. Bedding planes within the study area are generally parallel to S_2 foliation (see section 3.4); mapped S_2 foliations in Fig. 3.1, therefore represent the bedding planes as well..

On the basis of cross-cutting and refolding relationships observed over a large range of scales, the structures in the metasedimentary, metavolcanic and intrusive rocks of the northwestern Pontiac Subprovince have been divided into five groups, referred to as D_1 through D_5. Structures within the Lac Opasatica gneisses are classified as pre-D_1 structures. This represents the first time that such a detailed structural classification has been provided for a part of the Pontiac Subprovince. However, it must be noted that classification and interpretation of different structural events presented by this study are inferred to be the most reasonable ones on the basis of the present database, and better interpretations will most likely result from further more detailed studies.

Other than folds and faults related to different deformational events, three shear zones are first described here as being structures along which major movements have occurred during structural evolution of the study area. Part of one of these shear zones (Montbeillard shear zone) was first mapped and described by van de Walle (1978).

3.2. Pre-D_1 structures

This group of structures is restricted to the Lac Opasatica gneisses, and includes a gneissic foliation, and an associated mineral elongation lineation defined by alignment of the crystal aggregates. The deformational event is referred to as pre-D_1, to distinguish it from the deformational events that affected the Pontiac sedimentary rocks. Gneissose rocks of the Lac Opasatica area are cross-cut by I-type granitoids similar to those of Lac Frechette complex,

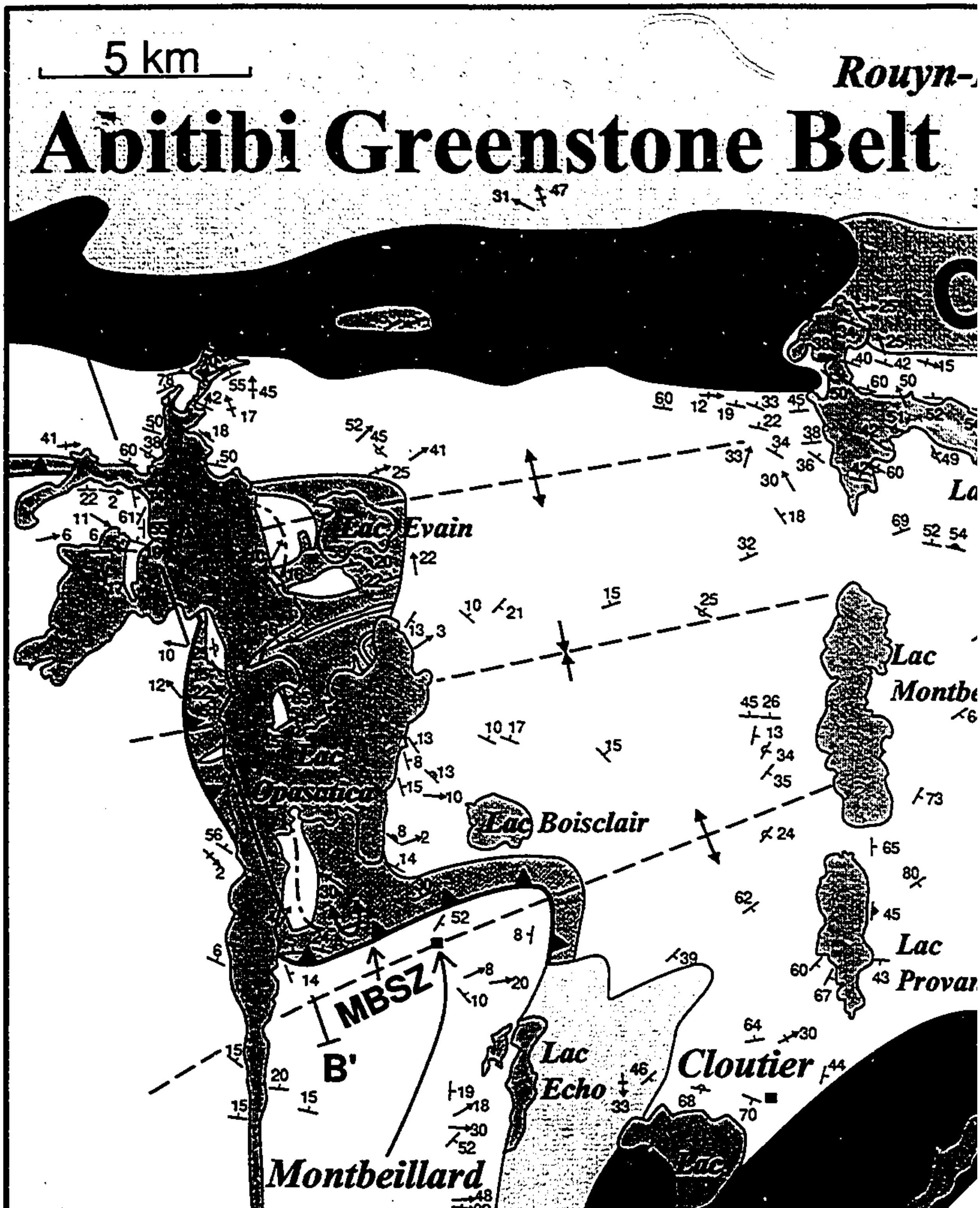

Fig. 3.1. Structural geology map of the northwestern Pontiac Subprovince. Foliations within the D batholith represent measurements from metasedimentary enclaves within the pluton, an within the Lac Frechette complex represent foliation of the igneous rock.

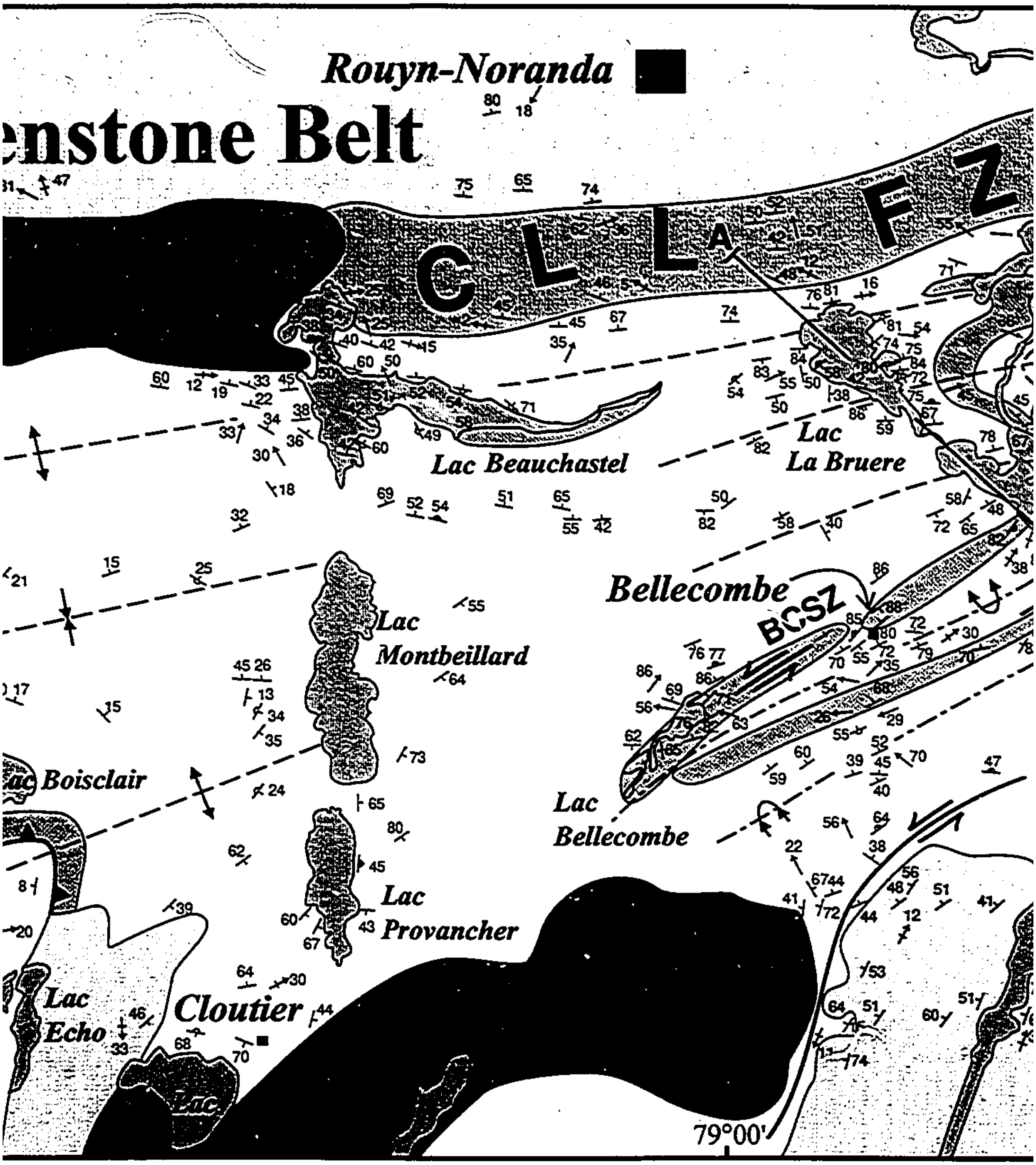

ern Pontiac Subprovince. Foliations within the Decelles metasedimentary enclaves within the pluton, and those ent foliation of the igneous rock.

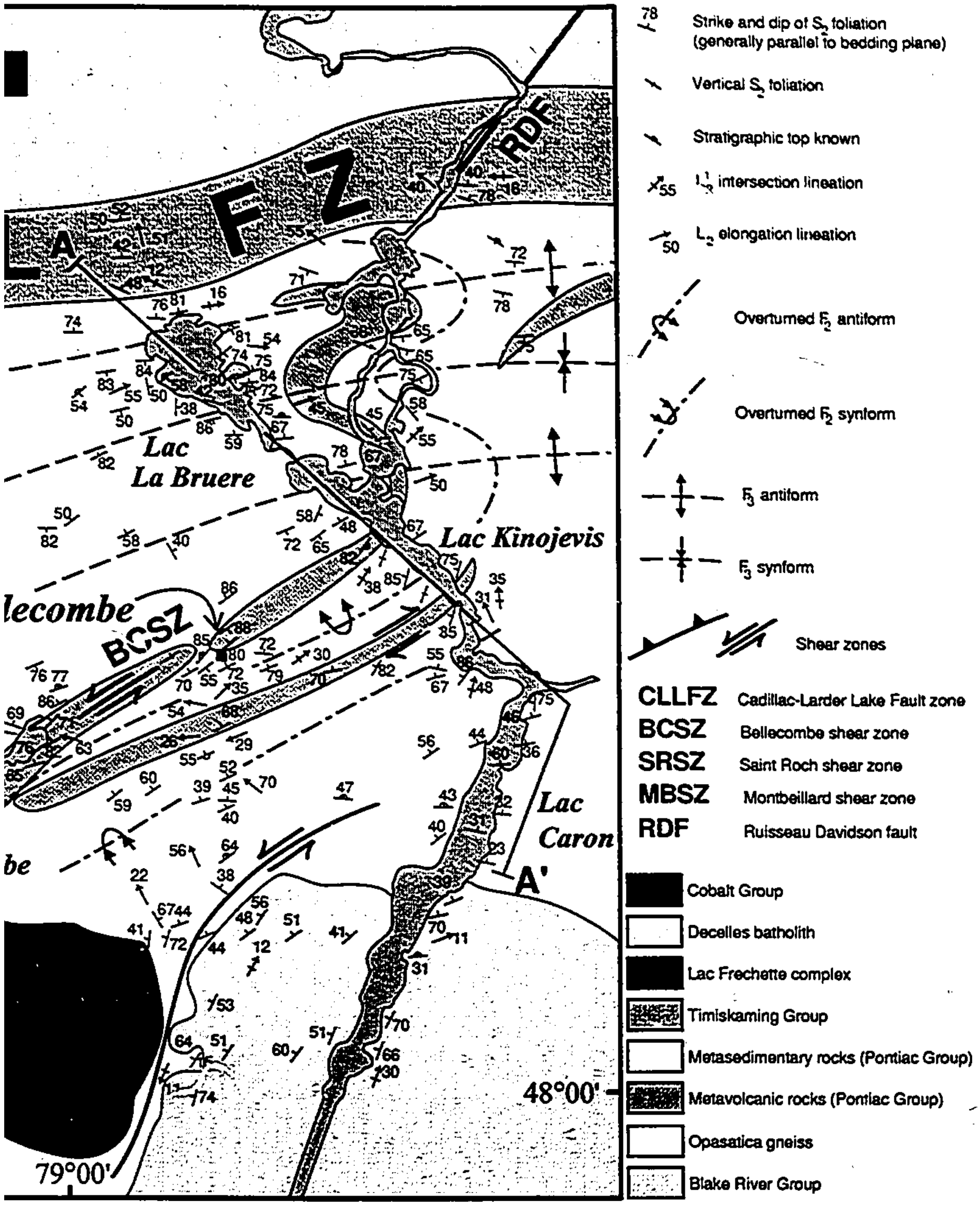
Strike and dip of S2 foliation (generally parallel to bedding plane)
Vertical S2 foliation
Stratigraphic top known
L1-2 intersection lineation
L2 elongation lineation
Overturned F2 antiform
Overturned F2 synform
F3 antiform
F3 synform
Shear zones
CLLFZ Cadillac-Larder Lake Fault zone
BCSZ Bellecombe shear zone
SRSZ Saint Roch shear zone
MBSZ Montbeillard shear zone
RDF Ruisseau Davidson fault
Cobalt Group
Decelles batholith
Lac Frechette complex
Timiskaming Group
Metasedimentary rocks (Pontiac Group)
Metavolcanic rocks (Pontiac Group)
Opasatica gneiss
Blake River Group
Lac La Bruere
Lac Kinojevis
Lac Caron
lecombe
BCSZ
RDF
A
A'
48°00'
79°00'

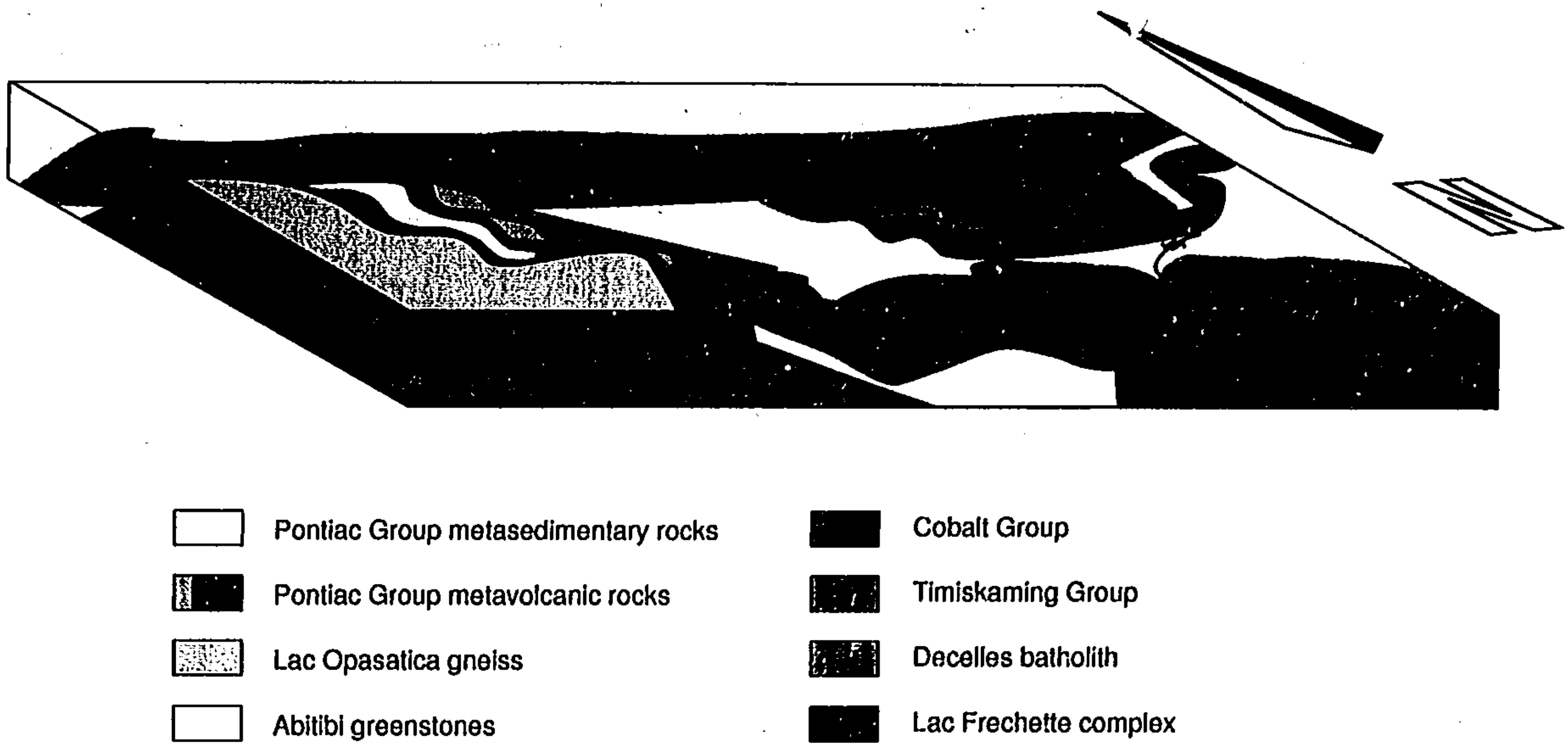

Fig. 3.2. Block diagram illustrating spatial relationship between different rock types in the northwestern Pontiac Subprovince. Note D_3 folding of D_2 nappes.

where the intrusions show no sign of penetrative deformation. The gneissosity therefore developed before intrusion of these I-type intrusions.

The pre-D_1 foliation is defined by alignment of flat quartz and feldspar crystals, and segregation of biotite and amphibole crystals parallel to foliation. Foliation planes are usually concordant with the S_2 foliation within the overlying Pontiac Group, which is separated along the Montbeillard shear zone from the gneisses (Fig. 3.1). However, the mineral elongation lineation within the gneisses is predominantly east-trending (Fig. 3.3), which is almost perpendicular to the L_2 elongation lineation within the Pontiac Group rocks. Quartz *c*-axis fabrics in the orthogneisses from the vicinity of the Lac Opasatica indicate a point maximum of *c*-axes parallel to the extension lineation (Fig. 3.4), that can be interpreted as recording either a pure shear strain (with the Z-axis of the strain ellipse being sub-vertical) or a very high non-coaxial strain, with a top-to-the-west sense of shear. Parallelism of the quartz *c*-axes with the direction of maximum finite strain indicates a prismatic slip system in the [0001] direction. This type of slip system in quartz is documented to be characteristic of high-temperature (above 700°C) deformation (Blacic 1971, Nicolas and Poirier 1976).

Investigation of relationships between orientation of *c*-axes and sub-grain boundaries in the quartz-rich samples of Lac Opasatica gneiss indicates that the sub-grain boundaries are mostly parallel to the *c*-axes (Fig. 3.5). This may be a result of rigid body rotation during the same deformational event, or a later minor simple shear event resulting in differential rotation of subgrains, which have slipped along subgrain boundaries parallel to the *c*-axes. The classic view about rigid body rotation of crystals does not support the first interpretation, because it requires that subgrain boundaries developed during rigid body rotation must be generally perpendicular to the orientation of the slip system within the crystals. The second interpretation seems more viable, which is similar to the interpretation of Lloyd *et al.* (1992) for development of subgrains during shear zone formation. They suggested that at low (simple) shear strains, subgrains may develop and have differential rotation in a domino-style of intergranular deformation.

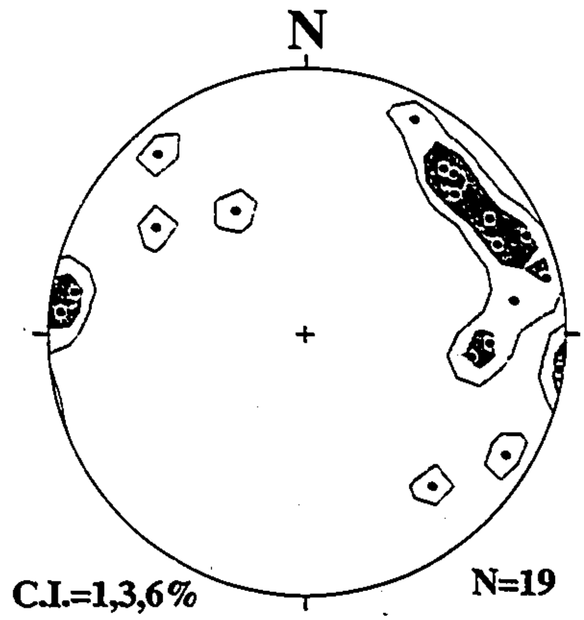

Fig. 3.3. Contoured lower hemisphere equal-area projection of pre-D_1 mineral elongation lineation within the Lac Opasatica gneisses.

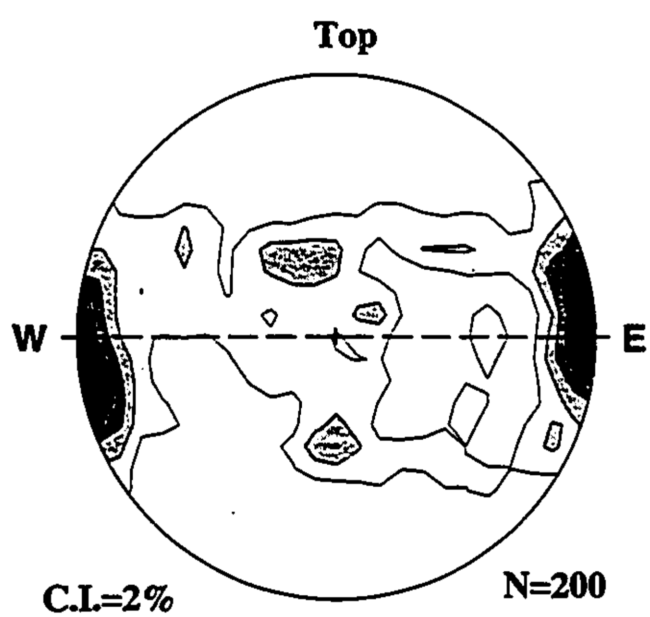

Fig. 3.4. Contoured lower hemisphere equal-area projection of quartz *c*-axis fabric within an orthogneissic sample of Lac Opasatica gneiss. The horizontal dashed line represents the foliation plane, and the mineral elongation lineation is oriented east-west.

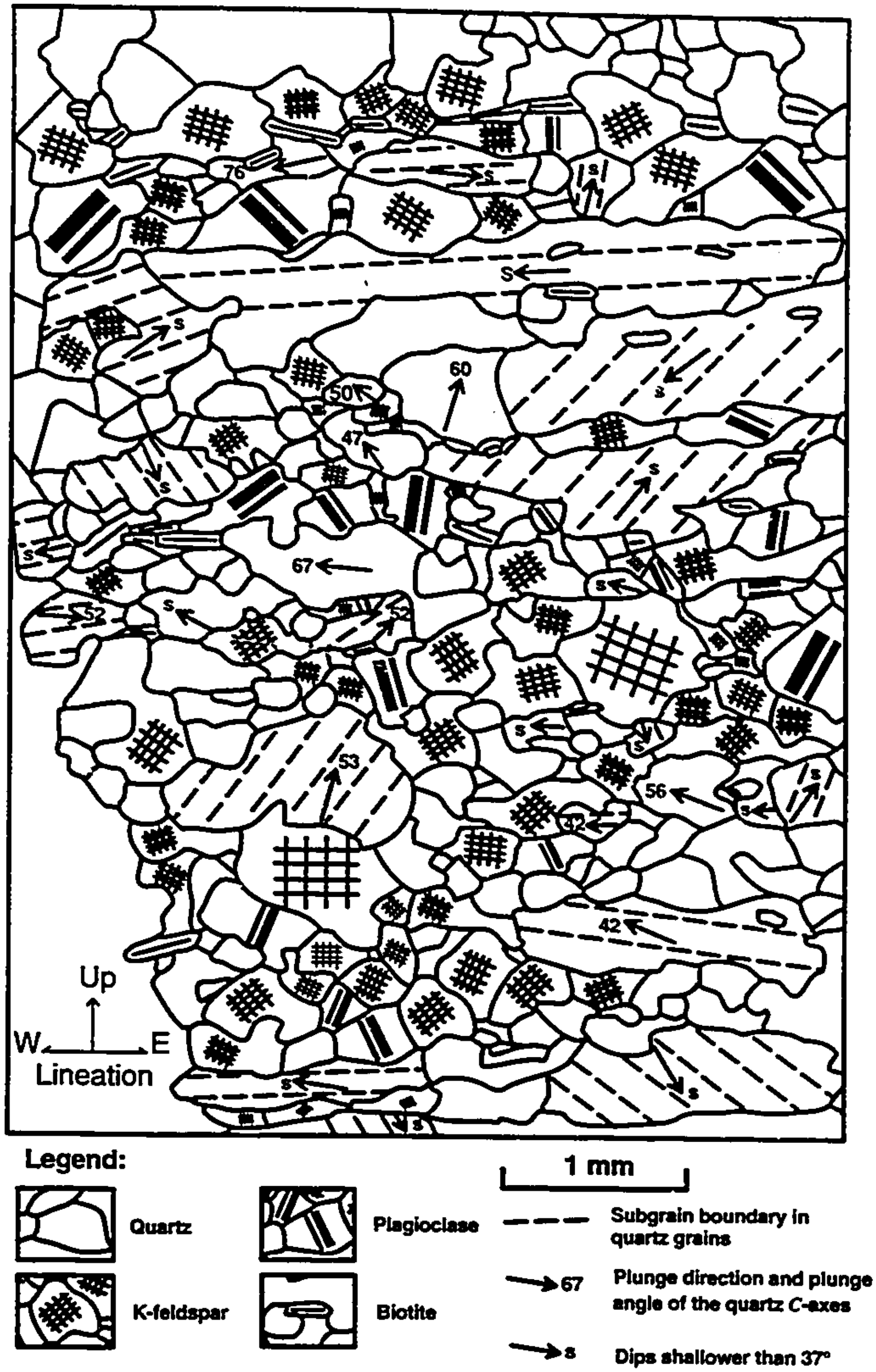

Fig. 3.5. Microfabric map of part of a thin section from the Lac Opasatica gneiss. Note the relationship between the subgrain boundaries and orientation of the quartz *c*-axes.

3.3. D_1 structures

D_1 structures have been largely overprinted during the subsequent D_2 event. Many structures considered by previous workers as D_1 structures, when studied in detail, appear to be D_2 structures that have totally or partially overprinted the D_1 structures. Evidence of D_1 structures is preserved essentially as relics of the S_1 foliation within the microlithons of the S_2 differentiated crenulation, in strain shadows around porphyroblasts, or as inclusion trails within porphyroblasts. Penetrative foliations, that are evident everywhere in the metasedimentary rocks of the Pontiac Group, when studied under the microscope, are revealed as small-scale differentiated crenulation foliations, with S_1 preserved as folded trails of biotite crystal flakes, or straight inclusion trails within the staurolite porphyroblasts, and crenulated inclusion trails within the kyanite porphyroblasts (Fig. 3.6). In thin-sections, general orientation of crenulated S_1 within S_2 foliation accords with orientation of S_1 preserved within the staurolite porphyroblasts. Since staurolites in all samples include only straight inclusion trails related to undeformed S_1 foliation, they are considered to be syn-D_1 porphyroblasts. Study of inclusion trails in the staurolite porphyroblasts indicates that they follow a preferred orientation usually at a high-angle to the S_2 foliation (Fig. 3.7). As is discussed in the next section, when the effects of later deformational events are removed, the S_1 foliation is generally steeper than the S_2 foliation. This indicates that D_1 was associated with development of a steep foliation probably during thickening of the crust prior to the D_2 event. On the basis of an axial planar relationship with the S_1 foliation, some rootless folds, preserved here and there, are interpreted as refolded, originally upright F_1 folds.

Because of the pervasive overprinting of D_1 structures by D_2, reconstruction of the D_1 finite strain pattern is difficult. Orientation of the L_2^1 intersection lineation shows a rather scattered pattern within the study area, which is an effect of later deformational events superposed on D_1 and D_2 structures (Fig. 3.8). However, accepting the tectonic model of present study (Chapter 6), east-trending structures are most probable for the D_1 event. Moreover, some east-trending inclined to recumbent folds of D_2 event appear to be (upright) F_1

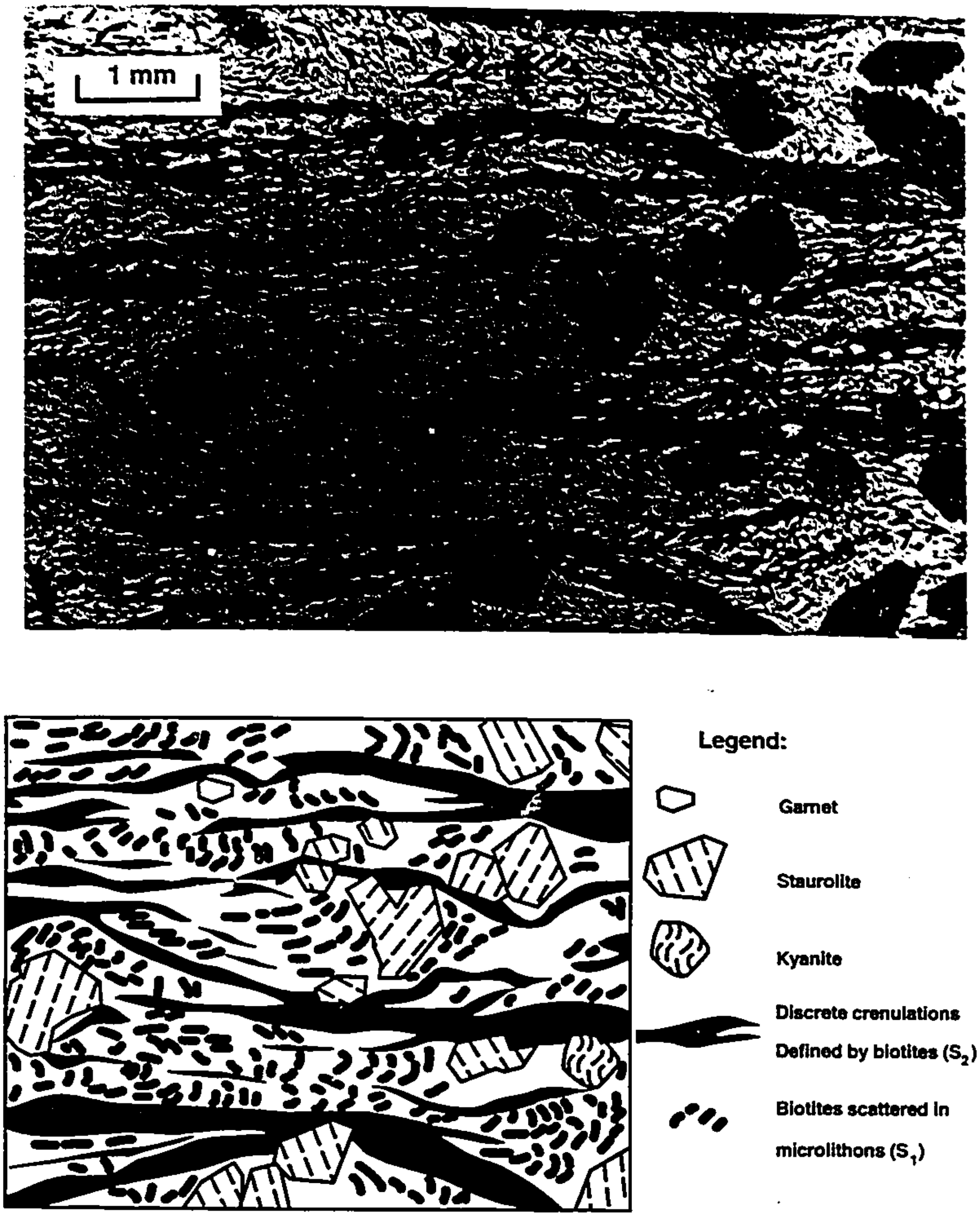

Fig. 3.6. Photomicrograph and sketch showing relationship between S_1 and S_2 foliations. Note preservation of S_1 within microlithons of S_2. Also note difference between straight inclusion trails within the staurolite porphyroblasts and crenulated inclusion trails within the kyanite porphyroblasts.

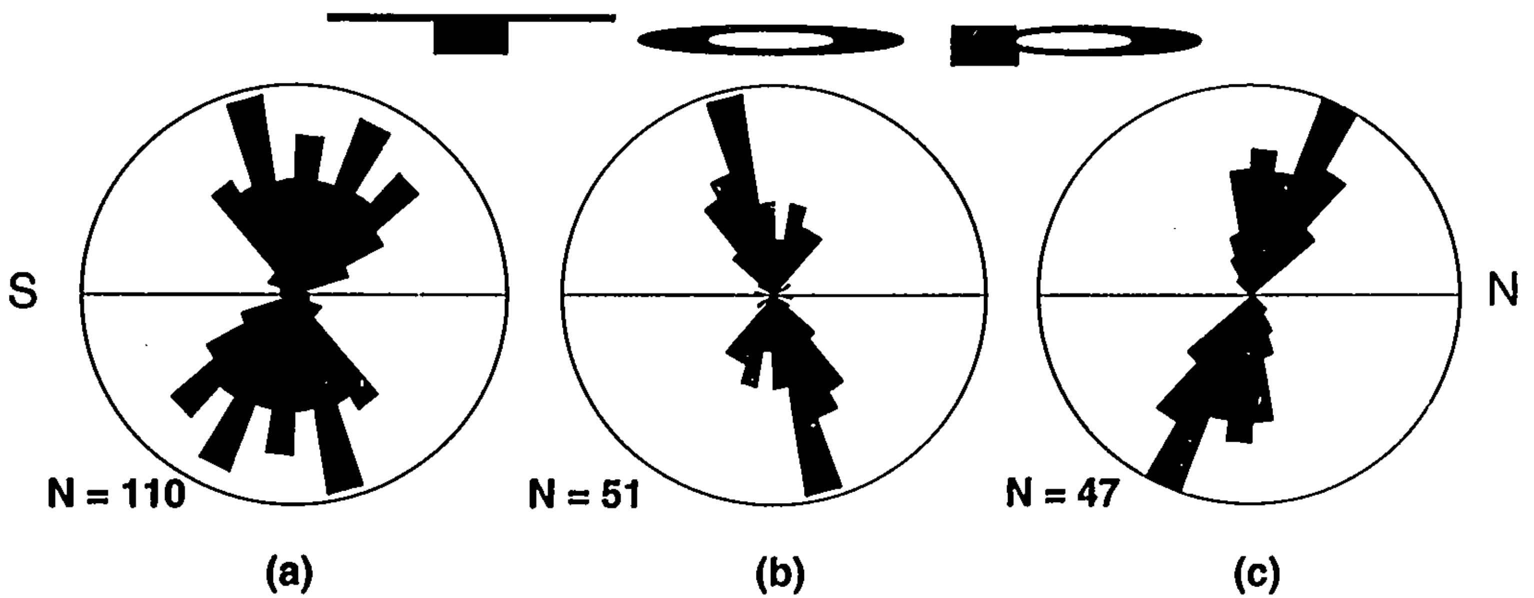

Fig. 3.7. Rose diagrams showing preferred orientation of S_1 inclusion trails within staurolite porphyroblasts of three metasedimentary rock samples. The straight horizontal lines represent the orientation of the S_2 foliation.

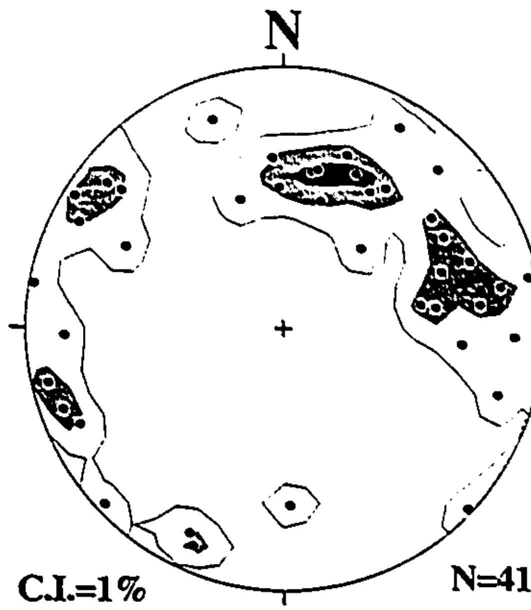

Fig. 3.8. Contoured lower hemisphere equal-area projection of L^1_2 intersection lineation.

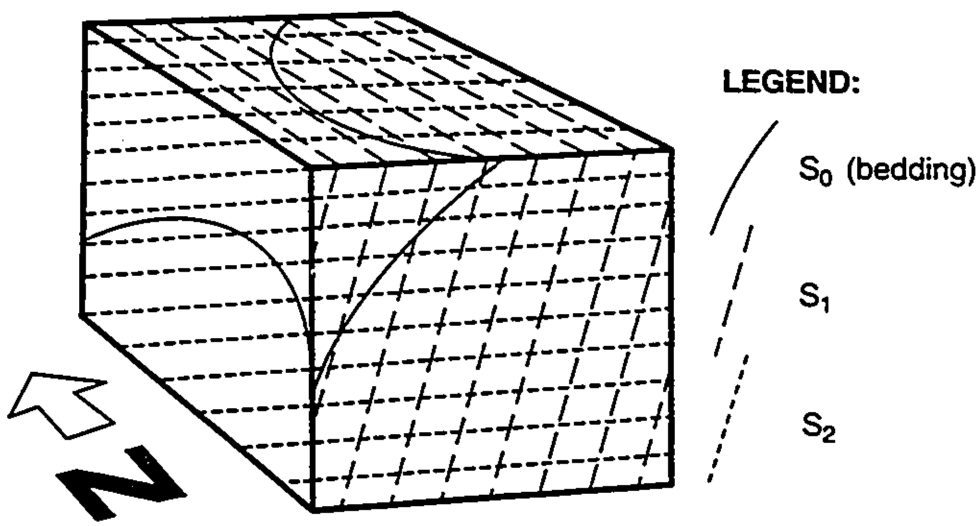

Fig. 3.9. Block diagram illustrating relationships between S_0, S_1 and S_2 foliations in an outcrop 5 km south of the Bellecombe village.

folds that have been further modified into F_2 folds. Figure 3.9 illustrates the geometric relationships between S_0, and the S_1 and S_2 foliations in the Pontiac Group metasedimentary rocks south of Bellecombe village (Fig. 3.1).

Sequential crystallization of biotite, garnet and staurolite during the D_1 event, and crystallization of kyanite and sillimanite during the D_2 event, indicates that both temperature and pressure were rising during the D_1 event (see related discussions in Chapter 4, and in section 3.4 of the present chapter). Metamorphic grade of the Pontiac metasedimentary rocks increases from biotite grade into sillimanite grade with increasing distance to the south of the Cadillac-Larder Lake fault zone. Maximum pressure estimations for the Pontiac metasedimentary rocks is as high as 7.2 kbar (see Chapter 4), while pressure estimation from metavolcanic rocks close to the Cadillac-Larder Lake fault zone shows pressures of about 5 kbar (Morin *et al.* 1993). Metamorphic pressure and temperature of the Abitibi volcanic rocks north of the Cadillac-Larder Lake fault zone are lower than metamorphic grade of Timiskaming and Pontiac Groups south of the fault zone (Powell *et al.* 1993). This information suggests that, when pressure and temperature of these rocks were close to peak metamorphic conditions, a considerable thickness of Abitibi rocks was over the rocks in the Pontiac Subprovince. Since stratigraphic relationships imply that Abitibi rocks are older than Pontiac rocks (see section 2.1), and are resting with a north-dipping tectonic contact over these metasedimentary rocks, the present reverse sequence must have been developed during a large scale thrusting event before peak metamorphic conditions, along the Cadillac-Larder Lake fault zone. Because D_2 is a syn-peak metamorphism event, the major thrusting is inferred to have occurred during D_1.

D_1 is also considered to have been responsible for folding and emergence out of water of the Pontiac Group rocks and the start of Timiskaming Group deposition. Presence of the Timiskaming Group in the footwall of the Cadillac-Larder Lake fault zone, and predominance of volcanic and igneous clasts derived from the Abitibi greenstone belt within this detrital sedimentary succession are compatible with deposition of the Timiskaming Group in a foreland basin during the south-vergent thrusting of the Abitibi over the Pontiac Subprovince.

3.3.1. Plutonism during D_1

Temporal relationships between sedimentation in the Pontiac basin, intrusion of I-type granitoids, and peak metamorphic conditions, established through geochronologic data (see Chapter 5), indicate that emplacement of I-type granitoid rocks including the Lac Frechette complex was ongoing during D_1. The Lac Frechette complex and other igneous rocks with similar composition, that are scattered throughout the study area, are not observed anywhere to cut across D_2 structures. As will be discussed in the next section, the eastern margin of the Lac Frechette complex, and small intermediate intrusions within the Bellecombe shear zone comparable with the Lac Frechette complex, show a foliation that is concordant and very similar to S_2 foliation in the Pontiac metasedimentary rocks.

South of Cloutier village (Fig. 3.1), small mafic to intermediate intrusions of the Lac Frechette complex show strong deformation in accordance with D_2 deformation within the host Pontiac metasedimentary rocks (Fig. 3.10). Syn-D_2 S-type pegmatites in this area cross-cut the I-type intrusions. The aforementioned observations indicate that I-type granites were emplaced before the D_2 deformational event.

3.4. D_2 structures

D_2 structures resulted from development of SSE-oriented nappes after crustal thickening produced by the D_1 event. The study area is speculated to include a nappe structure that was transported south-southeastward along the Montbeillard and possibly Saint Roch shear zones (Fig. 3.1, 3.2). These two shear zones, therefore may be considered as thrust faults that existed at the base of the nappe. Metavolcanic layers within the Pontiac metasedimentary rocks provide a good marker that delineates the nappe structures. One metavolcanic unit present in the eastern half of the study area, extends from Lac Bellecombe to the Lac Kinojevis and Lac Bruère areas; another metavolcanic unitoutcrops in the west, along the shores of Lac Opasatica . In Fig. 3.11, two cross-sections illustrate the nappe structures in

Fig. 3.10. Marginal zone of I-type Lac Frechette complex, south side of Cloutier village (Fig. 3.1). Note accordance of deformation and boudinage of the dark intrusive rocks with F_2 folds within the host Pontiac Group rocks. Also note intrusion of (light) syn-D_2 S-type granite into gashes in the I-type intrusions, developed during D_2 event. Horizontal surface; north toward the right side of page.

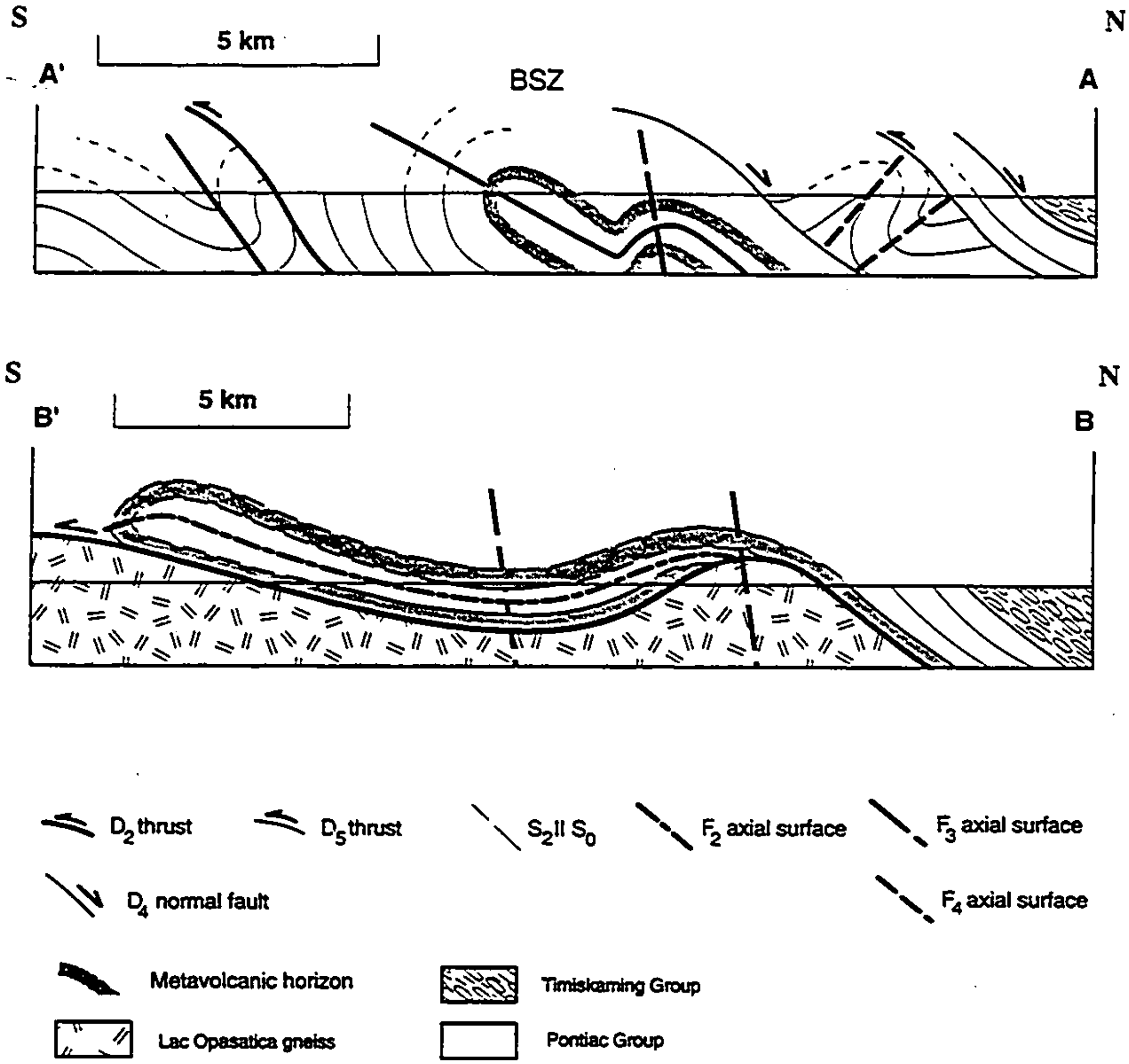

Fig. 3.11. Structural cross-sections of eastern (top) and western (bottom) parts of the study area. For location of the cross-sections see Fig. 3.1.

these areas. The eastern nappe is either terminated laterally (as is speculated within the block diagram of Fig. 3.2) or it is a continuation of the western nappe, partially buried at greater depths in the middle part of the study area.

S_2 foliation is the predominant, regionally penetrative foliation in the study area, generally parallel to bedding plane within sedimentary rocks of the Pontiac Group. It is a differentiated crenulation foliation defined by cleavage bands containing strongly oriented biotite and muscovite crystals, and microlithons on the order of 1-3 mm thick, within which S_1 is preserved as folded trails of biotite crystals, and straight or crenulated inclusion trails within staurolite and kyanite porphyroblasts (Fig. 3.6). F_2 folds are isoclinal overturned and recumbent folds, axial surfaces of which usually dip at a small angle to north-northwest (Fig. 3.12). Mesoscale F_2 folds are usually associated with axial-planar S_2 foliation; however, large-scale asymmetric F_2 folds were observed within the shear zones (see section 3.4.1), and they often fold S_2 foliation.

S_2 generally dips at a small angle to the north-northwest, and the dip angle of S_2 is generally shallower than that of the S_1 foliation. This observation may be explained through a model in which upright structures associated with D_1 preserved their steep orientations both in normal and overturned limbs of the D_2 nappes. Thus the hinge areas of the D_2 nappes are the only places where above-mentioned relationship between S_1 and S_2 is not found. The crenulated S_1 within microlithons of the regionally pervasive S_2 foliation is overgrown by kyanite crystals (Fig. 3.13). Using this fact, and the observation that staurolite is the last prograde metamorphic mineral that records the D_1 event through its crystallization, it may be concluded that D_2 was an event that started early during peak-metamorphic conditions.

A strongly developed, generally north-northwest-plunging L_2 elongation lineation is another important structural feature of the D_2 event (Fig. 3.14). This lineation is best visible within elongated pebbles of conglomerates of the Timiskaming Group, and within pillow structures of the volcanic unit within the Bellecombe shear zone (Fig. 3.15). It is also visible within the quartz veins that cross-cut the Pontiac and Timiskaming Group rocks, where it is

Fig. 3.12. North-dipping recumbent second-order folds in the overturned limb of a south-southeast-vergent first order F_2 fold affecting Pontiac Group metasedimentary strata along the eastern shores of Lac Opasatica. The outcrop is few tens of metres above the Montbeillard shear zone. View looking east.

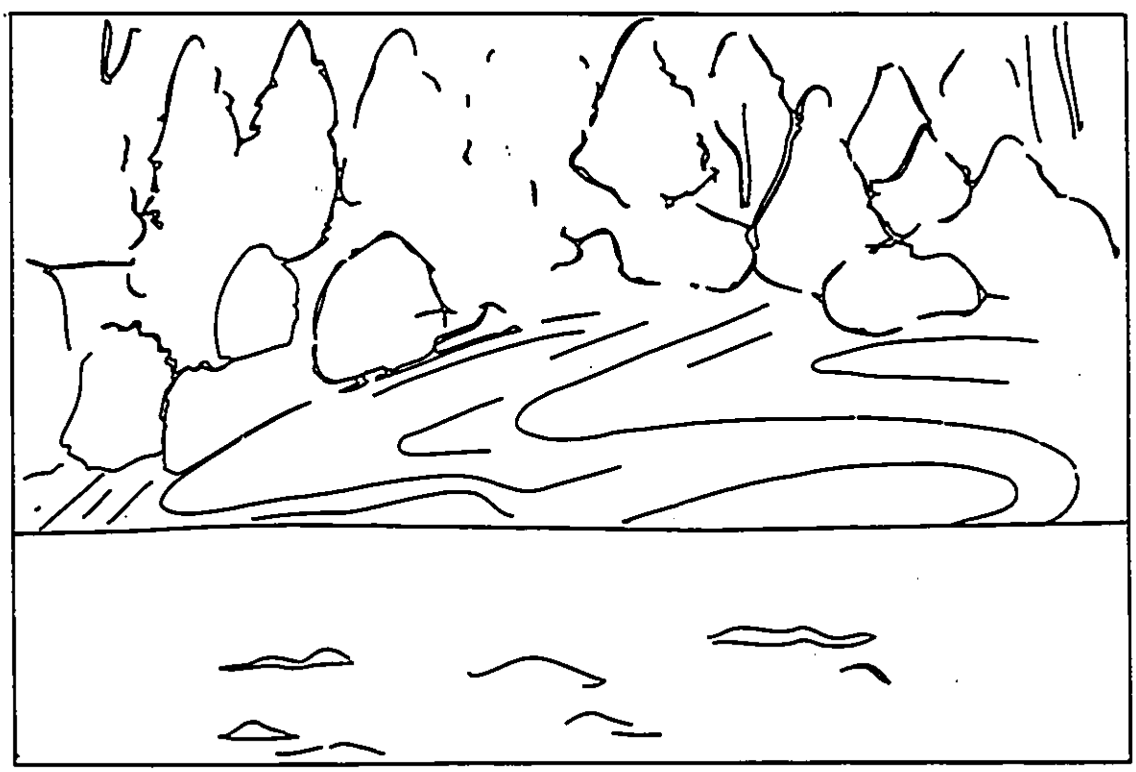

Fig. 3.13. Photomicrograph showing crenulated inclusion trails (folded S_1) within a kyanite (Ky) porphyroblast. Staurolite (St) porphyroblasts are also present in the thin-section.

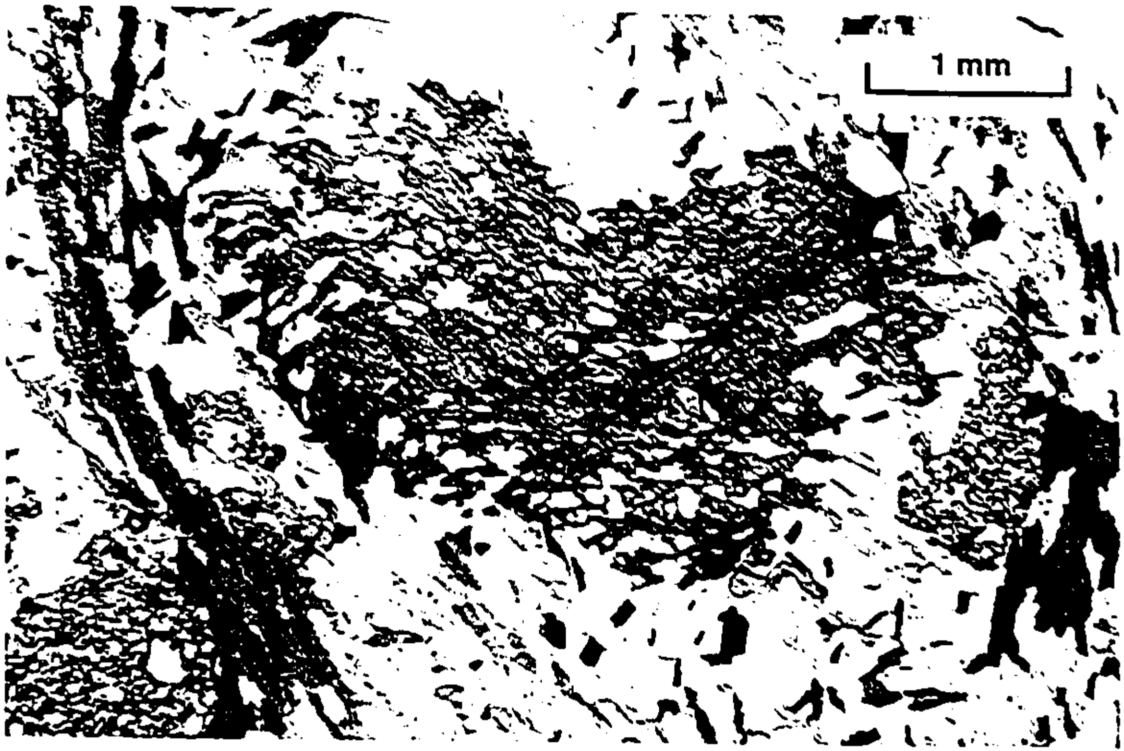
1 mm

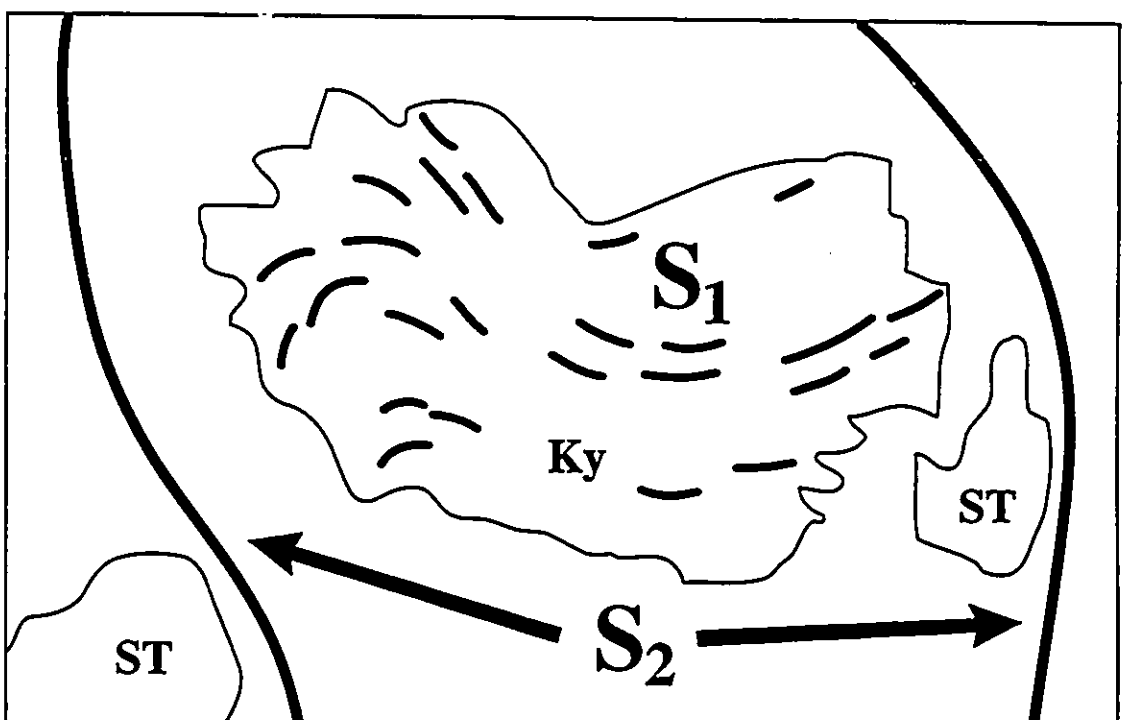
S1
Ky
ST
ST
S2

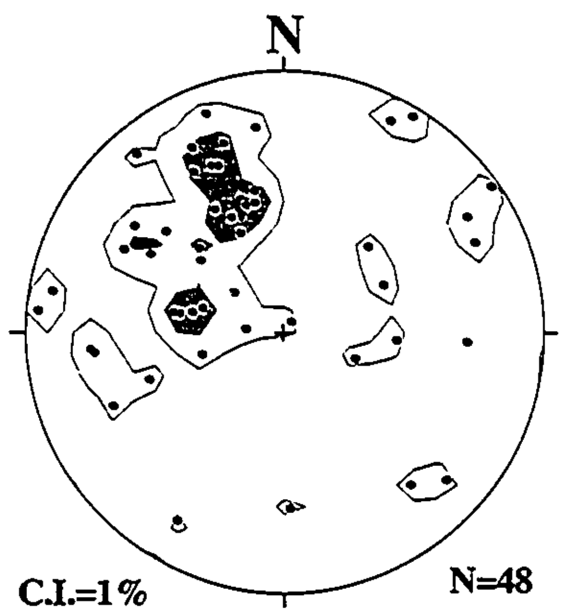

Fig. 3.14. Contoured lower hemisphere equal-area projection of L_2 elongation lineation.

Fig. 3.15b. Elongated pillow structures within the metavolcanic rocks of the Pontiac Group in Bellecombe shear zone, near Lac Bellecombe. Elongation of the pillows are parallel to a mineral elongation lineation of amphiboles within these rocks. Also visible in this photograph are extension fractures that are transverse to the elongation lineation. Vertical face. View looking southeast.

Fig. 3.15a. Highly elongated pebbles within the Timiskaming Group, close to the Cadillac-Larder Lake fault zone. Vertical face. View looking south.

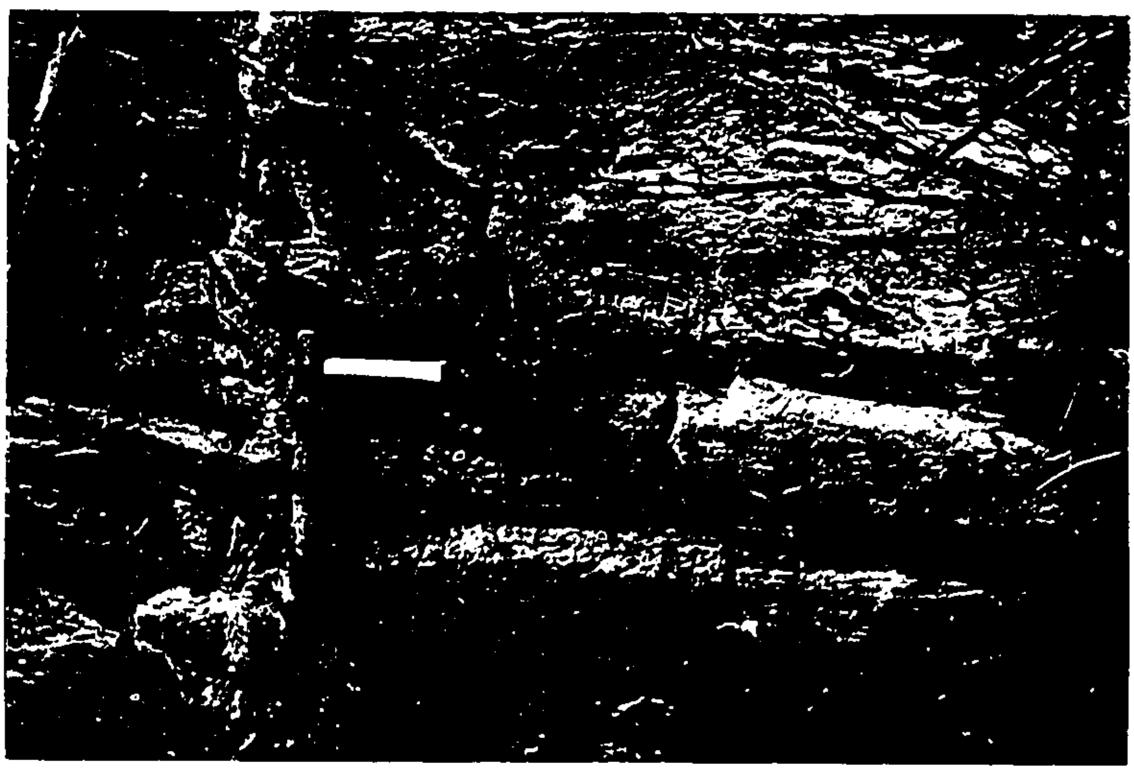

expressed as parallel rods of quartz aggregates. Within the Pontiac metasedimentary rocks, mineral lineation parallel to elongation lineation is defined by alignment of quartz, feldspar and biotite crystals aggregates, whereas in the metavolcanic rocks of the Pontiac Group it is represented by a preferred orientation of amphibole crystals.

Asymmetrical shear-sense indicators associated with the regionally penetrative S_2 foliation are rare; moreover, preferred orientation of the straight inclusion trails within the staurolite porphyroblasts (see Fig. 3.7) indicates that no rigid body rotation of the porphyroblasts has occurred after their crystallization (and during D_2). This evidence suggests that the fabric records a predominantly coaxial deformation. D_2 deformation has, however, been locally partitioned into apparently very high-strain shear zones (see section 3.4.1), within which evidence of a highly non-coaxial strain history is preserved. Lack of evidence for simple shear parallel to the foliation plane, together with a considerable amount of shortening normal to the foliation, suggest that both foliation and lineation have developed as a result of predominantly coaxial shear strain during the D_2 event.

Macroscopic and microscopic evidence reveals a great amount of shortening perpendicular to the S_2 foliation. Pre-D_2 quartz veins oblique to S_2 foliation show a considerable amount of shortening through folding perpendicular to the foliation planes. Measuring folded length of one of these quartz veins indicates a shortening of about fifty percent (Fig. 3.16), as is the case for S-type granitic dykes that are highly oblique to the S_2 foliation (Fig. 3.17). Granitic dykes and other relatively rigid bodies (e.g. quartz veins and lamprophyric dykes) parallel to the foliation are usually boudinaged.

3.4.1. Shear zones

Three shear zones have been identified in the study area (Fig. 3.1). Intrusion and deformation of syn-peak metamorphic S-type granitic sills and dykes within two of these shear zones (Montbeillard and Saint Roch shear zones), along with microstructural evidence (see section 3.4), establish that they were active during D_2. Parallelism of these shear zones with

Fig. 3.16. Photograph of a folded quartz vein cutting across S_2 foliation and deformed during D_2 event. Measurement of length of the vein indicates about 50 percent shortening parallel to the length of the vein.

Fig. 3.17. Folding of an S-type granitic dyke perpendicular to S_2 foliation.

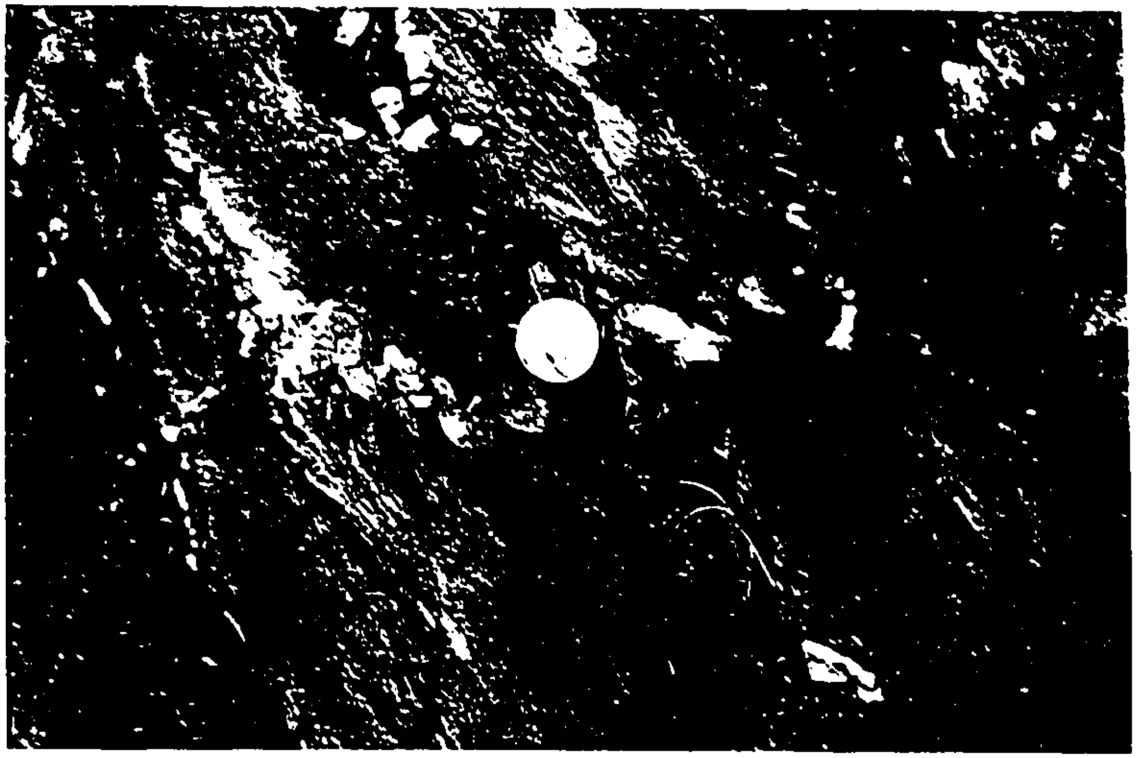

generally recumbent F_2 folds suggests that they were shallow-dipping zones of deformation, that were later folded along with F_2 folds. The shear sense indicators along these shear zones, after correction for later folding events, point to a generally top-to-the-south-southeast transport direction. Later during the D_3 event the Saint Roch shear zone was folded and tilted into its present steep orientation (Fig. 3.2), so that it has been misinterpreted as a transpressive sinistral shear zone (Benn *et al.* 1994).

Montbeillard shear zone

The Montbeillard shear zone (see Fig. 3.1) is a shallow-dipping shear zone that separates the metasedimentary and metavolcanic rocks of the Pontiac Group from the underlying Lac Opasatica gneisses. The shear zone is considered to be the sole thrust fault of the western nappe. Above this shear zone, which is best observed along the shores of Lac Opasatica, the metasedimentary and metavolcanic rocks of the Pontiac Group are deformed into south-southeast-vergent asymmetric and overturned folds (see Fig. 3.12, also see Fig. 5 in Appendix D). Figure 3.18 illustrates two asymmetric boudins within the Montbeillard shear zone, that have undergone antithetic rotation during a top-to-the-south-southeast movement. The shear direction, measured perpendicular to the long axes of the boudins, is 140°. S-type garnet-bearing granitic sills and dykes are intruded and deformed along this ductile shear zone. Presence of granitic leucosomes at the tips of the boudins (Fig. 3.18) suggest that shearing has occurred during the peak metamorphic conditions.

South of Lac Evain, close to Montbeillard shear zone, a crenulation, which is axial planar to recumbent F_2 folds, is superimposed on S_2 foliation (Fig. 3.19). Both crenulations in this area are north-dipping; however, the S_2 foliation is steeper than the later larger-scale crenulation. This superposition relationship is interpreted as a result of non-coaxial deformation within the shear zones. In the shear zones deformation of the rocks has caused asymmetric folding, and rotation of the S_2 foliation. Rotation of S_2 along with the limb of an asymmetric F_2 fold, may have changed position of the foliation plane with respect to the coaxial strain

Fig. 3.18. Asymmetric boudins within the Montbeillard shear zone. Antithetic rotation of the boudins indicate a top-to-southeast (to right in photograph) movement along the shear zone.

Fig. 3.19. Photomicrograph and sketch of S_2 foliation (solid lines) with superimposed shallow-dipping crenulation foliation (dashed lines). Dashed lines are drawn along areas where S_2 foliations are more closely spaced; these lines coincide with the macroscopic foliation of the rock in field. Folded trails of biotites within S_2 microlithons (in photomicrograph) represent S_1 foliation.

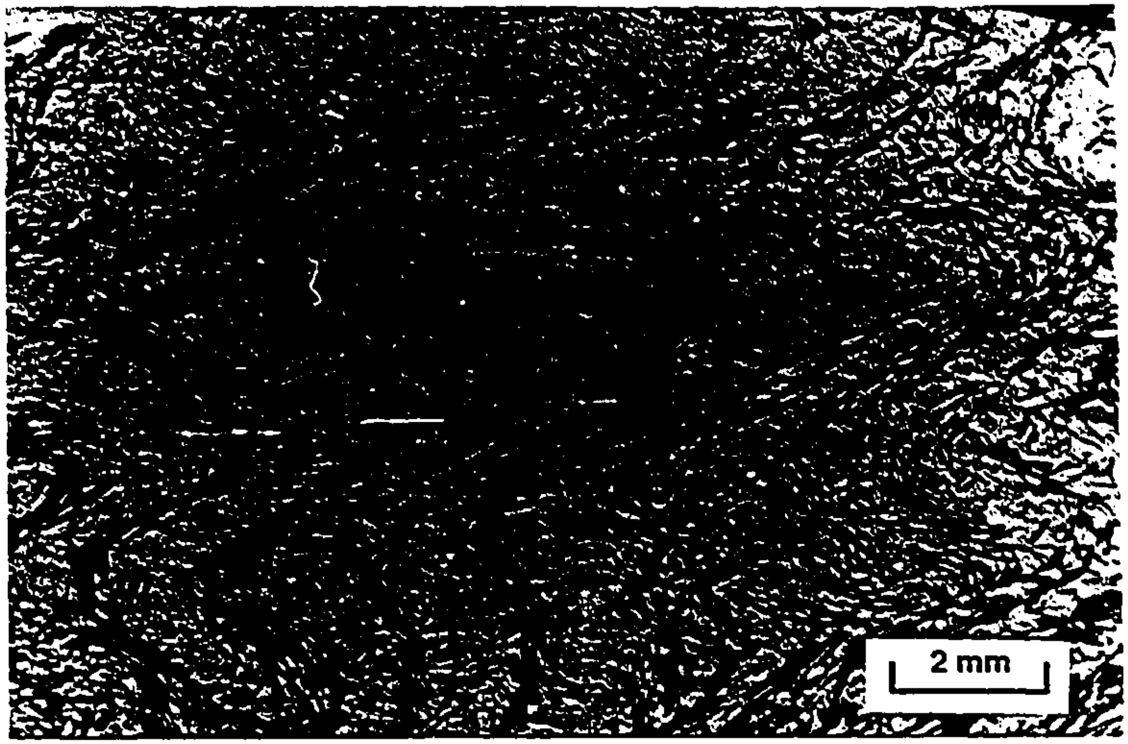
2 mm

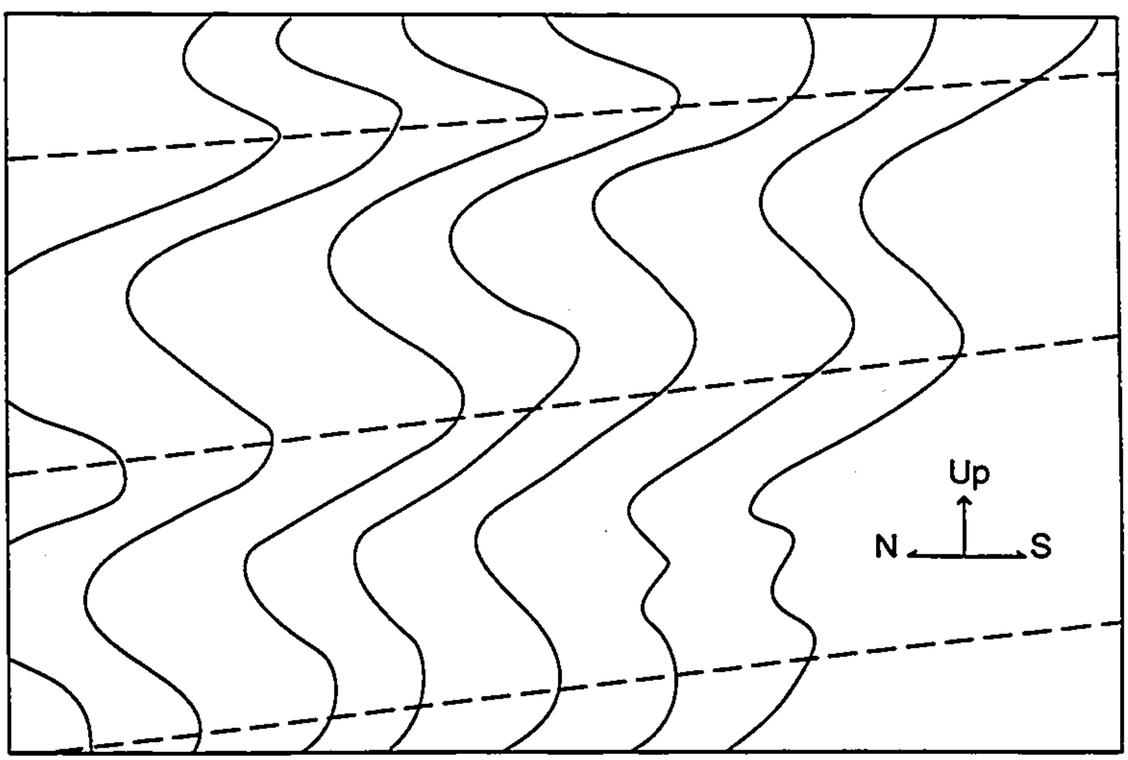
Up
N
S

field. Further deformation of the rock through coaxial shear has probably caused superposition of a shallow-dipping crenulation on S_2, parallel to axial planes of F_2 folds. The second crenulation is therefore considered to be a D_2 microstructure.

Saint Roch shear zone

The Saint Roch shear zone is another shear zone along which extensive syn-tectonic intrusion of the S-type pegmatites and granites has taken place. It outcrops extensively in the southeastern part of the map area, between the Decelles granites and the Lac Frechette complex, where it has been folded into a steep orientation (032°/65°NW) by the subsequent D_3 event. The S-type granites and related pegmatites were emplaced within the shear zone as dykes and sills (Fig. 3.20). Dykes that cross-cut S_0 surfaces, and S_2 foliations at high angle when emplaced, were later rotated into orientations close to the foliation within the shear zone. The rotation is more evident where S_2 foliation close to these dykes are deflected because of the dyke rotation. When reconstructed into their pre-deformation state, the dykes appear to have been emplaced in a tension gash array consistent with apparent sinistral movement along the shear zone. Apparent sinistral strike-slip kinematics have otherwise been established using small-scale sinistral tension gashes, sinistral drag folds, and antithetic rotation of quartz and granitic veins within the shear zone. Because of being at a low angle to the shear zone boundaries, the sills on the contrary, show no evidence of synthetic rotation. Instead the shear zone-related deformation of these intrusive bodies has occurred instead as asymmetric boudinage, with boudins showing antithetic rotation in many places (Fig. 3.21). Small granitic dykes, in which folding related to the D_2 event may be documented are very few; however, even where they plot in the shortening quadrant of the strain field, no major folding was observed.

The granodioritic Lac Frechette pluton shows a strong foliation at its eastern margin, within the Saint Roch shear zone (Fig. 3.22). Strong alignment of biotite crystal flakes, and flattened felsic minerals along the foliation, indicate ductile deformation of the rock presumably

Fig. 3.20. S-type granitic dykes and sills within the Saint Roch shear zone. Note rotation of dykes with respect to sills and foliation within the Pontiac metasedimentary rocks.

Fig. 3.21. Antithetic rotation of boudins of pegmatitic sills within the Saint Roch shear zone. The antithetic rotation suggests sinistral shear, in accordance with other kinematic indicators such as asymmetrically folded quartz veins (also visible in this photograph, near the pen.

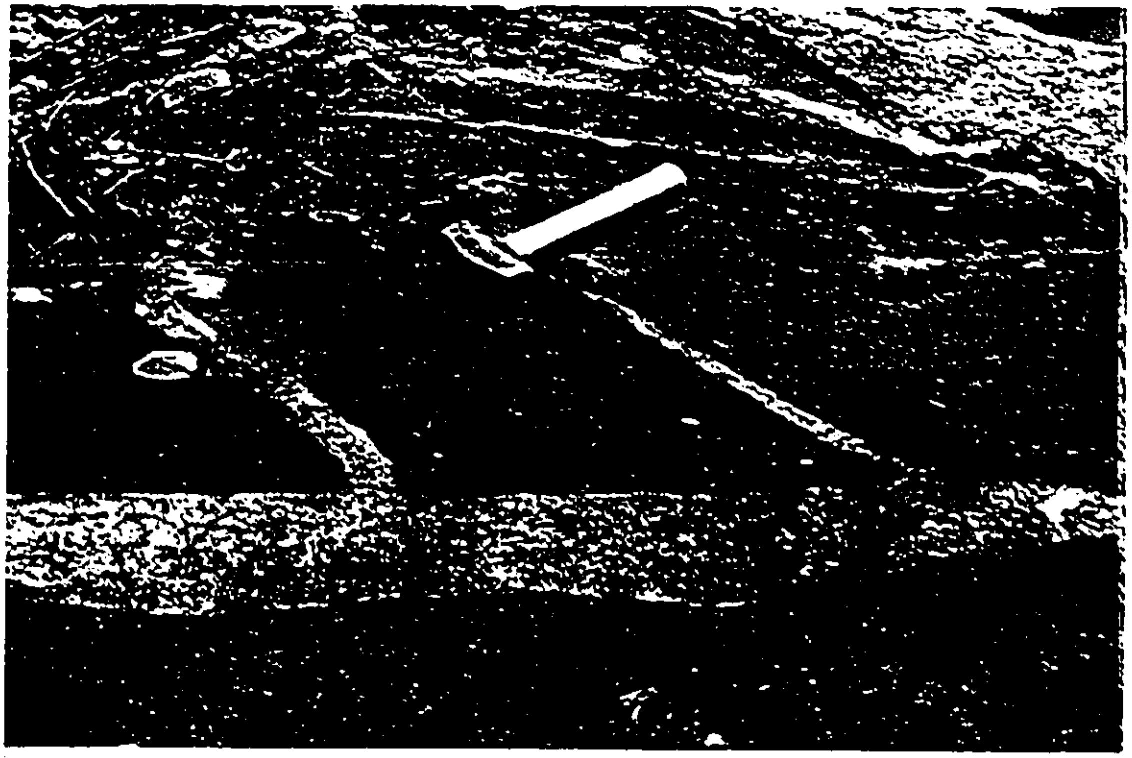

under high temperatures. This presumption along with concordance in texture and orientation with S_2 foliation in the Pontiac metasedimentary rocks near the contact with the plutonic body, suggest that the foliation developed during the D_2 deformational event.

Presence of the shear zone in the footwall of the eastern nappe suggests that it might have been the sole thrust for this nappe, and if both nappes of the study area are in fact extensions of an individual nappe structure, the Saint Roch shear zone may be considered as a continuation of the Montbeillard shear zone.

Bellecombe shear zone

The Bellecombe shear zone is a steep northeast-trending, steeply northwest-dipping zone of intense folding and faulting (see Fig. 3.1 for the location). Because of later superposed deformational events, F_2 folds in this shear zone have variable plunges; however their axial planes are dominantly parallel to the shear zone. L_2 elongation lineation is very well developed within the shear zone, and is usually very steep. Another generation of folds (present within the shear zone) are smaller in scale compared to F_2 folds, and are usually associated with an axial planar crenulation foliation. They are best developed within short limbs of the asymmetric folds. Lineations related to these crenulations in some places make a 90° angle with crenulation

lineations of S_2 foliation (Fig. 3.23). Axial planar orientation of the asymmetric folds with respect to the orientation of the shear zone implies a sinistral sense of shear for the Bellecombe shear zone. These are late structures that may be related to the D_3 event. However, dominance of D_2-related ductile structures (folds and elongation lineation) indicates that this shear zone, like the other two shear zones within the study area, had a major period of activity during the D_2 event.

Intermediate intrusions, comparable in composition with Lac Frechette complex, and lamprophyric dykes are extensively intruded within this shear zone. Some small dykes of these rocks are intruded along surfaces parallel to bedding, and interconnected along features that

Fig. 3.22. Photomicrograph of S_2 foliation developed at the margin of the Lac Frechette granitoid complex in Saint Roch shear zone. Large crystal in the centre of the photomicrograph is hornblende: minerals within the background are K-feldspar, quartz, biotite and amphibole.

Fig. 3.23. Superimposed microfolding on a quartz vein parallel to S_0. Microfolds with horizontal and vertical axes are related to S_2 and S_3 crenulations respectively. Diameter of coin is 26 mm.

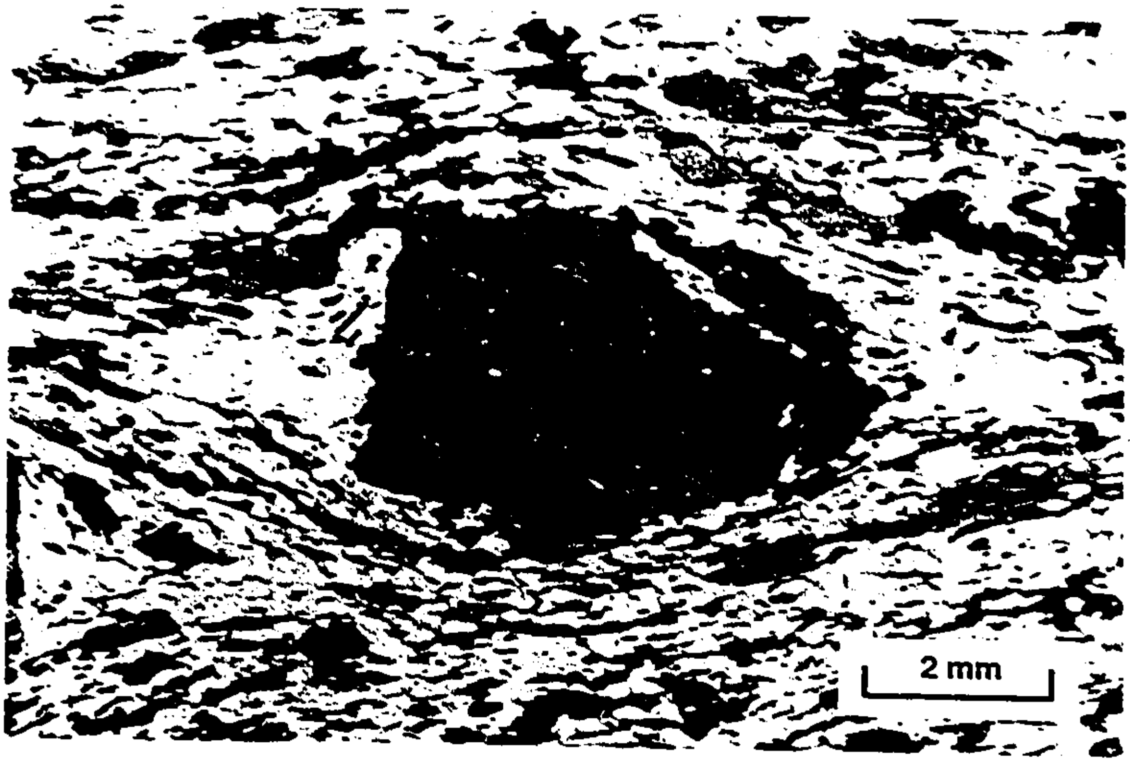
2 mm

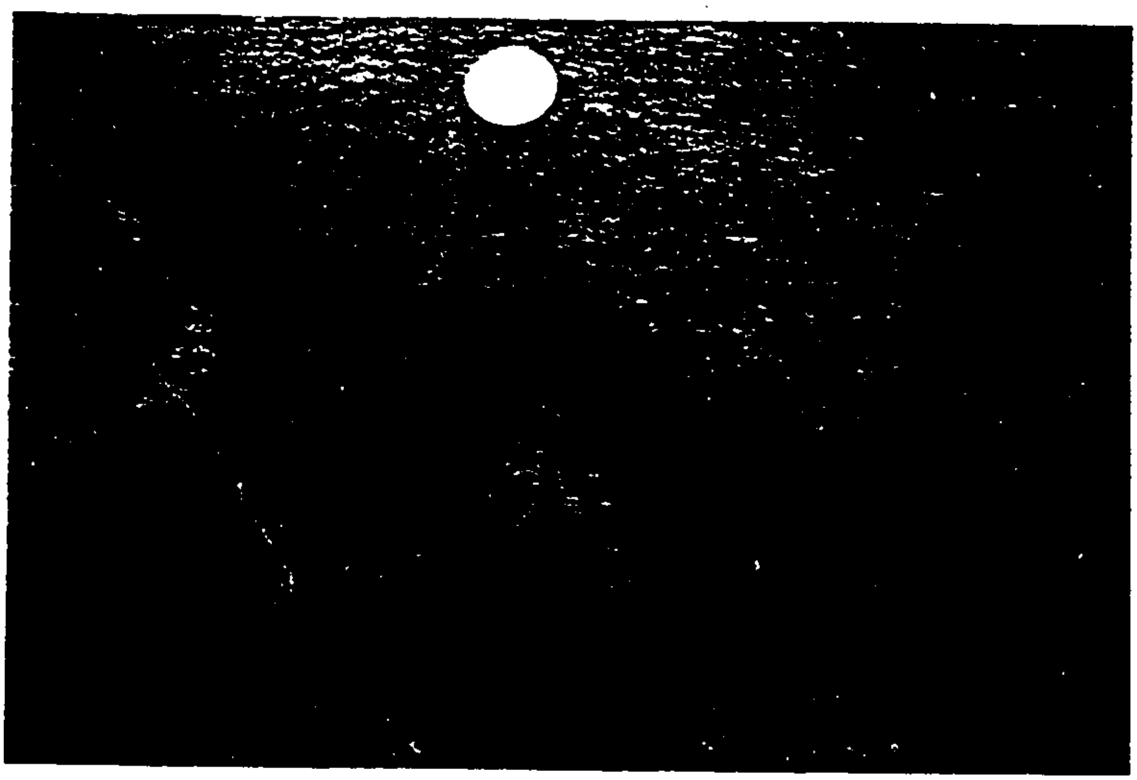

resemble tension gashes. Unlike other D_2 shear zones, no S-type intrusion was observed within the Bellecombe shear zone. This may be because of the occurrence of the shear zone higher in the crust, with respect to the other two shear zones.

Another characteristic of the Bellecombe shear zone is its coincidence with a relatively continuous unit of metavolcanic rocks within the Pontiac Group (see map in Fig. 3.1). This unit, which is composed of metamorphosed komatiitic and basaltic rocks, may have acted as a décollement surface along which the hanging wall block was transported. Part of this unit is now folded into a steep northeast trending belt of sheared rocks extending from the Lac Bellecombe area into the Lac Caron and Lac Bruère areas, where it is folded around axial surfaces of F_3 folds. Another rather dissected volcanic unit runs parallel to the Bellecombe shear zone (Fig. 3.1). This unit may be traced intermittently to the northeastern part of the study area, and is a continuation of the same volcanic unit in the Bellecombe shear zone that was folded during the D_2 and D_3 events.

3.4.2. Plutonism during D_2

A large volume of S-type granites, that are interpreted as the product of melting of the metasedimentary rocks of the Pontiac Group, occur within the southern part of the study area. S-type granites are usually observed to cross-cut S_2 foliation or intrude along axial planes of F_2 folds (Fig. 3.24). Late stages of these granites appear to be folded by F_2 folds (see Fig. 3.17). Shortening and folding of steep granitic dykes perpendicular to the S_2 foliation indicate that a considerable amount of D_2 strain occurred even after intrusion of these dykes.

As was earlier concluded in this section, relationships between the metamorphic growth of porphyroblasts and microstructures indicate that the D_2 event started early, during peak metamorphic conditions. On the other hand, S-type granites have been produced through melting of metasedimentary rocks of the Pontiac Group during peak metamorphic conditions (see section 4.2). Related intrusive rocks must therefore have been emplaced sometime after beginning of the D_2 event (in other words S-type granites are considered as syn-D_2 intrusions).

Fig. 3.24. Photograph showing intrusion of the S-type granites along the axial surface of F_2 folds within Pontiac metasedimentary rocks. Looking east.

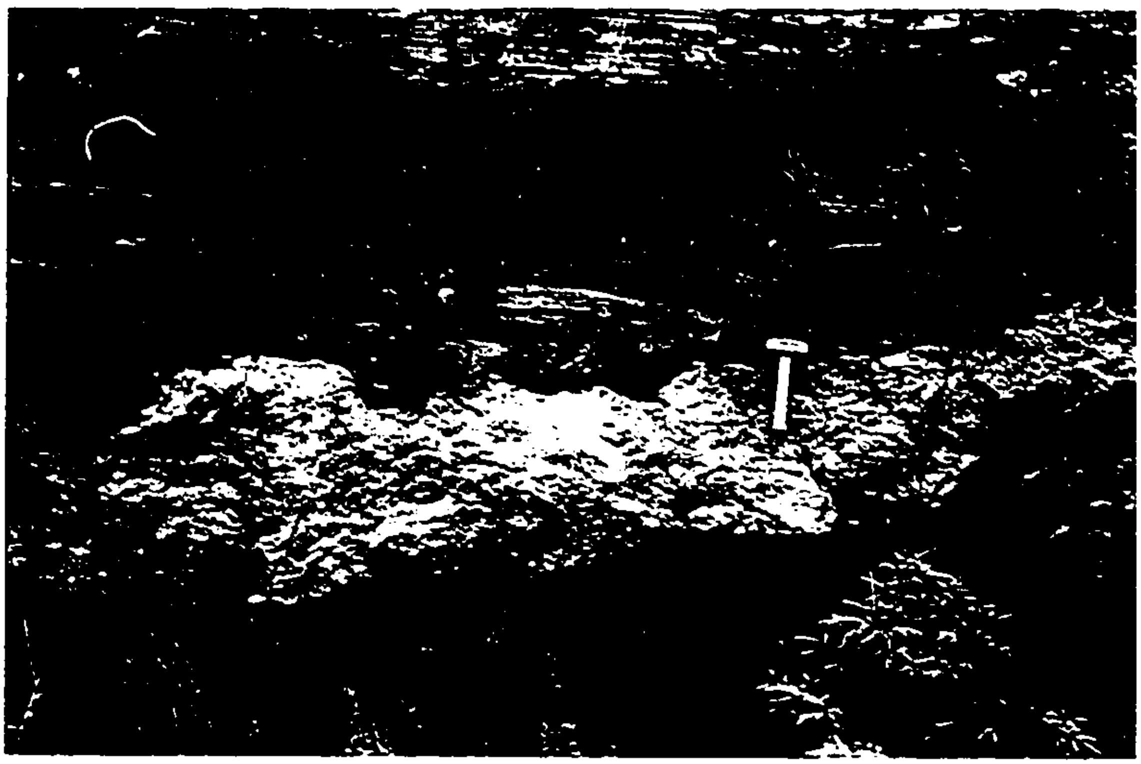

Unlike the S-type granites, small intrusions of I-type granites were generally emplaced as sills along the bedding. The orientations of D_2 structures within xenoliths of the Pontiac metasedimentary rocks in the S-type granites are traceable and concordant at the map scale.

3.5. D_3 structures

North-south bulk regional shortening produced east trending folds related to the D_3 event. Upright to slightly northerly dipping F_4 folds have affected all of the older structures. D_3 folding of Lac Opasatica gneisses, and the Bellecombe, Montbeillard and Saint Roch shear zones is evident both in map (Fig. 3.1) and outcrop scale.

Because of the occurrence of the D_3 after consolidation of the Decelles batholith, it acted as a relatively rigid body that impinged and deflected the F_3 fold axes, such that F_3 axial-surface-traces follow the outline of the batholith. D_3 reactivation of the Saint Roch and Bellecombe shear zones may have accommodated some of the differential shortening between the eastern and western parts of the study area. Some crenulations within these shear zones, superimposed on the S_2 foliation, may be related to this deformational event (Fig. 3.25, also see Fig. 3.23). These crenulations are best developed on the short limb of S-shape folds within the shear zone.

3.6. D_4 structures

In the vicinity of the Cadillac-Larder Lake fault zone, and within this zone, earlier foliations in metasedimentary rocks of the Pontiac and Timiskaming Groups are affected by north-dipping normal faults. These structures have a brittle-ductile nature, and their normal top-to- the-north movement are well documented by shear sense indicators, including drag folds and asymmetric boudinage of quartz veins (Fig. 3.26). Large- and small-scale crenulations have developed within the short limb of the drag folds associated with the normal faulting. The crenulations dip at a small angle northward, and nowhere appear to be folded by F_3 folds. Neither normal faults nor crenulations of similar character have been found within the Early

Fig. 3.25. Superimposed microfolding on the S_0 surface of the Pontiac metasedimentary rocks within the Saint Roch shear zone. Microfolds with subhorizontal and steep axes are related to D_2 and D_3 events respectively. Vertical face. View looking west-northwest.

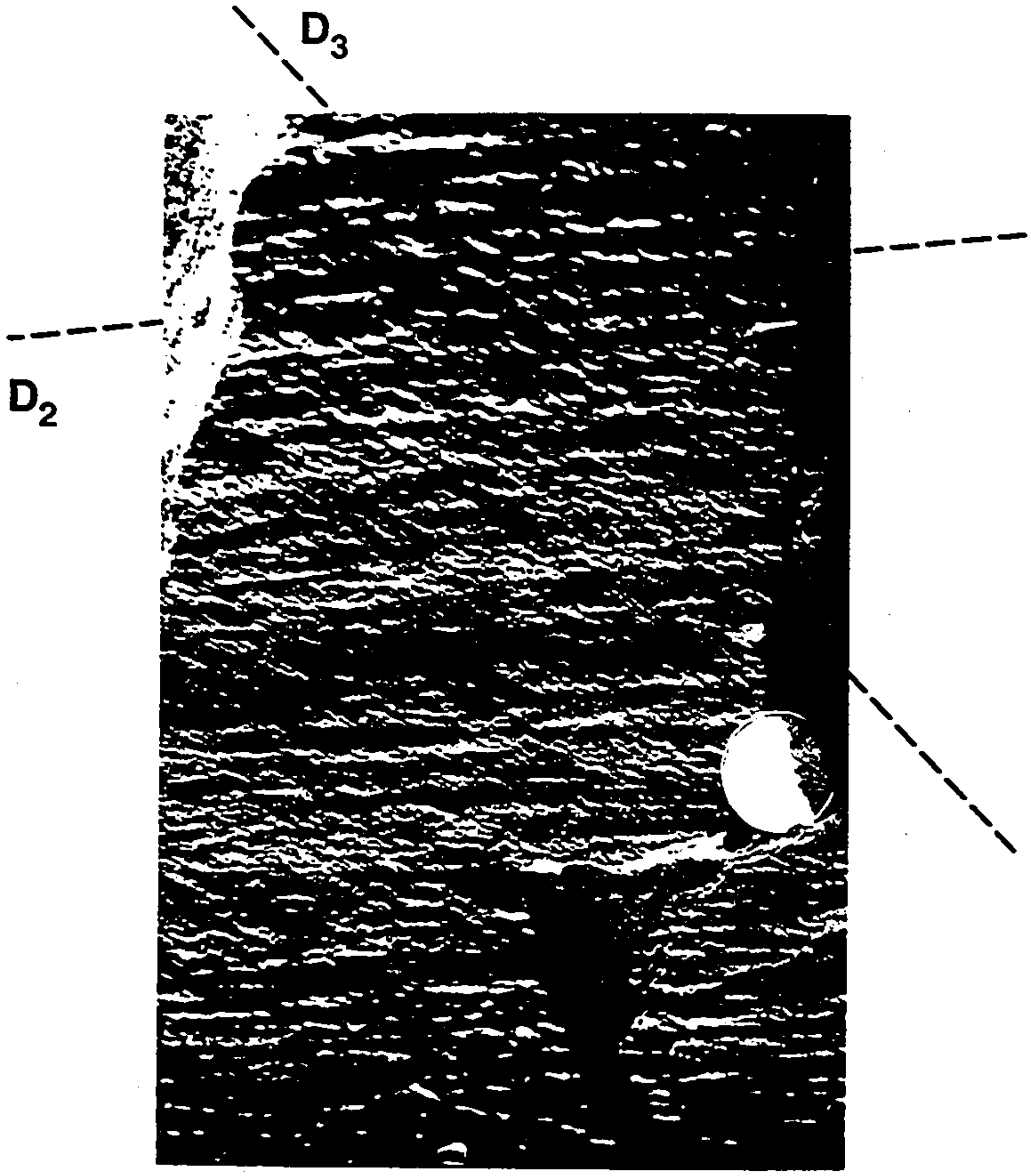
D3
D2

Fig. 3.26a. Quartz vein asymmetric boudins, folds and crenulations within the Pontiac metasedimentary rocks close to the Cadillac-Larder Lake fault zone. Shear sense indicators point to a top-to-the-north movement. Looking east.

Fig. 3.26b. Drag folds related to a top-to-the-north movement along the Cadillac-Larder Lake fault zone within the Timiskaming Group. Looking east.

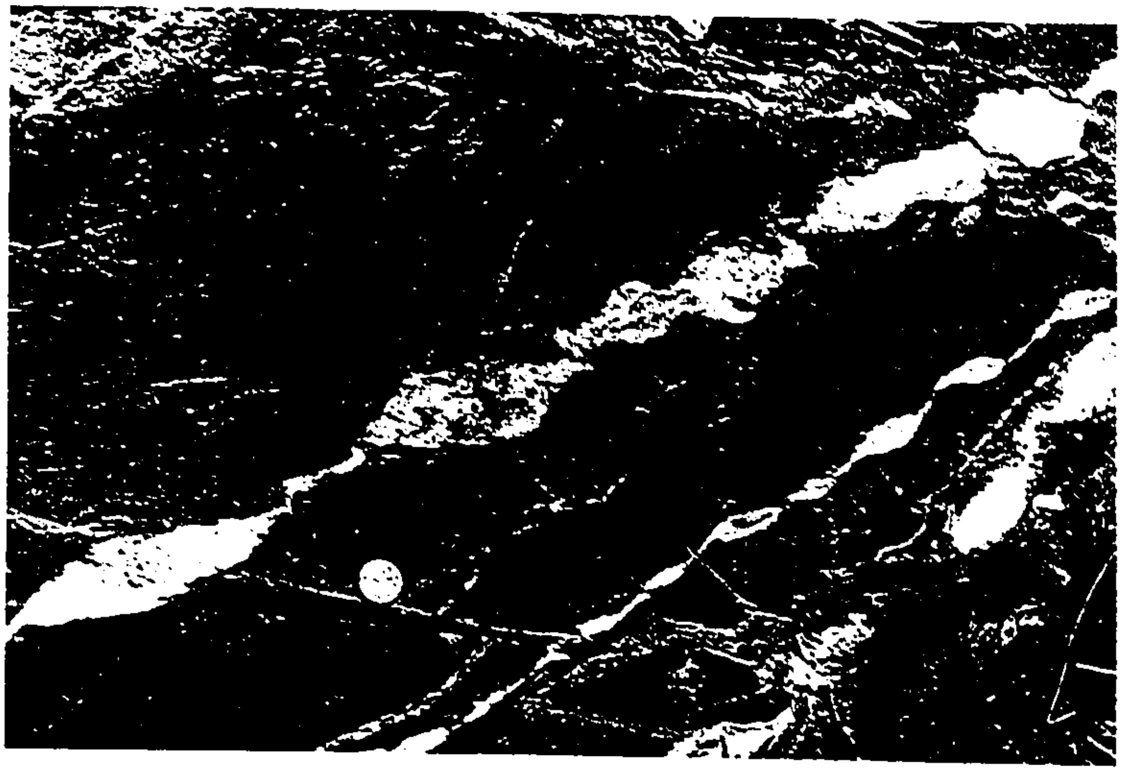

Proterozoic sedimentary rocks of the Cobalt Group. These structures therefore are interpreted as results of an extensional event following the D_3 contractional event and before deposition of the Early Proterozoic sedimentary sequence, that involved reactivation of the Cadillac-Larder Lake fault zone as a normal fault zone.

3.7. D_5 structures

Late east-trending south-vergent brittle thrusting, evident both in the Cadillac-Larder Lake fault zone and elsewhere in the northwestern Pontiac Subprovince, is interpreted to have been the last major shortening event of rocks in the area. A thrust fault of this type cuts older ductile and brittle-ductile structures of the Timiskaming Group and the cross-cutting granitic and syenitic intrusive body in northwestern part of the study area (Fig. 3.27). Sedimentary rocks of the Cobalt Group in the hanging wall of this fault are highly fractured. No movement was documented along these fractures, and no small-scale folding has affected these rocks in the hanging wall; however, the sedimentary layers dip about 12° towards north. In contrast, farther south in the footwall of this brittle thrust fault, bedding within these sedimentary rocks has undergone a relatively tight folding. The fold axes trend east-northeast and plunge gently westward. No cleavage is associated with this folding; however, because of the void spaces that have been developed between the sedimentary layers, the folds must be related to post diagenetic tectonic deformation. No relics of mineralization that might have been weathered out is present in these void spaces. A schematic cross-section of the thrust fault is represented (Fig. 3.28) as an interpretation for deformational relationships in the hanging wall and footwall of the above-described fault.

Northeast-trending sinistral and northwest-trending dextral brittle faults on which elongated lakes such as Lac Kinojevis and Lac Caron are formed, and also similar sets of kink bands developed in the Pontiac metasedimentary rocks (also see Dimroth *et al.* 1982), may also be interpreted as conjugate shear sets developed during this structural event. The conjugate sets

Fig. 3.27. Brittle south-vergent thrust fault related to the D_5 event, cutting and displacing the Timiskaming Group, and a syenite porphyry intrusive body. View looking east.

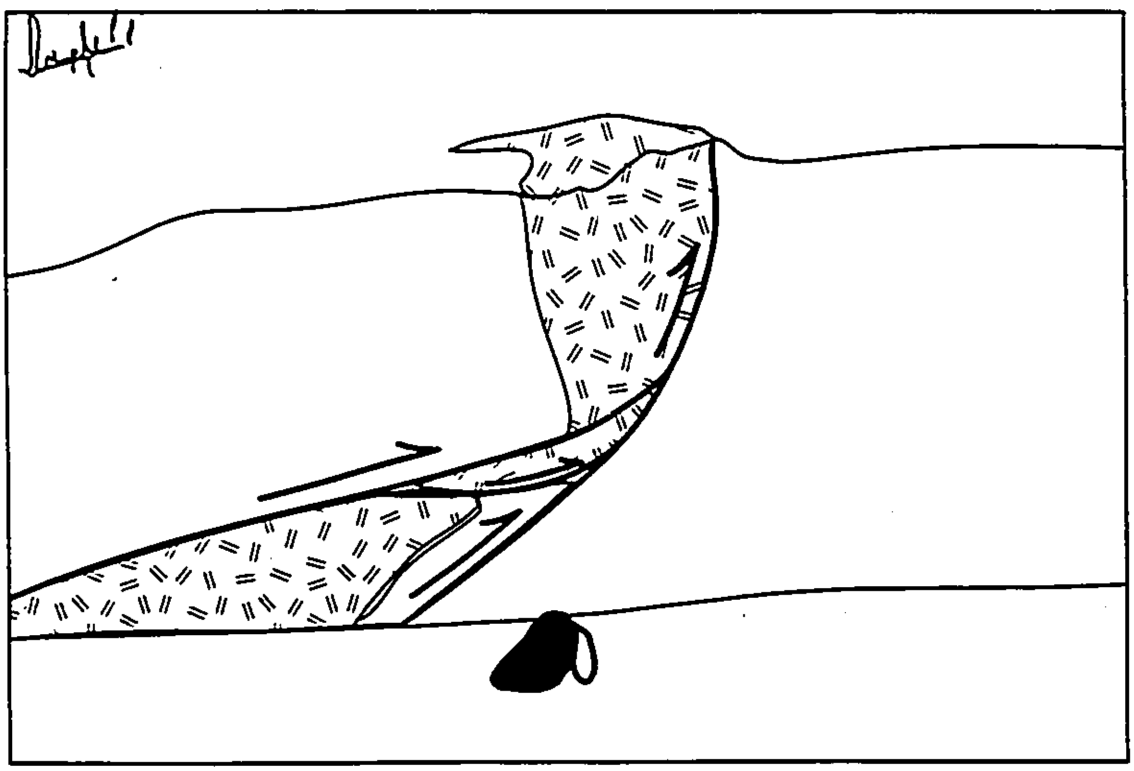

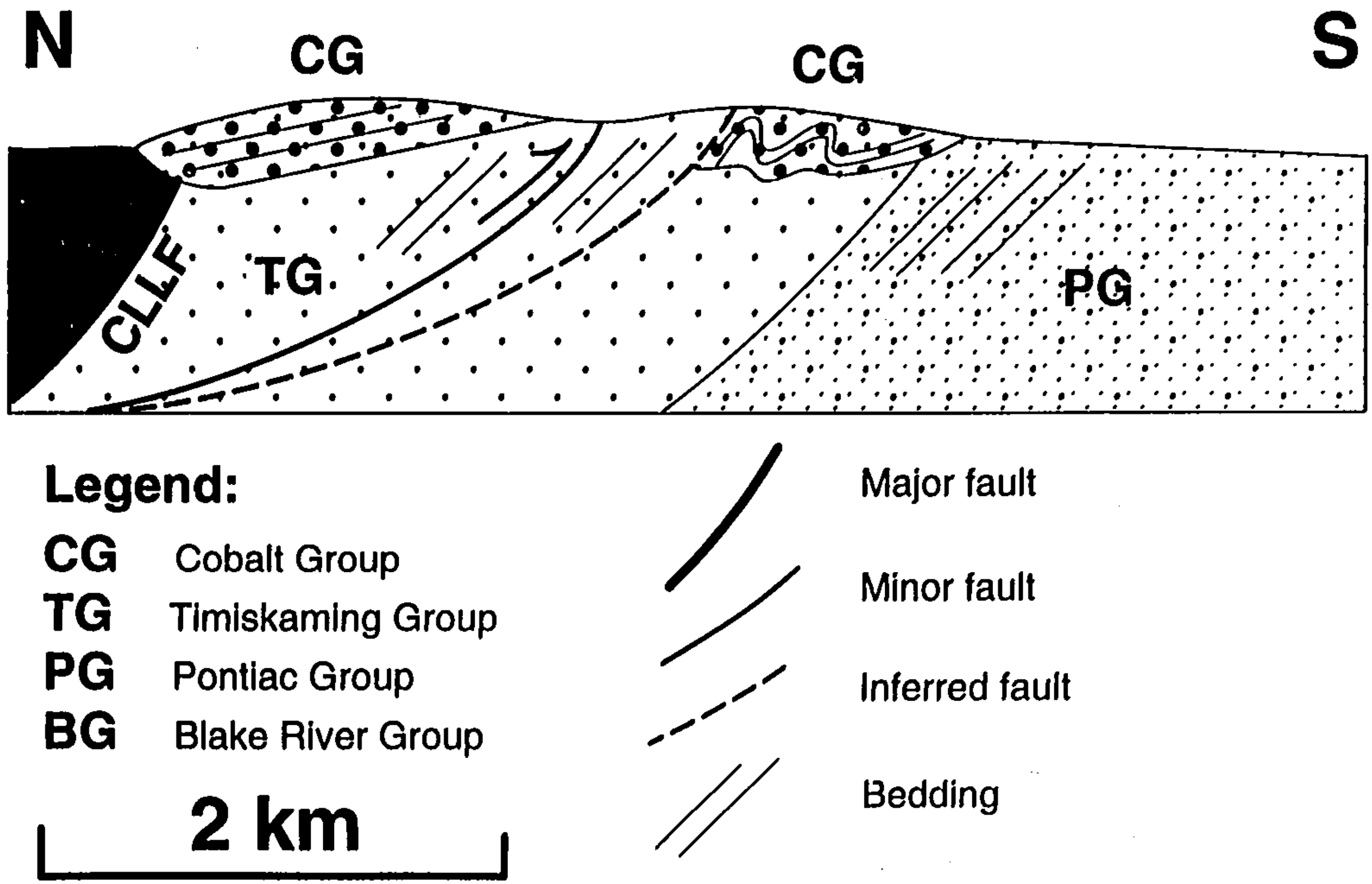

Fig. 3.28. Schematic cross-section showing an interpretation for D_5 thrusting affected Timiskaming and Cobalt Groups in northwestern part of the study area.

of faults and kink bands cut across and displace F_4 folds in the area. The northeast-striking Ruisseau Davidson fault (Goulet 1978) is a sinistral fault of this type that has displaced older structures in the northwestern part of the study area (see Fig. 3.1).

D_5 structures are different from D_4 structures in that they are relatively brittle structures that affect Early Proterozoic sedimentary rocks.

Powell and Hodgson (1992) have documented deformation of the Gowganda Formation (Cobalt Group) by post-Early Proterozoic reactivation of the Archean Cadillac-Larder Lake fault zone, in the Matachewan area. These structures are described as an array of right-stepping, en echelon folds with variably developed axial-planar cleavage, aligned along the trend of the northeast-southwest-trending basement faults. Kinematics of this deformation, as described by Powell and Hodgson (1992), do not properly fit with that of D_5 event within the study area; however, deformational event itself indicates reactivation of major Archean structures in Early Proterozoic.

3.8. Analysis of structural data

On the basis of structural style the study area is divided into three different zones: the Beauchastel, Opasatica and Bellecombe zones (Fig. 3.29). Structural differentiation of these three zones has mostly taken place during the D_3 event. Orientation analysis of the S_2 foliation, that constitutes the most penetrative planar structure in the metasedimentary rocks of the Pontiac Group, is used for description of the structural style in each structural zone.

The Beauchastel zone is parallel to and close to the Cadillac-Larder Lake fault zone, and hence has many features in common with this fault zone. F_3 folds in this zone are isoclinal with axial surfaces that strike parallel to the Cadillac-Larder Lake fault zone (i.e. east-trending and dip steeply to the north). F_3 axes plunge gently to moderately east-northeast. F_3 folding of S_2 foliation in this zone is well illustrated by dispersion of the poles to S_2 along a partial great circle (Fig. 3.30a).

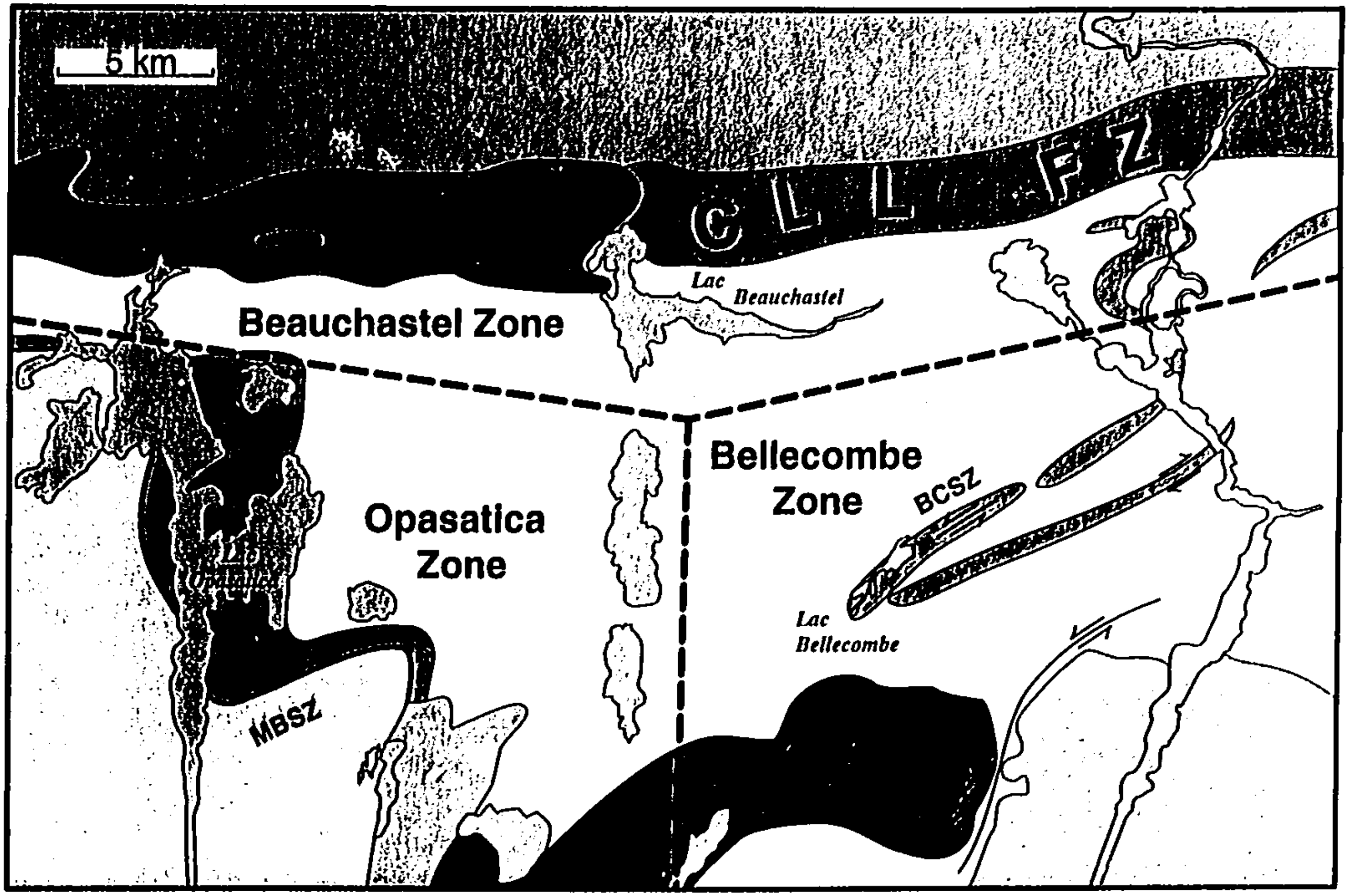

Fig. 3.29. Map illustrating structural zones defined for structural analysis of the study area.

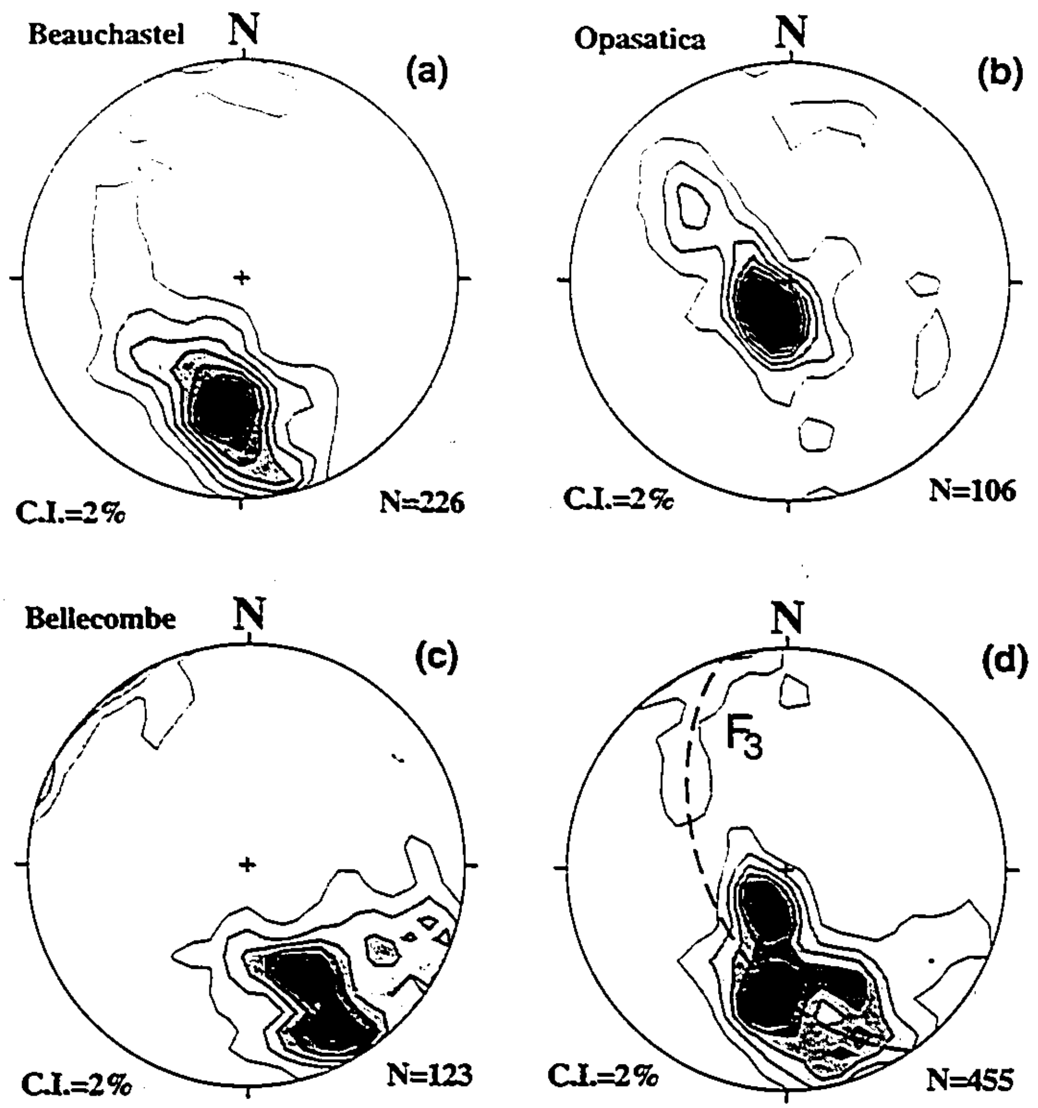

Fig. 3.30. Contoured lower hemisphere equal-area projection of poles to S_2 foliation within (a) Beauchastel, (b) Opasatica, and (c) Bellecombe structural zones. (d) illustrates stereographic projection resulted from plotting of a combination of data from all zones. Dashed line represents a great circle that is interpreted as a result of F_3 folding.

F_3 folds in the Opasatica zone are more open compared with those in the Beauchastel zone. Thus S_2 foliations within the Opasatica zone have smaller dips compared to other zones (Fig. 3.30b). F_3 fold axes in this zone plunge gently towards the east-northeast (Fig. 3.1). In the western part of this zone, the axial traces of F_3 folds are moderately deflected southwest. This change in trend of the folds resulted from impingement of Decelles batholith and other large plutons into the eastern part of the study area during the D_3 event.

The trend of the structures in the Bellecombe zone differs from that in the two other zones. This difference is well reflected by a change in curvature of the traces of axial surfaces of the F_3 folds east of the study area (see Fig. 3.1). Because the D_3 event occurred after consolidation of Decelles and Lac Frechette plutons, it is likely that a major part of shortening during the D_3 event was taken up by less competent rocks of the Pontiac Group rather than the granitic bodies. These plutons therefore appear to have acted as relatively rigid inclusions that protruded and deflected the F_3 folding pattern in the Pontiac metasedimentary rocks.

Statistical analysis of S_2 in Bellecombe zone (Fig. 3.30c) indicates that distribution of this penetrative foliation shows two close maxima in the SE quadrant. These two maxima reflect folding of S_2 by F_2 isoclinal folds, which in turn have been folded and rotated into steeper positions during D_3.

Figure 3.30d illustrates a combination of the poles to S_2 foliation in all zones. Dispersion of the poles along a great circle is interpreted as early folding of S_2 by F_3.

Measured mesoscopic fold axes (Fig. 3.31) are dominantly related to D_2 and D_3. In the Beauchastel zone they plunge generally east-northeast (Fig. 3.31a). Away from the Cadillac-Larder Lake fault zone, in the Bellecombe and Opasatica zones, mesoscopic fold axes are more scattered (Fig. 3.31b,c). Non-cylindrical F_2 folds, are presumably represented by variably plunging fold axes in all three zones.

L_2^1 intersection lineations (Fig. 3.32) in the Beauchastel and Bellecombe zones are correlative with great circles that define S_2 in each zone (compare with Fig. 3.30). Axes of

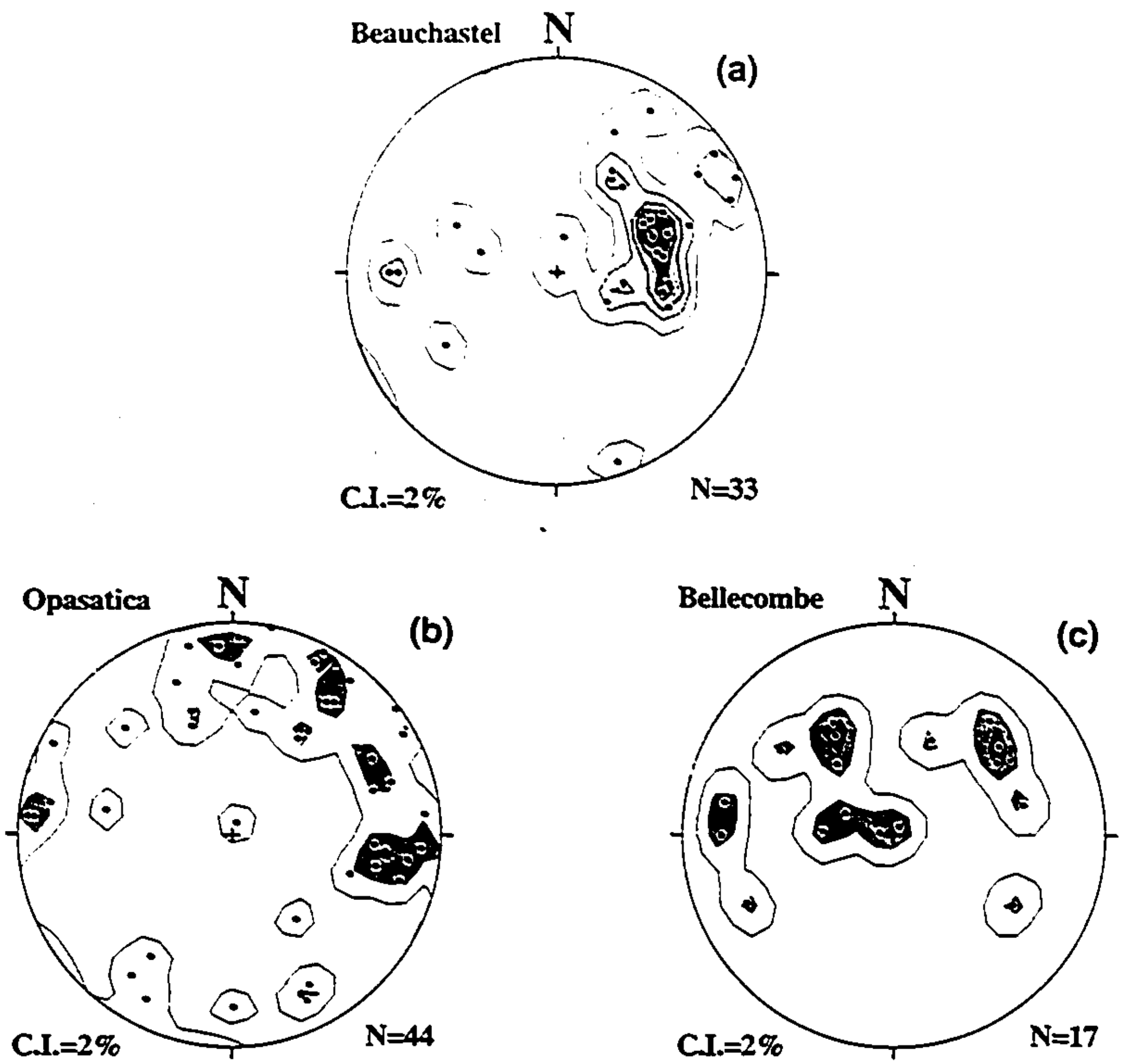

Fig. 3.31. Contoured lower hemisphere equal-area projection of mesoscopic fold axes within (a) Beauchastel, (b) Opasatica, and (c) Bellecombe structural zones.

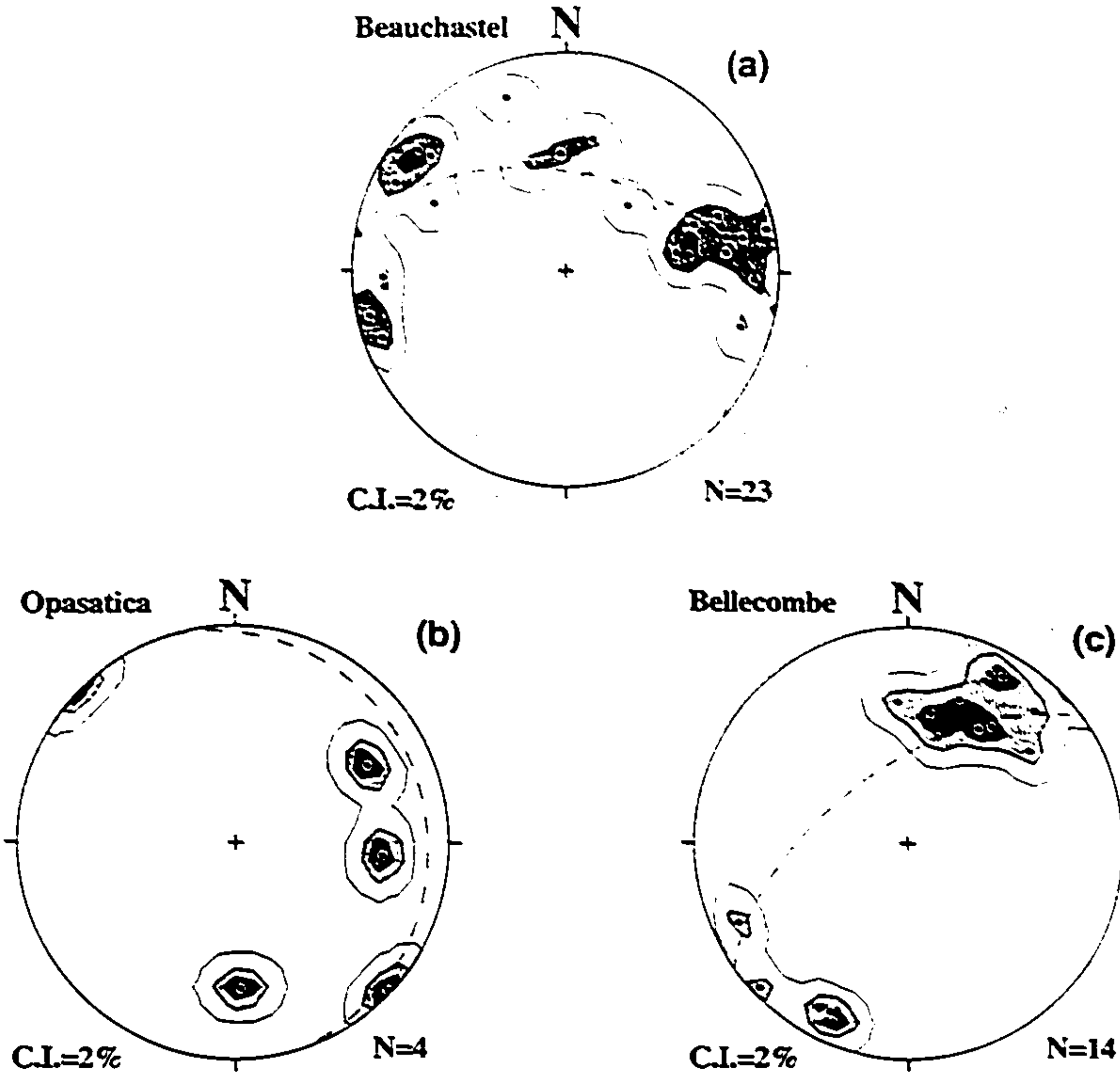

Fig. 3.32. Contoured lower hemisphere equal-area projection of L_2^1 intersection lineation within (a) Beauchastel, (b) Opasatica, and (c) Bellecombe structural zones. Dashed lines represent great circles corresponding to S_2 in each zone.

folds measured on quartz veins show a similar correlation with S_2 foliation (Figs. 3.33 and 3.30).

North-northwest plunging and east-northeast plunging maxima on the stereographic projection representing distribution of elongation lineations in the Beauchastel zone (Fig. 3.34a) are interpreted as being related respectively to the D_2 and D_3. Orientation of the latter maximum accords with that of F_3 fold axes within the same structural zone (compare with Fig. 3.31a). The major maximum on the stereographic projection representing the Bellecombe zone (Fig. 3.34b) is related to L_2. Difference between this (L_2) maximum and that in the Beauchastel zone is interpreted to be the result of an increasing of dip, and rotation of the D_2 structures in this zone because of impingement of the Decelles batholith in the eastern part of the study area. Elongation lineations in the Opasatica zone (Fig. 3.34c) are basically measured in the Lac Opasatica gneiss domain and represent the pre-D_1 deformation.

An abrupt change is observed in the style of deformation across the Cadillac-Larder Lake fault zone. North of the Cadillac-Larder Lake fault zone within the greenstones of the southern Abitibi, the style of deformation is predominantly brittle. Deformation within these rocks has essentially occurred as brittle low- to high-angle faulting. Foliation development, and highly ductile folds, comparable to those in the Pontiac Subprovince, are not observed within these volcanic rocks. However, it must be kept in mind that F_3 folds are comparable to similar east-trending folds within the Abitibi Subprovince.

3.8.1. Comparison with previous structural studies within the Pontiac Subprovince

The presence of a north-trending F_1 fold set, defined by of Goulet (1978) to be one of the major structural features of the Rouyn-Beauchastel area, is not documented by the present study.

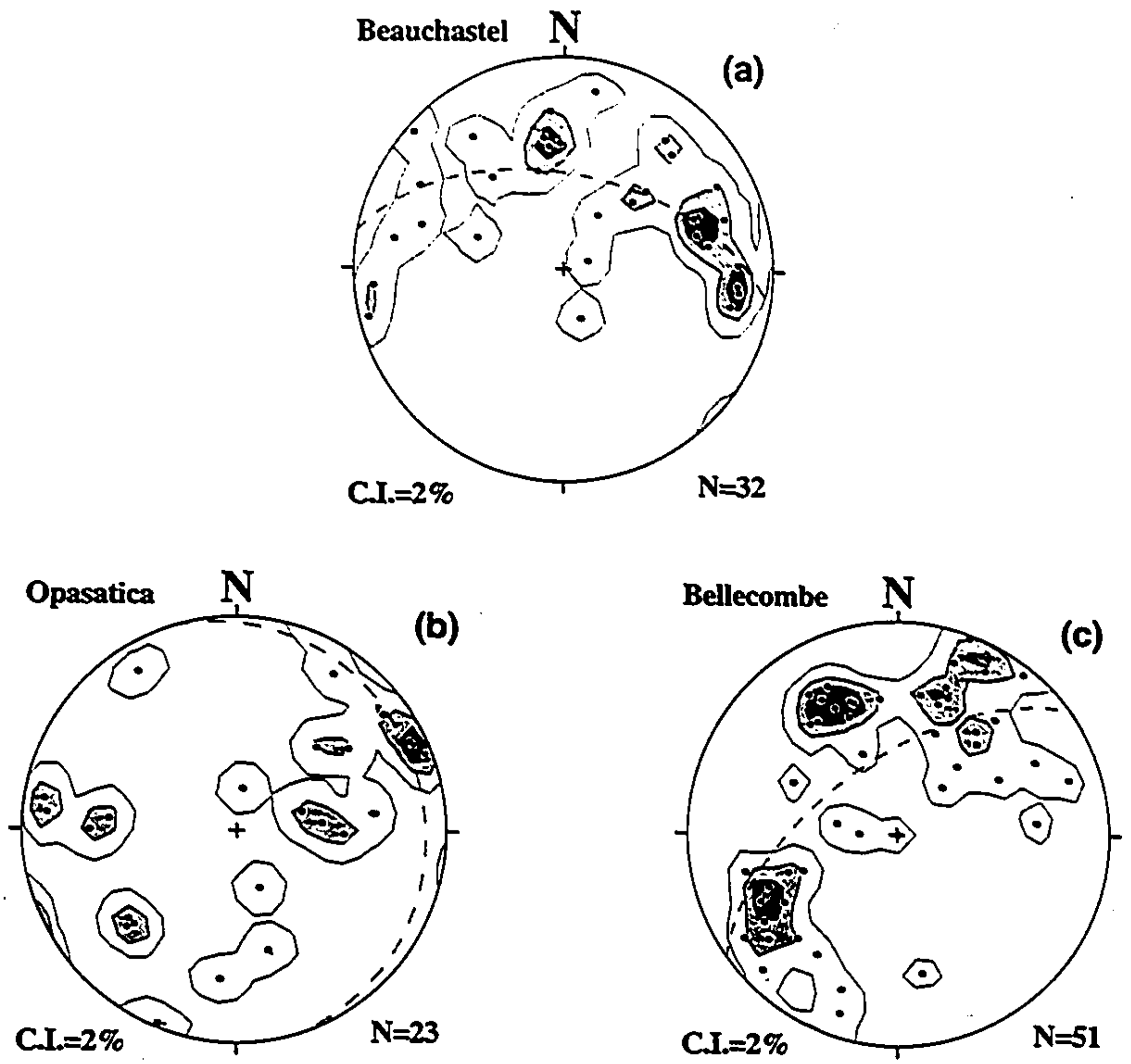

Fig. 3.33. Contoured lower hemisphere equal-area projection of quartz vein fold axes within (a) Beauchastel, (b) Opasatica, and (c) Bellecombe structural zones. Dashed lines represent great circles corresponding to S_2 in each zone.

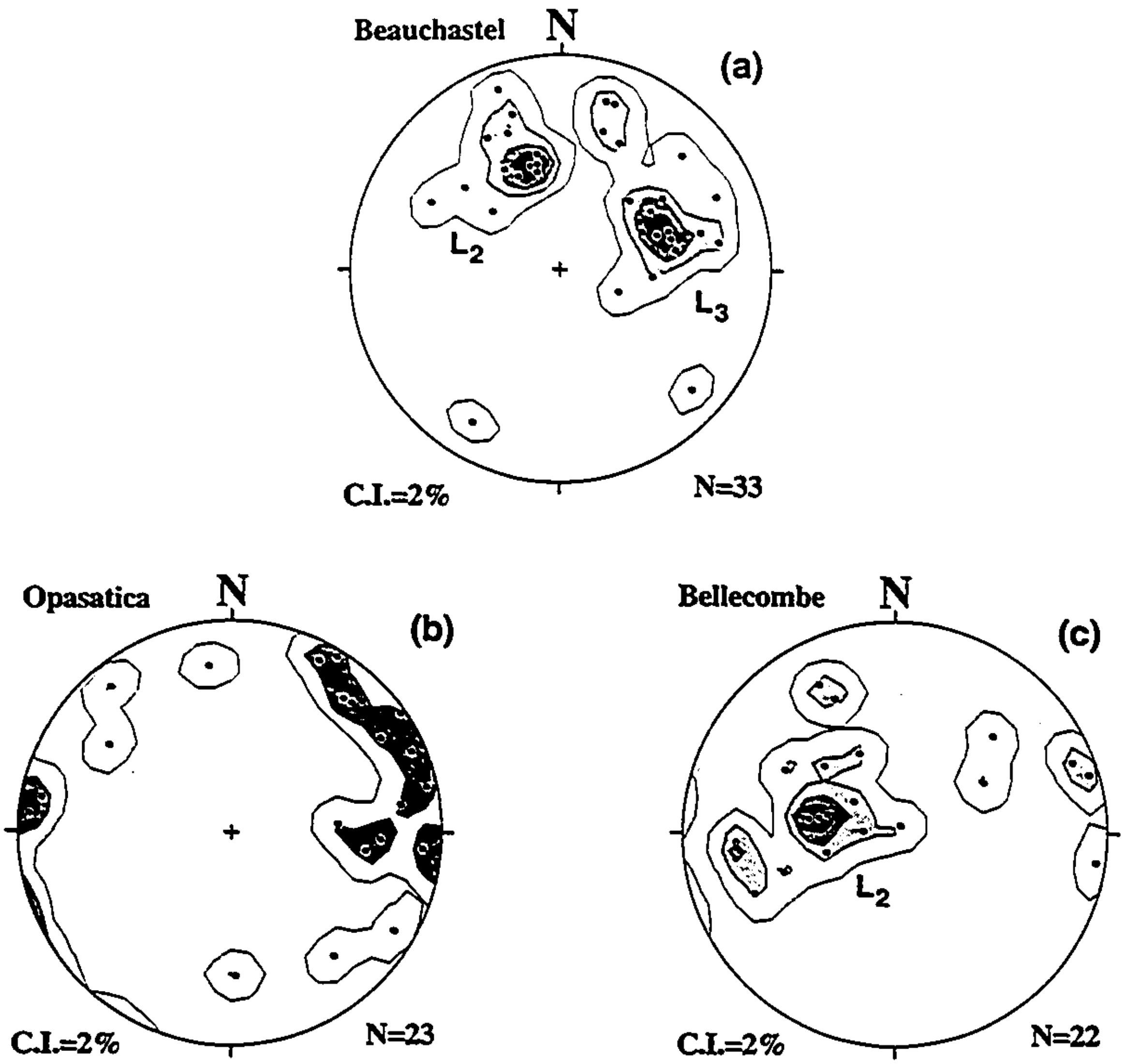

Fig. 3.34. Contoured lower hemisphere equal-area projection of elongation lineations within (a) Beauchastel, (b) Opasatica, and (c) Bellecombe structural zones.

Camiré and Burg (1993) divided the study area into two major nappe structures, the boundary of which was defined by an abrupt change in structural style and metamorphic facies. They described two phases of close to isoclinal folding that are evident in the upper nappe but are absent from the lower nappe. Comparison of different structural features mapped for this study from different regions reveals continuity of these features throughout the study area. This is in contrast with the findings of Camiré and Burg (1993); moreover, study of metamorphic facies within the area indicates that the mineral assemblage, defined by these workers to be characteristic of the lower nappe (see Camiré and Burg 1993), is common within their upper nappe. The metavolcanic band exposed along the Kinojevis River is interpreted by Camiré and Burg (1993) as a folded klippen structure thrust onto the sedimentary rocks of Pontiac before the peak of metamorphism. However, the present study indicates that the metavolcanic band is part of a rather continuous autochthonous volcanic unit within the Pontiac sedimentary sequence, that shares very similar structural features with these sedimentary rocks.

3.9. Summary and conclusions

Metasedimentary, metavolcanic, and plutonic rocks within the northwestern Pontiac Subprovince have undergone a complex sequence of deformational events. The resultant structures are best visible within the metasedimentary rocks of the Pontiac Group, and may be summarized as follows:

On the basis of microstructural analyses, D_1 was associated with steep (east-trending) foliation axial planar to upright F_1 folds. D_1 microstructures in the northwestern Pontiac Subprovince record prograde conditions before attainment of peak metamorphic conditions, most probably the result of early crustal thickening. Structural and metamorphic relationships between the southern Abitibi greenstone belt and Pontiac Subprovince indicate that D_1 was associated with large-scale thrusting of the Abitibi Subprovince over the Pontiac Subprovince. The Timiskaming Group was deposited within a foreland basin in front of the Abitibi greenstone belt, and affected by D_2 deformational event and regional metamorphism. This sedimentary group marks emergence of sedimentary rocks and the end of deposition within the Pontiac basin during the D_1 event.

D_2 was a south-southeast-directed nappe development event that was associated with shallow-dipping structures developed during and after peak metamorphic conditions as demonstrated by relationships between these structures and peak metamorphic minerals, as well as their relationship with syn-peak metamorphic S-type granites. A penetrative regional crenulation foliation (S_2) axial planar to the recumbent F_2 folds is the most prominent feature of the D_2 event. S_1 foliation is preserved as folded trails of biotite, and/or straight or crenulated inclusion trails within the microlithons of S_2 foliation. This event presumably marks a period of high grade deformation of the rocks at greater depths as compared to the D_1 event. The generally shallow nature of S_2 foliation compared to S_1 foliation, suggests that foliation development during D_2 event has occurred with the Z-direction of the bulk regional finite strain ellipse being vertical.

D_3 represents a north-south contractional event that superimposed east-trending generally upright folds on F_3 folds. These structures are comparable to similar east-trending structures within the Abitibi Subprovince.

D_4, which is confined to the vicinity of the Cadillac-Larder Lake fault zone, is an extensional event that resulted in normal faulting reactivation of this fault zone.

D_5 appears to be the most recent contractional event that produced kinks and brittle south-vergent thrusts which have affected all older structures within the study area.

Gneissose structure of the Lac Opasatica gneisses and related mineral elongation lineation developed during a pre-D_1 event, that is not traceable into the Pontiac Group rocks.

4. Metamorphism

4.1. Introduction

The study of metamorphism within Archean terranes is very important for a better understanding of the early thermal history of Earth's crust and its orogens. Metamorphism is considered by some to be responsible for ore deposition within these old terranes through remobilization of elements by metamorphic fluids. Late Archean (*ca.* 2.7 Ga) lode gold mineralization in the Superior Province of Canada was a syn- to late-peak metamorphic event (Kerrich and Cassidy 1994).

The first accounts of metamorphism in the Pontiac Subprovince were by Wilson (1909, 1962) who noted the presence of biotite, chlorite and sericite in siliceous mica schists of the Pontiac Group in the Rouyn-Beauchastel area. He also described metamorphosed volcanic rocks within this region. Jolly (1978), in his proposed metamorphic zonation of the Abitibi belt, placed the Pontiac Subprovince within the amphibolite facies. He introduced the first metamorphic isograd map of the subprovince (Jolly 1978), for which he defined east-trending isograds of garnet, staurolite, kyanite and sillimanite in order towards the south. Van de Walle (1978) mapped the same isograds in more detail within the Montbeillard area of the northwestern Pontiac Subprovince. On the basis of the occurrence of mineral assemblages, Goulet (1978) mapped a biotite-epidote isograd and a staurolite-biotite isograd in the Rouyn-Beauchastel area of the Pontiac Subprovince. He reported the presence farther south of both fibrous and prismatic sillimanite in the metasedimentary rocks. On the basis of crystal shape, he suggested that the prismatic sillimanite was probably a pseudomorph after andalusite. Goulet suggested that amphibolite facies metamorphism in the central part of the Pontiac Subprovince was likely a very late tectonic phenomenon, probably related to the intrusion of large granodiorite and trondhjemite-tonalite massifs. Camiré *et al.* (1993), accepting a similar southward increasing metamorphic grade, suggested that southward-inclined drag folds and low-angle ductile shear zones in the northwestern Pontiac Subprovince developed during a Barrovian-type metamorphism.

The present investigation of metamorphism in the study area was focused on the timing of the metamorphic events with respect to established structural events and major magmatic episodes. Study of metamorphic assemblages along with their relationships to microstructural features within different samples permit, for the first time, estimates of metamorphic pressures and temperatures, and also the construction of a P-T path for amphibolite facies rocks of the northwestern part of the Pontiac Subprovince.

4.2. Mineral assemblages and metamorphic reactions

Hand specimens of the Pontiac Group metasedimentary rocks within the study area are biotite-rich schists (metagraywacke) that show at least one penetrative metamorphic foliation (S_2), spaced on the order of 1 millimeter. The foliation is essentially parallel to the original layering (bedding) of the metasedimentary rocks. Other metamorphic minerals (muscovite, garnet, staurolite, and kyanite) may also be detected in the field. In thin-sections, metamorphic mineral assemblages consist of various combinations of quartz, plagioclase, chlorite, biotite, muscovite, garnet, epidote, tourmaline, staurolite, kyanite, and sillimanite. K-feldspar is present in few samples from the sillimanite zone. Microscopic zircon crystals are present in some of the thin-sections. Chloritoid is not present in any examined sample from the Pontiac metasedimentary rocks, but the aluminum-rich composition of the rocks suggests that it might have been present during the early stages of prograde metamorphism. Oxide and sulfide minerals detected through microscopic study of polished thin-sections include rutile, ilmenite, magnetite, hematite, pyrite, chalcopyrite, pyrrhotite and pentlandite. The metamorphic facies of the Pontiac Group is in a relatively clear contrast with the metamorphic facies in the southern Abitibi, which, except for small amphibolite facies aureoles around plutons, is of sub-greenschist to greenschist facies (Jolly 1978, Powell 1993, 1995).

Based on different progressive metamorphic reactions, four different isograds are mapped in the northwestern Pontiac Subprovince: these are the '+garnet', '+staurolite', '+kyanite', and '+sillimanite' isograds (Fig. 4.1). Detailed study of the rocks in the field and in thin-sections has allowed defining a more precise location of these isograds compared to those mapped by Jolly (1978), van de Walle (1978), Goulet (1978), Camiré *et al.* (1993), and Benn *et al.* (1994). An increase in metamorphic grade from north to south is inferred from the distribution of isograds in Fig. 4.1. No petrologic data in the third dimension are available to constrain the dip of the isograd surfaces in the study area. Because the isograds are based on the first appearance of the metamorphic minerals, small-scale post-peak metamorphism folding and/or faulting of the isograds were not detectable.

The areas delimited by the four mapped isograds are referred to as the biotite, garnet, staurolite, kyanite and sillimanite zones. Table 4.1 represents common mineral assemblages within each zone (for mineral name abbreviations see Table 4.2).

The mineral assemblages in the metavolcanic rocks of the Pontiac Group include amphiboles (pargasite), biotite, garnet, epidote, chlorite, serpentine, plagioclase, K-feldspar, quartz, and carbonates (calcite and dolomite).

4.3. Microstructural relationships and metamorphic reactions

Mineral assemblages within different metamorphic zones and their microstructural relationships are here described to define possible metamorphic reactions responsible for the present distribution of metamorphic mineral assemblages within the study area, and to propose a scheme for the metamorphic evolution of this terrane. However, it must be noted that because of a lack of comprehensive knowledge on bulk geochemistry of the rocks, the proposed scheme is far from a solid approach.

Biotite is the most abundant metamorphic mineral, occurring as crystals defining a foliation in the metasedimentary rocks of the Pontiac Group. Later deformation of biotites in these foliation planes and their microstructural relationship with other metamorphic or non-

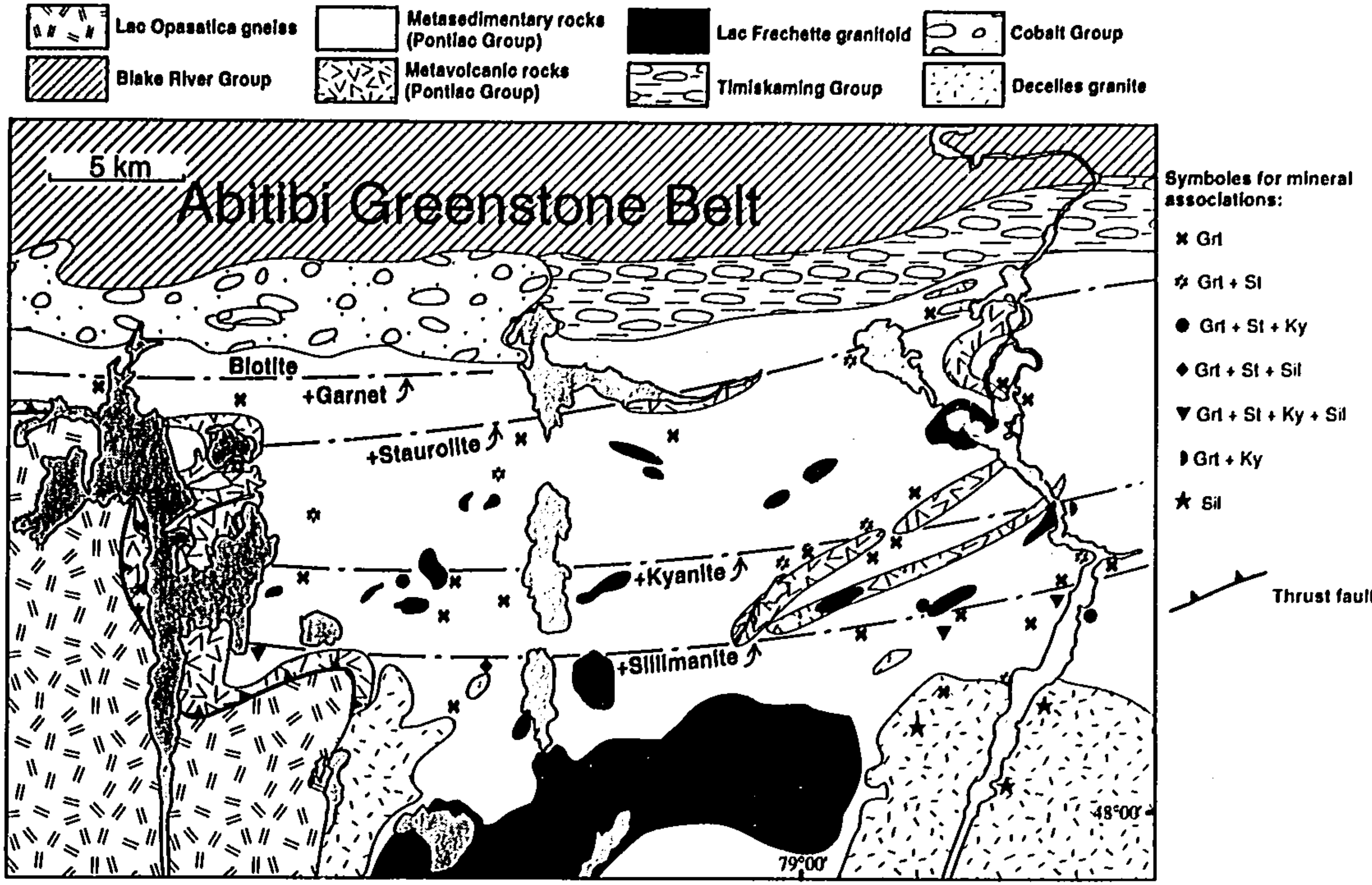

Fig. 4.1. Metamorphic isograds in metasedimentary rocks of northwestern Pontiac Subprovince. Metamorphic mineral associations within different metamorphic zones are shown by symbols. Biotite and muscovite are present in most of the samples. For more details on geology and structure of the area see Figs. 2.2 and 3.1. Most of the isograds are located farther north compared to those that have been earlier mapped (Jolly 1978, van de Walle 1978, Goulet 1978, and Camiré et al. 1993).

Table 4.1. Representative mineral assemblages within different metamorphic zones of the study area. For location of samples see Fig. 4.2.

	Bt zone	Grt zone		Staurolite zone		Kyanite zone						Sillimanite zone		
	PM 68	PM 2	PM 123	PM 1	JL 3	JL 34	JL 48	JL 14	PM 35	PM 17	JL 39	JL 44	JL 41	JL 25
Qtz	+	+	+	+	+	+	+	+	+	+	+	+	+	+
Pl	*	*	+	*	+	*	*	*	+	+	*	*	*	*
Bt	*	*	+	*	*	*	*	*	+	+	*	*	*	*
Ms	-	+	+	+	*	+	*	+	+	*	+	*	*	*
Chl	*	*	+	*	+	*	+	+	+	+	+	+	*	+
Grt	-	*	*	*	*	*	*	*	*	+	*	*	*	*
St	-	-	-	*	+	*	+	+	-	-	*	+	*	+
Ky	-	-	-	-	-	*	+	+	+	-	-	+	-	-
Sil	-	-	-	-	-	-	-	-	-	-	-	*	-	+
Ep	+	-	-	-	-	-	-	-	-	-	-	-	-	-
Tur	+	+	-	-	-	+	+	-	-	-	-	-	-	-
Rt	+	+	N	+	N	+	N	N	N	N	N	+	N	N
Ilm	+	N	N	+	N	N	N	N	N	N	N	+	N	N
Mag	N	+	N	+	N	+	N	N	N	N	N	N	N	N
Hem	N	N	N	N	N	S	N	N	N	N	N	N	N	N
Py	N	+	N	+	N	+	N	N	N	N	N	+	N	N
Ccp	+	N	N	+	N	N	N	N	N	N	N	+	N	N
Po	+	N	N	N	N	N	N	N	N	N	N	N	N	N
Pn	+	N	N	N	N	N	N	N	N	N	N	N	N	N

\+ present
* present, mineral analyzed; see Tables 4.3, 4.6, and Appendix E.
\- absent
N opaque minerals not studied
S secondary

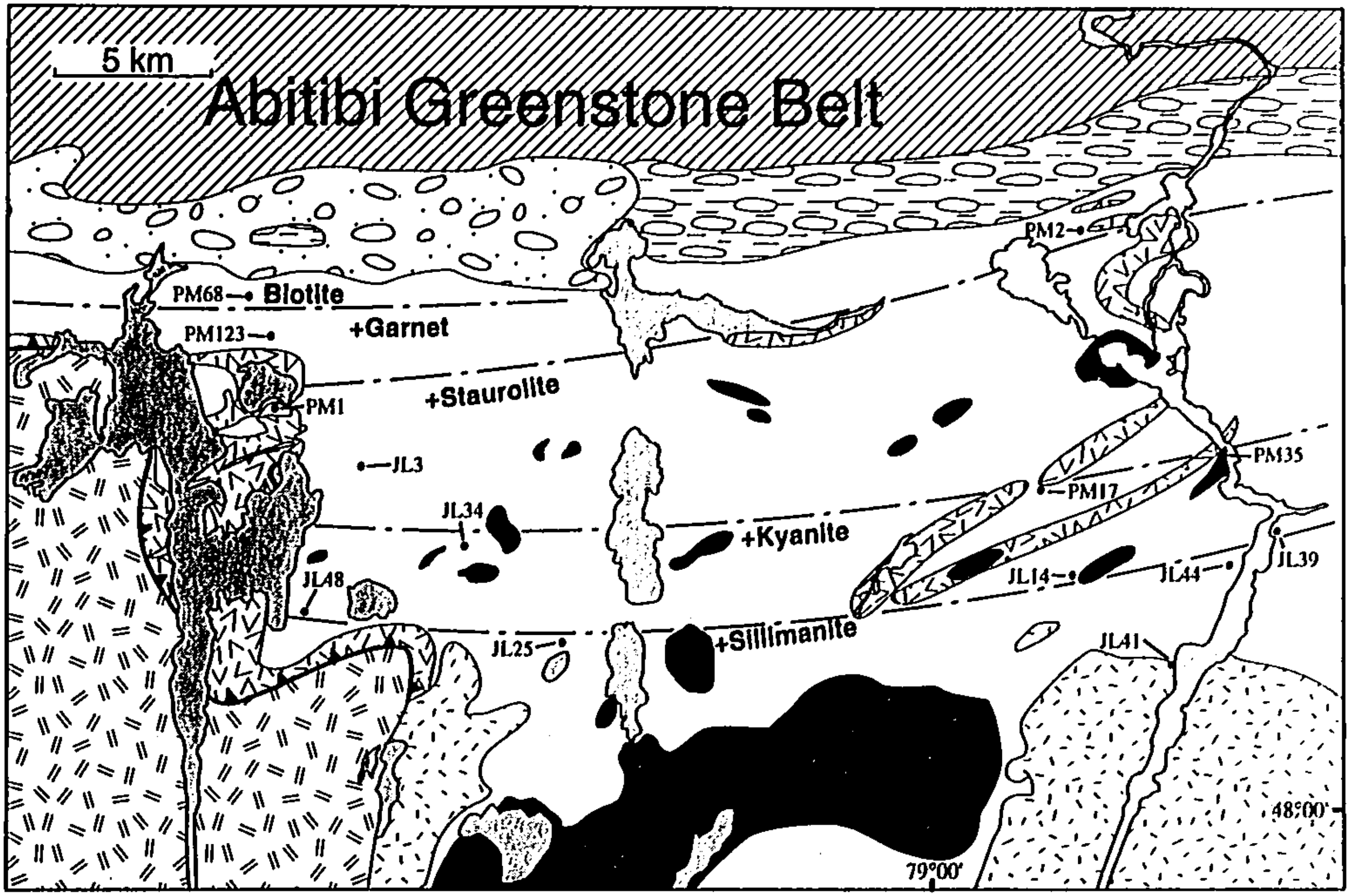

Fig. 4.2. Distribution of samples used for mineral analyses.

Table 4.2. Mineral and component names, mineral symbols (after Kretz 1983), and simplified formulas.

Mineral	Abb.	Formula
garnet	Grt	$(Fe,Mg,Mn,Ca)_3 (Al,Fe^{3+})_2 Si_3 O_{12}$
almandine	Alm	$Fe_3 Al_2 Si_3 O_{12}$
pyrope	Prp	$Mg_3 Al_2 Si_3 O_{12}$
spessartine	Sps	$Mn_3 Al_2 Si_3 O_{12}$
grossular	Grs	$Ca_3 Al_2 Si_3 O_{12}$
andradite	Adr	$Ca_3 Fe^{3+}{}_2 Si_3 O_{12}$
aluminum silicate	Als	$Al_2 Si O_5$
sillimanite	Sil	$Al_2 Si O_5$
kyanite	Ky	$Al_2 Si O_5$
andalusite	And	$Al_2 Si O_5$
staurolite	St	$(Fe,Mg)_4 Al_{18} Si_{7.5} O_{44} (OH)_4$
chloritoid	Cld	$(Fe,Mg)_2 (Al,Fe^{3+}) Al_3 Si_2 O_{10} (OH)_4$
zoisite	Zo	$Ca_2 Al_3 Si_3 O_{12} (OH)$
epidote	Ep	$Ca_2 (Al,Fe^{3+})_3 Si_3 O_{12} (OH)$
tourmaline	Tur	$Na (Mg,Fe,Fe^{3+})_3 Al (OH,F)_4$
pargasite	Prg	$Na Ca_2 Mg_4 Al_3 Si_6 O_{22} (OH)_2$
Fe pargasite	FePrg	$Na Ca_2 Fe_4 Al_3 Si_6 O_{22} (OH)_2$
anthophyllite	At	$(Mg,Fe)_7 Si_8 O_{22} (OH)_2$
Fe anthophyllite	FeAt	$Fe_7 Si_8 O_{22} (OH)_2$
tremolite	Tr	$Ca_2 Mg_5 Si_8 O_{22} (OH)_2$
actinolite	Act	$Ca_2 (Mg,Fe)_5 Si_8 O_{22} (OH)_2$
Fe actinolite	FeAct	$Ca_2 Fe_5 Si_8 O_{22} (OH)_2$
hornblende	Hbl	$(Ca,Na)_{2-3} (Mg,Fe,Fe^{3+},Al)_5 (Si,Al)_8 O_{22} (OH)_2$
muscovite	Ms	$K Al_3 Si_3 O_{10} (OH)_2$

Table 4.2. Continued.

Mineral	Abb.	Formula
paragonite	Pg	$Na\ Al_3\ Si_3\ O_{10}\ (OH)_2$
biotite	Bt	$K\ (Mg,Fe,Fe^{3+},Ti,Al,\pm)_3\ (Si,Al)_4\ O_{10}\ (OH)_2$
phlogopite	Ph	$K\ Mg_3\ Al\ Si_3\ O_{10}\ (OH)_2$
annite	Ann	$K\ Fe_3\ Al\ Si_3\ O_{10}\ (OH)_2$
chlorite	Chl	$(Fe,Mg,Al)_6\ (Si,Al)_4\ O_{10}\ (OH)_8$
Fe chlorite	FeChl	$Fe_5\ Al_2\ Si_3\ O_{10}\ (OH)_8$
Mg chlorite	MgChl	$Mg_5\ Al_2\ Si_3\ O_{10}\ (OH)_8$
K-feldspar	Kf	$K\ Al\ Si_3\ O_8$
plagoclase	Pl	$(Na\ Al\ Si_3\ O_8),(Ca\ Al_2\ Si_2\ O_8)$
albite	Ab	$Na\ Al\ Si_3\ O_8$
anorthite	An	$Ca\ Al_2\ Si_2\ O_8$
quartz	Qtz	$Si\ O_2$
calcite	Cal	$Ca\ CO_3$
magnetite	Mag	$Fe_3\ O_4$
hematite	Hem	$Fe_2\ O_3$
ilmenite	Ilm	$Fe\ Ti\ O_3$
rutile	Rt	$Ti\ O_2$
pyrite	Py	$Fe\ S_2$
chalcopyrite	Ccp	$Cu\ Fe\ S_2$
pyrrhotite	Po	$Fe\ S$
pentlandite	Pn	$(Fe\ Ni)_9\ S_8$

metamorphic minerals provide information about the relative ages of the successive structural events, metamorphic reactions, and interrelationship of structural and metamorphic events. Crenulation foliations, for example, are essentially produced by microfolding of the previous foliations. With continued deformation, these microfolds have evolved into discrete bands of biotite separating quartz- and feldspar-rich microlithons, in which folded trails of biotite flakes still preserve partial relics of the earlier cleavage (Fig. 3.6). Inside and close to the discrete cleavage planes, quartz and feldspar are present as small flat crystals between the biotite flakes (Fig. 4.3), showing that constituent elements of quartz and feldspar have diffused from areas of high stress between the biotite flakes into areas of low stress in the microlithons.

Based on microstructural evidence, white micas in the metasediments may be divided into two groups, here referred to as first- and second-generation white micas. The first generation has a comparatively smaller crystal size and is aligned together with biotite in the S_2 foliation. Prograde reactions appear to be responsible for development of these crystals. The second generation has a larger crystal size and overgrows the S_2 foliation. Large crystals of this generation have overgrown many biotite-rich domains, fringe some staurolite crystals (Figs. 4.4 and 4.5), and totally replace staurolite or kyanite porphyroblasts.

On the basis of the presence or lack of inclusions, garnets in metasedimentary rocks of the Pontiac Group may be divided into two groups. The inclusions, commonly quartz, locally show a preferred planar orientation, and end at an inclusion-free rim. The inclusion trails in the garnets are usually parallel to planar inclusion trails in the staurolite crystals. Having a broad stability field, and being involved in many different metamorphic reactions, garnet has been produced at different stages of the progressive and retrogressive metamorphism; different generations of garnet are therefore expected. In some samples, garnet that has overgrown the S_2 foliation represents a younger generation. Some garnets from the kyanite and sillimanite zones have grown inside the S_2 microlithons, but since they have grown on, and at the expense of, the staurolite crystals (with planar inclusion trails), they have inherited the old S_1 inclusion

Fig. 4.3. Flat quartz and plagioclase crystals between biotite crystals (brownish yellow) close to S_2 foliation. Removal of these crystals by diffusion from higher differential stress areas within S_2 foliation has resulted in passive concentration of biotites along foliation planes. Cross-polarized light.

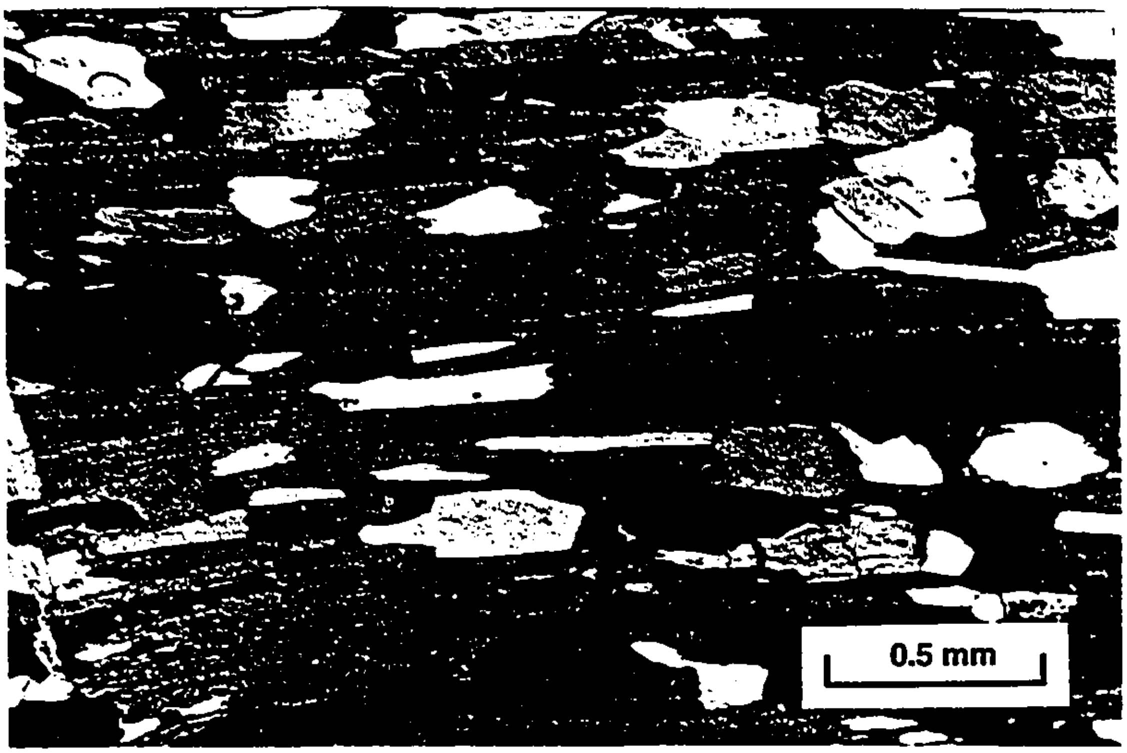
0.5 mm

Fig. 4.4. Overgrowth of second-generation muscovite along S_2 foliation. Cross-polarized light.

Fig. 4.5. Replacement of staurolite on the rim by second-generation muscovite. Partially cross-polarized light.

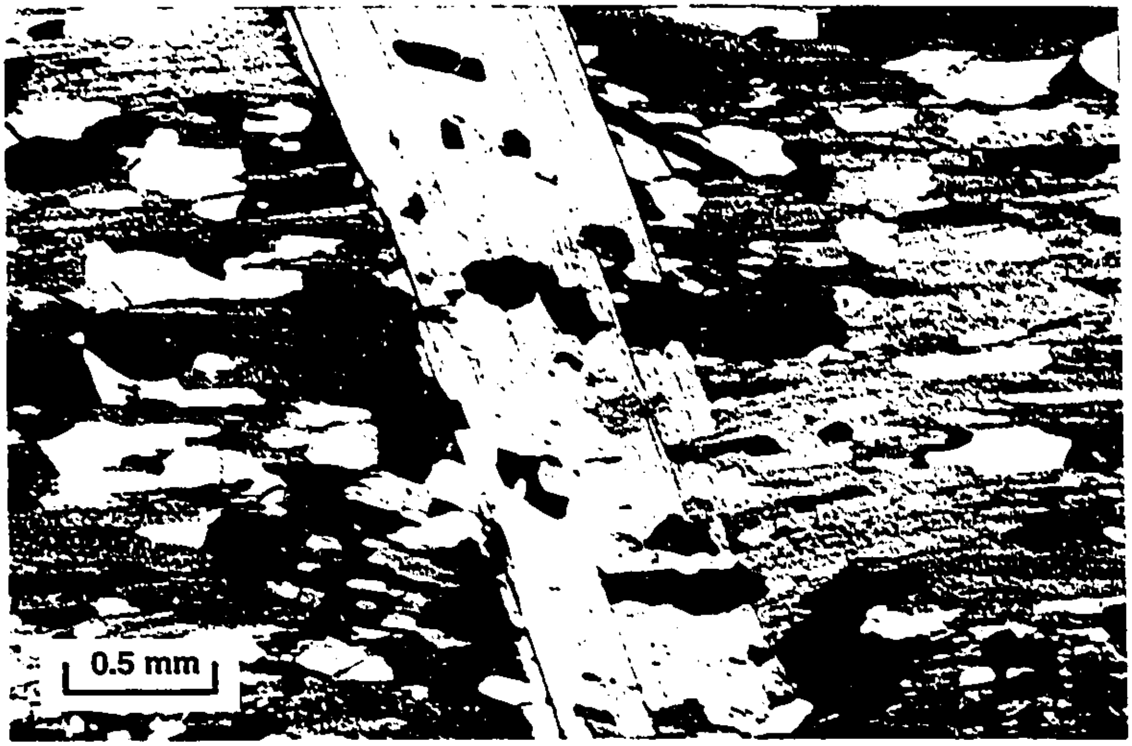
0.5 mm

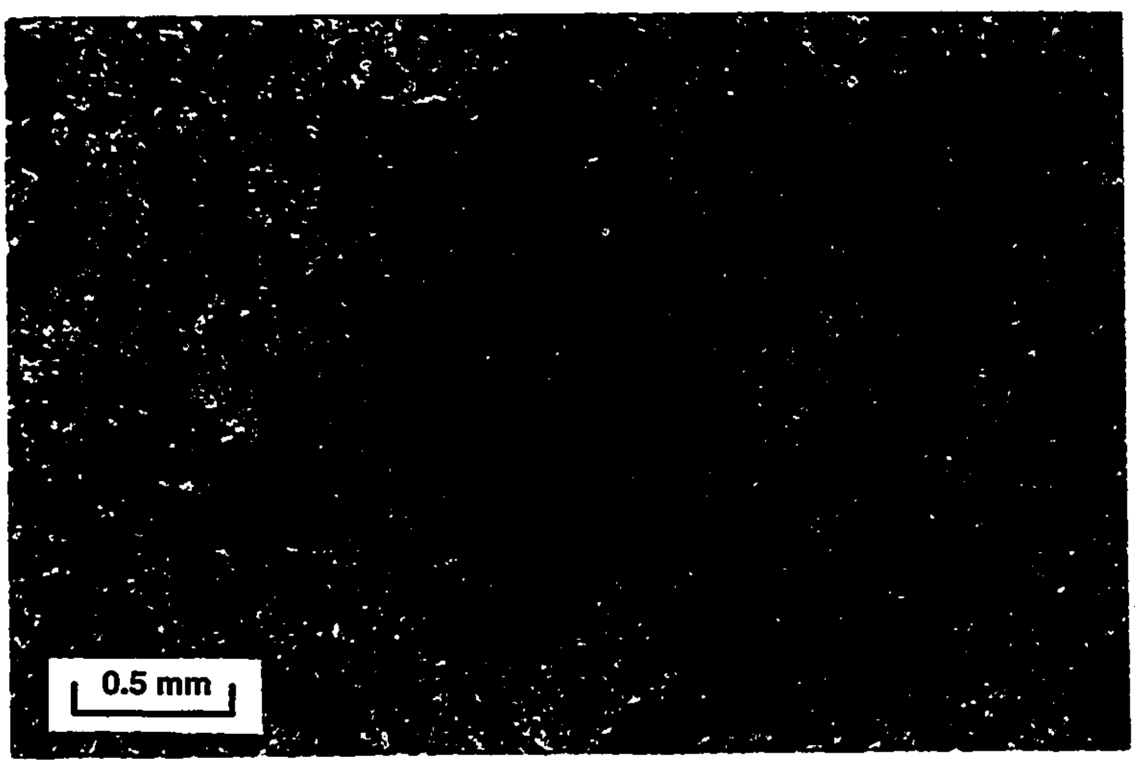
0.5 mm

trails. The appearance of almandine, pyrope and spessartine components of the garnets at the +garnet isograd may be related to the following reactions:

$$2Chl + 4Qtz = 3Grt + 8H_2O \quad (1)$$

$$3Chl + Ms + 3Qtz = Bt + 4Grt + 12H_2O \quad (2)$$

Reaction (1) was investigated experimentally by Hsu (1968), and (2) was proposed by Kretz (1994). Because they have negative ΔS°, most of the reactions that consume anorthite and produce grossular are retrograde reactions; the following prograde reaction is therefore possible for the appearance of grossular in the garnet zone (Crawford 1977):

$$4Zo + Qtz = Grs + 5An + 2H_20 \quad (3)$$

The following reaction (Kretz 1994) is among a few progressive reaction that result in the development of grossular from anorthite:

$$Chl + An + Qtz = Grt + 4H_2O \quad (4)$$

Staurolites constitute the largest and most abundant porphyroblasts in the central and southern parts of the study area. The poikiloblastic crystals have abundant quartz inclusions and some inclusions of biotite, that are aligned to define a preferred orientation mostly discordant with the surrounding S_2 foliation. Since the quartz inclusions are usually elongated, they are probably older grains engulfed by the growing staurolite rather than being a product of stauroiite-producing reactions (see related discussions in Carmichael 1969 p.250). In most of the staurolite porphyroblasts, the straight inclusion trails of quartz end at an inclusion-free rim, while in one thin-section, inclusion trails that are slightly curved at the rim of the crystals have been observed. Because of a high aluminum content, staurolite-producing reactions require consumption of other aluminum-rich minerals. The Al-silicates appear only in rocks that are higher in grade compared to rocks in the staurolite zone. They were either present and totally used up in the staurolite-forming reactions (see Hoschek 1969, and Spear and Cheney 1989), or reactions involving consumption of muscovite and production of biotite, similar to the next two reactions, may be proposed for this process:

$$Chl + 9Grt + 8Ms = 2St + 8Bt + 15Qtz \qquad (5)$$

$$31Chl + 41Ms = 8St + 41Bt + 33Qtz + 108H_20 \qquad (6)$$

Staurolite porphyroblasts in some samples are partially or totally replaced by muscovite crystals. Reactions (5) and (6), in a retrograde manner, seem to be responsible for the consumption of staurolite and growth of muscovite.

Chlorite is present in many samples, usually as a retrograde replacement of biotite, garnet and staurolite. Reactions (1), (2), (5) and (6), therefore, may be responsible for these retrogressions. In some kyanite- and staurolite-bearing samples, relatively large porphyroblasts of chlorite have grown on discrete biotite-rich crenulation planes of the S_2 foliation (Fig. 4.6). Cross-cutting relationships of the chlorite crystals with respect to older crystals in these samples is quite similar to that of muscovite porphyroblasts, suggesting synchronous development of these minerals through the above-mentioned reactions. This is an agreement with the presence of rutile inclusions in chlorite crystals that have grown on the biotite-rich domains. The rutile crystals probably represent concentrations of titanium left over from consumption of biotites.

Chloritoid has not been observed in metasedimentary rocks of the Pontiac Group. Parts of the Timiskaming Group, however, are rich in chloritoid, where the mineral is associated with quartz, feldspar, sericite, and carbonate minerals.

Kyanite porphyroblasts overgrow the crenulated S_1 foliation. Inclusion trails of quartz in poikiloblastic crystals of this mineral, unlike trails in staurolite porphyroblasts, are usually sigmoidal (Fig. 3.13). This relationship, which is observed in individual thin-sections, provides evidence for timing of foliation development with respect to the metamorphic events. The staurolites have grown during and/or after development of S_1 foliation, but before D_2, whereas kyanite crystals have grown during and/or after crenulation of S_1, presumably during

D_2, when staurolite growth had apparently ceased. In other words, staurolite is the last prograde metamorphic mineral that records D_1, and S_1 has developed at a lower metamorphic grade compared to S_2, which is considered to be syn-peak metamorphic. Garnet, as inclusions in kyanite, is common, which may indicate their involvement in the kyanite-producing reactions. The kyanite porphyroblasts are usually close to staurolite; moreover, staurolites are a possible source for the aluminum required for the growth of kyanite. Reactions similar to (7), (8) and (9) may provide a good approximation for consumption of the staurolite and production of kyanite (coefficients are balanced using the formulae from Table 4.2).

$$6St + 17Grt + 25Ms = 96Als + 25\,Bt + 12H_2O \qquad (7)$$

$$6St + 8Ms + 17Qtz = 62Als + 8Bt + 12H_2O \qquad (8)$$

$$6St + 25Qtz = 46Als + 8Grt + 12H_2O \qquad (9)$$

Sillimanite in samples from the metasedimentary rocks are of the fibrolite type; no prismatic sillimanite was observed in any thin-section. Although growth patterns of the fibrolite are very diverse, they have mostly developed on biotite crystals (Fig. 4.7), so that they seem to have grown at the expense of those crystals. Needles of fibrolite are also common within quartz grains. Relatively low aluminum content of biotite and immobility of this element compared to other elements, makes explanation of the growth of the fibrolite on biotite troublesome. Carmichael (1969) tried to overcome this difficulty in rocks with similar composition and microstructures to those in present study area, by proposing reactions that involve ions as well as minerals, and used some of them as intermediates for others to change from biotite into sillimanite. From study of the textures of individual thin-sections, he deduced a set of metasomatic cation-exchange reactions, which proceed in different microscopic domains of the rock, but which add up on the scale of the whole thin-section to give a balanced metamorphic reaction.

In staurolite-rich samples from the study area, fibrolite has grown on biotite close to staurolite porphyroblasts, suggesting reactions similar to reactions (7), (8) and (9), during

Fig. 4.6. Overgrowth of chlorite (bundle of steeply inclined crystals near centre) on S_2 foliation. Cross-polarized light.

Fig. 4.7. Fibrolite developed on biotite crystals within S_2 foliation close to a staurolite crystal. Plane-polarized light.

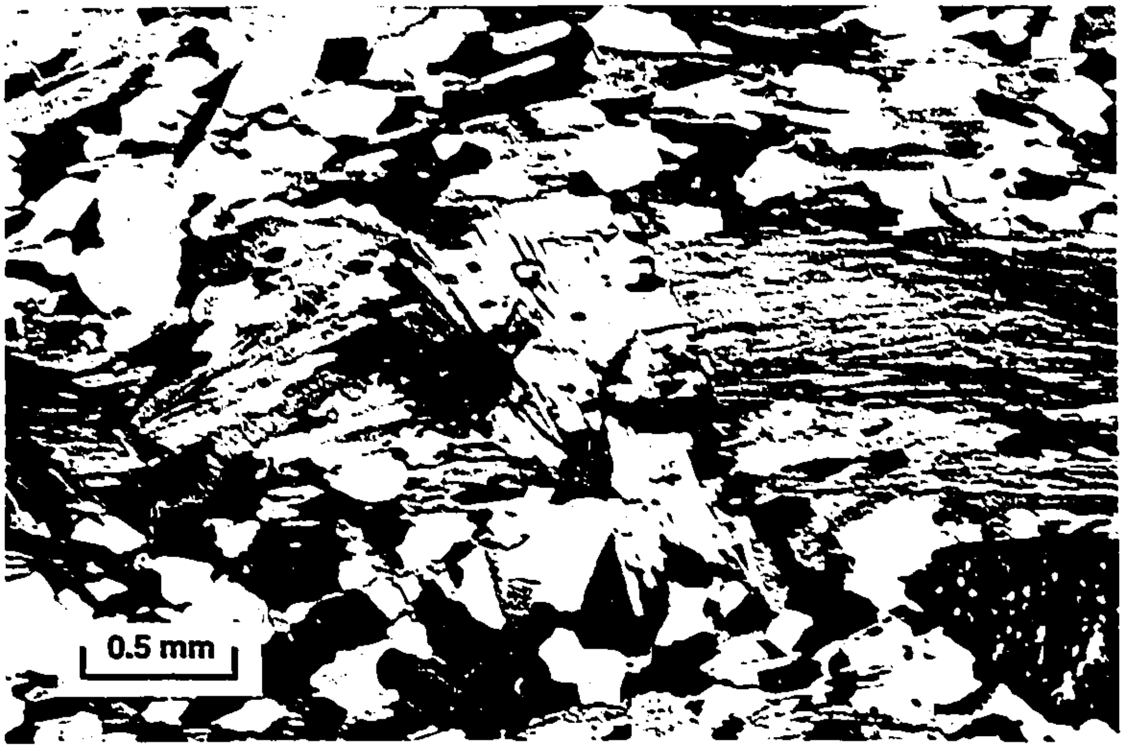
0.5 mm

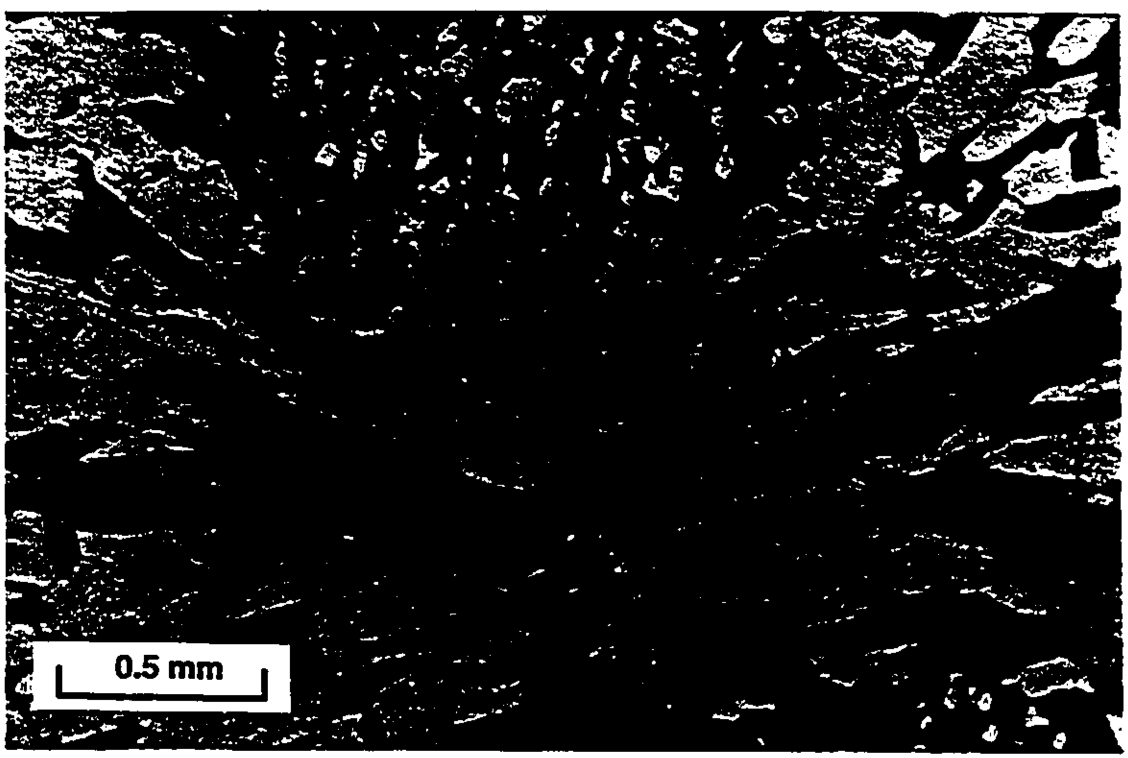
0.5 mm

which less mobile aluminum ions have traveled short distances to produce sillimanite on biotite crystals that have served as a substrate for them. Growth of fibrolite on muscovite and kyanite (Fig. 4.8) is common in the samples, suggesting reactions (10) and (11):

$$Ky = Sil \tag{10}$$

A sample from an outcrop about 30 km south of the southern border of the study area, northwest of Angliers, indicates production of fibrolite at the expense of muscovite. The fibrolite has grown on the muscovite porphyroblasts with no sign of kyanite, staurolite, or garnet in either thin-section or outcrop. K-feldspar has been detected through staining of the sample. An appropriate reaction for this case would therefore be (after Harker 1932):

$$Ms + Qtz = Kf + Sil + H_2O \tag{11}$$

Quartz crystals towards the southern part of the study area occur as coarser grains due to annealing recrystallization under high temperature conditions, as indicated by straight grain boundaries between the crystals joining at approximately 120°, reflecting textural equilibrium.

Biotite is disappeared in the rocks that may be considered as a transition between the metasedimentary rocks of the Pontiac Group and the S-type granites. These rocks, that may be called migmatites, preserve a rough pattern of the foliation within metasedimentary rocks of the sillimanite zone, but are extensively recrystallized, and have a granitic appearance. Reaction (12) may be written for the disappearance (after Hodges and Crowley 1985).

$$Bt + 2Sil + Qtz = Ms + Grt \tag{12}$$

North of Saint Roch, large nests of sillimanite are present within the Decelles granitic rocks. Reactions involved in melting of the metasedimentary rocks of the Pontiac Group may be summarized as below (from Yardley 1989):

$$Ms + Qtz + H_2O = Sil + melt \tag{13}$$

$$Ms + Bt + Qtz + H_2O = Sil + melt \tag{14}$$

$$Ms + Qtz = Kf + Sil + melt \tag{15}$$

Fig. 4.8. Growth of fibrolite on, and partly at the expense of kyanite. Plane-polarized light.

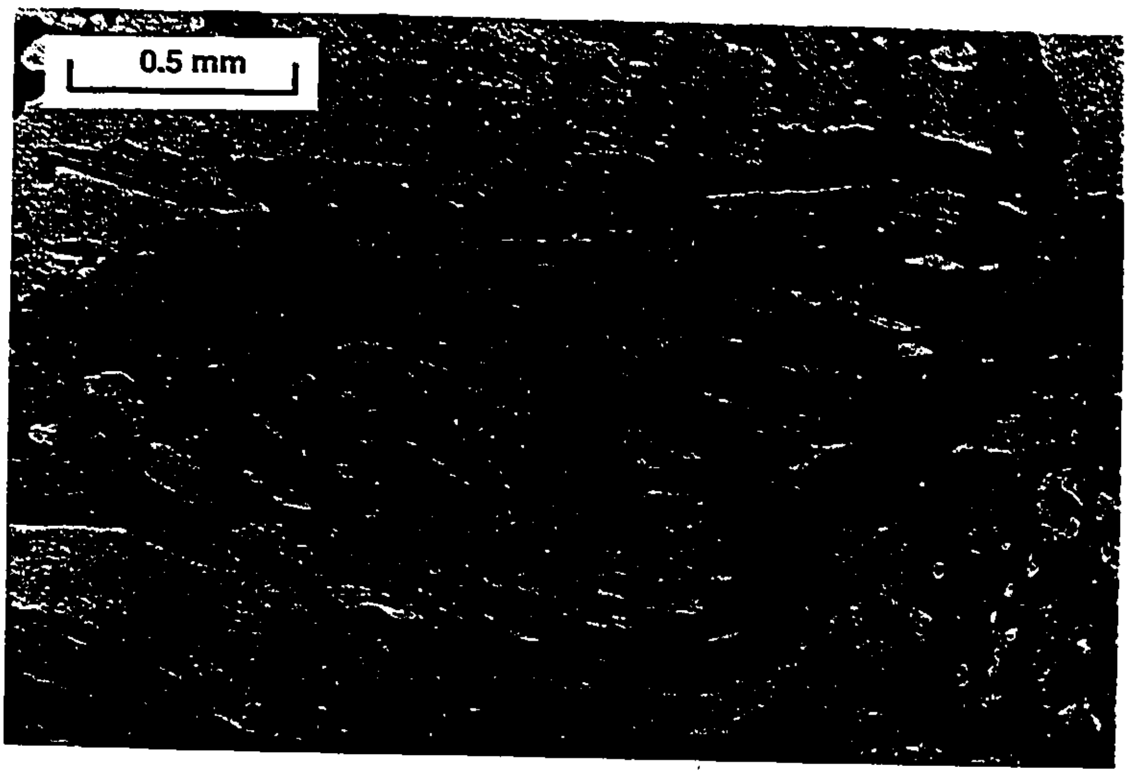
0.5 mm

A recrystallization process seems to be responsible for growth of plagioclases in the fine-grained metasediments of the northern part of the study area during metamorphism. The porphyroblasts of plagioclase have a poikiloblastic texture (small biotite inclusions). Preferred orientation of the biotite inclusions is generally discordant with respect to external S_2 foliation.

Tourmaline usually appears in metasedimentary samples all the way from the biotite into sillimanite zones. Relatively small crystals of this mineral are usually associated with biotites, and concentric change in their colour may represent chemical zoning.

4.4. Mineral compositions

Minerals used in the study of variations in mineral compositions, and the thermobarometry estimations, were analyzed using the electron microprobe. Some crystals of garnet, biotite and staurolite were analyzed at different points to determine if they are zoned. Zoned crystals can be thought of as a chemical tape recorder in which the history of crystallization is recorded. The reason for studying zoned crystals is that they may hold a key to understanding the chemical reaction history of a sample, and hence its P-T history (Spear 1993).

4.4.1. Minerals from the metasedimentary rocks

To assess variations of the mineral compositions at progressively higher metamorphic conditions, compositions of different minerals in the biotite, garnet, staurolite, kyanite, and sillimanite zones have been compared (Table 4.3).

The average composition of biotite within the metasedimentary rocks is almost midway between phlogopite and annite, their atomic Mg content being slightly higher than that of Fe. Profiles, across the crystals, show an increase in Fe/Fe+Mg ratio from core to rim.

Except for an unusually high value in a sample from the garnet zone, the Fe/Fe+Mg (Fe represents total Fe) ratio of biotite shows a regular increase from lower to higher grade rocks in the metasedimentary rock samples (see Table 4.3). Excluding the same sample from

Table 4.3. Representative compositions from electron microprobe analyses of minerals (in metasedimentary rocks) from different metamorphic zones within northwestern Pontiac Subprovince.

Biotite

Sample No:	BT68	BT2	BT1	BT34	BT41
Metamorphic zone	Biotite	Garnet	Staurolite	Kyanite	Sillimanite
SiO_2	37.91	36.54	36.98	35.42	36.28
Al_2O_3	18.85	19.36	20.13	19.76	20.19
TiO_2	1.72	1.41	1.51	1.51	1.58
Cr_2O_3	0.05	0.13	0.12	0.00	0.06
FeO	16.31	18.61	16.56	16.73	16.69
MnO	0.06	0.22	0.07	0.10	0.02
MgO	12.24	11.33	11.83	11.32	11.00
CaO	0.08	0.00	0.00	0.04	0.06
K_2O	9.84	9.33	9.56	9.29	9.08
Na_2O	0.00	0.00	0.00	0.73	0.34
Cl	0.00	0.02	0.04	0.00	0.00
Total	97.06	96.95	96.8	94.90	95.30
Formula (basis 22 atoms of oxygen)					
Si	5.577	5.425	5.439	5.349	5.420
[4]Al	2.443	2.575	2.561	2.651	2.580
[6]Al	0.813	0.813	0.928	0.865	0.976
Ti	0.190	0.158	0.167	0.172	0.178
Cr	0.006	0.015	0.014	0.000	0.007
Fe	1.999	2.311	2.037	2.113	2.086
Mn	0.007	0.028	0.008	0.013	0.002
Mg	2.674	2.507	2.594	2.549	2.450
Ca	0.013	0.000	0.000	0.007	0.010
K	1.839	1.768	1.793	1.790	1.730
Na	0.000	0.000	0.000	0.213	0.097
Cl	0.000	0.006	0.009	0.000	0.000
Fe/Fe+Mg	0.428	0.480	0.440	0.453	0.460

Fe denotes total iron as Fe^{2+}

Muscovite

Sample No:	MS3	MS17	MS48	MS25	MS44
Metamorphic zone	Staurolite	Kyanite	Kyanite	Sillimanite	Sillimanite
SiO_2	46.23	46.97	46.58	46.70	46.98
Al_2O_3	37.07	36.87	35.55	36.70	36.01
TiO_2	0.15	0.44	0.27	0.59	0.27
Cr_2O_3	0.11	0.11	0.09	0.04	0.11
FeO	0.95	0.91	1.85	1.18	1.03
MnO	0.06	0.00	0.03	0.03	0.02
MgO	0.28	0.27	0.30	0.12	0.39
CaO	0.12	0.13	0.16	0.14	0.14
K_2O	9.18	9.59	9.30	9.56	9.19
BaO	0.69	0.40	0.68	0.33	0.46
Na_2O	1.25	1.23	1.52	0.83	1.07
Cl	0.00	0.00	0.00	0.00	0.00
Total	96.09	96.92	96.33	96.31	95.67
Formula (basis 22 atoms of oxygen)					
Si	6.087	6.126	6.159	6.126	6.194
[4]Al	1.913	1.874	1.841	1.874	1.806
[6]Al	3.841	3.793	3.700	3.800	3.790
Ti	0.015	0.043	0.027	0.058	0.027
Cr	0.011	0.011	0.009	0.004	0.012
Fe	0.105	0.099	0.204	0.130	0.114
Mn	0.007	0.000	0.003	0.003	0.002
Mg	0.054	0.053	0.059	0.041	0.077
Ca	0.017	0.018	0.023	0.019	0.020
K	1.543	1.595	1.569	1.599	1.546
Ba	0.036	0.021	0.035	0.017	0.024
Na	0.319	0.312	0.390	0.210	0.275
Cl	0.000	0.000	0.000	0.000	0.000

Chlorite

Sample No:	CH68	CH2	CH1	CH34	CH41
Metamorphic zone	Biotite	Garnet	Staurolite	Kyanite	Sillimanite
SiO_2	25.48	26.63	25.4	25.16	25.31
Al_2O_3	23.27	22.63	24.22	23.93	24.06
TiO_2	0.14	0.07	0.13	0.14	0.12
Cr_2O_3	0.40	0.32	0.16	0.20	0.17
FeO	21.48	20.39	21.84	23.24	22.08
MnO	0.31	0.24	0.17	0.26	0.29
MgO	18.42	18.67	17.71	17.89	18.47
CaO	0.00	0.04	0.03	0.06	0.00
K_2O	0.00	0.04	0.00	0.01	0.00
Cl	0.00	0.00	0.00	0.00	0.00
Total	89.50	89.03	89.66	90.89	90.50
Formula (basis 28 atoms of oxygen)					
Si	5.153	5.369	5.122	5.052	5.070
[4]Al	2.847	2.631	2.878	2.948	2.930
[6]Al	2.700	2.745	2.880	2.715	2.751
Ti	0.021	0.011	0.019	0.021	0.018
Cr	0.063	0.050	0.025	0.031	0.027
Fe	3.632	3.437	3.684	3.902	3.699
Mn	0.053	0.041	0.029	0.044	0.049
Mg	5.551	5.610	5.325	5.354	5.514
Ca	0.000	0.009	0.007	0.012	0.000
K	0.000	0.010	0.000	0.002	0.000
Cl	0.000	0.000	0.000	0.000	0.000
Fe/Fe+Mg	0.395	0.380	0.409	0.422	0.402

Table 4.3. Continued.

Garnet

Sample No:	GT2	GT1	GT34	GT41
Metamorphic zone	Garnet	Staurolite	Kyanite	Sillimanite
SiO_2	37.49	37.79	36.8	37.70
Al_2O_3	21.28	21.36	21.24	21.76
TiO_2	0.05	0.07	0.05	0.00
FeO	28.75	29.16	30.49	30.51
MnO	7.90	5.25	4.74	4.54
MgO	2.16	2.44	3.37	3.68
CaO	3.32	5.20	2.85	3.13
Total	100.95	101.27	99.6	101.32
Formula (basis 24 atoms of oxygen)				
Si	5.990	5.987	5.931	5.950
$^{[4]}Al$	0.010	0.013	0.069	0.050
$^{[6]}Al$	3.999	3.975	3.967	3.998
Ti	0.006	0.008	0.007	0.000
Fe	3.841	3.864	4.109	4.027
Mn	1.070	0.704	0.647	0.607
Mg	0.515	0.575	0.809	0.866
Ca	0.569	0.882	0.493	0.529
Fe/Fe+Mg	0.8818	0.8705	0.8355	0.8230

Staurolite

Sample No:	ST1	ST34	ST41
Metamorphic zone	Staurolite	Kyanite	Sillimanite
SiO_2	27.96	27.87	28.10
Al_2O_3	54.34	53.43	54.99
TiO_2	0.70	0.54	0.54
FeO	12.84	13.04	13.03
MnO	0.37	0.34	0.30
MgO	1.72	2.01	1.58
ZnO	0.37	0.22	0.22
Total	98.3	97.45	98.76
Formula (basis 46 atoms of oxygen)			
Si	7.704	7.753	7.699
Al	17.651	17.519	17.755
Ti	0.146	0.112	0.112
Fe	2.959	3.034	3.047
Mn	0.086	0.079	0.069
Mg	0.705	0.833	0.902
Zn	0.074	0.045	0.045
Fe/Fe+Mg	0.8076	0.7846	0.7716

Kyanite and sillimanite

Sample No:	KT34	KT44	SL44
Metamorphic zone	Kyanite	Sillimanite	Sillimanite
SiO_2	37.36	38.22	37.30
TiO_2	0.00	0.00	0.17
Al_2O_3	62.63	61.69	58.36
FeO	0.24	0.21	1.99
MnO	0.03	0.00	0.02
MgO	0.16	0.34	1.45
ZnO	0.02	0.07	0.00
Total	100.13	100.53	99.29
Formula (basis 20 atoms of oxygen)			
Si	4.031	4.104	4.102
Ti	0.000	0.000	0.014
Al	7.924	7.809	7.564
Fe	0.022	0.019	0.183
Mn	0.003	0.000	0.002
Mg	0.026	0.054	0.237
Zn	0.001	0.005	0.000

Plagioclase

Sample No:	PL68	PL2	PL1	PL34	PL41
Metamorphic zone	Biotite	Garnet	Staurolite	Kyanite	Sillimanite
SiO_2	62.67	62.50	62.31	61.85	61.00
Al_2O_3	24.21	23.61	24.63	23.96	24.39
K_2O	0.99	0.04	0.29	0.00	0.03
CaO	3.29	4.77	5.38	5.49	5.95
Na_2O	8.99	8.44	8.14	8.63	8.39
FeO	0.18	0.17	0.20	0.11	0.04
Total	100.33	99.53	100.95	100.04	99.80
Formula (basis 20 atoms of oxygen)					
Si	5.535	5.549	5.472	5.486	5.432
Al	2.521	2.471	2.550	2.505	2.560
K	0.112	0.004	0.033	0.000	0.003
Ca	0.311	0.454	0.506	0.521	0.568
Na	1.539	1.453	1.386	1.485	1.448
Fe	0.013	0.013	0.015	0.008	0.003
Ca/Ca+Na+K	0.159	0.238	0.263	0.260	0.281

Fe denotes total iron as Fe^{2+}

the garnet zone, the potassium contents of the biotites appear to decrease from lower grade rocks to higher grade rocks. Wet chemical analyses of mineral separates of biotites from five samples of metasedimentary rocks, indicate Fe^{2+}/Fe-total ratios between 95 and 99 percent (Table 4.5).

Garnets both in metasedimentary and metavolcanic rocks are close to the almandine end-member (Tables 4.3 and 4.4). Calcium contents of garnets from the metavolcanic rocks, however, are higher relative to garnets from the metasedimentary rocks. Microprobe analyses of points midway between core and rim of the garnet crystals show a decrease in Fe/Fe+Mg ratio from lower to higher grade samples. The calcium content of the garnet crystals does not show a regular increasing or decreasing pattern, but manganese shows a rather regular decrease towards higher grade rocks.

Several garnet crystals from different samples were examined for chemical zoning (Table 4.6). From 26 garnet crystals selected for this investigation, 18 show an increase, and 5 show a decrease in Fe/Fe+Mg ratio from core to rim. Three other crystals show little change in this ratio. With regard to calcium content, 19 crystals show a decrease, and 7 crystals show an increase. Fifteen garnets show a negative correlation between trend of change in Fe and Ca content from core to rim of the crystals. Three different garnet crystals in sample JL34 from the kyanite zone show different zoning patterns for calcium. Two of them show a decrease in calcium content from core to rim (crystals number 1 and 2); the other one shows a reverse pattern (crystal number 3). This may represent two different generations of garnet in the same sample, the first generation having crystallized during prograde (crystal number 3), and second generation during retrograde metamorphism (crystals number 1 and 2). The manganese content of the crystals generally increases towards the rims.

Through study of zonation within garnets from different metamorphic grades, Yardley (1977) suggested that garnets which homogenize by diffusion commonly have margins enriched in Mn, which he has interpreted as a retrograde phenomenon. He also suggested that elimination of zoning for grains 1-2 mm in diameter occurs at about 640°C±30°C. If true, most

Table 4.4. Representative compositions from electron microprobe analyses of minerals in metavolcanic and igneous rocks within northwestern Pontiac Subprovince.

Biotite

Sample No:	BT19	BT22	BT90	BT96	BT97
Rock type	Monzonite	Lamprophyre	Metavolcanic	Metavolcanic	Metavolcanic
SiO_2	36.78	37.66	35.43	34.52	34.74
Al_2O_3	15.38	16.05	17.27	17.09	17.24
TiO_2	2.40	2.19	1.89	2.21	2.74
Cr_2O_3	0.11	0.11	0.03	0.01	0.09
FeO	19.72	13.80	23.51	23.64	21.83
MnO	0.25	0.22	0.28	0.15	0.08
MgO	11.89	15.10	8.66	8.59	9.50
CaO	0.01	0.08	0.19	0.10	0.09
K_2O	8.95	9.64	9.20	8.62	9.06
Na_2O	0.16	0.09	0.00	0.13	0.20
Cl	0.04	0.01	0.00	0.00	0.00
Total	95.69	94.95	96.46	95.06	95.97
Formula (basis 22 atoms of oxygen)					
Si	5.588	5.610	5.445	5.385	5.355
$^{[4]}Al$	2.412	2.390	2.555	2.615	2.645
$^{[6]}Al$	0.342	0.428	0.573	0.527	0.487
Ti	0.274	0.245	0.219	0.260	0.317
Cr	0.013	0.013	0.004	0.001	0.011
Fe	2.505	1.720	3.022	3.084	2.814
Mn	0.032	0.028	0.037	0.020	0.010
Mg	2.694	3.353	1.983	1.997	2.183
Ca	0.002	0.013	0.031	0.017	0.015
K	1.734	1.833	1.805	1.716	1.782
Na	0.048	0.027	0.000	0.041	0.059
Cl	0.010	0.003	0.000	0.000	0.000
Fe/Fe+Mg	0.482	0.339	0.604	0.607	0.563

Fe denotes total iron as Fe^{2+}

Garnet

Sample No:	GT90	GT96	GT97	GT112
Rock type	Metavolcanic	Metavolcanic	Metavolcanic	Metavolcanic
SiO_2	37.72	37.42	37.74	37.77
Al_2O_3	20.75	21.18	21.16	20.47
TiO_2	0.11	0.15	0.17	0.21
FeO	28.22	28.83	28.79	19.78
MnO	6.77	3.72	3.87	7.08
MgO	1.20	1.37	1.83	0.90
CaO	6.17	7.98	7.10	13.37
Total	100.94	100.65	100.66	99.58
Formula (basis 24 atoms of oxygen)				
Si	6.034	5.973	6.005	6.033
$^{[4]}Al$	0.000	0.027	0.000	0.000
$^{[6]}Al$	3.912	3.958	3.968	3.855
Ti	0.013	0.018	0.020	0.025
Fe	3.776	3.849	3.831	2.643
Mn	0.917	0.503	0.521	0.958
Mg	0.286	0.325	0.434	0.213
Ca	1.058	1.365	1.211	2.288
Fe/Fe+Mg	0.930	0.922	0.898	0.925

Table 4.4. Continued.

Amphibole

Sample No:	HB18	HB19	HB116	HB22
Rock type	Monzonite	Monzonite	Syenite	Lamprophyre
SiO_2	51.30	48.66	47.44	53.10
Al_2O_3	4.72	6.62	5.58	3.37
TiO_2	0.24	0.44	0.38	0.08
Cr_2O_3	0.00	0.00	0.00	0.00
FeO	13.94	16.08	18.66	9.43
MnO	0.25	0.28	0.40	0.30
MgO	14.94	12.84	12.05	17.50
CaO	12.17	12.32	11.46	12.89
K_2O	0.43	0.55	0.59	0.12
Na_2O	0.88	0.96	1.43	0.35
Total	98.87	98.75	97.99	97.14
Formula (basis 23 atoms of oxygen)				
Si	7.393	7.129	7.120	7.598
$^{[4]}Al$	0.607	0.871	0.880	0.402
$^{[6]}Al$	0.195	0.273	0.107	0.166
Ti	0.026	0.049	0.043	0.009
Cr	0.000	0.000	0.000	0.000
Fe	1.680	1.970	2.343	1.129
Mn	0.031	0.034	0.051	0.036
Mg	3.208	2.803	2.695	3.732
Ca	1.879	1.934	1.843	1.977
K	0.079	0.103	0.112	0.023
Na	0.245	0.272	0.416	0.097
Fe/Fe+Mg	0.3437	0.4127	0.4651	0.2323

Fe denotes total iron as Fe^{2+}

Amphibole

Sample No:	HB90	HB96	HB97	HB112
Rock type	Meavolcanic	Meavolcanic	Meavolcanic	Meavolcanic
SiO_2	40.40	41.82	39.63	40.07
Al_2O_3	14.87	13.40	14.91	15.59
TiO_2	0.40	0.72	0.61	0.38
Cr_2O_3	0.00	0.00	0.00	0.00
FeO	22.25	19.56	23.07	20.75
MnO	0.61	0.26	0.36	0.48
MgO	6.00	8.25	5.84	5.80
CaO	11.14	11.57	11.29	11.89
K_2O	0.62	0.58	0.78	1.21
Na_2O	1.68	1.35	1.38	0.97
Total	97.97	97.51	97.87	97.14
Formula (basis 23 atoms of oxygen)				
Si	6.205	6.355	6.127	6.180
$^{[4]}Al$	1.795	1.645	1.873	1.820
$^{[6]}Al$	0.897	0.756	0.843	1.014
Ti	0.047	0.082	0.071	0.045
Cr	0.000	0.000	0.000	0.000
Fe	2.859	2.485	2.983	2.676
Mn	0.080	0.034	0.047	0.062
Mg	1.375	1.869	1.346	1.334
Ca	1.834	1.883	1.870	1.964
K	0.122	0.112	0.154	0.237
Na	0.500	0.397	0.415	0.291
Fe/Fe+Mg	0.6752	0.5707	0.6891	0.6673

Table 4.5. Comparison of wet chemical (ferrous iron) and electron microprobe (total iron) of biotite from metasedimentary rock samples.

Sample No.	JL7	JL34	JL39	JL41	JL44
%FeO WA	16.05	16.54	17.45	16.19	15.93
%FeO (total) MA	16.97	16.73	17.62	16.69	16.48

WA: wet chemical analyses MA: electron microprobe analyses

Table 4.6. Compositional zoning within the garnet crystals from metasedimentary rocks of Pontiac Group. Elements are normalized on the basis of a 24 oxygen atoms formula.

Sample No.	PM123			PM35		
Crystal No.	one			one		
Position	core	mid	rim	core	mid	rim
Fe	4.124	4.301	4.309	3.852	3.927	3.808
Mn	0.605	0.525	0.580	0.825	0.943	1.258
Mg	0.619	0.672	0.670	0.620	0.521	0.439
Ca	0.661	0.565	0.479	0.536	0.599	0.485
Total	6.009	6.063	6.038	5.833	5.990	5.990
Fe/Fe+Mg	0.869	0.865	0.865	0.861	0.883	0.897
Ca/Fe+Mg+Mn+Ca	0.110	0.093	0.079	0.092	0.100	0.081

Sample No.	JL3					
Crystal No.	one			two		
Position	core	mid	rim	core	mid	rim
Fe	4.259	4.418	4.455	4.269	4.322	4.392
Mn	0.587	0.567	0.660	0.491	0.511	0.587
Mg	0.701	0.804	0.619	0.773	0.780	0.746
Ca	0.466	0.311	0.284	0.471	0.426	0.321
Total	6.013	6.100	6.018	6.004	6.039	6.046
Fe/Fe+Mg	0.859	0.846	0.878	0.847	0.847	0.855
Ca/Fe+Mg+Mn+Ca	0.077	0.051	0.047	0.078	0.071	0.053

Sample No.	JL34							
Crystal No.	one			two				
Position	core	mid	rim	rim	mid	core	mid	rim
Fe	4.105	4.074	4.141	4.128	4.127	4.115	4.109	4.170
Mn	0.575	0.602	0.763	0.609	0.547	0.581	0.647	0.829
Mg	0.736	0.832	0.677	0.758	0.842	0.822	0.809	0.583
Ca	0.550	0.529	0.438	0.522	0.529	0.513	0.493	0.395
Total	5.966	6.037	6.019	6.017	6.045	6.031	6.058	5.977
Fe/Fe+Mg	0.848	0.830	0.859	0.845	0.831	0.834	0.836	0.877
Ca/Fe+Mg+Mn+Ca	0.092	0.088	0.073	0.087	0.088	0.085	0.081	0.066

Sample No.	JL34						
Crystal No.	three						
Position	rim	mid	mid	core	mid	mid	rim
Fe	4.110	4.110	4.253	4.269	4.270	4.179	4.091
Mn	0.874	0.625	0.586	0.590	0.606	0.730	0.798
Mg	0.604	0.803	0.870	0.894	0.799	0.764	0.663
Ca	0.406	0.367	0.310	0.285	0.347	0.325	0.443
Total	5.994	5.905	6.019	6.038	6.022	5.998	5.995
Fe/Fe+Mg	0.872	0.837	0.830	0.827	0.842	0.845	0.861
Ca/Fe+Mg+Mn+Ca	0.068	0.062	0.052	0.047	0.058	0.054	0.074

Sample No.	JL44					
Crystal No.	one			two		
Position	core	mid	rim	core	mid	rim
Fe	4.099	3.316	4.044	4.032	4.051	4.065
Mn	0.710	0.575	0.877	0.630	0.673	0.781
Mg	0.793	0.742	0.676	0.849	0.840	0.778
Ca	0.436	0.330	0.400	0.528	0.421	0.428
Total	6.038	4.963	5.997	6.039	5.985	6.052
Fe/Fe+Mg	0.838	0.817	0.857	0.826	0.828	0.839
Ca/Fe+Mg+Mn+Ca	0.072	0.066	0.067	0.087	0.070	0.071

Sample No.	JL14				
Crystal No.	one				
Position	rim	mid	mid	mid	core
Fe	4.206	4.135	4.181	4.105	3.891
Mn	0.856	0.748	0.777	0.769	0.727
Mg	0.725	0.830	0.824	0.824	0.809
Ca	0.308	0.269	0.315	0.312	0.310
Total	6.095	5.982	6.097	6.010	5.737
Fe/Fe+Mg	0.853	0.833	0.835	0.833	0.828
Ca/Fe+Mg+Mn+Ca	0.051	0.045	0.052	0.052	0.054

garnets from the present study have not undergone diffusion that may have resulted in homogenization of the crystals because maximum temperature estimates for the rock samples within the study area are about 630°C (see section 4.5). However, enrichment in Mn at the rims of most garnet crystals may indicate that they developed during the retrograde part of the P-T path. Based on his studies Kretz (personal communication) suggests that Mn enrichment at margins of garnet is very common in not homogenized crystals as well. He further attributes Mn reversal in garnet crystals to delayed Mn-(Mg,Fe) exchange with biotite, and not to a retrograde reaction.

Staurolites are rich in iron relative to magnesium (see Table 4.3), and iron generally shows an increase in concentration from centre to rims of the crystals. Distribution of iron, magnesium and manganese in staurolite samples from different zones indicates that Fe/Fe+Mg ratios and manganese content s decreases towards the sillimanite zone.

Figure 4.9 illustrates various mineral associations and their compositions in biotite, garnet, staurolite, kyanite and sillimanite zones through AFM diagrams. Boundary curves for mineral-forming reactions that possibly occurred are shown in Fig. 4.10. These univariant boundaries represent model reactions; under natural conditions they would be more complex. These boundaries are plotted on the basis of experimental data (see captions in Fig. 4.10 for references). The boundary curves do not agree with the garnet-biotite thermometry results for the representative samples from different metamorphic zones. Most of the boundary curves in the diagram must be shifted to the left to encompass samples with present compositions. The reason possibly lies with differences between the activity of the mineral components and water in experimental assemblages, the basis for construction of the boundary curves, and natural assemblages from the study area. Most of the experiments have been carried out with almost pure mineral end-members, and with the activity of water being very close to one. A decrease in activity of water from 1 to 0.5 at about 5 kbar would result in a shift of boundary curves of between 80°C and 130°C to the left (Fig. 9 in Hoschek 1969).

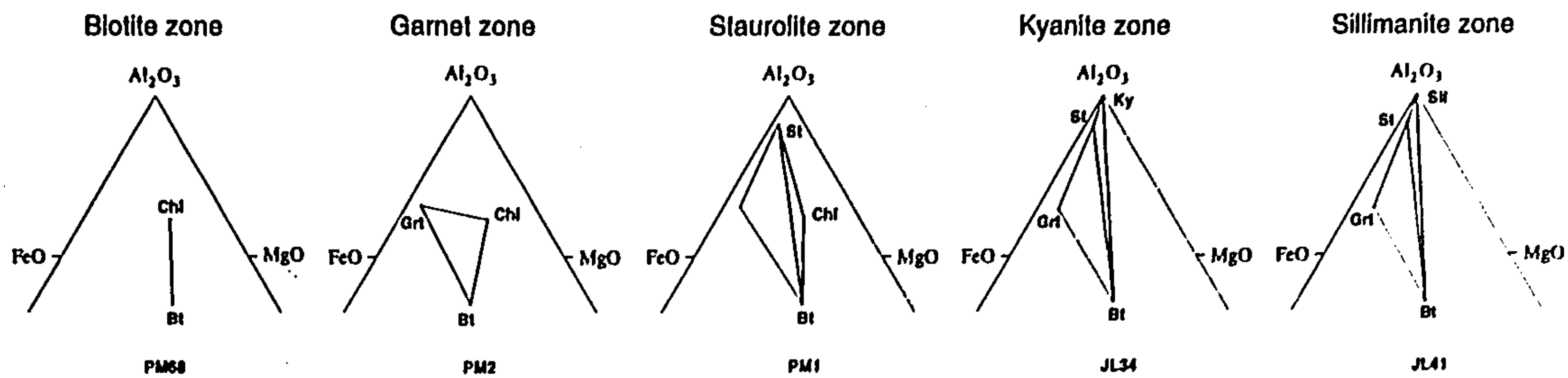

Fig. 4.9. AFM diagrams showing the various mineral associations and their compositions within different metamorphic zones of the study area. Sample numbers are shown below the diagrams.

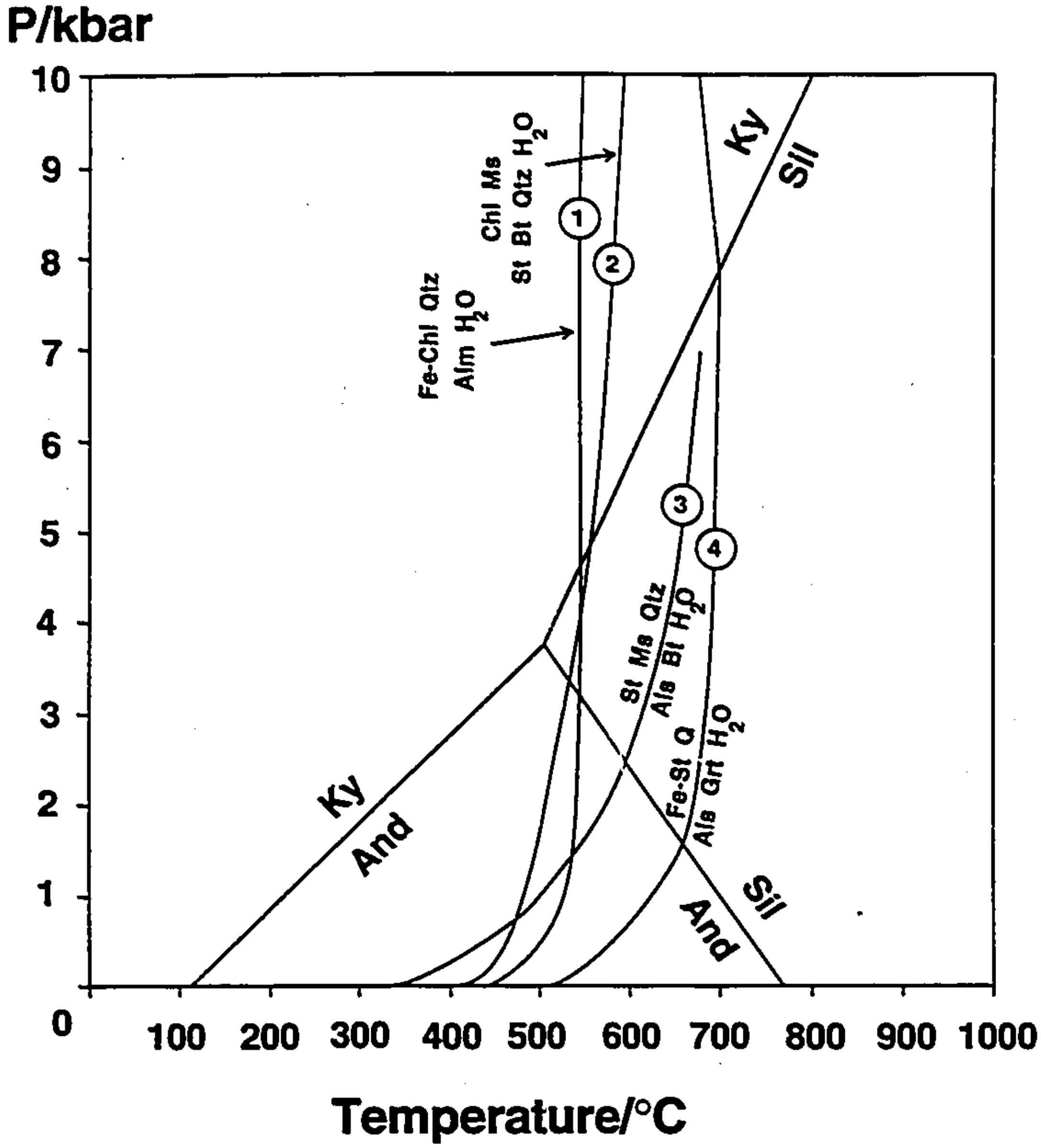

Fig. 4.10. Boundary curves postulated to be responsible for variation of mineral assemblages of metasedimentary rocks within different metamorphic zones of the study area. References for the boundary curves are: 1) Hsu (1968); 2) Hoschek (1969); 3) Hoschek (1969); 4) Richardson (1968), kyanite domain part of the curve is from Ganguly (1972), and Dutrow and Holdaway (1989); aluminum silicate boundary curves are from Holdaway (1971). Both Fe- and Mg-rich chlorite were used as starting material for reaction 2; Mg/Mg+Fe ratios of the staurolite and biotite involved in reaction 3 are 0.17 and 0.48 respectively.

Iron and magnesium contents of the kyanite are low, but analyses of fibrolite crystal aggregates, which have grown on biotite substrates, show a considerable amount of iron and magnesium. This is, in most part, due to the presence of these elements in the biotite that is the background for the fibrolite crystals (see Table 4.3).

Plagioclase from the metasedimentary rocks has an average composition of oligoclase, with very small departures from this norm (see Table 4.3). This uniformity in composition along with the presumption that plagioclase crystals were originally detrital, and therefore might had various compositions, indicate that an equilibrium state of chemical composition between the plagioclase and other minerals occurred during metamorphism of the sedimentary rocks. Anorthite content of the plagioclases increases towards the higher grade rocks (see Table 4.3). This is not in agreement with the fractional crystallization model of Spear *et al.* (1991), whereby "over most P-T paths as garnet grows, plagioclase must be consumed and it must become more albitic". Crystallization of garnet is not the only process that affects anorthite content of the plagioclases in the pelitic rocks. Other reactions such as the crystallization of paragonite or muscovite may change the composition of plagioclase in these rocks. Moreover, if one assumes that the only process affecting plagioclase composition is the crystallization of garnet, negative enthalpy of anorthite breakdown reaction (reactions 2 and 3 in Table 4.7) requires that over most P-T paths consumption of grossular component of garnets must result in enrichment of plagioclases in anorthite component (present study).

4.4.2. Minerals from the metavolcanic and igneous rocks

Biotites from the metavolcanic rocks, unlike those from the metasedimentary rocks, are closer to the annite end-member. Titanium content is higher in biotites from the metavolcanic rocks (Table 4.4) compared to biotites from the metasedimentary rocks. The difference is probably due to different compositions of the protoliths.

Table 4.7. Equilibria reactions used in thermobarometry calculations. Assemblages on the left are stable on the high side of the P-axis variable, or the high side of the T-axis variable for sub-vertical reaction boundaries. ΔS° (J K^{-1}) and ΔV° (J bar^{-1}) at (298,1) were calculated using the thermodynamic database of Berman (1988, 1991).

	Reactions for metasedimentary rocks:	ΔS°	ΔV°
1)	phl + alm = ann + prp	-13.3	-0.31
2)	grs + Qtz + 2Sil = 3an	-112.1	-5.45
3)	grs + Qtz + 2Ky = 3an	-139.1	-6.59
4)	alm + Ms = 2Sil + Qtz + ann	-21.2	-2.12
5)	alm + Ms = 2Ky + Qtz + ann	5.8	-0.98
6)	alm + grs + Ms = 3an + ann	-133.3	-7.57
7)	prp + grs + Ms = 3an + phl	-120.1	-7.26
8)	prp + Ms = phl + Qtz + 2Sil	-8.0	-1.81
9)	prp + Ms = phl + Qtz + 2Ky	19.0	-0.67
10)	6St + 48Qtz + 23grs = 8alm + 69an + 12W	-4906.7	-121.92
11)	6St + 48Qtz + 23grs + 8phl = 8ann + 69an + 8prp + 12W	-5012.9	-124.41

Table 4.7. Continued.

	Reactions for metavolcanic rocks:	ΔS°	ΔV°
1)	3Prg + 18Qtz + phl + 2grs + alm = 3ab +ann + 6an + 3Tr	-199.6	-14.19
2)	3Prg + 18Qtz + prp + 2grs = 3ab + 6an + 3Tr	-186.4	-13.88
3)	3Tr + 5ann = 5phl + 3FeAct	-87.3	-0.78
4)	4ann + 3Prg = 3FePrg + 4phl	-99.0	-0.29
5)	alm + phl = prp + ann	-13.3	-0.31
6)	15Prg + 90Qtz + 10grs + 5alm = 15ab + 30an + 12Tr + 3FeAct	-1085.5	-71.73
7)	3Prg + 18Qtz + 2grs + 4ann + alm = 3ab + 6an + 4phl + 3FeAct	-286.9	-14.97
8)	15Prg + 72Qtz + 8grs + 4alm = 12ab + 24an + 12Tr + 3FePrg	-897.6	-57.05
9)	3 FePrg + 18Qtz + 5phl + 2grs + alm = 3ab + 5ann + 6an + 3Tr	-100.6	-13.90
10)	3Prg + 18Qtz + prp + 2grs + 5ann = 3ab + 6an + 5phl + 3FeAct	-273.7	-14.66
11)	3FePrg + 18Qtz + prp + 4phl + 2grs = 3ab + 4ann + 6an + 3Tr	-87.4	-13.59
12)	5FePrg + 4Tr = 4FeAct + 5Prg	48.6	-0.56
13)	3Tr + 5alm = 5prp + 3FeAct	-153.7	-2.33
14)	5alm + 2grs + 18Qtz + 3Prg = 3FeAct + 4prp + 6an + 3ab	-340.1	-16.21
15)	3Prg + 4alm = 4prp + 3FePrg	-152.1	-1.53
16)	2grs + 5prp + 18Qtz + 3FePrg = 3Tr + 6an + 4alm + 3ab	-34.2	-12.35
17)	3FePrg + 18Qtz + 2grs + alm = 3ab + 6an + 3FeAct	-187.9	-14.68
18)	15FePrg + 90Qtz + 5prp + 10grs = 15ab + 30an + 3Tr + 12FeAct	-786.0	-71.07
19)	15FePrg + 72Qtz + 4prp + 8grs = 12ab + 24an + 12FeAct + 3Prg	-599.7	-57.19
20)	3FePrg + 18Qtz + prp + 2grs + ann = 3ab + 6an + phl + 3FeAct	-174.7	-14.37

Amphiboles in the metavolcanic rocks are close to pargasite in composition and are rich in iron (Fig. 4.11); amphiboles in the intrusive rocks of the Lac Frechette complex are close to hornblende, and are rich in magnesium (see Table 4.4).

Electron microprobe profiles across two large (2.5 and 3.5 mm in diameter) garnet crystals from a metavolcanic sample in the Pontiac Group show an interesting pattern: iron contents show first a decrease and then an increase from core to the rim of the two crystals. This zonation pattern of iron shows a spectacular negative correlation with zonation of calcium in the crystals (Fig. 4.12). Plagioclase appears to be rare, and K-feldspar constitutes the major feldspar of the rock. Abundant amphiboles in the rock are the only calcium- and iron-rich minerals that might have had an exchange of these two elements with garnet crystals during metamorphism. The following reaction may be a good approximation for the metamorphic reaction:

$$\mathrm{Grs + FeAt = Alm + FeAct} \qquad (16)$$

Amphiboles in a lamprophyric rock sample (JL22) intruding Pontiac metasedimentary rocks have crystallized at the expense of biotite. This is evident from amphibole crystals that still preserve parts of the biotite crystals in their cores. A gradual change in colour and other optical characteristics is shown by the two minerals in core and rim of the mineral complex (Fig. 4.13). Calcite, quartz and K-feldspar are present in the rock; the following reaction is, therefore, suggested for this mineral transformation:

$$\mathrm{5Bt + 6Cal + 24Qtz = 3Act + 5Kf + 6CO_2 + 2H_2O} \qquad (17)$$

A garnet vein occurs within a syenitic intrusion close to the Cadillac-Larder Lake fault zone. The garnet is typically different from garnets within the metasedimentary and metavolcanic rocks. On the basis of microprobe analyses, the garnet belongs to the andradite end member (see Appendix F for composition of the mineral). In thin-section the mineral

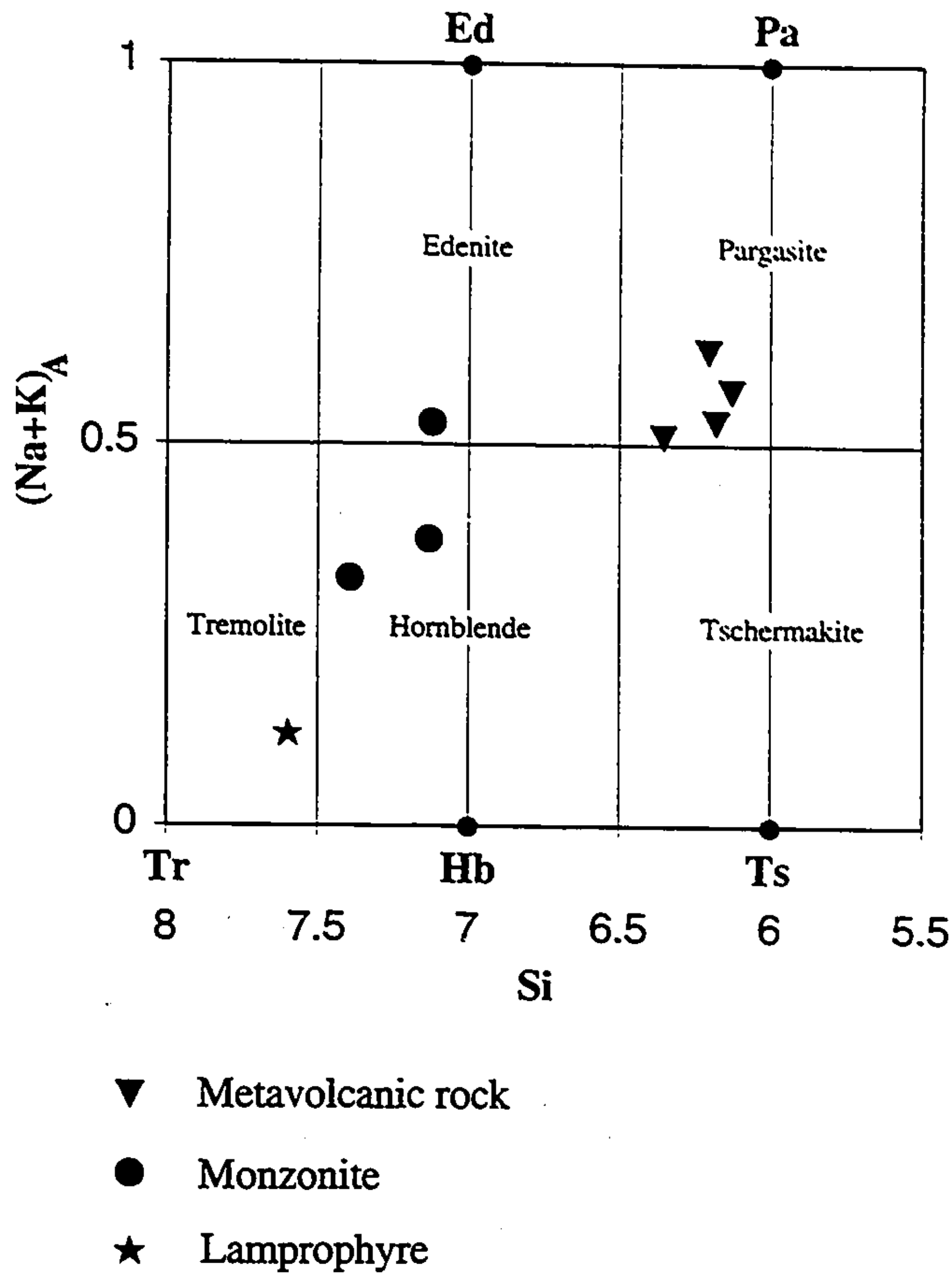

Fig. 4.11. Composition of amphiboles from different rock types within the northwestern Pontiac Subprovince. Mineral compositions are normalized on the basis of a 23 oxygen atom formula.

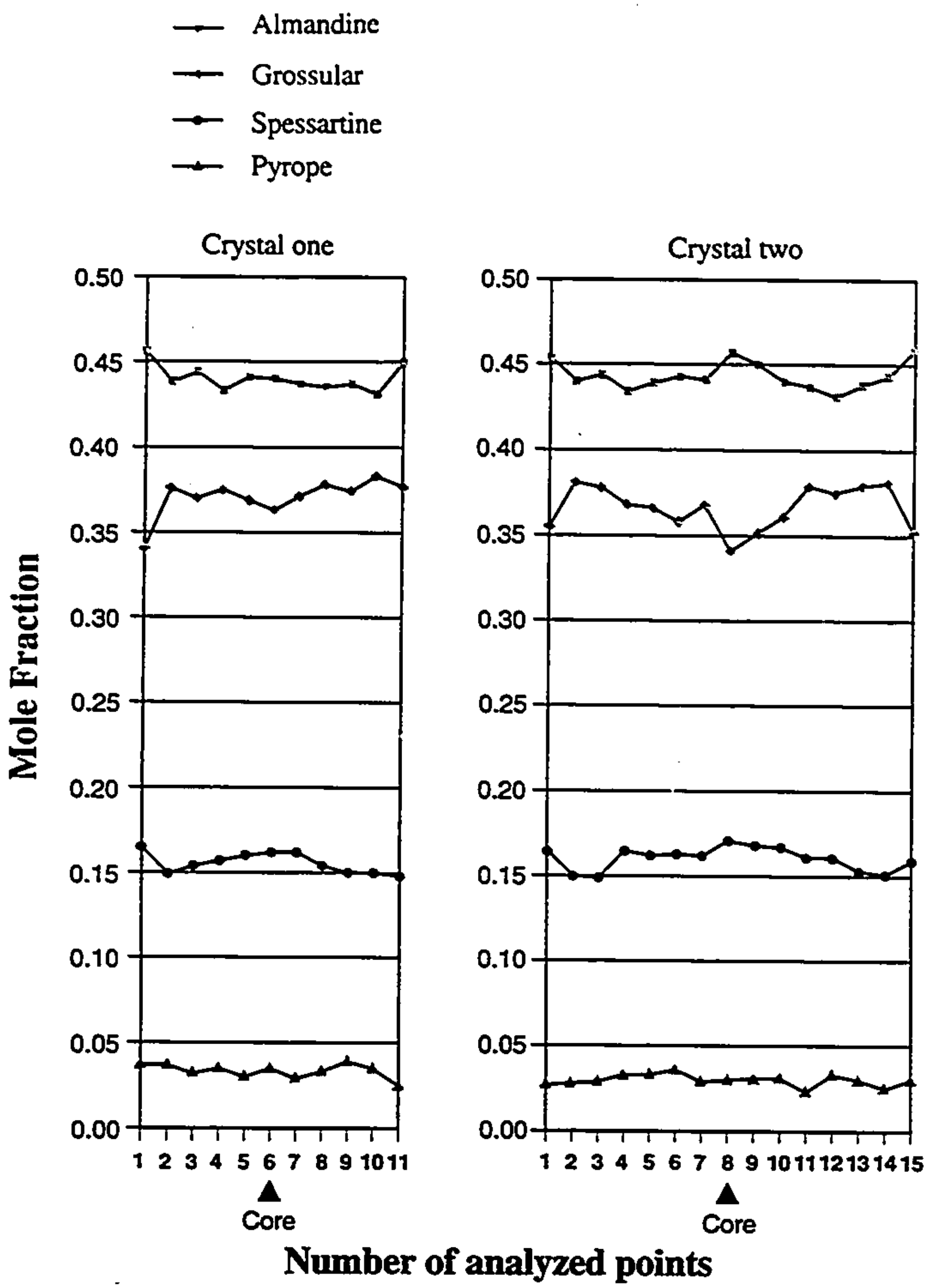

Fig. 4.12. Compositional zoning within two garnet crystals from a metavolcanic rock sample of the Pontiac Group. Data points are connected by straight lines, it must be noted however that in reality a smooth function is expected. Note negative correlation of almandine and grossular components.

Fig. 4.13. Photomicrograph illustrating growth of amphibole at the expense of biotite. Note the transitional zone between biotite crystal in the core and amphibole crystal at the rim. Plane-polarized light.

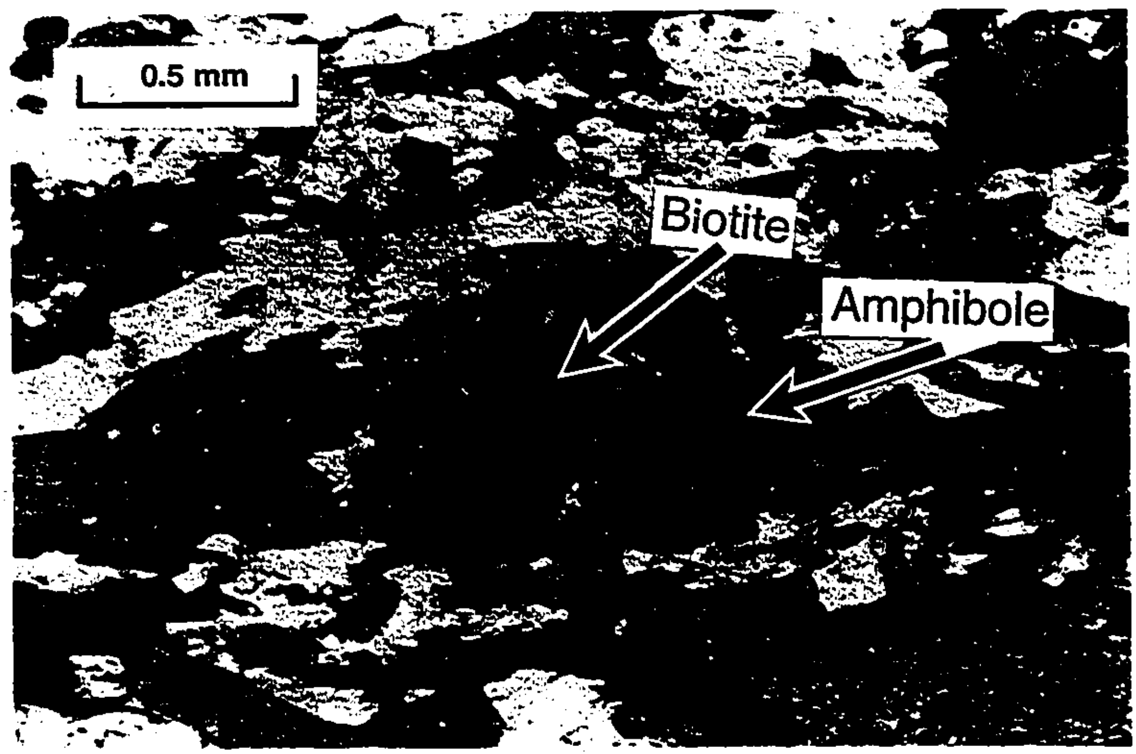
0.5 mm
Biotite
Amphibole

shows crystals with zones of anisotropy. Development of this garnet vein may be related to the main phase of metamorphism within the study area.

4.5. Paleo-pressure and paleo-temperature estimations for samples from the Pontiac Subprovince

Some mineral assemblages in the metasedimentary rocks of the Pontiac Group are suitable for estimation of paleo-pressures and paleo-temperatures. The minerals were analyzed by electron microprobe and the results were used in the TWEEQU (Thermobarometry With Estimation of EQUilibration state) program (Berman 1991) to estimate the equilibria within the mineral assemblages. For comparison, the conventional garnet biotite geothermometer and anorthite breakdown barometer (where aluminum silicates were available in the sample) were used to calculate paleo-pressures and paleo-temperatures for the individual samples.

4.5.1. Geothermobarometry using the TWEEQU method

The method uses the standard form of equations (a) and (b) for geothermometry and geobarometry (Berman 1991).

$$T = \frac{(\Delta H^{\circ} + \Delta V^{\circ}(P-1))}{(\Delta S^{\circ} - R\ln K)} \tag{a}$$

$$P = \frac{(-RT\ln K - \Delta H^{\circ} + T\Delta S^{\circ})}{\Delta V^{\circ}} \tag{b}$$

where T is temperature in kelvin, ΔH° is standard state enthalpy of reaction at 1 bar and 298 kelvin, ΔV° is the volume change for the reaction, P is pressure in bars, ΔS° is the standard state entropy of the reaction at 1 bar and 298 kelvin, R is the gas constant, and K is equilibrium constant for the reaction, given by:

$$K = \prod_{i}^{n} a_i^{\nu_i} \tag{c}$$

with a_i equal to the activity of phase component i, and ν_i equal to stoichiometric reaction coefficient.

Through the program, the positions of all possible equilibria among components of a given mineral assemblage may be computed and plotted in P-T space. An average pressure and temperature deduced from all intersections is calculated and reported. The program calculations are performed utilizing an internally consistent set of thermodynamic data (Berman 1988) for the end members and solution properties, so that thermobarometric consistency is guaranteed (Berman 1991). After plotting the lines representing the equilibria for different metamorphic reactions, the software calculates pressure and temperature estimates for the samples on the basis of intersection point(s) between the lines.

The essential thermometer used in the program is the garnet-biotite exchange reaction. Reactions used for barometry in metasedimentary samples include the anorthite breakdown reaction known as GASP (Garnet, Al-silicate, SiO_2, Plagioclase) , SGAM (SiO_2, Garnet, Al-silicate, Muscovite, Biotite; abbreviation and calibration from McMullin *et al.* 1991), and other reactions summarized in Table 4.7. The GASP geobarometer was first proposed by Kretz (1964), and has been made popular by Ghent (1976). The SGAM barometer was first proposed by Ghent and Stout (1981).

Figure 4.14 illustrates the calculated P-T diagrams for the samples from the Pontiac Group. Minimum and maximum temperatures calculated for the metasedimentary samples are about 520°C and 620°C respectively, and minimum and maximum pressures are about 3.9 and 7.2 kbar respectively. P-T calculations for two metavolcanic samples from the Opasatica gneiss assemblage show paleo-pressures and paleo-temperatures of about 4.8 kbar and 530°C, and 7.3 kbar and 640°C respectively (see Fig. 4.14).

Locations of the samples analyzed for thermobarometry, and their paleo-pressure and paleo-temperature estimations, are shown in Fig. 4.15.

Fig. 4.14. P-T diagrams illustrating geothermobarometry results for metasedimentary samples and metavolcanic samples (last two diagrams), calculated using the TWEEQU method. Numbers on the boundary curves indicate metamorphic reactions listed in Table 4.7. Boxes within the grids indicate sample number, and estimated temperatures and pressures. References for solution models of different minerals are as follows: Garnet - Berman (1990); Biotite - McMullin *et al.* (1991); Plagioclase - Fuhrman and Lindsley (1988); Muscovite - Chatterjee and Froese (1975); Amphiboles - Margules solution model Mäder and Berman (1992)

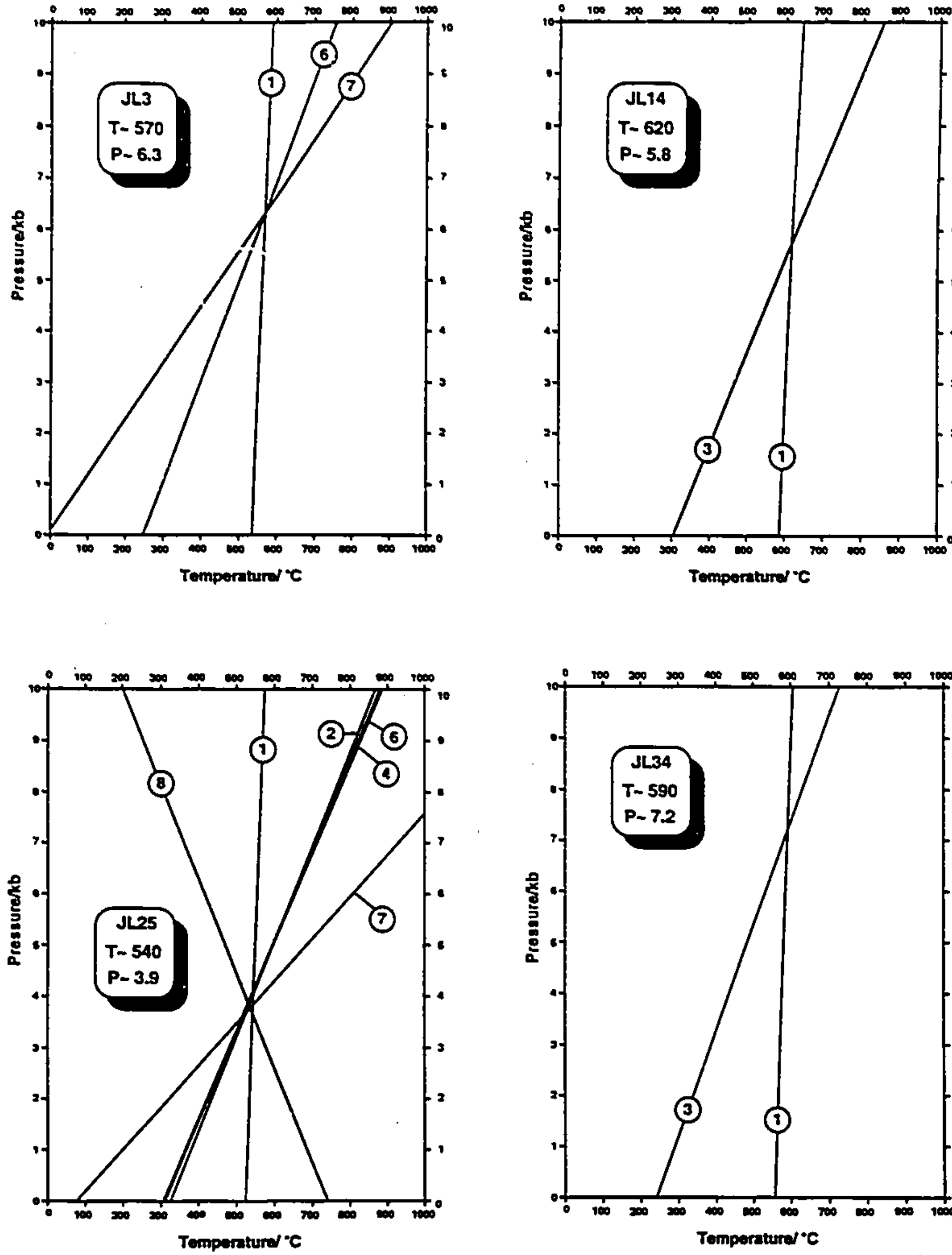
JL3
T~ 570
P~ 6.3
Pressure/kb
Temperature/ °C
JL14
T~ 620
P~ 5.8
Pressure/kb
Temperature/ °C
JL25
T~ 540
P~ 3.9
Pressure/kb
Temperature/ °C
JL34
T~ 590
P~ 7.2
Pressure/kb
Temperature/ °C

Fig. 4.14.

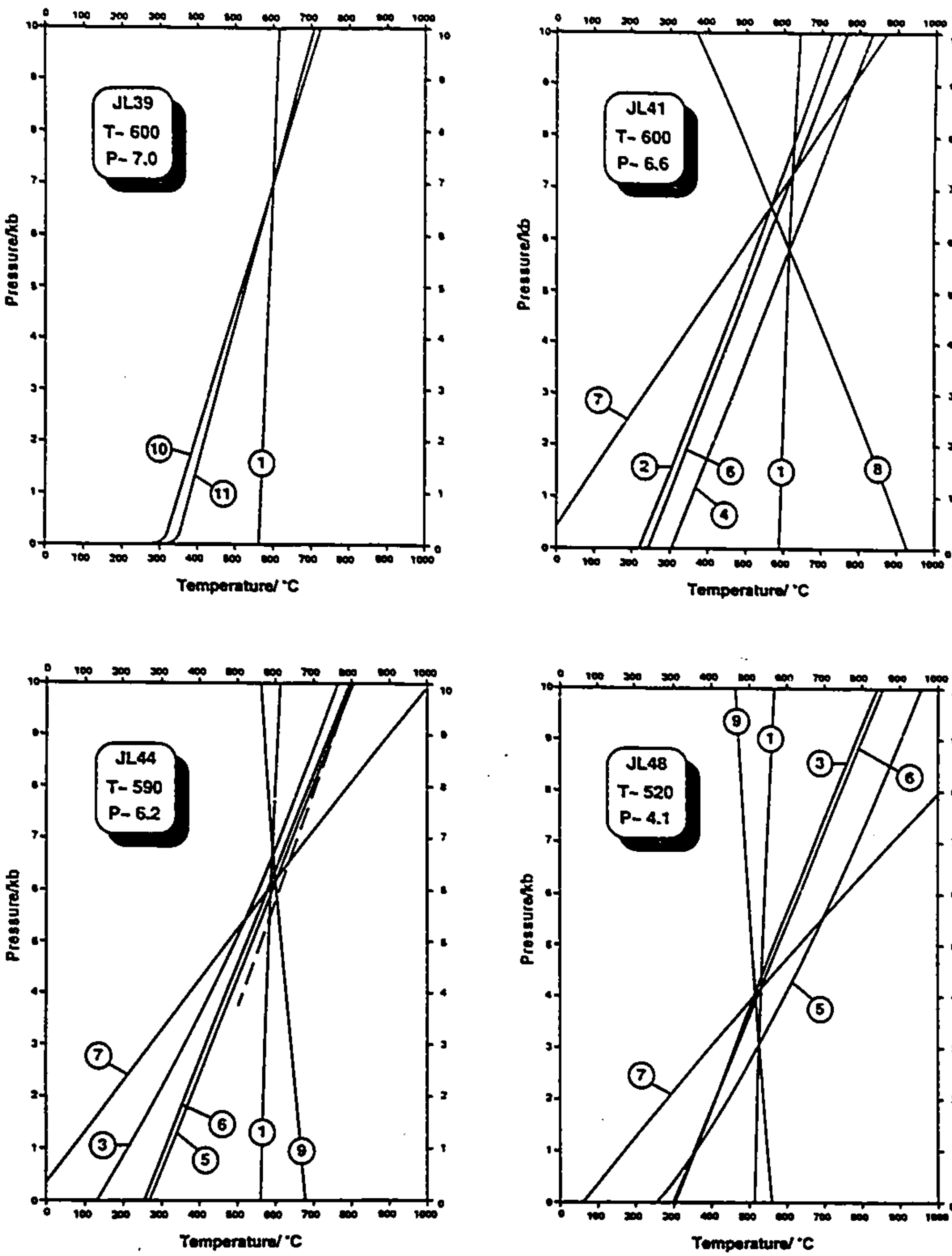

Fig. 4.14. Continued. Dashed line in lower left diagram shows kyanite-sillimanite boundary curve (from Holdaway 1971).

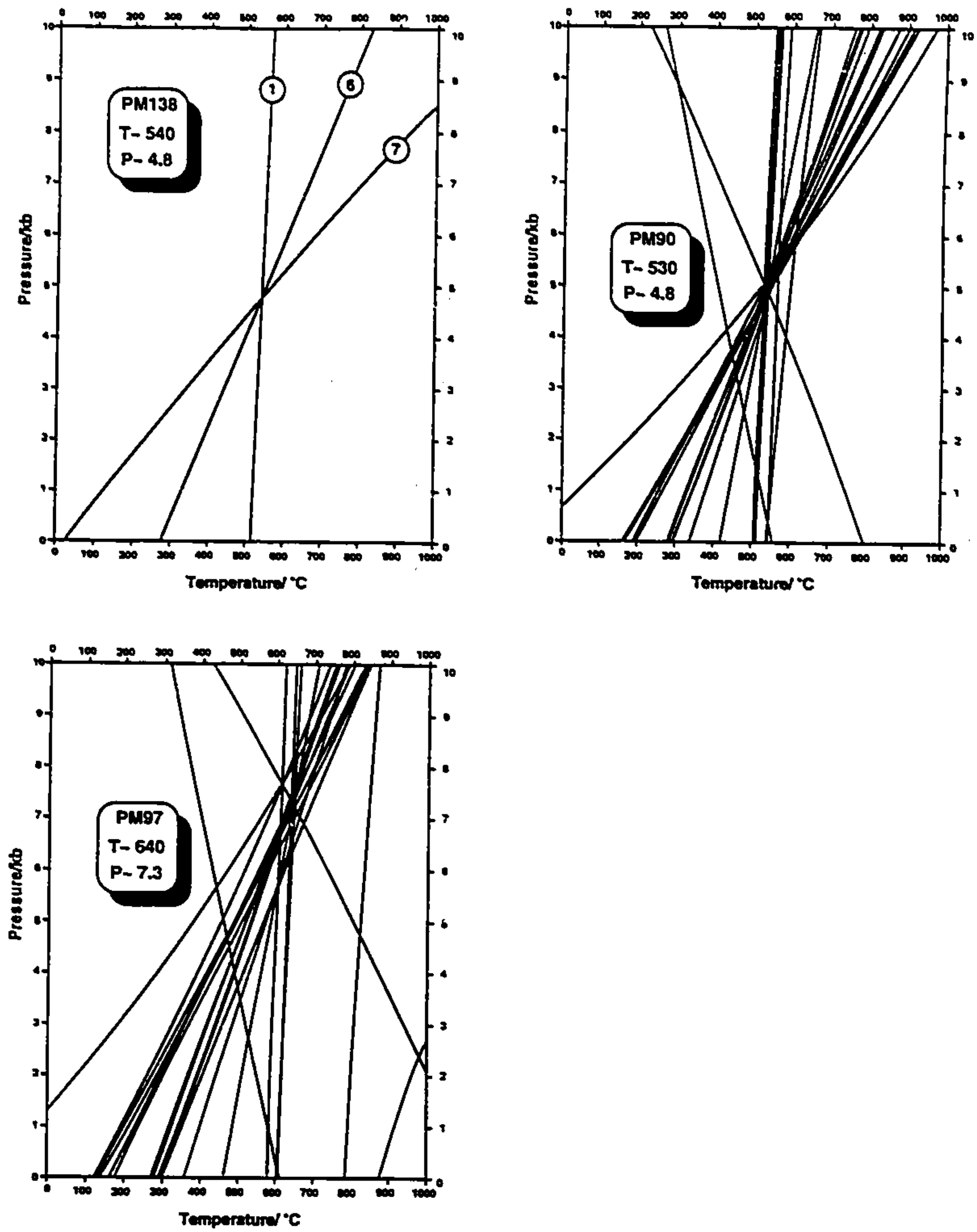

Fig. 4.14.Continued.

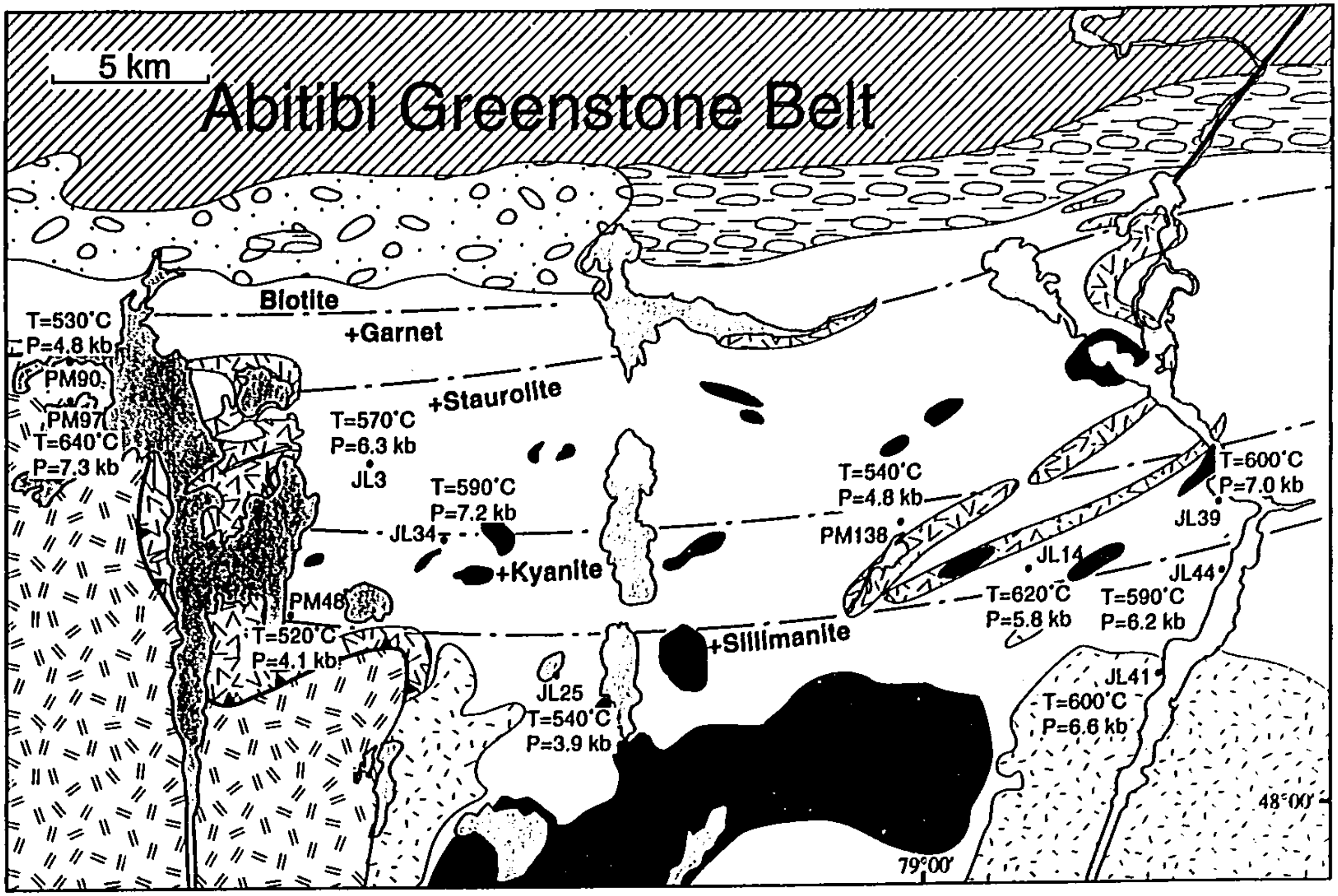

Fig. 4.15. Distribution of the samples selected for thermobarometry calculations, and related paleo-temperature and paleo-pressure estimations.

4.5.2. Conventional geothermobarometry

The distribution of Mg and Fe^{2+} between biotite and garnet in metamorphic rocks may be used as a geologic thermometer (Thompson 1976a, b). Electron microprobe analyses of biotites and garnets from metasedimentary and metavolcanic rocks of the study area were used in equation (d) (Kretz 1994) to calculate the temperatures of these rocks during the regional metamorphism:

$$T = \frac{2780 + 258[Ca]}{\ln K_D + 0.235[Ca] + 1.51} \qquad \text{(d)}$$

where $[Ca]$ is the calcium content of garnet, and K_D is the distribution coefficient of the exchange reaction.

In samples where aluminum silicates are present, the anorthite breakdown equilibrium was used to constrain the metamorphic pressure. Calculations were made through equation (e) (Newton and Haselton 1981):

$$P = \frac{-RT\ln(a_{grs} / a_{an}) + \Delta V^{\circ}.P^{\circ}}{\Delta V^{\circ}} \qquad \text{(e)}$$

where a_{grs} and a_{an} are activities of grossular and anorthite components in garnet and plagioclase, and P° is the equilibrium pressure of the end-member reaction at the temperature of interest, calculated by equations (f) and (g) respectively, from Koziol and Newton (1988) and Robie and Hemingway (1984):

$$P^{\circ} = 22.80T - 7317 \text{ (with kyanite)} \qquad \text{(f)}$$

$$P^{\circ} = 23.4T - 6310 \text{ (with sillimanite)} \qquad \text{(g)}$$

The thermodynamic data set of Berman (1988) was used for the calculations; a_{an} were calculated by means of the Newton-Charlu-Kleppa (1980) equation. Resulting pressure and temperature estimates are summarized in Table 4.8. TWEEQU thermobarometry results for the individual samples are shown in this table for comparison.

Table 4.8. Temperature and pressure estimates for 6 aluminum silicate-bearing samples through conventional and TWEEQU methods. MZ is the abbreviation for "metamorphic zone".

		Garnet				Biotite		Plagioclase			Conventional		TWEEQU	
MZ	Sample	FeO	MgO	CaO	MnO	FeO	MgO	CaO	Na_2O	K_2O	T/°C	P/kbar	T/°C	P/kbar
Ky	JL14	31.30	3.55	1.61	5.77	18.90	11.18	5.04	8.58	0.06	660	8.0	620	5.8
Sil	JL25	29.24	2.89	1.83	8.27	17.16	10.83	5.90	8.14	0.15	630	7.5	540	3.9
Ky	JL34	30.49	3.37	2.85	4.74	16.73	11.32	5.49	8.63	0.00	660	9.5	590	7.2
Sil	JL44	30.66	3.78	2.84	4.40	16.48	12.11	6.96	7.54	0.03	660	9.0	590	6.2
Ky	JL48	30.27	2.79	1.98	7.38	17.80	11.03	5.67	8.26	0.11	620	7.4	520	4.1

4.5.3. Comparison and interpretation of results

Figure 4.16 illustrates the distribution of estimated points calculated through both methods for different samples within the P-T space (also see Table 4.8). Most samples are plotted within the kyanite stability domain, close to the kyanite-sillimanite boundary curve. As may be noticed from Fig. 4.16, pressure and temperature estimations obtain by the TWEEQU method are lower than those of the conventional method. Excluding samples JL25 and JL48 that show some evidence of alteration, the pressure and temperature differences for individual samples are about 2.5 kbar and 60°C respectively. Proposed explanations for the discrepancy are discussed in Appendix G.

The TWEEQU estimations are concentrated in clusters that are closer to the kyanite-sillimanite boundary curve, compared to those obtained by the conventional method. Considering the presence of kyanite and/or sillimanite in 6 samples, the TWEEQU results are preferred and considered to be more realistic. The occurrence of estimates for sillimanite-bearing samples that fall in the kyanite stability field, and vise versa may be resolved through errors of about ±50°C and ±1 kbar respectively for thermometry and barometry estimations (for a detailed discussion on error propagation for barometers see Kohn and Spear 1991a, b).

Excluding samples PM48 and JL25, which show relatively low pressures compared to their counterparts within kyanite and sillimanite zone, the average of estimations for different samples indicates that regional metamorphism of rocks in northwestern Pontiac Subprovince occurred at about 590°C and 6.2 kbar. In samples PM48 and JL25, biotites show chloritization, and garnets are more rich in Mn compared to their counterparts within other studied samples (see Table 4.8). This phenomenon has probably resulted from a local retrograde process.

The paleo-pressure and paleo-temperatures for 9 samples show an average T/z (Temperature over depth) ratio of 26°C/km. This ratio is even less than values suggested for geothermal gradients of some Phanerozoic orogens (Table 4.9).

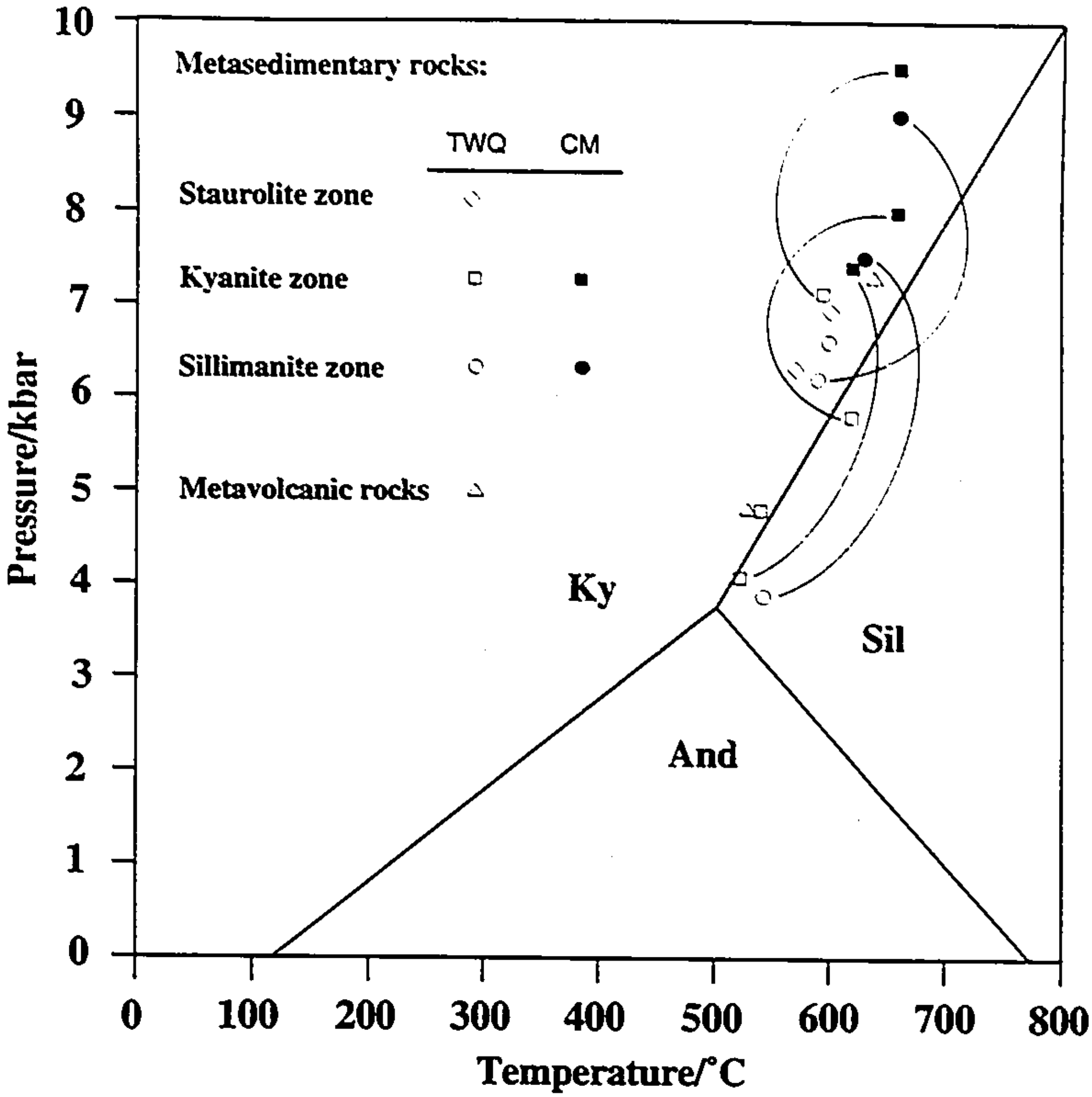

Fig. 4.16. Distribution of estimated pressures and temperatures for different rock samples in PT space. P-T estimations for individual samples through conventional (CM) and TWEEQU (TWQ) methods are connected by tie lines for comparison.

Table 4.9. Estimated geothermal gradients (T/z) of some Phanerozoic orogens.

Orogen	[§]Average estimated T/z (°C/km)
*Tauern window, Alpine orogen (Late Mesozoic)	38
†Himalayan orogen, (Cenozoic)	26
‡Acadian Orogen (Devonian)	20
¥Cordillera Darwin, (Late Mesozoic)	23
Average	27

*Based on 6 estimations (from Selverstone *et al.* 1984, and Selverstone and Spear 1985)

†Based on 5 estimations (from Hubard 1989)

‡Based on one estimation (from Hames *et al.* 1989)

¥Based on 52 estimations (Kohn *et al.* 1993)

§Depths are calculated on the basis of an average crustal density of 2850 kg m^{-3}

4.6. Estimation of a pressure-temperature (P-T) path for metamorphic rocks in the Pontiac Group

Progressive and retrogressive reactions between the minerals were deduced from changes in mineral assemblages from low grade rocks into higher grade ones, and microstructural relationships of the minerals. These data were combined with results of thermobarometric calculations, with special emphasis on the compositional zoning in the garnet crystals, to derive a P-T path for metasedimentary rocks of the Pontiac Group. Geochronologic data from the present study and other sources, along with relative ages of structural and thermal events were used to constrain the P-T path within a time framework.

Figure 4.17 illustrates the P-T path constructed for metasedimentary rocks of the Pontiac Group. The major part of the path was constructed on the basis of P-T data and microstructural relationships from relatively higher grade rock samples from kyanite and sillimanite zones. Evidence indicating the relationship of porphyroblast growth to microstructures is well preserved in these samples (see related discussion in section 4.3). Garnets from these samples show an increase in activity of almandine, and a decrease in the activity of grossular components from core to rim of the crystals. This compositional zoning pattern in garnets, probably developed during retrogression of the staurolites through reaction (5) , records part of the retrogressive path. P-T calculations on the basis of analyses of points at the core, middle and rim of these garnets show reducing pressures and temperatures (see composition of the garnet crystal from sample JL14 in Table 4.6). Five points within the P-T grid were calculated on the basis of compositional zoning of a garnet crystal from sample JL14. These points were used to plot part of the P-T path in Fig. 4.17.

The compressional D_1 structural event was synchronous with early progressive metamorphism, during which sequential metamorphic reactions resulted in the appearance and growth of biotite, garnet and staurolite. Because staurolite is the last prograde metamorphic mineral that records the D_1 event, this event should have finished before development of kyanite porphyroblasts (reaction boundary number 3 in Fig. 4.10). The D_1 event was followed

Fig. 4.17. Suggested P-T path for metasedimentary rocks within northwestern Pontiac Subprovince. The thicker path is plotted for a sample from the kyanite zone, and the thinner path is suggested for rocks that have been buried to greater depths, and undergone melting into S-type granites. Deformational events D_1, D_2 and D_3 are shown on the shallower path. Boundary curves are the same as in Fig. 4.10. The dashed curve is the H_2O-saturated solidus of muscovite granite (after Huang and Wyllie 1973).

Explanations for criteria used in construction of the P-T path (for more details on geochronologic data see Chapter 5):

A: The youngest detrital zircon ages (2683 Ma) from the metasedimentary rocks of the Pontiac Group provide a maximum age for the beginning of the D_2 deformational event.

B: Staurolite porphyroblasts overgrow S_1 foliation.

C: Kyanite porphyroblasts overgrow S_2 crenulations.

D: Overgrowth of fibrolite on kyanite.

E: Crosses represent P-T estimations and error bars (±50°C, ±1kbar) for core to rim composition of a garnet crystal from the kyanite zone (sample JL14).

F: Oldest monazites (closure temperature = 700°C) dated from the S-type granites.

G: Average $^{40}Ar/^{39}Ar$ cooling age of amphiboles at about 530°C.

H: Schematic illustration of increase in pressure due to D_3 compressional event.

I: Average $^{40}Ar/^{39}Ar$ cooling age of muscovites at about 350°C.

J: Relatively fast cooling rate due to D_4 extensional event after D_3.

K: Average $^{40}Ar/^{39}Ar$ cooling age of biotite at about 280°C.

L: Depositional age of the Gowganda formation at about 2300 Ma provides a minimum age for exposure of the metasedimentary rocks at the surface.

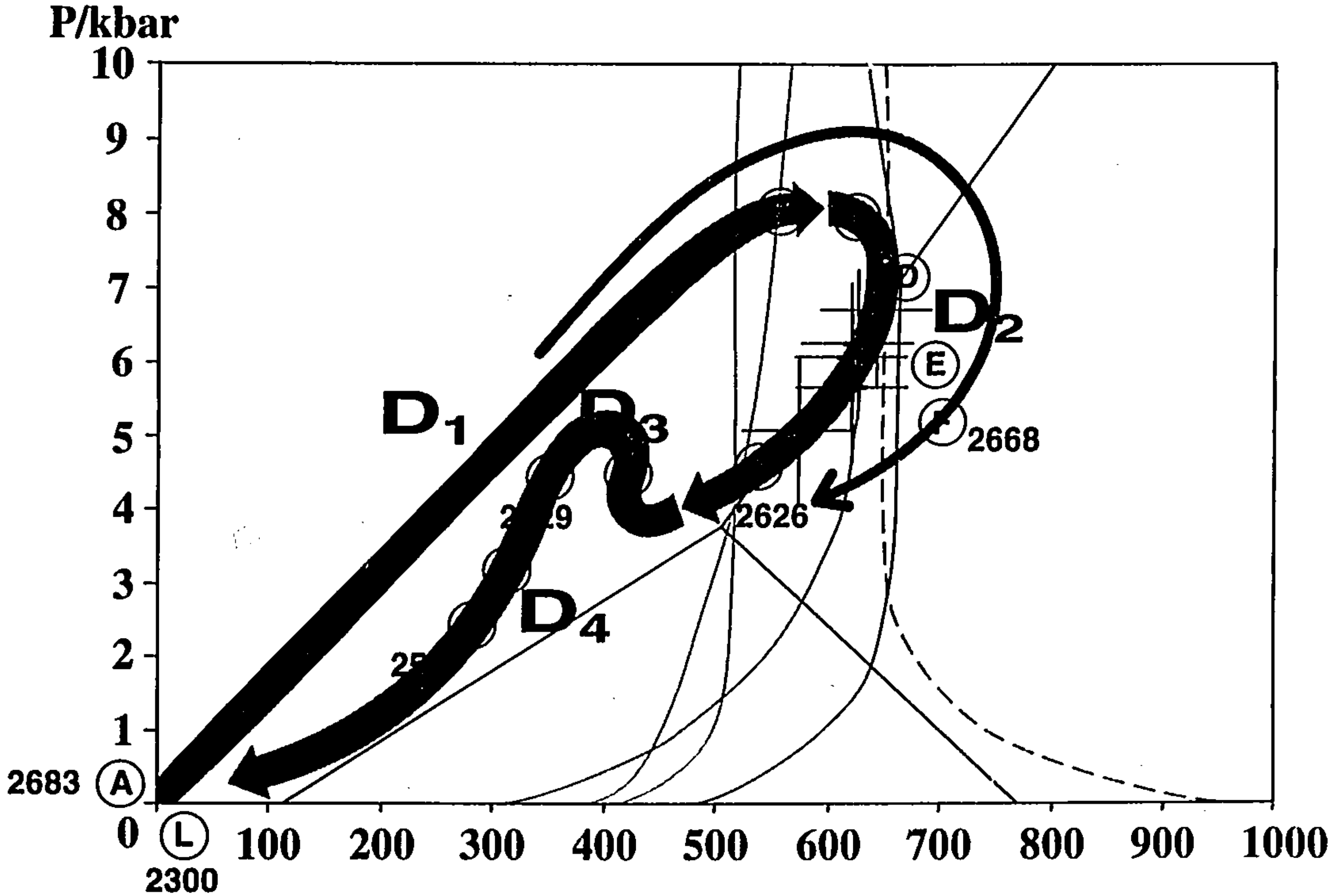

Fig. 4.17. Suggested P-T path for metasedimentary rocks within northwestern Pontiac Subprovince.

by D_2 nappe-development. This was a syn-peak metamorphism event during which kyanite and sillimanite first started to form and grow. S-type granites, derived from the metasedimentary rocks, were produced, emplaced and deformed during this event. D_3 and D_4 and D_5 events apparently had relatively minor contributions to the pressure and temperature of the rocks.

The youngest (*ca.* 2683 Ma) detrital zircon from the Pontiac metasedimentary rocks defines the maximum age for the D_1 event. The age of the oldest monazites from S-type granitic bodies (*ca.* 2668 Ma) may be used as an approximation for the age of the D_2 event (U/Pb dating from Mortensen and Card 1993). $^{40}Ar/^{39}Ar$ cooling ages (see section 5.2) of the biotites and muscovites recovered from the metasedimentary samples have been used to place some constraints on the retrograde part of the P-T path. An important (D_4) extensional event after D_3 deformational event is considered to be responsible for crustal thinning, and appearance of Pontiac metasedimentary rocks at the surface before deposition of the Huronian Supergroup at about 2500 Ma (see related discussion in Chapter 6). A relatively fast cooling rate of about 5°C/Ma, deduced from $^{40}Ar/^{39}Ar$ dating of muscovites and biotites from the metasedimentary rocks, is considered to have resulted from the above-mentioned extensional event (see related discussion in Chapter 5). Most parts of the Pontiac Group rocks that now crop out at the surface must have been exposed at the surface before deposition of the Gowganda Formation (Cobalt Group). The unconformity surface between the two rock units is present in the northwestern part of the study area. This implies that Pontiac Group rocks must have returned to the surface before about 2300 Ma, an approximate age for sedimentation of the Gowganda Formation (Fairbairn *et al.* 1969).

4.7. Cause of regional metamorphism within the Pontiac Subprovince

Clockwise metamorphic P-T paths, typical of Phanerozoic orogenic belts (see Selverstone *et al.* 1984, Selverstone and Spear 1985, Hubard 1989, Kohn *et al.* 1993), are considered to be the result of burial of the rocks to great depths through crustal thickening by large-scale thrusting, heating of the rocks at depth, and their return to surface as a result of uplift and erosion (England 1984, Oxburgh and England 1980). Comparatively early high and late low slope (dP/dT) of the P-T path is interpreted to be a result of a relatively fast rate of burial through large-scale thrusting events, and a slow rate of exhumation through erosion of the overburden (Oxburgh and England 1980). Within this framework, the increase in temperature is considered to be a consequence of thermal relaxation of the thickened crust (England 1984). Steeper geotherms during peak metamorphic conditions are, therefore, believed to be established by a thicker crust which contains much more heat-producing isotopes compared to a crust of average thickness.

An investigation of distribution of heat producing isotopes (U, Th, K) within metasedimentary, metavolcanic, and igneous rocks of the Pontiac and Abitibi Subprovinces (Table 4.10) indicates that heat production values of these rocks in Late Archean were considerably lower than values for Phanerozoic crustal assemblages. The regional metamorphism of the Pontiac Subprovince, therefore, was not simply induced by a thickened heat-producing crust. Superficial distribution of rocks in the Pontiac Subprovince (Fig. 2.1) indicates that the granitoid rocks, considered to be I-type intrusions, constitute about 15 percent of the outcrops within the subprovince. Intrusion of these granitoid rocks, therefore must have transferred a considerable amount of heat from the mantle into the crust of the Pontiac Subprovince.

As may be inferred from the constructed P-T path, the time span between the end of deposition within the Pontiac basin and peak metamorphic conditions was relatively short (about 10 Ma). Considering the fact that in all clockwise P-T paths, peak pressures occur before peak temperatures, the path implies that the orogen reached its maximum thickness in less than 10 Ma. Cooling of the crust on the retrograde part of the P-T path, however, was considerably slower, as is revealed by geochronological data.

Table 4.10. Present day concentration of heat producing radioisotopes and calculated Late Archean heat production in different rocks considered to be involved in thickening of Pontiac Subprovince crust. Values for average Archean upper crust (AAUC) and present upper crust are quoted for comparison. Heat production calculations are on the basis of formula 4-8 in Turcotte and Schubert (1982).

	Rock type	location	U (ppm)	Th (ppm)	K(%)	Specific gravity ($kg\ m^{-3}$)	Heat production (μWm^{-3})
1	Volcanics	Evain (Rouyn)	0.56	1.20	0.660	2800	0.704
2	Volcanics	Val-d'Or	0.63	2.30	0.550	2750	0.775
3*	Pontiac Group	Pontiac Subprovince	2.46	8.31	0.058	2720	2.042
4†	Pontiac Group	Pontiac Subprovince	1.83	6.87	0.056	2720	1.582
5‡	Pontiac Group	Pontiac Subprovince	2.06	6.20	0.038	2720	1.642
6	Timiskaming Group	Pontiac Subprovince	1.17	4.25	0.030	2780	0.636
7	I-type granites	Pontiac Subprovince	1.30	3.20	0.060	2650	0.967
8	S-type granites	Pontiac Subprovince	3.70	13.70	0.090	2650	3.092
9	Tonalitic gneiss	Pontiac Subprovince	2.05	1.80	0.036	2700	1.259
10	AAUC		0.75	2.90	0.750	2780	0.988
11	PUC		2.50	10.50	2.740	2780	3.469

Sources for concentrations of heat producing elements: 1,2 Mareschal *et al* . (1989); 3,8 Feng *et al.* (1993b); 4,6 Camire *et al.* (1993); 5 Ujike (1984); 6,7 Feng *et al.* (1993a), 9,10 Taylor and McLennan (1981). *Based on ten analyses †Based on seven analyses ‡ Based on three analyses

4.8. Summary and conclusions

Sedimentary and volcanic rocks of the Pontiac Group underwent amphibolite-facies (high-temperature moderate-pressure) metamorphism during the Late Archean (*ca.* 2670 Ma). Southward in the study area, metamorphic grade of the metasedimentary rocks increases from the biotite to the sillimanite zone. This increase towards the south, where granitic rocks of the Decelles batholith and migmatitic rocks of the Pontiac Group are exposed on the surface, and the presence of metamorphic minerals within these granites, may be used for the interpretation that the S-type granites were produced by melting of the Pontiac Group during peak metamorphic conditions. Geothermobarometry estimations for different samples from the study area indicate that peak regional metamorphism in northwestern Pontiac Subprovince occurred at about 590°C and 6.2 kbar. Maximum equilibrium paleo-temperatures and paleo-pressures estimated for these rocks are about 620°C and 7.2 kbar respectively. The maximum estimated paleo-pressure from the study area implies that the studied rocks were buried to maximum depths of about 26 km probably during a major collisional event.

A compilation of data from mineral reactions, microstructural relationships, thermobarometry, and geochronology was used for estimation of a P-T path for the metamorphic history of the study area. The resulting P-T path is among the few first attempts so far carried out for reconstruction of the metamorphic history of Archean terranes. Estimated pressures and temperatures for several samples from the study area, and the clockwise pattern of the suggested P-T path are similar to those documented for regional metamorphism of different Phanerozoic collisional belts. The P-T path is paired with the deformational history of the Pontiac Subprovince, whereby the crust was first thickened during a compressional event, and then started to become thin, presumably as a result of erosion during the D_2 event. Peak amphibolite facies metamorphism of the crust, and intrusion of S-type granites, occurred during this event. High temperatures during metamorphism were responsible for softening of the mid-crustal rocks and their reduction into a thinner pile. A relatively low value (as compared to Phanerozoic orogens) for the T/z (temperature/depth) ratio resulted from thermobarometry estimations indicates that thermal gradients in the Pontiac Subprovince during Late Archean time were not higher than at the present time. This observation supports the view that continental geothermal gradients in the Archean were not steeper than those of the Phanerozoic time (Bickle 1978, Burke and Kidd 1978, England 1979). Intrusion of voluminous I-type granites in the absence of a high heat-generating crust is suggested to be responsible for a major part of the heat contribution for regional metamorphism of the crustal rocks.

5. Geochronology

5.1. Introduction

Geochronological studies of basement rocks within the Abitibi and Pontiac Subprovinces began more than two decades ago (cf. Steiger and Wasserburg 1969). Acquisition of abundant high precision age data from different rock types have resulted in a better understanding of timing and nature of geological processes in these two subprovinces within this relatively short time span. Many ambiguities in stratigraphic relations that resulted from simple conclusions based solely on superposition relationships [such as that proposed by Imreh (1973) for stratigraphic relationship between the Pontiac Group and the Angliers-Belleterre greenstones], have been eliminated through the application of advanced methods for absolute age determination.

The $^{40}Ar/^{39}Ar$ dating method, that has been extensively used for thermal evolution studies of different types of Phanerozoic terranes, has been recently employed for similar investigations in the Abitibi and Pontiac Subprovinces. Feng and Kerrich (1992) interpreted $^{40}Ar/^{39}Ar$ ages from igneous and metamorphic rocks of the Abitibi and Pontiac Subprovinces in terms of two major thermal events affecting these two subprovinces at about *ca.* 2690 to *ca.* 2670 Ma, and *ca.* 2660 to *ca.* 2630 Ma. The earlier thermal activity was accompanied by intrusion of voluminous syntectonic plutons and caused low-pressure, greenschist facies metamorphism in the Southern Volcanic Zone of Abitibi Subprovince, and intermediate-pressure metamorphism in the Pontiac Subprovince. The second thermal event was coeval with the emplacement of syncollisional, S-type granites in the Pontiac Subprovince and the higher grade Lacorne block of the Abitibi, and reset the K-Ar systems in neighbouring pre-existing rocks (Feng and Kerrich 1992).

Powell *et al.* (1995) studied volcanic and sedimentary rocks and alterations in the southern Abitibi and northern Pontiac Subprovinces using the $^{40}Ar/^{39}Ar$ dating method. Based on their study, they divided the area into three domains: 1) zones of impermeable rock in the southern Abitibi, with cooling rates of >8°C/Ma; 2) zones of impermeable rock that are associated with monzogranite plutons in the northern Pontiac, with apparent cooling rates of 1-2°C/Ma; and 3) permeable high-strain zones (e.g. Cadillac-Larder Lake fault zone), with apparent cooling rates of <1°C/Ma. Powell *et al.* (1995) suggested that discrete hydrothermal events have affected the high strain Cadillac-Larder Lake fault zone over a period of at least 250 Ma, from peak metamorphism at *ca.* 2660 Ma to the retrogression age (deduced from $^{40}Ar/^{39}Ar$ analyses) of amphiboles *ca.* 2420 Ma.

Analysis of $^{40}Ar/^{39}Ar$ age spectrums, combined with U/Pb, Pb/Pb, and Rb/Sr dating methods for different minerals with different closure temperatures, provide a valuable tool for investigation of thermal and tectonic evolution of different terranes. Dispersed geochronologic data from the Pontiac and Abitibi Subprovince, along with $^{40}Ar/^{39}Ar$ dates from this study, will be used here to construct a time framework for depositional, magmatic, metamorphic, and deformational events within the Pontiac Subprovince. A compilation of the geochronologic data used in this construction is summarized in Table 5.1 along with related references. Table 5.2 shows summarized $^{40}Ar/^{39}Ar$ analytical data from this study. Data for constraints on ages of the Cobalt Group and mafic dyke swarms are from studies carried out elsewhere in the Superior Province.

5.2. $^{40}Ar/^{39}Ar$ dating on samples from the Pontiac Subprovince

5.2.1. Sample selection and analytical methods

Fourteen samples from the metasedimentary, metavolcanic and plutonic rocks of the Pontiac Subprovince were selected for $^{40}Ar/^{39}Ar$ study (Table 5.2). Petrographic examination was performed in order to avoid altered rock samples. Sample sites, and the metamorphic zones from which they have been collected, are shown in Fig. 5.1 (also see Table 5.2). Mineral separation was carried out through crushing and grinding the rock samples, followed

Table 5.1. Summary of geochronological data related to the Pontiac and Abitibi Subprovinces.

A: Gneisses

Rock type	Mineral	Method	Age (Ma)	Interpretation	Reference
Lac Opasatica gneiss	titanite	U/Pb	2660±6		Machado *et al.* (1991a)
Baie des Lys orthogneiss	zircon zircon titanite	U/Pb U/Pb U/Pb	2686 (core) 2648 (overgrowth) 2637±3	minimum age minimum age	Machado *et al.* (1991a)
Lac de Quinze gneiss	zircon titanite	U/Pb U/Pb	2695±1 2673±4		Mortensen & Card (1993)
Tonalitic gneiss from Opatica belt	zircon	U/Pb	2825±3	oldest zircons so far dated within the Opatica belt	Davis *et al.* (1993)

B: Volcanic rocks

Rock type	Mineral	Method	Age (Ma)	Interpretation	Reference
Belleterre rhyolite	zircon	U/Pb	2686±2		Carignan *et al.* (1992)
Belleterre volcanic breccia	zircon	Pb/Pb	2690±2		Mortensen & Card (1993)
Belleterre synvolcanic intrusion	zircon	Pb/Pb	2685±1	maximum crystallization age	Mortensen & Card (1993)
Baby Volcanics	zircon	Pb/Pb	2682±1	maximum crystallization age	Mortensen & Card (1993)
southern Abitibi volcanics	zircon	U/Pb	2750 to 2670	development of southern Abitibi belt	Corfu (1993)
Blake River volcanics	zircon	U/Pb	2703-2698	culmination of eruption of Blake River Group	Mortensen (1993b)
Blake River rhyolite	zircon	U/Pb	2701±2		Corfu *et al.* (1989)
Pacaud felsite (southern Abitibi belt)	zircon	U/Pb	2747	maximum volcanism age in southern Abitibi	Mortensen (1993b)
Lac des Ventes flow (Northern Abitibi belt)	zircon	U/Pb	2759	maximum volcanism age in Northern volcanic zone	Mortensen (1993a)

Table 5.1. Continued.

C: Metasedimentary and related rock types

Rock type	Mineral	Method	Age (Ma)	Interpretation	Reference
Pontiac metasediments	detrital zircon	U/Pb	2686	maximum depositional age	Davis (1991)
Pontiac metasediments	detrital zircon	U/Pb	2740 to 2700	young zircon population	Gariepy *et al.* (1984)
Pontiac metasediments	detrital zircon	U/Pb	2940	old zircon population	Gariepy *et al.* (1984)
Pontiac metasediments	detrital zircon	U/Pb	2683±3	maximum depositional age	Mortensen & Card (1993)
Metasediments of Lacorne block	detrital zircon	Pb/Pb	2691±8 to 3042±6		Feng & Kerrich (1991)
Timiskaming metasediments	detrital zircon	U/Pb	2679	upper age limit for deposition of Timiskaming	Davis (1991)
Timiskaming metasediments	detrital zircon	U/Pb	2980		Davis (1991)
syenite cutting the Timiskaming Group	zircon	U/Pb	2673±3	minimum depositional age	Davis (1991)
Cadillac metasediments	detrital zircon	U/Pb	2688	maximum depositional age	Davis (1991)
Kewagama metasediments	detrital zircon	U/Pb	2687	maximum depositional age	Davis (1991)

Table 5.1. Continued

D: I-type granitoids and related intrusive rocks

Rock type	Mineral	Method	Age (Ma)	Interpretation	Reference
Lac Frechette pluton	zircon	U/Pb	2681+2/-1	maximum crystallization age	Mortensen & Card (1993)
Lac Frechette pluton (another locality)	zircon	U/Pb	2685±3	crystallization age	Mortensen & Card (1993)
Lac Remigny pluton	zircon	U/Pb	2680±1	maximum crystallization age	Mortensen & Card (1993)
Lac Simard monzonite	zircon & titanite	U/Pb	2686+4/-3		Machado *et al.* (1991a)
Lac Maple monzogranite	zircon	U/Pb	2678+3/-2		Machado *et al.* (1991a)
Tour de Belleterre monzodiorite	zircon	U/Pb	2669±3		Machado *et al.* (1991a)
Belleterre-Fugerville tonalite	zircon	U/Pb	2705±5		Carignan *et al.* (1992)
anorthositic gabbro south of the Baby-Belleterre	zircon	U/Pb	2694±2		Carignan *et al.* (1992)

C: S-type granites

Rock type	Mineral	Method	Age (Ma)	Interpretation	Reference
Decelles complex	monazite	U/Pb	2668±1	crystallization age	Mortensen & Card (1993)
Decelles complex (another locality)	monazite	U/Pb	2663±1	crystallization age	Mortensen & Card (1993)
Halle monzogranite (Decelles batholith)	zircon & monazite	U/Pb	2632±3		Machado *et al.* (1991a)

Table 5.1. Continued

E: Metamorphic events

Rock type	Mineral	Method	Age (Ma)	Interpretation	Reference
Igneous & metamorphic rocks from Pontiac & Abitibi Subprovinces	Muscovite, Biotite & Amphibole	Ar/Ar	2690-2670	early thermal activity in Abitibi and Pontiac Subprovinces	Feng *et al.* (1992)
Igneous & metamorphic rocks from Pontiac & Abitibi Subprovinces	Muscovite, Bioite & Amphibole	Ar/Ar	2660-2630	second thermal activity in Abitibi and Pontiac Subprovinces	Feng *et al.* (1992)
auriferous alterations	rutile & titanite	U/Pb	2625±7	Abitibi gold mineralization age	Jemielita *et al.* (1990)
Archean high-grade rocks south of Grenville front	metamorphic minerals	Pb/Pb	2508-2653	minimum age for Archean granulite facies metamorphism	Gariepy *et al.* (1990)
Archean amphibolite grade migmatites in Grenville front	zircon, monazite & titanite	U/Pb	2650±4		Krogh (1994)
Archean granulite grade gneisses in Grenville front	monazite	U/Pb	2643±5		Krogh (1994)

F: Other related ages

Rock type	Mineral	Method	Age (Ma)	Interpretation	Reference
Matachewan dyke swarm	zircon	U/Pb	2454+3/-2	Upper age limit for deposition of Cobalt Group	Heaman (1988)
Nipissing dyke swarm	baddeleyite	U/Pb	2219	Lower age limit for deposition of Cobalt Group	Corfu & Andrews (1986)
Sediments of Gowganda Formation	whole rock	Rb/Sr	2288±87	age of deposition	Fairbairn *et al.* (1969)

Table 5.2. Summary of characteristics of $^{40}Ar/^{39}Ar$ data analyses for different samples from the study area.

Sample No.	Rock type	Mineral	Metamorphic zone	Plateau age(Ma)	% ^{39}Ar	Correlation age(Ma)	% ^{39}Ar	Maximum age(Ma)
PM58	Lac Frechette granite	amphibole		2607±8	42.3	2604±20	42.3	2611±5
JL19	Lac Frechette granite	amphibole		2649±13	61.3	2668±15	30.6	2977±28
JL19	Lac Frechette granite	biotite		2604±11	28.1	2570±18	60.1	2612±16
PM16	Lamprophyre	amphibole		2562±10	62.2	2424±8	62.2	2596±11
JL20	Lamprophyre	amphibole		1221±12	95.0	1144±217	14.4	1391±41
PM97	Metavolcanic	amphibole		2622±28	73.2	2575±20	80.6	2626±30
PM90	Metavolcanic	biotite		2551±16	15.0	2486±9	14.4	2551±16
PM101	Metasedimentary	biotite	staurolite	2510±8	85.2	2510±6	75.4	2517±11
JL1	Metasedimentary	biotite	kyanite	2565±12	72.6	2557±6	52.9	2579±6
PM54	Metasedimentary	biotite	staurolite	2502±9	72.2	2502±8	82.6	2532±30
PM57	Metasedimentary	biotite	sillimanite	2506±10	37.3	2458±13	42.0	2514±6
JL25	Metasedimentary	biotite	sillimanite	2220±26	3.9			2220±25
JL25	Metasedimentary	muscovite	sillimanite	2555±10	23.5	2468±13	17.0	2557±9
JL41	Metasedimentary	biotite	sillimanite	2480±9	24.5	2411±19	29.7	2482±9
JL41	Metasedimentary	muscovite	sillimanite	2530±9	63.3	2530±38	63.3	2554±11
JL44	Metasedimentary	biotite	sillimanite	2503±10	47.4	2496±18	53.7	2540±13
JL44	Metasedimentary	muscovite	sillimanite	2529±11	61.4	2512±12	39.7	2594±9
JL18	Decelles granite	muscovite		2502±11	62.3	2496±24	68.2	2512±9

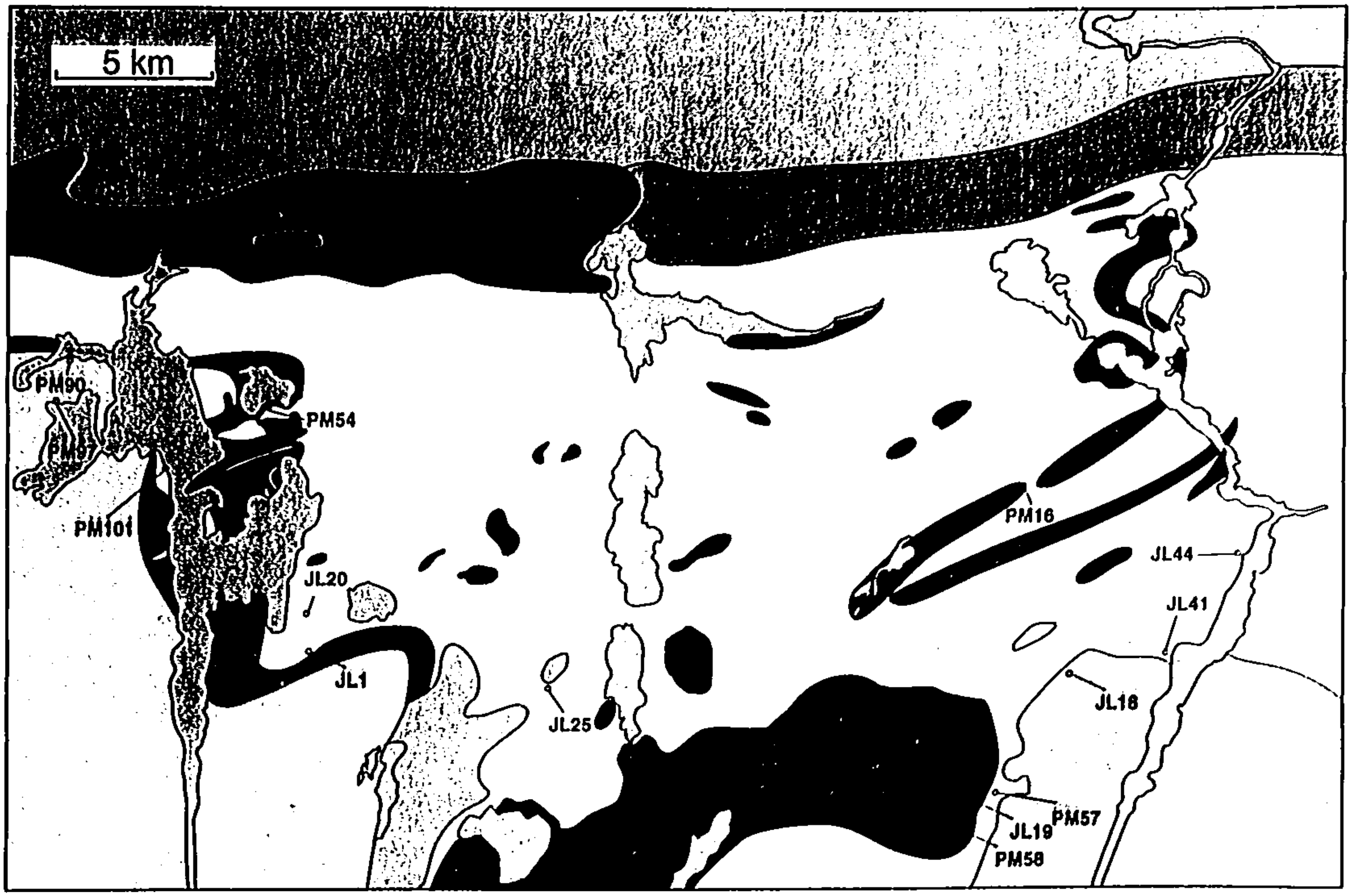

Fig. 5.1. Location map for the samples used in $^{40}Ar/^{39}Ar$ dating.

by use of magnetic and heavy-liquid separation methods. The final samples were hand-picked, and had about 99% purity. Biotite and muscovite were separated from metasedimentary rocks, and biotite and amphibole from metavolcanic and plutonic rocks. The metavolcanic rocks samples have an intermediate composition, and are rich in amphiboles. Plutonic rock samples include two granodioritic specimens from the eastern margin of the Lac Frechette complex, and two samples from lamprophyric dykes from the Bellecombe shear zone and the vicinity of Montbeillard village. A muscovite mineral separate (JL18) was obtained from a leucogranitic sample of the Decelles batholith.

Mineral separates were sent to Queen's University, Kingston, Ontario, for irradiation and step-heating (section 1.3). Amphiboles were heated at 8 steps between 800° and 1200°C, biotites at 10 steps between 500° and 1200°C, and muscovites at 10 steps between 650° and 1200°C.

5.2.2. Results

Table 5.3 and Fig. 5.2 show the results of the step-heating experiments on the samples. Through the text, the term 'plateau' refers to a number of high-temperature gas fractions that yield $^{40}Ar/^{39}Ar$ ages with overlap in error, and the term 'disturbed age spectrum' refers to an uneven spectrum that shows major argon loss subsequent to crystallization and rapid cooling.

As may be noticed from Fig. 5.2, age spectra of different step-heated minerals from almost all samples are relatively undisturbed. An exception is the spectra for biotites from sample JL25 (Fig. 5.2H), for which disturbed early steps may be a record of an argon loss due to local thermal disturbances. Comparative study of the analyzed minerals, both in thin-section and in mineral separates, indicates that size of the crystals in this sample is comparable to average crystal-size of other samples, and hence the disturbances may not be related to small grain size of the minerals.

Amphibole plateau ages for two samples from the granodioritic Lac Frechette complex are 2607±8 and 2649±13 (Fig. 5.2B, D). A lamprophyric sample (PM16, Fig. 5.2A) from the

Table 5.3. Step heating isotopic analyses of dated samples from the northwestern Pontiac Subprovince.

Temp./°C	$^{36}Ar/^{40}Ar$	$^{39}Ar/^{40}Ar$	Ca/K	%^{40}Ar	%^{39}Ar	$^{40}Ar/^{39}Ar$	Age/Ma
PM58, Amphibole (J=0.033918); Sample mass=98.0 mg							
800	107.16E-6	11.43E-3	5.16	96.48	36.00	84.709	2442.86±39.86
900	12.80E-6	10.39E-3	5.35	99.25	25.85	95.893	2611.44±5.14
940	23.35E-6	10.43E-3	5.29	98.84	14.31	95.220	2601.72±6.56
980	18.57E-6	10.64E-3	5.25	99.97	10.29	94.536	2591.80±6.38
1000	47.69E-6	11.41E-3	5.14	99.96	3.12	88.906	2507.99±7.15
1030	84.68E-6	11.65E-3	6.72	99.96	1.81	88.010	2494.27±6.41
1080	36.76E-6	11.48E-3	8.73	99.96	6.52	88.084	2495.41±6.08
1200	238.79E-6	9.80E-3	7.34	90.18	2.11	94.834	2596.13±24.64

Temp./°C	$^{36}Ar/^{40}Ar$	$^{39}Ar/^{40}Ar$	Ca/K	%^{40}Ar	%^{39}Ar	$^{40}Ar/^{39}Ar$	Age/Ma
JL19, Amphibole (J=0.033504); Sample mass=100.0 mg							
800	851.46E-6	5.96E-3	0.77	74.14	3.43	125.562	2976.70±27.69
900	744.82E-6	8.08E-3	7.21	77.16	6.08	96.510	2603.34±26.42
940	30.09E-6	9.37E-3	13.35	97.70	6.21	105.787	2731.16±11.44
980	13.78E-6	9.66E-3	15.34	99.36	14.60	103.915	2706.09±31.56
1020	12.89E-6	10.04E-3	14.37	98.83	39.07	99.194	2641.27±12.93
1060	54.67E-6	10.09E-3	14.62	99.97	7.31	100.735	2662.67±15.34
1100	10.89E-6	9.89E-3	15.24	98.49	14.90	100.816	2663.79±10.49
1200	11.55E-6	9.74E-3	15.92	97.67	8.40	102.278	2683.87±22.91

Temp./°C	$^{36}Ar/^{40}Ar$	$^{39}Ar/^{40}Ar$	Ca/K	%^{40}Ar	%^{39}Ar	$^{40}Ar/^{39}Ar$	Age/Ma
JL19, Biotite (J=0.033444); Sample mass=100.0 mg							
500	228.58E-6	12.10E+3	0.00	92.65	5.98	77.092	2300.00±23.78
540	264.46E-6	10.00E-3	0.00	91.52	4.30	92.180	2538.00±12.16
580	7.81E-3	311.10E-3	15.80	99.22	0.45	10.630	548.77±300.25
640	638.56E-6	8.70E-3	0.00	80.95	13.15	93.247	2553.69±6.75
690	62.08E-6	10.45E-3	0.00	97.78	8.87	93.924	2563.59±10.53
770	5.97E-6	10.89E-3	0.04	99.31	7.10	91.668	2530.41±11.23
850	8.96E-6	10.72E-3	0.00	99.97	13.35	93.546	2558.07±4.24
930	7.13E-6	10.53E-3	0.19	99.55	18.68	94.795	2576.23±8.52
990	21.82E-6	10.32E-3	0.00	99.08	15.97	96.318	2598.13±7.72
1200	19.53E-6	10.22E-3	0.12	98.79	12.14	97.321	2612.41±16.30

Table 5.3. Continued.

Temp./°C	$^{36}Ar/^{40}Ar$	$^{39}Ar/^{40}Ar$	Ca/K	%^{40}Ar	%^{39}Ar	$^{40}Ar/^{39}Ar$	Age/Ma
PM16, Amphibole (J=0.033813); Sample mass=101.0 mg							
800	386.64E-6	26.13E-3	0.86	87.74	18.66	33.899	1377.81±18.14
900	38.45E-6	12.10E-3	16.96	99.96	24.78	83.604	2421.19±8.88
940	11.79E-6	11.88E-3	18.50	98.16	13.33	83.902	2425.94±6.61
980	7.78E-6	11.93E-3	17.34	98.21	11.58	83.647	2421.88±17.54
1010	78.24E-6	12.23E-3	15.81	99.96	5.60	83.667	2422.19±12.34
1060	57.24E-6	11.75E-3	17.56	96.15	6.90	83.650	2421.92±9.42
1100	9.86E-6	10.80E-3	20.72	97.80	9.61	92.319	2555.02±8.61
1200	42.63E-6	10.59E-3	25.61	96.26	9.54	93.262	2568.93±10.85

Temp./°C	$^{36}Ar/^{40}Ar$	$^{39}Ar/^{40}Ar$	Ca/K	%^{40}Ar	%^{39}Ar	$^{40}Ar/^{39}Ar$	Age/Ma
PM97, Amphibole (J=0.033985); Sample mass=100.0 mg							
800	988.19E-6	13.83E-3	6.85	69.00	3.95	51.198	1818.41±52.84
900	96.36E-6	11.82E-3	11.84	95.86	10.26	82.207	2405.51±12.70
940	168.19E-6	9.82E-3	11.91	94.43	62.52	96.742	2626.34±29.48
980	80.68E-6	12.02E-3	11.83	94.79	3.54	81.191	2389.03±48.18
1010	110.21E-6	11.48E-3	12.77	99.95	3.11	89.929	2526.18±36.90
1060	18.60E-6	10.93E-3	13.15	97.90	4.25	91.984	2556.99±32.02
1100	15.98E-6	10.53E-3	18.18	97.84	10.71	94.553	2594.76±18.71
1200	364.19E-6	10.02E-3	31.06	81.59	1.66	89.049	2512.83±70.85

Temp./°C	$^{36}Ar/^{40}Ar$	$^{39}Ar/^{40}Ar$	Ca/K	%^{40}Ar	%^{39}Ar	$^{40}Ar/^{39}Ar$	Age/Ma
JL20, Amphibole (J=0.033586); Sample mass=100.0 mg							
800	44.12E-6	35.00E-3	7.47	99.90	42.70	28.942	1225.12±17.75
900	471.24E-6	29.69E-3	60.65	77.74	9.92	28.996	1226.77±31.72
940	379.10E-6	30.42E-3	7.06	85.77	3.99	29.195	1232.86±50.04
980	178.50E-6	32.44E-3	11.16	90.62	3.92	29.197	1232.93±38.89
1010	152.04E-6	31.05E-3	28.09	88.60	3.06	30.763	1280.20±33.64
1040	317.91E-6	26.20E-3	47.83	81.04	1.90	34.585	1390.66±45.09
1080	106.60E-6	33.86E-3	6.82	93.44	5.54	28.600	1214.55±17.97
1200	150.53E-6	33.51E-3	2.78	94.39	28.97	28.513	1211.87±18.45

Table 5.3. Continued.

Temp./°C	$^{36}Ar/^{40}Ar$	$^{39}Ar/^{40}Ar$	Ca/K	%^{40}Ar	%^{39}Ar	$^{40}Ar/^{39}Ar$	Age/Ma
PM101. Biotite (J=0.034015); Sample mass=100.0 mg							
500	938.82E-6	17.12E-3	0.11	71.79	6.51	42.212	1606.16±19.97
540	1.27E-3	7.82E-3	0.00	62.47	8.31	80.090	2372.14±18.47
580	399.17E-6	9.93E-3	0.00	88.01	11.47	88.835	2510.76±20.03
640	220.05E-6	10.53E-3	0.00	93.30	13.11	88.777	2509.88±11.50
690	308.88E-6	10.24E-3	0.00	90.59	8.48	88.764	2509.69±10.66
770	146.84E-6	10.85E-3	0.00	95.38	9.80	88.167	2500.55±10.79
850	130.00E-9	11.29E-3	0.00	99.76	13.59	88.557	2506.52±6.90
930	153.37E-6	10.72E-3	0.00	95.28	17.14	89.087	2514.61±7.72
990	30.26E-6	11.15E-3	0.02	98.64	7.47	88.883	2511.50±10.22
1200	97.32E-6	10.88E-3	0.59	95.61	3.85	89.271	2517.42±10.52

Temp./°C	$^{36}Ar/^{40}Ar$	$^{39}Ar/^{40}Ar$	Ca/K	%^{40}Ar	%^{39}Ar	$^{40}Ar/^{39}Ar$	Age/Ma
JL1. Biotite (J=0.033378); Sample mass=100.0 mg							
500	312.61E-6	32.53E-3	0.18	89.62	7.78	27.901	1187.41±15.51
540	643.15E-6	9.75E-3	0.00	79.60	1.57	83.053	2395.19±39.28
580	27.74E-6	10.83E-3	0.00	99.40	2.15	93.114	2549.05±24.15
640	3.90E-6	10.92E-3	0.00	98.88	3.12	91.461	2524.66±15.31
690	639.47E-6	9.11E-3	0.00	80.50	3.57	89.013	2487.91±10.21
770	3.28E-3	389.00E-6	0.00	3.01	9.20	77.262	2300.28±1044
850	111.84E-6	10.33E-3	0.00	96.32	8.89	93.613	2556.35±12.36
930	17.44E-6	10.45E-3	0.00	99.34	31.02	95.189	2579.21±5.98
990	180.00E-9	10.67E-3	0.06	99.73	16.84	93.715	2557.84±9.78
1200	2.09E-3	4.11E-3	0.05	38.17	15.85	93.119	2549.13±15.86

Temp./°C	$^{36}Ar/^{40}Ar$	$^{39}Ar/^{40}Ar$	Ca/K	%^{40}Ar	%^{39}Ar	$^{40}Ar/^{39}Ar$	Age/Ma
PM54, Biotite (J=0.033854); Sample mass=100.0 mg							
500	598.44E-6	23.61E-3	0.31	80.39	3.24	34.869	1406.35±40.40
540	6.51E-6	14.98E-3	0.00	99.42	6.47	66.905	2134.70±24.41
580	63.56E-6	11.48E-3	0.00	97.63	7.73	85.485	2452.55±20.69
640	820.00E-9	11.32E-3	0.00	99.76	15.32	88.396	2497.64±13.83
690	18.29E-6	11.25E-3	0.05	99.04	9.17	88.435	2498.24±14.72
770	820.00E-9	11.40E-3	0.00	99.12	4.60	87.674	2486.56±10.00
850	1.33E-6	11.24E-3	0.00	99.72	13.69	89.009	2507.00±22.46
930	5.66E-6	11.25E-3	0.00	99.92	19.87	89.038	2507.43±11.03
990	580.00E-9	11.29E-3	0.00	99.50	9.58	88.631	2501.23±13.19
1200	51.48E-6	10.86E-3	0.00	97.67	10.34	90.648	2531.77±29.99

Table 5.3. Continued.

Temp./°C	$^{36}Ar/^{40}Ar$	$^{39}Ar/^{40}Ar$	Ca/K	%^{40}Ar	%^{39}Ar	$^{40}Ar/^{39}Ar$	Age/Ma
JL25, Biotite (J=0.033667); Sample mass=100.0 mg							
500	2.61E-3	4.96E-3	0.00	22.60	2.14	46.152	1691.48±132.4
540	14.58E-6	38.99E-3	0.06	97.29	7.18	25.756	1126.49±16.54
580	7.27E-6	23.83E-3	0.00	98.43	7.83	42.047	1591.12±11.14
640	9.08E-6	17.86E-3	0.01	98.81	11.78	55.835	1908.22±7.32
690	25.77E-6	16.76E-3	0.04	99.71	9.78	60.110	1996.21±10.91
770	11.82E-6	16.08E-3	0.07	99.03	16.65	61.991	2033.60±8.84
850	382.05E-6	14.95E-3	0.28	88.07	14.22	59.343	1980.73±9.68
930	6.40E-6	15.97E-3	0.32	99.04	15.31	62.484	2043.28±7.05
990	120.76E-6	14.73E-3	0.40	95.44	11.20	65.488	2101.13±18.16
1200	82.97E-6	13.56E-3	1.52	93.03	3.91	71.958	2219.76±25.38

Temp./°C	$^{36}Ar/^{40}Ar$	$^{39}Ar/^{40}Ar$	Ca/K	%^{40}Ar	%^{39}Ar	$^{40}Ar/^{39}Ar$	Age/Ma
PM90, Biotite (J=0.033953); Sample mass=100.0 mg							
500	139.07E-6	24.16E-3	0.31	95.28	10.37	39.686	1539.48±31.67
540	8.09E-6	16.68E-3	0.14	97.20	1.50	59.824	2000.67±33.76
580	678.66E-6	12.94E-3	0.22	78.24	1.42	61.776	2039.68±32.17
640	9.11E-6	11.31E-3	0.00	99.54	16.69	88.219	2498.88±11.97
690	12.58E-6	10.87E-3	0.00	99.43	15.04	91.692	2551.35±15.90
770	13.09E-6	11.56E-3	0.00	99.43	19.03	86.157	2466.98±7.26
850	3.71E-6	11.42E-3	0.03	99.72	21.58	87.498	2487.80±6.23
930	18.31E-6	11.41E-3	0.00	99.14	10.82	87.143	2482.31±7.71
990	820.00E-9	11.38E-3	0.30	98.70	2.73	87.866	2493.45±12.97
1200	759.08E-6	9.33E-3	3.82	72.81	0.82	83.132	2419.15±72.76

Temp./°C	$^{36}Ar/^{40}Ar$	$^{39}Ar/^{40}Ar$	Ca/K	%^{40}Ar	%^{39}Ar	$^{40}Ar/^{39}Ar$	Age/Ma
JL25, Muscovite (J=0.033639); Sample mass=100.0 mg							
650	23.96E-6	11.57E-3	0.00	99.17	34.11	85.820	2449.25±11.78
730	2.74E-6	11.25E-3	0.00	99.81	13.51	88.930	2497.16±10.19
780	7.40E-6	11.55E-3	0.33	99.04	2.93	86.800	2464.49±34.90
830	11.62E-6	11.56E-3	0.00	99.73	5.89	86.829	2464.94±11.89
870	1.21E-6	11.37E-3	0.02	98.77	2.97	87.921	2481.76±14.21
910	30.75E-6	11.47E-3	0.01	97.94	3.20	86.384	2458.04±15.69
950	6.53E-6	11.23E-3	0.00	99.23	6.83	88.851	2495.96±11.45
990	10.45E-6	11.04E-3	0.00	99.11	7.07	90.311	2518.05±5.28
1050	910.00E-9	10.76E-3	0.00	99.74	21.51	92.909	2556.67±9.01
1200	192.87E-6	10.25E-3	0.02	91.18	1.98	91.993	2543.15±22.41

Table 5.3. Continued.

Temp./°C	$^{36}Ar/^{40}Ar$	$^{39}Ar/^{40}Ar$	Ca/K	%^{40}Ar	%^{39}Ar	$^{40}Ar/^{39}Ar$	Age/Ma
PM57, Biotite (J=0.033881); Sample mass=100.0 mg							
500	77.76E-6	15.81E-3	0.00	97.13	6.01	61.800	2037.57±23.13
540	2.30E-6	11.75E-3	0.00	99.71	13.03	85.076	2447.20±20.11
580	2.72E-6	11.33E-3	0.00	99.90	15.86	88.355	2498.10±13.25
640	3.02E-6	11.17E-3	0.00	99.70	13.46	89.418	2514.30±5.57
690	8.58E-6	11.22E-3	0.00	99.12	4.01	88.900	2506.41±9.98
770	1.96E-6	11.37E-3	0.00	99.74	14.69	87.866	2490.59±7.76
850	5.04E-6	11.71E-3	0.00	99.92	14.04	85.518	2454.14±3.86
930	9.03E-6	11.82E-3	0.00	99.81	6.81	84.823	2443.20±9.84
990	5.35E-6	11.63E-3	0.00	99.42	8.09	85.856	2459.43±11.19
1200	64.76E-6	11.03E-3	0.12	96.73	4.00	88.932	2506.90±9.84

Temp./°C	$^{36}Ar/^{40}Ar$	$^{39}Ar/^{40}Ar$	Ca/K	%^{40}Ar	%^{39}Ar	$^{40}Ar/^{39}Ar$	Age/Ma
JL14, Biotite (J=0.033769); Sample mass=100.0 mg							
500	607.27E-6	14.18E-3	0.06	81.58	8.43	57.879	1954.44±20.65
540	43.59E-6	12.25E-3	0.00	98.04	6.12	80.566	2370.39±15.19
580	1.57E-6	11.66E-3	0.00	99.69	16.27	85.709	2452.69±12.37
640	8.83E-6	11.38E-3	0.00	99.43	13.56	87.624	2482.40±9.28
690	4.67E-6	11.45E-3	0.00	99.61	7.68	87.433	2479.46±8.70
770	11.81E-6	11.83E-3	0.00	99.96	11.42	84.845	2439.11±5.41
850	162.13E-6	11.59E-3	0.19	94.60	6.84	82.145	2396.05±13.95
930	21.42E-6	11.98E-3	0.00	99.00	13.47	82.979	2409.47±13.47
990	9.37E-6	11.90E-3	0.00	99.31	12.92	83.799	2422.56±12.03
1200	184.39E-6	10.90E-3	0.11	92.16	3.29	86.710	2468.28±11.72

Temp./°C	$^{36}Ar/^{40}Ar$	$^{39}Ar/^{40}Ar$	Ca/K	%^{40}Ar	%^{39}Ar	$^{40}Ar/^{39}Ar$	Age/Ma
JL41, Muscovite (J=0.033744); Sample mass=100.0 mg							
650	108.19E-6	11.08E-3	0.00	96.43	5.59	87.409	2478.09±43.03
750	6.40E-6	10.98E-3	0.00	99.74	56.88	90.936	2531.65±5.91
790	14.91E-6	11.14E-3	0.00	99.96	4.65	90.165	2520.09±10.02
830	16.60E-6	11.30E-3	0.14	99.27	1.81	88.953	2501.73±42.69
870	17.46E-6	11.19E-3	0.00	99.87	3.57	89.800	2514.57±8.80
910	892.26E-6	7.97E-3	0.00	73.20	2.85	92.436	2553.95±10.81
950	16.36E-6	11.10E-3	0.00	98.96	4.48	89.638	2512.13±5.61
990	18.87E-6	11.09E-3	0.00	98.92	5.09	89.693	2512.96±6.71
1050	10.87E-6	11.01E-3	0.00	99.35	9.57	90.508	2525.23±6.04
1200	108.37E-6	10.64E-3	0.00	96.00	5.51	90.988	2523.44±5.56

Table 5.3. Continued.

Temp./°C	$^{36}Ar/^{40}Ar$	$^{39}Ar/^{40}Ar$	Ca/K	$\%^{40}Ar$	$\%^{39}Ar$	$^{40}Ar/^{39}Ar$	Age/Ma
JL44, Biotite (J=0.033719); Sample mass=100.0 mg							
500	327.60E-6	22.09E-3	0.00	87.89	2.67	40.886	1563.3±44.50
540	4.70E-6	12.95E-3	0.11	98.60	3.41	77.117	2311.08±9.87
580	6.34E-6	12.04E-3	0.00	98.79	3.95	82.935	2406.80±15.81
640	6.71E-6	10.94E-3	0.00	99.97	18.13	91.567	2540.06±13.29
690	4.51E-6	11.02E-3	0.00	99.43	9.15	90.633	2526.10±10.67
770	20.05E-6	11.22E-3	0.00	99.08	12.90	88.614	2495.57±11.30
850	8.49E-6	11.19E-3	0.00	99.47	16.02	89.152	2503.76±11.11
930	4.71E-6	11.17E-3	0.00	99.60	18.50	89.427	2507.93±7.52
990	4.22E-6	10.93E-3	0.00	99.33	8.99	91.343	2536.73±16.82
1200	85.70E-6	10.01E-3	0.13	96.24	6.27	97.340	2624.00±10.84

Temp./°C	$^{36}Ar/^{40}Ar$	$^{39}Ar/^{40}Ar$	Ca/K	$\%^{40}Ar$	$\%^{39}Ar$	$^{40}Ar/^{39}Ar$	Age/Ma
JL44, Muscovite (J=0.033693); Sample mass=100.0 mg							
650	39.16E-6	13.23E-3	0.00	98.19	6.85	74.734	2269.37±15.29
730	23.73E-6	10.86E-3	0.00	99.14	27.62	91.409	2536.65±11.49
780	7.13E-6	11.03E-3	0.00	99.54	16.82	90.466	2522.55±10.16
830	15.96E-6	11.18E-3	0.03	98.82	5.76	89.020	2500.70±15.19
870	10.21E-6	11.08E-3	0.00	98.86	4.89	89.947	2514.74±10.50
910	740.00E-9	11.07E-3	0.14	99.29	5.91	90.351	2520.82±13.33
950	1.13E-6	10.98E-3	0.00	99.31	6.20	91.088	2531.86±11.41
990	1.43E-6	10.87E-3	0.00	99.34	6.72	92.020	2545.73±10.39
1050	8.09E-6	10.75E-3	0.00	99.34	12.91	92.778	2556.93±7.15
1200	127.46E-6	10.10E-3	0.00	95.04	6.32	95.328	2594.12±8.86

Temp./°C	$^{36}Ar/^{40}Ar$	$^{39}Ar/^{40}Ar$	Ca/K	$\%^{40}Ar$	$\%^{39}Ar$	$^{40}Ar/^{39}Ar$	Age/Ma
JL18, Muscovite (J=0.033411); Sample mass=100.0 mg							
650	107.99E-6	12.06E-3	0.00	96.19	5.14	80.270	2351.51±19.00
730	14.64E-6	11.40E-3	0.00	99.30	12.70	87.346	2463.77±7.83
780	5.83E-6	11.47E-3	0.00	99.58	5.51	87.354	2463.91±8.39
830	10.88E-6	11.27E-3	0.00	99.28	8.44	88.473	2481.04±12.91
870	8.50E-6	11.35E-3	0.00	99.67	5.93	88.319	2478.68±11.74
910	27.69E-6	11.30E-3	0.00	99.48	2.58	89.225	2492.45±18.69
950	3.29E-6	11.23E-3	0.00	99.39	7.36	88.932	2488.01±9.86
990	2.23E-6	11.17E-3	0.00	99.73	12.31	89.554	2497.42±7.74
1050	1.18E-6	11.10E-3	0.00	99.80	30.41	90.043	2504.80±4.73
1200	30.19E-6	10.95E-3	0.00	98.39	9.61	90.554	2512.46±8.63

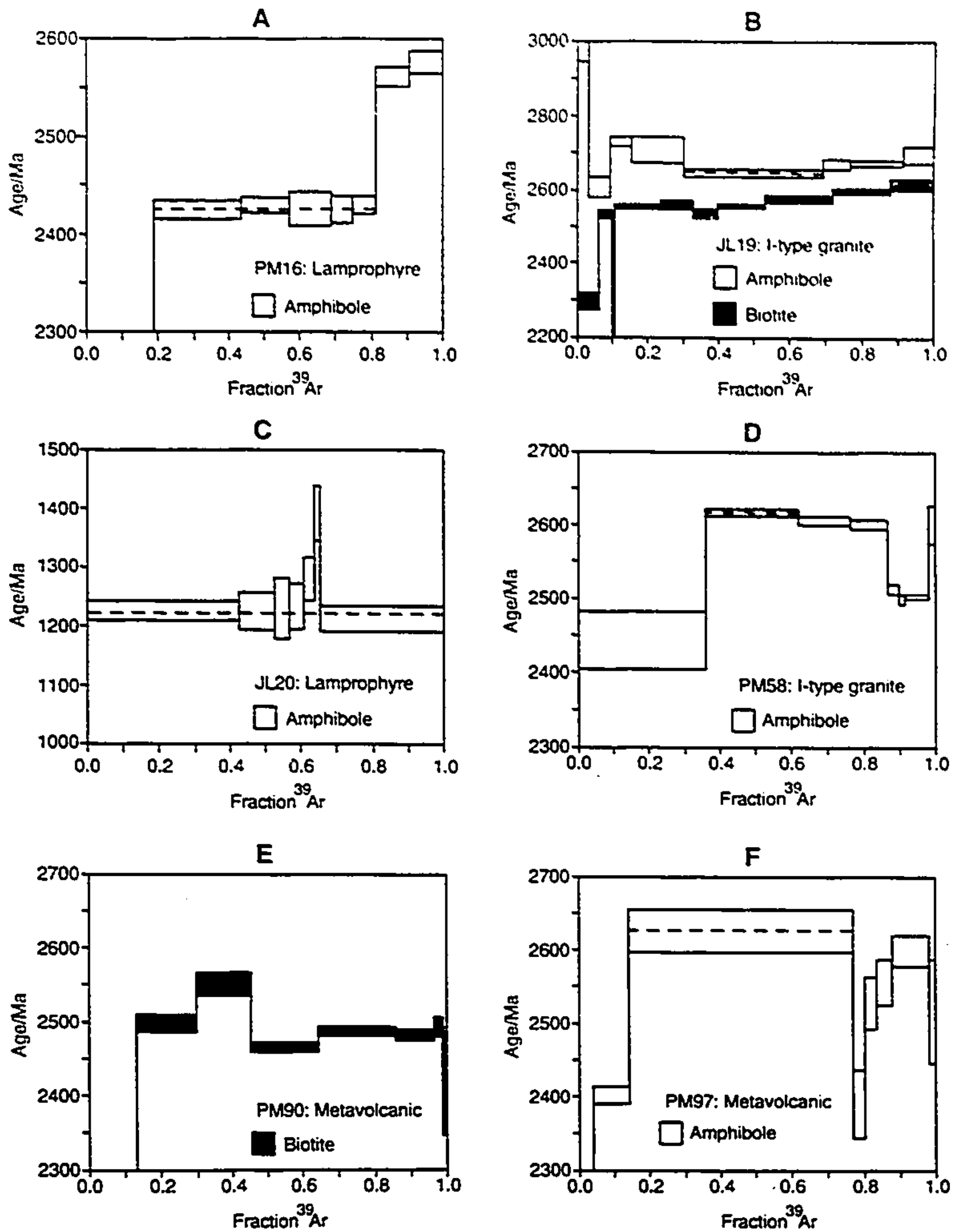

Fig. 5.2. $^{40}Ar/^{39}Ar$ age spectra resulted from step-heating of amphiboles, muscovites, and biotites in different rock types of the study area.

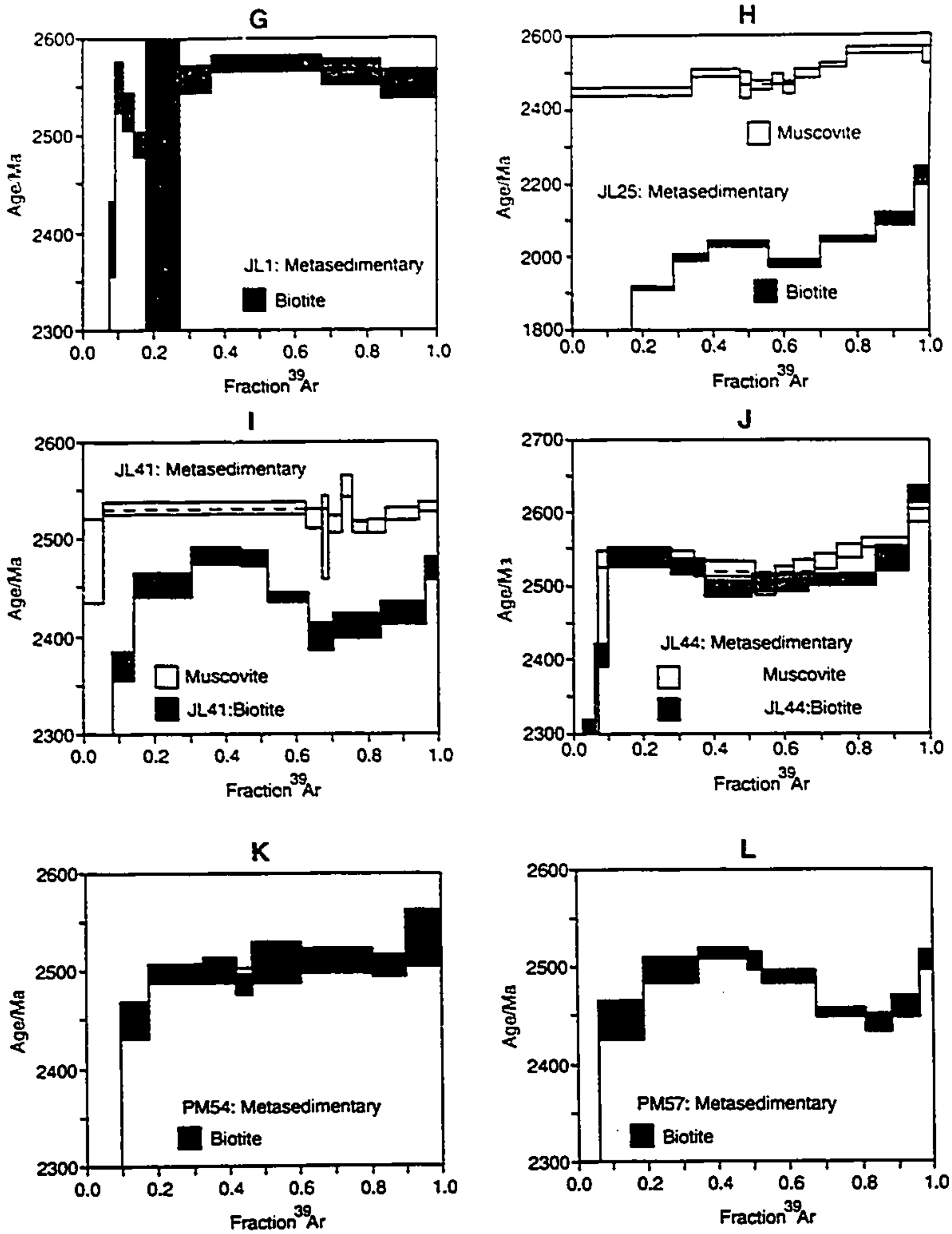

Fig. 5.2. Continued.

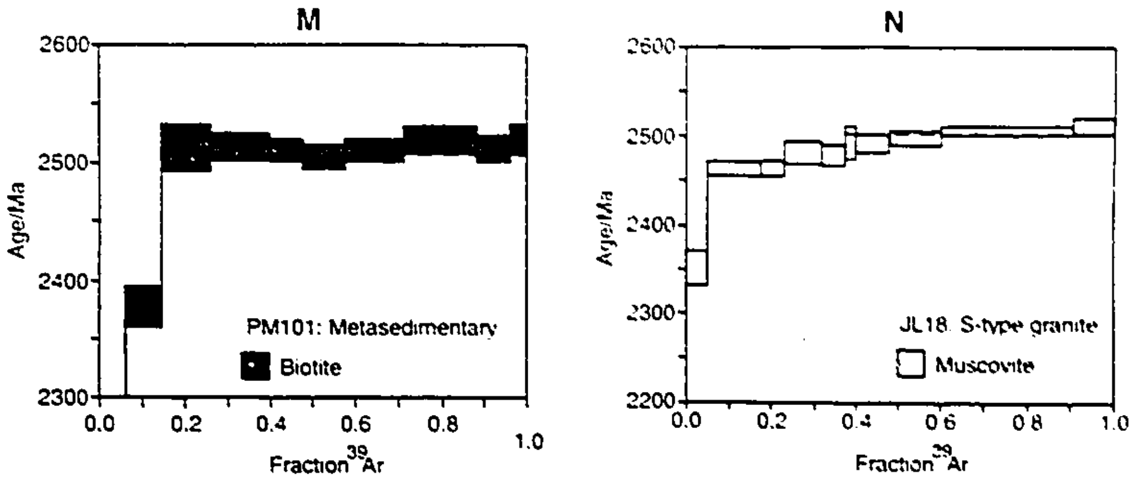

Fig. 5.2. Continued.

Bellecombe shear zone has an amphibole plateau age of 2422±9 Ma. For this sample another (smaller) plateau, however, may be placed at about 2562±10 Ma, which is still about 60 Ma younger than the two amphibole ages from granodioritic rocks. The lamprophyre, therefore, is considered to be considerably younger than the Lac Frechette complex, and belongs to a renewal of magmatic event. A 2673±2 Ma emplacement age has been dated for a lamprophyric dyke in southern Abitibi area (Wyman and Kerrich 1987). Biotites from the granodioritic sample JL19 (Fig. 5.2B) show a plateau age of 2604±11 Ma, which is about 37 Ma younger than the amphibole plateau age for the same sample.

The amphibole plateau age of 2622±28 Ma for a metavolcanic sample (PM97, Fig. 5.2F) from the Lac Opasatica gneiss domain is similar to that of dated amphiboles from the granodioritic samples. An average amphibole plateau (cooling) age of 2626 Ma is suggested for two granodioritic samples and a metavolcanic sample. Another metavolcanic sample (PM90) from the same domain shows a biotite plateau age of 2551±16 Ma.

Amphiboles of a lamprophyric sample (JL20, Fig. 5.2C) from east of Lac Opasatica show a consistent undisturbed plateau age of 1221±12 Ma, corresponding to 95% of ^{39}Ar. This dated lamprophyre therefore represents the youngest igneous activity within the Pontiac Subprovince.

Biotite plateau ages from metasedimentary rocks of the Pontiac Group (Figs. 5.2G to M) range from 2480±9 to 2565±12 Ma. Sample JL25 shows an extraordinarily younger age of 2220±26 Ma, probably resulting from a late local thermal disturbance. An average biotite age of about 2517 Ma (excluding sample JL25, and including metavolcanic sample PM90) may be calculated for seven rock samples.

Plateau ages for muscovites from metasedimentary samples range from 2502±11 to 2555±10 Ma. An average muscovite age of about 2529 Ma was calculated for four analyzed samples of metasedimentary rocks.

5.2.3. Interpretation

$^{40}Ar/^{39}Ar$ plateau age of amphiboles from two granodioritic samples of the Lac Frechette complex (Fig. 5.2 B, D) are about 50 Ma younger than the *ca.* 2681 Ma U/Pb zircon age of this plutonic complex (Mortensen and Card 1993). Biotites dated from one of these samples (JL19) yielded an age of 2604±11 Ma (about 90 Ma older than the average for biotites from the metasedimentary and metavolcanic rocks). A comparison of biotite compositions (see Tables 4.3 and 4.4) indicates that there is almost no difference between biotites from the metasedimentary rocks and biotites from the granodioritic sample in terms of magnesium content. The large difference in plateau ages, therefore, may not be related to different closure temperatures; this may be because of a difference in the phlogopite content of biotites in the igneous and metasedimentary samples (the effect of phlogopite content on argon retentivity of biotites is discussed in Harrison *et al.* 1985). No major difference in grain size is present between the biotite crystals from different igneous and metasedimentary samples.

A proposed cooling history of the Pontiac Subprovince, as suggested by $^{40}Ar/^{39}Ar$ data analyses from this study, combined with U/Pb dating data from other studies, is illustrated in Fig. 5.3. Closure temperatures of different minerals, used in construction of the cooling history diagram, are summarized in Table 5.4.

Considering the U/Pb zircon age of 2681 Ma (Mortensen & Card 1993) to be the crystallization age of the Lac Frechette complex, the average $^{40}Ar/^{39}Ar$ age of 2628 Ma for the amphiboles from the same pluton suggests a cooling rate of about 5°C/Ma. A similar calculation based on the difference between U/Pb zircon age, and $^{40}Ar/^{39}Ar$ biotite age for the Lac Frechette complex, suggests a cooling rate of about 7°C/Ma for this plutonic body. Comparing the suggested average muscovite age of 2529 to that of amphiboles indicates a slower cooling rate of about 2°C/Ma between closure temperatures of amphibole and muscovite. A similar comparison between average $^{40}Ar/^{39}Ar$ ages of muscovites and biotites suggests a cooling rate of about 6°C/Ma between temperatures of about 350° and 280°C (closure temperatures of muscovite and biotite respectively) for the study area. Calculation of

Table 5.4. Closure temperatures (T_c) for different minerals used in estimation of cooling history.

Mineral	Method	T_c	References
zircon	U/Pb	>800°C	Heaman & Parrish (1991)
monazite	U/Pb	700°C	Parrish 1990, Copeland *et al.* 1988
titanite	U/Pb	600°C	Tucker *et al.* 1987, Heaman & Parrish (1991)
amphibole	Ar/Ar	530±40°C	Harrison (1981), McDougall & Harrison (1988)
muscovite	Ar/Ar	350°C	Purdy & Jäger (1976)
biotite	Ar/Ar	280±40°C	Harrison *et al.* (1985)

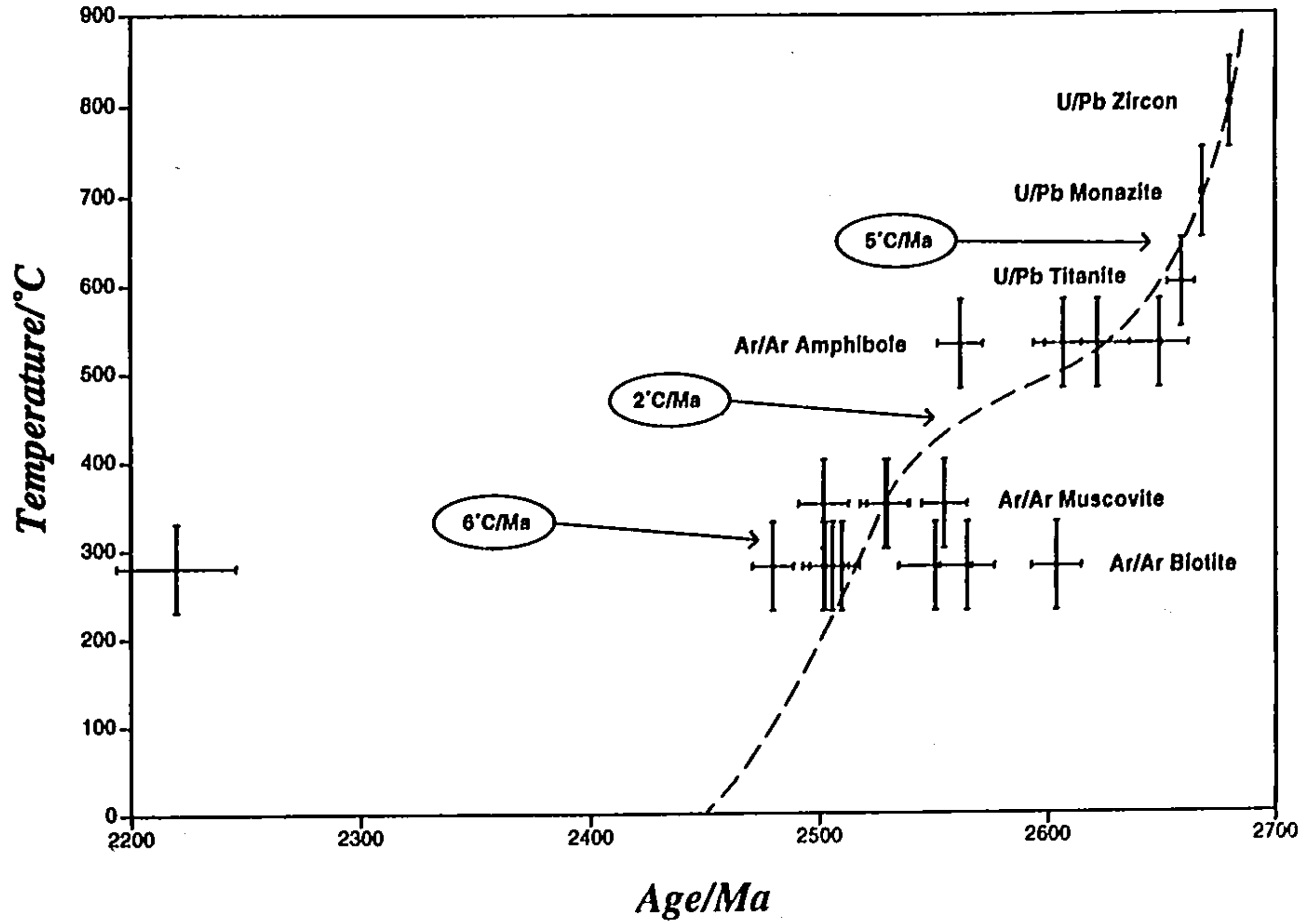

Fig. 5.3. Cooling history of rocks within the northwestern Pontiac Subprovince, constructed on the basis of $^{40}Ar/^{39}Ar$ ages of different minerals. The dashed line represents suggested cooling curve. U/Pb titanite (2660±6, Lac Opasatica gneiss), monazite (2668±1, Decelles batholith) and zircon (2681+2/-1, Lac Frechette complex) ages are from Machado *et al.* (1991a), and Mortensen and Card (1993).

the cooling rate between the closure temperatures of muscovite and biotite for individual metasedimentary samples JL41 and JL44 show values of about 1.5° and 3°C/Ma for these samples.

Assuming that the crust followed a similar Tt path following closure of biotite, the map section would have been exposed on the surface at about 2450 Ma (see Fig. 5.3). This accords with maximum depositional ages for the Huronian Supergroup, which were unconformably deposited on the Pontiac and Timiskaming Group rocks.

The wide distribution of cooling ages for amphibole, muscovite and biotite (as high as 124 Ma for the latter mineral) may have resulted from a very slow cooling through closure temperatures of the minerals. Another possible interpretation is that the minerals were subjected to one or more younger thermal events. No major magmatic activity has occurred within the study area after *ca.* 2630 Ma; moreover, intrusion of the Early Proterozoic dykes does not appear to have caused an important thermal disturbance within the rocks of the area. Multiple tectonic reactivation of the terrane is suggested to be responsible for later possible thermal effects and/or persistence of relatively high temperatures within a thickened crust.

5.3. Synthesis of geochronologic data for the Pontiac Subprovince

In this section, available geochronological data for the Pontiac and Abitibi Subprovinces (summarized in Table 5.1) are compiled with new $^{40}Ar/^{39}Ar$ analyses and geologic data from this study, to develop a time framework for the geologic evolution of the study area.

5.3.1. Depositional and magmatic history

The oldest documented zircon crystallization ages within the Pontiac Subprovince come from the Belleterre-Fugerville tonalite (2705±5 Ma, Carignan *et al.* 1992), the Lac des Quinze gneiss (2695±1 Ma, Mortensen & Card 1993), an anorthositic gabbro body south of the Baby-Belleterre belt (2694±2 Ma, Carignan *et al.* 1992), and from the Belleterre volcanic breccia

(2690±2 Ma, Mortensen & Card 1993). These ages are not in accordance with the relatively younger population of detrital zircons within the Pontiac metasedimentary rocks. As will be discussed in Chapter 6, these relatively old volcanic, plutonic and gneissic rocks are proposed to be predecessors of the relatively young Pontiac sedimentary basin. Granodioritic intrusions such as Lac Frechette complex, Lac Remigny pluton and Lac Simard pluton, with ages similar to the population of detrital zircons within the Pontiac Group metasedimentary rocks, and geochemical characteristics similar to arc-magmatic series (Feng *et al.* 1993), are interpreted as representing subduction-related magmatism during last stages of sedimentation in the Pontiac basin, and closure of the basin at about 2680 Ma due to a collisional event.

Due to similarity in composition and structure with the Lac de Quinze gneisses (Keith Benn, personal communication), the Lac Opasatica gneisses are suggested to have been developed during the same structural event. The only date on the Lac Opasatica gneisses is a titanite age (2660±6 Ma, Machado *et al.* 1991a) which probably indicates the cooling and/or metamorphic age of these rocks.

U/Pb ages of detrital zircons from the Pontiac metasedimentary rocks (Davis 1991, Gariépy *et al.* 1984, Mortensen & Card 1993) range from *ca.* 2940 Ma to *ca.* 2683 Ma. Sedimentation within the Pontiac sedimentary basin, must therefore have finished sometime after *ca.* 2683 Ma. Detrital zircons from Cadillac and Kewagama sedimentary units within Abitibi Subprovince yielded zircon ages (*ca.* 2687-2688 Ma, Davis 1991), similar to the youngest ages for detrital zircons within the Pontiac Group. The old zircon population ages of about *ca.* 2940 Ma (Gariépy *et al.* 1984) within the Pontiac Group appear to be quite different from the oldest absolute ages so far dated in the Abitibi greenstone belt or the Opatica belt farther north (see Table 5.1). The oldest magmatic zircon crystallization age so far dated within the Abitibi Subprovince is *ca.* 2759 Ma (Northern Volcanic Zone, Mortensen 1993a). However, based on Pb isotope data, Gariépy and Allègre (1985) suggested the presence of a 3.0 to 3.4 Ga inherited sialic crust component within the granitoid magmas of both the northern and southern Abitibi greenstone belts. So far the oldest zircon crystallization ages dated from the Lac Opatica gneiss belt are about *ca.* 2825 Ma (Davis *et al.* 1994, 1995). In Lacorne block, a metasedimentary and granitic terrane within the southern Abitibi Subprovince similar to Pontiac Subprovince, still older (3042±6 Ma) zircons have been dated (Feng & Kerrich 1991). Considering the age of the oldest dated rocks in the Abitibi Subprovince (*ca.* 2759 Ma, Mortensen 1993a), the Pontiac sedimentary basin must have been fed, at least partly, by erosion of a different and older terrane that does not outcrop in the southeastern Superior Province. However, Davis *et al.* (1994) have proposed the Opatica gneiss belt as a source for a moderately old population of zircons within the Pontiac metasedimentary rocks. Absence of old terranes in subprovinces surrounding the Pontiac Subprovince, and the presence of old (2.7 to 3.6 Ga, Goldich and Fischer 1986, Hoffman 1989) tonalitic to granodioritic orthogneisses and amphibolites within the Minnesota foreland in southwestern Superior Province, together suggest that this terrane may be a source for the old detrital zircons within the Pontiac sedimentary basin. Possible tectonic implications are discussed in Chapter 6. Considering relatively old I-type magmatism and gneiss formation in southwestern Pontiac Subprovince to be precursors of basin development (see Chapter 6), sedimentation in the basin must have started at about 2700 to 2690 Ma.

Ages of detrital zircons from the Timiskaming Group rocks range between *ca.* 2980 and *ca.* 2679 Ma (Davis 1991), similar to the Pontiac Group. Old detrital zircons within the Timiskaming Group may have been recycled from the Pontiac Group.

The only dated volcanic rocks within the Pontiac Subprovince are from the Baby and Belleterre volcanic belt situated in the southern part of the subprovince (see Fig. 2.1). Felsic volcanic rocks and related synvolcanic plutons of this belt show Pb/Pb zircon ages between *ca.* 2682 and *ca.* 2709 Ma (Mortensen and Card 1993). Considering the relatively younger ages of this volcanic belt compared to the southern Abitibi volcanic rocks, Mortensen and Card (1993) rejected the possibility that the belt is a klippe of the Abitibi belt emplaced over the Pontiac Subprovince.

Zircon and titanite ages for granitoid bodies that may be classified as I-type granites

(Lac Frechette, Lac Remigny, Lac Simard, Lac Maple and Tour de Belleterre granitoids) range between 2669±3 and 2686+4/-3 Ma (see Table 5.1 for references). A rather old (2705 ± 3) age is suggested for a tonalitic intrusion of Belleterre-Fugerville within the Baby-Belleterre belt (Carignan *et al.* 1992). Again, some discrepancy exists between old zircon ages of these granitoid bodies, and age of the youngest (2683±1 Ma) detrital zircons from the metasedimentary host rocks of the Pontiac Group.

Two samples from lamprophyric dykes intruded into the sedimentary rocks of the Pontiac Group were selected to be used for $^{40}Ar/^{39}Ar$ dating (see Table 5.2). Amphiboles from one of these samples (from the Bellecombe shear zone) indicates a plateau age of 2422±9 Ma. Another (smaller) plateau, however, may be placed at about 2562±10 Ma, which is still about 60 Ma younger than the average amphibole age of granodioritic and metavolcanic rocks within the study area. The lamprophyric body therefore is interpreted as indicative of igneous activity that occurred about 60 Ma after intrusion of the Lac Frechette complex. Another lamprophyric sample indicates amphibole ages that are much younger. A plateau age of 1221±12 Ma for amphiboles from this sample represent the youngest igneous activity so far dated within the Pontiac Subprovince.

Deposition of sedimentary rocks of the Cobalt group is bracketed by 2454 Ma date on diabase dykes of the Matachewan swarm (Heaman 1988, U/Pb zircon), which it unconformably overlies, and a *ca.* 2219 Ma date on diabase dykes and sills of the Nipissing swarm (Corfu and Andrews 1986, U/Pb baddeleyite), which are intruded into the sedimentary sequence.

No absolute age is available for mafic dyke swarms within the Pontiac Subprovince. However, van de Walle (1978), on the basis of orientation, composition, and cross-cutting relationships, has divided them into north-trending dykes comparable to the Matachewan dyke swarm (*ca.* 2454 Ma, Heaman 1988), and northeast-trending dykes of pre-Cobalt and post-Matachewan dyke swarm origin.

Age constraints on the S-type granites are discussed in the next section.

5.3.2. History of metamorphism

Constraints on the metamorphic history in the Pontiac Subprovince may essentially be inferred from absolute ages for S-type granites that are interpreted to result from the melting of sedimentary rocks within the Pontiac Group during peak metamorphic conditions (see Chapter 4). Monazites and zircons from the Decelles batholith, and from similar S-type granites and their related pegmatitic intrusions, give ages between *ca.* 2668 and *ca.* 2632 Ma (Mortensen & Card 1993, Machado *et al.* 1991a). Peak metamorphic conditions within the Pontiac Subprovince must therefore have been attained sometime before *ca.* 2668 Ma (so far maximum crystallization age of the S-type granites).

Zircon, monazite, titanite, and metamorphic minerals from samples within the Grenville front adjacent to the Pontiac Subprovince, yielded amphibolite and granulite facies Late Archean metamorphic ages between *ca.* 2653 and *ca.* 2508 Ma (Gariépy *et al.* 1990, Krogh 1994). These high-grade rocks may represent the equivalents of lower grade rocks of the Pontiac Subprovince that have been brought to the their present crustal level along the Grenville tectonic front. Relatively younger metamorphic ages from these high-grade rocks may be explained by slower cooling rates at greater depths.

Considering the age of the youngest detrital zircons from the Pontiac metasedimentary rocks (*ca.* 2683 Ma, Mortensen and Card 1993), a time interval of less than 15 Ma exists between the end of deposition within the Pontiac basin and melting of these sedimentary rocks. This phenomenon requires a relatively rapid increase in metamorphic temperature, which may have resulted from intrusion of voluminous I-type granitoid bodies within the Pontiac Subprovince (see Chapter 4).

Continuous intrusion of the I-type granites from *ca.* 2686 to *ca.* 2669 Ma, and renewed tectonic activities after peak metamorphic conditions may have caused a relatively slow cooling rate within the Pontiac Subprovince. Average cooling ages of about 2529 Ma from muscovite and *ca.* 2517 Ma from biotites within the Pontiac Subprovince rocks indicates that temperatures as high as 350°C and 280°C were persistent in crustal rocks of the area until *ca.* 150 Ma after attainment of peak metamorphic conditions.

The cooling history of the Pontiac Subprovince may be divided into an early relatively rapid, a middle relatively slow, and a late relatively rapid interval (see Fig. 5.3). On the basis of average $^{40}Ar/^{39}Ar$ plateau ages for amphiboles, muscovites and biotites from the study area, cooling rates of about 5°C/Ma , 2°C/Ma and 6°C/Ma are suggested for these three intervals. The early rapid interval records cooling of the crust after attainment of the peak metamorphic conditions during the D_2 event. The middle slow interval probably represents minor renewed crustal thickening during the D_3 contractional event. Finally, the late rapid interval may have resulted from the D_4 crustal extension preceding development of an early Proterozoic passive margin in which the Huronian Supergroup has been deposited.

A major difference between muscovite and biotite ages (about 335 Ma) in the metasedimentary sample JL25 may reflect a thermal disturbance of less than 350°C and more than 280°C (closure temperatures of muscovite and biotite respectively) of the rock between *ca.* 2529 and 2517 Ma (see Fig. 5.3). The sample is from an outcrop close to an exposure of a small S-type granitic intrusion; however, no dyke or other late intrusive body has been mapped close to the sample site. Also local tectonic activity (faulting) may have been responsible for thermal effects within the area. Thermobarometry of this sample from the sillimanite zone indicates re-equilibrium of the sample at lower pressures (about 4 kbar) compared to other samples within the sillimanite zone (see Fig. 4.14).

Geochronological and textural relationships between metamorphism and gold mineralization-related alterations indicate that Late Archean (*ca.* 2.7 Ga) lode gold mineralization in the Superior Province of Canada was a syn- to late-peak metamorphic event (Kerrich and Cassidy 1994). U/Pb ages for rutile and titanite in auriferous alteration at the Camflo mine in the Abitibi Subprovince indicates that gold deposition in this area (close to the Cadillac-Larder Lake fault zone) occurred at about 2625 Ma (Jemielita *et al.* 1990). These ages suggest that hydrothermal activities related to regional metamorphism were in effect up to about 45 Ma after attainment of peak metamorphic conditions.

5.3.3. Age constraints on structural events

Structures within the study area record six deformational events that have affected the Pontiac Subprovince during Late Archean and Early Proterozoic time (Chapter 3). Geochronologic data are used here to define some time constraints on these structural events.

The D_1 event is considered to be the first major deformational event after deposition of the Pontiac metasedimentary rocks, resulting in thickening of the sedimentary pile. This event appears to have been responsible for early folding and emergence (see sections 2.1.2 and 3.3) of the sedimentary rocks deposited within the Pontiac basin, and deposition of the Timiskaming sedimentary rocks. The age of this early event may be bracketed between the age of the youngest detrital zircon from the Pontiac metasedimentary rocks (2683±1 Ma) and peak metamorphism (2668±1 Ma), constrained by the oldest monazite ages from the S-type granitic rocks (ages from Mortensen & Card 1993). An approximate age of *ca.* 2680 Ma appears to be reasonable for the start of the D_1 event, because other than a *ca.* 2683 Ma age for the youngest zircons from the Pontiac Group, the youngest detrital zircons dated from the Timiskaming Group are about *ca.* 2679 Ma old. The Timiskaming Group is considered to be a syn-tectonic depositional system that was both deposited and deformed during the D_1 event (see section 3.3).

Before attainment of the peak metamorphic conditions within the subprovince, D_1 deformation ends and the D_2 event starts. S-type granites, on the other hand, are postulated to have been the result of melting of the Pontiac metasedimentary rocks during the peak metamorphic conditions. A maximum U/Pb monazite age of *ca.* 2668 Ma from the S-type granites within the subprovince may be considered the minimum age for the start of the syn-peak metamorphic D_2 event. Considering the probability of the presence of older S-type granites that have not been dated so far, an age of about *ca.* 2670 Ma is proposed for the beginning of the D_2 event.

S-type granitic dykes are deformed by the D_2 event. The youngest zircons from the S-type granites (*ca.* 2632 Ma, Machado *et al.* 1991a) may therefore be a tentative maximum age for the end of the D_2 event.

The D_2 event in temporal, structural, tectonic, and thermal aspects may be correlated with stage 4 in the Wawa gneiss domain described by Moser (1994). This event (*ca.* 2660-2637 Ma, based on intrusive relationships) in the Kapuskasing area has produced granulite facies gneisses which are later juxtaposed with greenschist facies rocks of the Abitibi Subprovince by an east-vergent thrust movement on the Ivanho Lake fault.

Temperatures remained as high as 350°C - 280°C until *ca.* 150 Ma after attainment of the peak metamorphic conditions (see section 5.3.2) indicating a very slow cooling rate of 2°C/Ma, which may reflect slow exhumation of deep crustal rocks. The D_3 event, that might have renewed crustal thickening after the D_2 event, probably resulted in a reduction of the exhumation rate, and hence the cooling rate of the crust. The age of thickening of the crust responsible for this change during the D_3 event may therefore have been limited between *ca.* 2626 Ma and *ca.* 2529 Ma. These two limits are the average cooling ages of amphiboles and muscovites within the study area, between which a slow cooling rate was prevalent.

The upper age limit of the D_3 contractional event, that resulted in east-trending folding and thrusting, may have been limited to the lower age limit for deposition of the Huronian Supergroup (*ca.* 2500 Ma), because this event does not affect the aforementioned sedimentary rocks.

An upper age limit may be established for the D_4 extensional event. As will be discussed in Chapter 6, this event resulted in development of basins in which the Cobalt Group rocks were deposited. A major extensional event is documented in the depositional record of the Huronian Supergroup, starting at about 2500 Ma (Zolani et *al.* 1984). Crustal extension that resulted in development of this passive margin sedimentary basin on the southern margin of the Superior Province, would have resulted in thinning of the crust. Normal faulting reactivation of the Cadillac-Larder Lake fault zone and a few structures within the southern Abitibi, resulting in development of half grabens for deposition of the Cobalt Group, may be correlated with this extensional event (Chapters 3 and 6). The late rapid cooling rate suggested for thermal evolution of the study area may record this extensional event in Late Archean and Early Proterozoic time.

The Early Proterozoic Gowganda Formation (Rb/Sr age *ca.* 2300 Ma, Fairbairn *et al.* 1969) of Huronian Supergroup was folded and probably faulted during the D_5 compressional event. A maximum age of about 2500 Ma may be suggested for this deformational event. On a more regional scale the deformation may be correlated with the Penokean orogeny (1.9-1.7 Ga., Barovich *et al.* 1989). This collisional event resulted in major east-trending folding and faulting in the southern Superior Province. According to Card (1978), Penokean shortening exceeded older (pre-Nipissing, 2.4 to 2.2 Ga) or younger (Grenvillian, 1.2 to 1.0 Ga) deformation of the fold belt within the southern Superior Province.

5.4. Summary and conclusions

Crustal evolution of the Pontiac Subprovince started at about 2700 to 2690 Ma, the time of initial deposition within the Pontiac sedimentary basin. The marine sedimentation probably continued until about 2680 Ma, when terrestrial deposition of the Timiskaming Group marked the termination of marine deposition. Sedimentation of the Timiskaming Group, interpreted as being deposited in a foreland basin over the Pontiac Subprovince, also marks the onset of D_1 deformation that lasted until about 2670 Ma. I-type granitoid plutons and other related intrusive bodies were emplaced in the crust during the same time interval as the D_1 event. The thickened crust attained peak metamorphic conditions at about 2670 Ma, when it started to reduce in thickness during the D_2 deformation. $^{40}Ar/^{39}Ar$ cooling ages of muscovites and biotites from metamorphic rocks of the Pontiac Subprovince indicate that temperatures as high as 350°C and 280°C were persistent in crustal rocks of the area until *ca.* 150 Ma after peak metamorphic conditions were reached. D_3 event resulted in another (minor) crustal thickening episode, that may have been limited between 2626 Ma and 2529 Ma. A relatively rapid interval of cooling history in the study area, deduced from cooling ages of muscovites and biotites, may have been related to D_4, a crustal extension that preceded development of a passive continental margin south of the Superior Subprovince, and deposition of the Huronian Supergroup. D_5 appears to have been a relatively young event comparable in age to the Penokean orogen. Construction of a cooling curve for samples from the study area reveals a generally slow cooling rate that ranges from 2° to 6°C/Ma.

6. Tectonics

6.1. Introduction

The tectonic settings of Archean terranes have been subjects of protracted debates. Some geologists have inferred that Archean tectonic environments involved predominantly vertical movement (Goodwin 1977, 1982, Hunter 1974, Baragar and McGlynn 1976, Archibald *et al.* 1978, Kroner 1981), whereas others have favoured plate tectonic processes similar to those active during Phanerozoic time (Engel and Kulm 1972, Burke *et al.* 1976, Windley and Smith 1976, Bickle 1978, Blackburn 1980, Windley 1981, Anhaeusser 1981).

The presence within Archean terranes of extensive komatiitic rocks, with liquidus temperatures of 1550-1650°C, suggests higher heat-flow from the mantle during the Archean compared to Proterozoic and Phanerozoic times (Bickle 1978, Sleep 1979, Nisbet and Walker 1982). Postulating a higher heat-flow from the mantle during the Archean, in turn, is considered to have required a plate tectonic regime different from present plate tectonic settings. The differences are considered to be: a greater numbers of spreading centres, faster plate movements, smaller average plate size, and thicker oceanic crust (Bickle 1978, Sleep 1979, Sleep and Windley 1982, Nisbet and Walker 1982, Nisbet and Fowler 1983, Abbott and Hoffman 1984, Hoffman and Ranalli 1988).

Accepting a plate tectonic scenario, Card (1989) has classified the subprovinces of the Superior Province into four types of belts: (1) volcanic-plutonic belts, which resemble island arcs; (2) metasedimentary belts, which resemble accretionary prisms; (3) plutonic complexes, which may have formed continental slivers within island arcs; and (4) high-grade gneiss complexes, most of which are simply deeper erosion levels of the other belt types. Presence of east trending belts of different lithologies and metamorphic grades with a southward decreasing trend in age across their strike, have been interpreted as evidence for successive accretion of the island arcs and accretionary prisms from north to south, responsible for aggregation of the Superior Province (Card, 1989).

The Pontiac Subprovince, which is essentially composed of metamorphosed turbiditic sedimentary rocks has in the same way been interpreted as an accretionary prism (Card 1989). The north-dipping boundary with Southern Abitibi along the Cadillac-Larder Lake fault Zone has led some geologists to interpret the prism to be related to a north-dipping subduction zone under the Abitibi island arc setting (Dimroth *et al.*, 1983b). Others have postulated a north- and south-dipping subduction zone framework during deposition of the Pontiac sedimentary pile (Kerrich and Feng 1992). Kerrich and Feng (1992), using some features of the Himalayan orogeny as a recent analog, suggested that the Abitibi and Pontiac Subprovinces represent two juxtaposed allochthonous terranes. A different tectonic interpretation postulates deposition of the Pontiac sediments in a synorogenic turbidite fan, fed by collision of the Superior and the Minnesota continents (Kimura *et al.*, 1993).

Detailed background on geologic data and their interpretations is given elsewhere in previous Chapters. General information on geologic events that are critical for the tectonic interpretation of present study are summarized here.

The oldest dated rocks within Abitibi Subprovince are volcanic flows in northern Abitibi with ages of *ca.* 2759 Ma (Lac des Ventes flow, Chibougamau area, Quebec: Mortensen 1993a). Volcanic rocks with approximately similar ages (*ca.* 2747 Ma) occur in southern Abitibi to the west of the Pontiac Subprovince (Pacaud felsite, Ontario: Mortensen 1993b). Culmination of volcanism in the Southern Volcanic Zone, represented by essentially felsic volcanic rocks in the Blake River Group, is considered to have occurred between 2703 and 2698 Ma (Mortensen 1993b). Felsic volcanism in the Baby-Belleterre belt of the Pontiac Subprovince appears to have started from *ca.* 2694 Ma (Carignan *et al.* 1992), and lasted until about 2682 Ma (Mortensen & Card 1993). The 2695 Ma U/Pb age of zircons from the Lac de Quinze ortho-gneiss (Mortensen & Card 1993) is comparable with felsic volcanism in the area.

Age of the youngest detrital zircon within the Pontiac metasedimentary rocks (2683±1 Ma, Mortensen & Card 1993) indicates that sedimentation in the Pontiac basin finished sometime after 2683 Ma. The Timiskaming Group, deposited unconformably on the Pontiac

Group, has received detrital zircons as young as 2679 Ma (Davis 1991). This conglomeratic metasedimentary group has a major component of clasts composed of felsic volcanic and igneous rocks comparable to felsic rocks in the Blake River Group. Investigation of sedimentology and stratigraphy of the Timiskaming and Pontiac Groups by Goulet (1978) and Dimroth *et al.* (1982) led them to propose that the Blake River Group rocks were a major source for sediments of the Pontiac and Timiskaming Groups.

A summary of tectonic models proposed for evolution of the southern Abitibi greenstone belt and Pontiac Subprovince is presented here for comparison.

6.1.1. Previous geodynamic models proposed for Abitibi greenstone belt and Pontiac Subprovince

Dimroth *et al.* (1983b), based on detailed mapping and regional synthesis, suggested a tectonic model for Late Archean evolution of the Abitibi greenstone belt, in which they postulated development of the volcanic succession of the greenstone belt over a north-dipping subduction zone (Fig. 6.1). Pontiac sedimentary rocks would have been deposited in the arc-trench gap of the oceanic arc system. Later during its tectonic history, the matured Abitibi island arc uplifted at the Cadillac-Larder Lake break and began to shed large volumes of coarse-grained sediments to the south (Timiskaming Group). The Cadillac-Larder Lake break at this time was active as a zone of (normal) growth faults associated with subsidence of the sedimentary basin to the south, and the volcanic arc to the north. An orogeny, the tectonic setting of which is not defined by Dimroth and his coworkers, resulted in termination of subduction, thrusting of the Abitibi belt over its foreland (Pontiac Subprovince) to the south, and folding within the whole area.

Based on structural, geochemical, sedimentological and geochronological studies, Ludden *et al.* (1986), and Ludden and Hubert (1986) suggested a tectonic model in which the Southern Volcanic Zone of the Abitibi greenstone belt formed in a series of rift basins which dissected an earlier-formed volcanic arc (the Northern Volcanic Zone). In this model, a south-

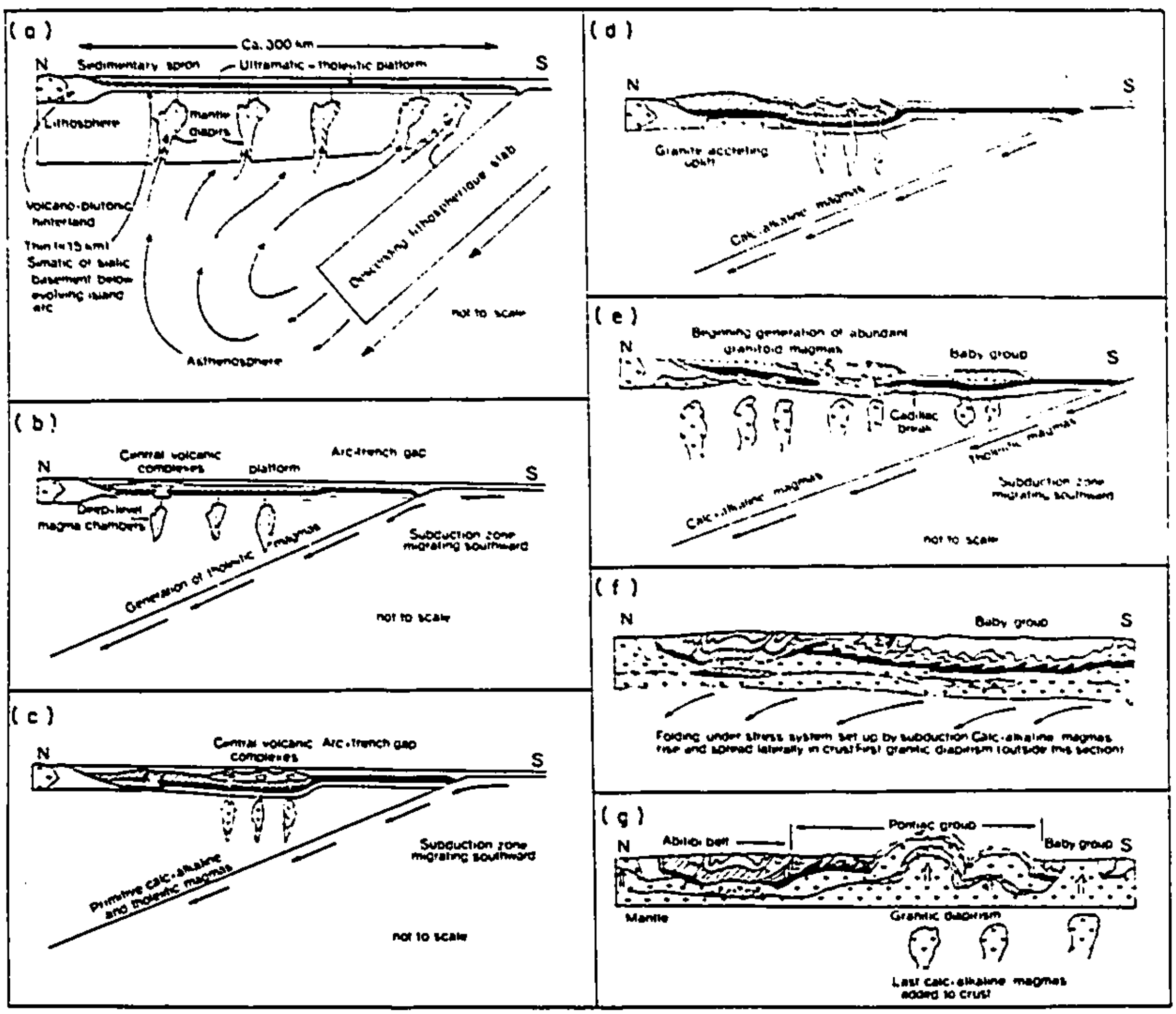

Fig. 6.1. Tectonic model proposed by Dimroth *et al.* (1983b) for evolution of the Abitibi and Pontiac Subprovinces. Stages (f) and (g) respectively represent commencement of orogeny in the area, and final uplift and doming up of Bellecombe Belt.

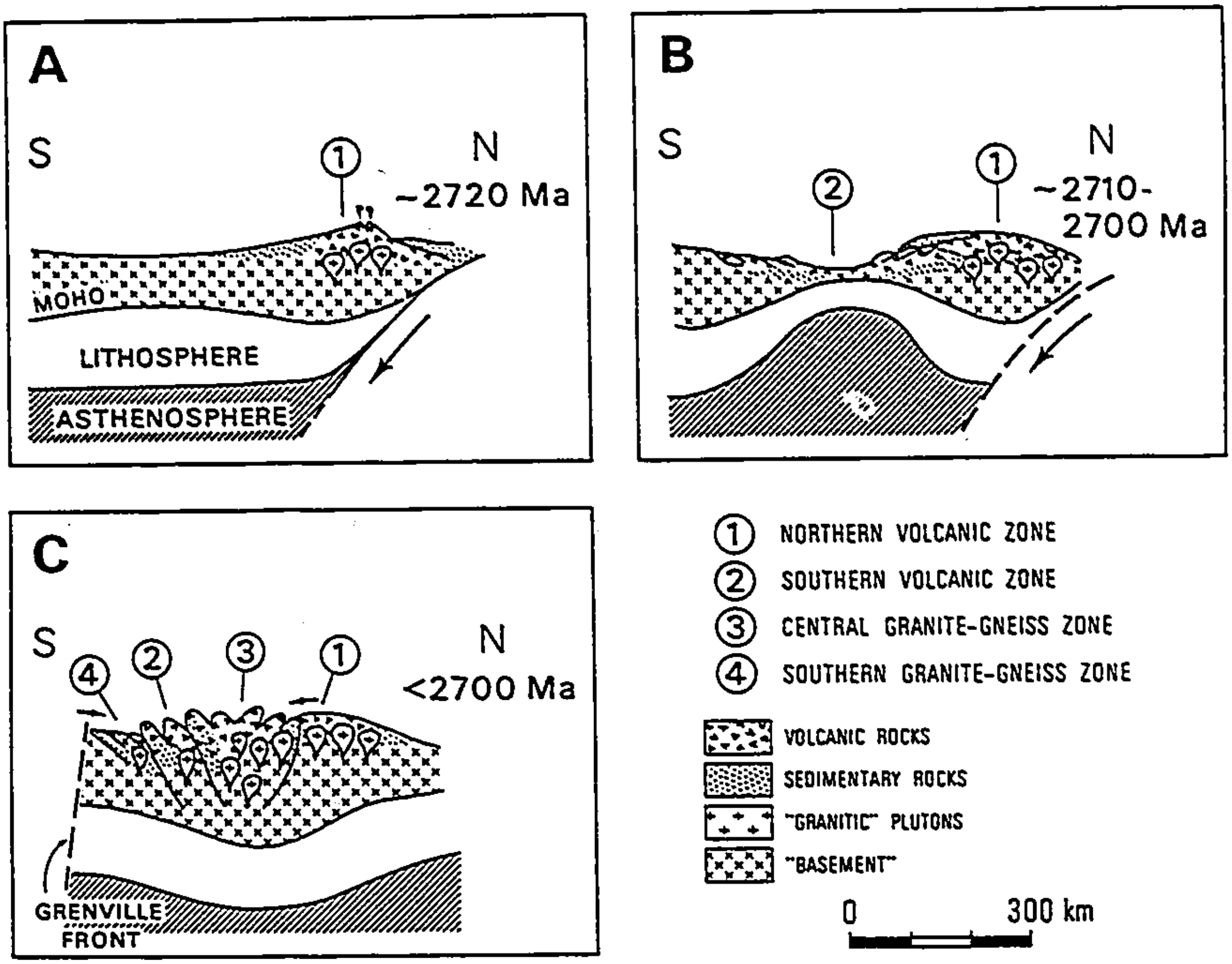

Fig. 6.2. Evolutionary model for the Abitibi belt (Ludden *et al.* 1986): (a) main volcanic phase in the Northern Volcanic Zone evolution (Andino-type plutonism); (b) deformation of Northern Volcanic Zone and main volcanic phase in Southern Volcanic Zone (ocean arc-type plutonism); (c) final orogenic phase (Kenoran) deformation of Northern Volcanic Zone and Southern Volcanic Zone, and emplacement of post orogenic (Hercynotype and Caledonian-type) granitoids.

dipping subduction zone existed under the Abitibi magmatic arc (Fig. 6.2). In their model, Ludden *et al.* (1986) proposed that the Pontiac sediments were, at least in part, contemporaneous with the extrusion of komatiitic volcanics and were shed from the Northern Volcanic Zone and older basement into deep-water rift basins in the Southern Volcanic Zone.

REE and trace element data from volcanic rocks of the Noranda area led Ujike and Goodwin (1987) to conclude that the most likely tectonic environment for these rocks in southern Abitibi was a backarc-type spreading setting above a primitive mantle diapir. They noted the similarity between the Noranda massive sulfide deposits and the Kuroko massive sulfide deposits of Japan which formed in a backarc spreading environment. Considering this idea, Jackson and Fyon (1991) accepted a backarc spreading environment or a transitional arc to backarc spreading environment as an alternative to the commonly invoked mature island-arc setting of the Blake River and possibly other calc-alkalic metavolcanic assemblages.

Hodgson and Hamilton (1989) expanded and modified the island-arc model of Dimroth *et al.* (1983b). In their model, north-dipping subduction formed island-arc assemblages on pre-existing oceanic crustal assemblages. Subduction led to terminal collision with the foreland basin along the leading edge of a southerly continental mass, now the Pontiac Subprovince. Collision involved southward overthrusting of the southern Abitibi greenstone belt over the Pontiac Subprovince, and synchronous development of molasse deposits of the Timiskaming Group.

Based on regional mapping, structural studies, and petrological studies, Jackson and Fyon (1991), and Jackson *et al.* (1994) suggested a four-stage evolutionary model that includes: 1) formation of submarine oceanic assemblages in a region of complex micro-plate interactions; 2) termination of submarine volcanism by collision of a large continental mass to the south at ~2700 Ma; 3) tectonic thickening during collision led to emergent sediment source area(s) for post-2700 Ma turbidite deposits, including both local deposits and a massive sediment influx to develop deposits of the Pontiac metasedimentary belt, which may represent a remnant of a major accretionary wedge; 4) terminal subduction at 2685 to 2675 Ma generated alkalic volcanic rocks and alluvial sediments in proximity to crustal-scale shear zones. They suggested that the collision at the stage 3 of the model may have been oblique, and involved 2.8 to 3.0 billion-year-old Minnesota River Valley gneiss terrane. To explain the juxtaposition and superposition of diverse volcanic assemblages in the southern part of the Abitibi greenstone belt, they cited the tectonic setting of the Indonesian region as an analog. In a more detailed tectonic model for the southern Abitibi greenstone belt, Jackson *et al.* (1994) ascribed deposition of the Blake River Group (in Quebec) to a rifted arc environment (Fig. 6.3).

Based on geochemical, geochronological and petrologic data, Kerrich and Feng (1992) suggested the following geodynamic model for evolution of the Abitibi and Pontiac Subprovinces (Fig. 6.4). Drift of a plate, perhaps the Pontiac Subprovince, caused oceanic subduction northward underneath an Andean-type margin, forming a set of ocean island and/or continental margin arcs, and backarc basins, where vast amounts of calc-alkaline volcanics (arc) and komatiitic magmas (backarc basin) were produced. As the arcs matured at about 2700 Ma during transpressive accretion, voluminous calc-alkaline to subalkaline magmas, and subsequently volumetrically minor alkaline or shoshonitic magmas (related to this subduction process) were intruded into different crustal levels within the Abitibi Southern Volcanic Zone at about 2690-2670 Ma. Concurrent with arc magmatism in the Abitibi Southern Volcanic Zone, a Tethys-type oceanic floor ahead of the Pontiac type microcontinent may have fractured, resulting in subduction of an oceanic plate southward under the Pontiac microcontinent to form the 2690-2670 Ma calc-alkaline to subalkaline and alkaline monzodiorite-monzonite-granodiorite-syenite plutons in the Pontiac Subprovince. Alternatively, a coeval subduction zone may have been operative south of the Pontiac microcontinent. Late tectonic subalkaline to alkaline magmas may be related to strike-slip structures that resulted from oblique subduction, similar to the association seen in the Trans-Himalayan belt. After ocean closure (~2680-2670 Ma?), collision between the Abitibi Southern Volcanic Zone and the Pontiac Subprovince occurred, the Abitibi belt being locally underthrust by the Pontiac microcontinent. lithospheric thickening enabled Pontiac-type sediments to undergo anatexis to form collisional garnet-

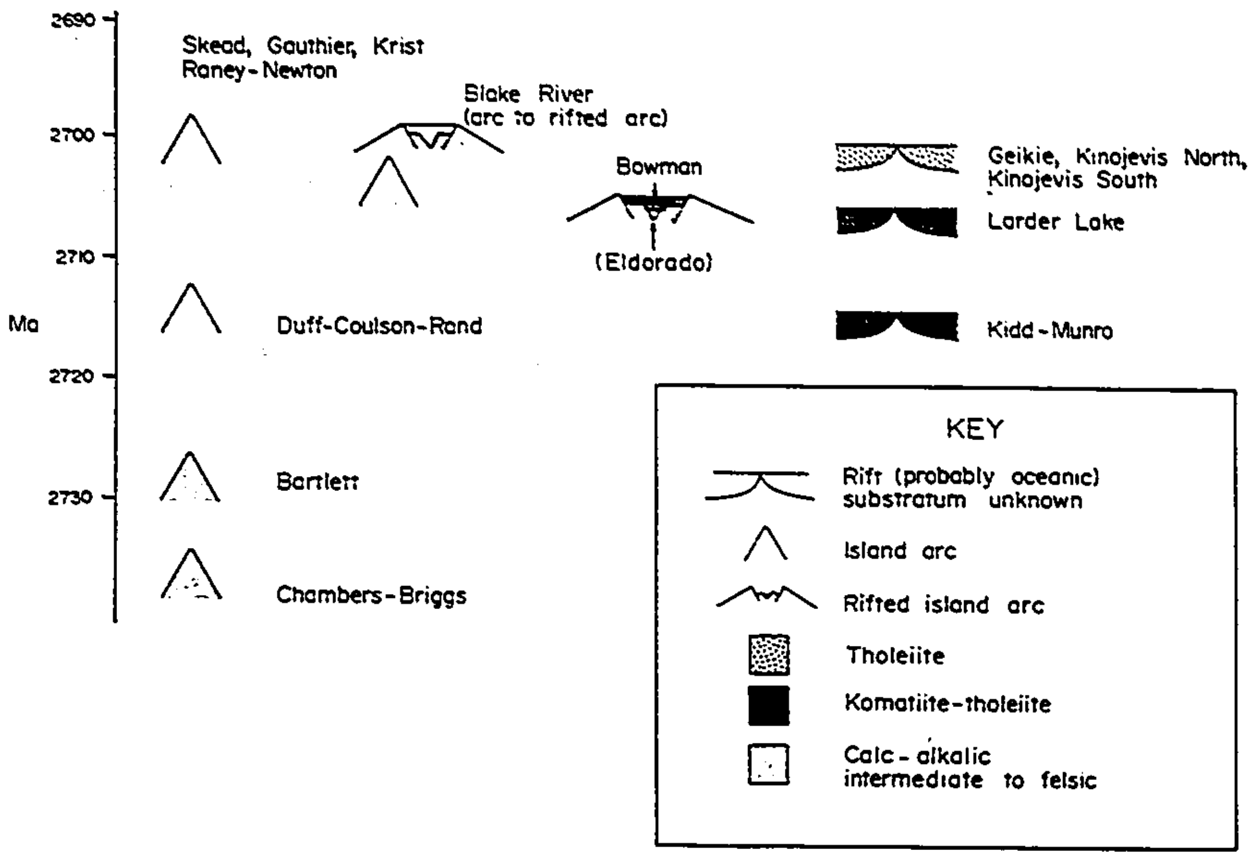

Fig. 6.3. Summary of age vs. interpreted tectonic environment of assemblages within southern Abitibi (Jackson *et al.* 1994).

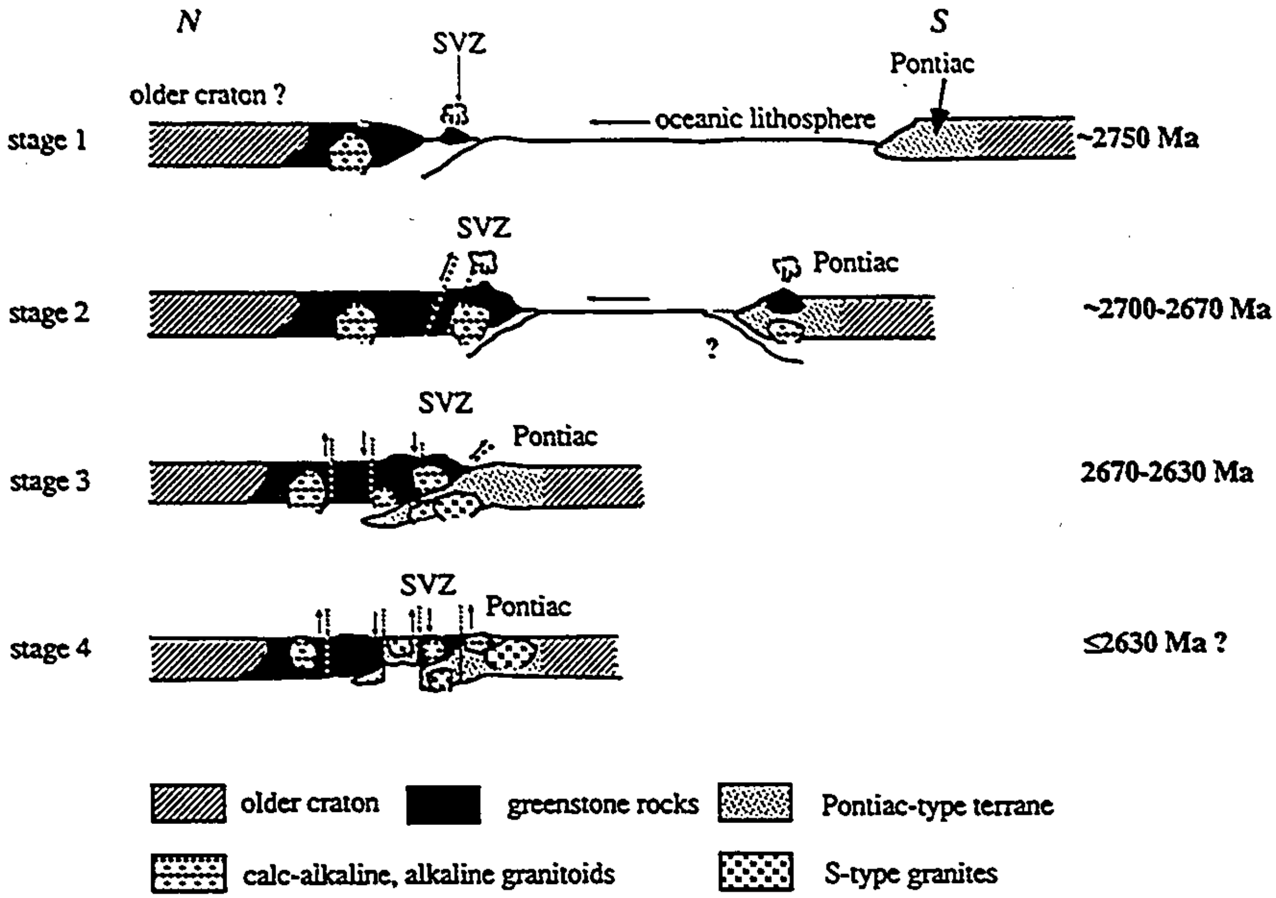

Fig. 6.4. Simplified tectonic model for the evolution of the Abitibi Southern Volcanic Zone and the Pontiac Subprovince (Kerrich and Feng 1992). Stage (1): oceanic subduction and arc volcanism; stage (2): plutonism, transcurrent tectonics and accompanied alkaline magmatism and gold; stage (3): arc-continent collision, reactivated gold; and stage (4): differential uplift.

muscovite granite series plutons (S-type) at about 2645 Ma. Differential uplift exposed part of the underthrust Pontiac plate as a tectonic window in the lower grade Abitibi greenstone belt, e.g. the Lacorne block, and the entire Pontiac Subprovince to the south of the boundary fault with the Abitibi Southern Volcanic Zone.

On the basis of U/Pb geochronologic data, Corfu (1993) postulated an essentially oceanic arc setting for the southern Abitibi greenstone belt. He further suggested development of the major volcanic sequences of the southern Abitibi in oceanic rifts formed by extension of an active arc, followed by an orogenic phase that involved two main periods of thrusting and folding accompanied by calc-alkalic and later alkalic magmatism.

Kimura *et al.* (1993) proposed that the Pontiac sedimentary rocks represent a deep sea fan deposited during collision of the Superior continent with another continental landmass (possibly the Minnesota foreland), resulting in uplift. They predicted the Pontiac, Quetico and potentially the English River sediments as belonging to the same sedimentary system (Fig. 6.5).

Progressively younger ages of the Abitibi Subprovince towards the south, and seismic-profile evidence for crustal layering of the subprovince is used by Jackson and Cruden (1995) to propose an arc-trench migration model for formation of the Abitibi greenstone belt (Fig. 6.6). Within the present crust of the Abitibi Subprovince, they defined an upper layer of greenschist facies rocks with upright structures and low seismic reflectivity, and a middle crust of amphibolite facies rocks with moderate to shallow-dipping structures and strong seismic reflectivity. They proposed that this crustal layering and the age progression resulted from accretion of oceanic assemblages followed by extensive mid-crustal magmatism linked to southward migration of an arc-trench system.

6.1.2. Evaluation of the proposed models

Dimroth *et al.* (1983b) were among the first geologists to propose a plate tectonic (island-arc) model for the Abitibi and Pontiac Subprovinces. Their idea about northward

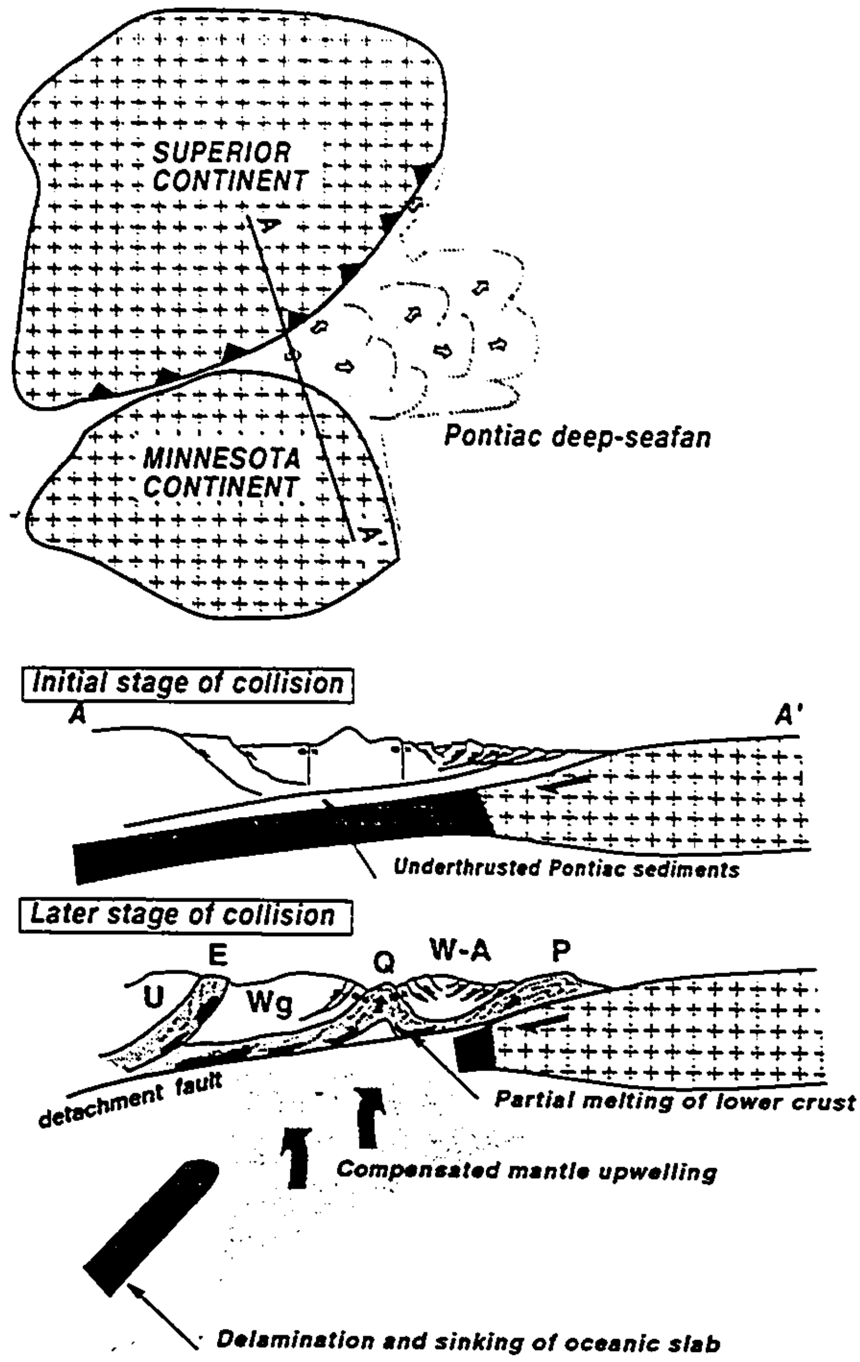

Fig. 6.5. Model proposed by (Kimura *et al.* 1993) for the final stage in the tectonic evolution of the Superior Province based on the interpretation of the Pontiac as a late stage syn-orogenic turbidite fan associated with a prograding orogen.

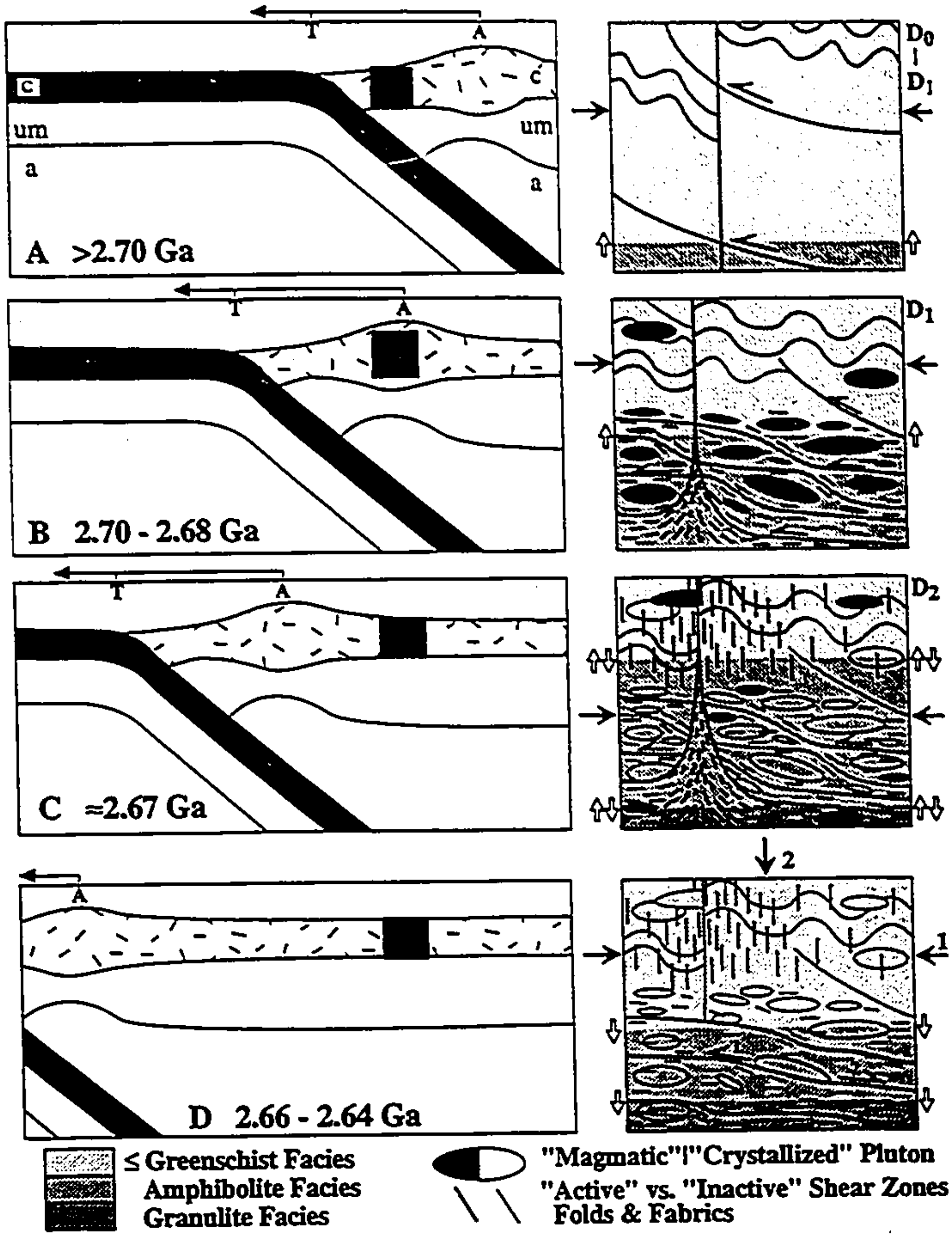

Fig. 6.6. Migrating arc (A) - trench (T) model of Abitibi greenstone belt crust (black rectangle) (Jackson and Cruden 1995). Ages are for the southern Abitibi greenstone belt. Crust, upper mantle, and asthenosphere indicated by c, um, and a, respectively.

subduction beneath the Abitibi greenstone belt was based on underthrusting of the foreland (Pontiac Subprovince) below the volcanic belt. However, in a subduction-related tectonic context, where accretionary prism sedimentation is the most important and essential depositional system, interpretation of the Pontiac sedimentary rocks as being deposited in an arc-trench gap leaves the model open to criticism. Because of the major change in type of sedimentation between the Pontiac and Timiskaming Groups, sedimentation of the Timiskaming Group appears to be related to a more catastrophic tectonic activity rather than maturing and uplift of the Abitibi island arc.

Considering the present geologic data, the tectonic model proposed by Ludden *et al.* (1986) appears to be able to explain major differences between the magmatism within Northern and Southern Volcanic Zones of the Abitibi Subprovince. It can also explain why mineral deposits in the Southern Volcanic Zone are mainly of syngenetic massive sulfide type, whereas in the Northern Volcanic Zone they are of porphyry-type. They also considered for the first time the probability of deposition of the Pontiac sedimentary rocks in an extensional tectonic setting. They argued that, because rifting is generally behind the volcanic arc in Phanerozoic examples, and the Southern Volcanic Zone represents volcanic activity resulting from rifting of the Northern Volcanic Zone, the subduction must therefore have been south-dipping. The reasoning arises from an incomplete model, which does not clearly deal with the other half of the dissected Northern Volcanic Zone. In other words, if Southern Volcanic Zone represents the volcanic succession resulted from the rifting of an arc, another arc terrane similar to Northern Volcanic Zone should be present south of the Southern Volcanic Zone.

Geochemical and ore deposit studies were used by Ujike and Goodwin (1987), Ludden *et al.* (1986), and Jackson and Fyon (1991) as a basis for comparison with Phanerozoic tectonic settings, and are very important for refined tectonic modeling of the Abitibi and Pontiac Subprovinces.

The tectonic model proposed by Hodgson and Hamilton (1989) is essentially the same as that suggested by Dimroth *et al.* (1983b). The only difference is in the tectonic setting proposed by Hodgson and Hamilton (1989) for the Timiskaming Group. They suggested that the Timiskaming Group rocks are molasse deposits that developed synchronously with southward overthrusting of the southern Abitibi greenstone belt over the Pontiac Subprovince, which is a likely setting for these detrital sedimentary rocks.

The suggested tectonic model of Jackson and Fyon (1991) is different from other models in postulating an early (~2700 Ma) collisional event. They suggested that during this event, a large continental mass to the south (probably the Minnesota River Valley gneiss terrane) collided with microplates now assembled in the Abitibi greenstone belt. The collision resulted in emergent areas shedding sediment into the Pontiac basin.

Kerrich and Feng (1992) considered the Pontiac Subprovince to represent a microcontinent prior to its collision with the Abitibi arc system. Postulating a continental nature for a package of turbiditic rocks, without introducing any basement for it, and before any subduction-or collision-related deformation and magmatism is open to question. The same assumption has lead Feng *et al.* (1993) to propose the Abitibi and Pontiac Subprovinces to be two different terranes that have been tectonically juxtaposed. Their suggestion for the Lacorne block as being a tectonic window of the Pontiac Subprovince within the Abitibi Subprovince appears to be reasonable.

The geochronologic approach of Corfu (1993) for his tectonic modeling essentially supports the arc extension model of Ludden *et al.* (1986).

The arc-trench migration model of Jackson and Cruden (1995) is not valid because backarc spreading, which is an integral part of the arc-trench migration scenario, is not taken into consideration by the model. Moreover, it is not clear how a crustal segment (representing the Abitibi greenstone belt) can move from forearc into arc and then backarc position (see Fig. 3 in Jackson and Cruden 1995).

6.2. Geodynamic model for Late Archean-Early Proterozoic evolution of the Pontiac Subprovince

Data from the present study are integrated with general geologic data along with geochronologic and geochemical data from different sources on the Abitibi and Pontiac Subprovinces, to support a refined geodynamic model for evolution of the Pontiac Subprovince in Late Archean-Early Proterozoic. The tectonic evolution of the subprovince in this model is described through five different evolutionary stages.

A tectonic setting similar to that of Phanerozoic backarc basins is proposed for the Late Archean evolution of the Pontiac Subprovince. Throughout the description of the model, different characteristics of Phanerozoic backarc basins are frequently referred to for comparison, and so their important geologic features are described here.

6.2.1. Characteristics of Phanerozoic backarc basins

Features of the Phanerozoic backarc basins from Taylor (1995) are summarized below.

Backarc basin development involves the splitting of volcanic arcs, initially forming rifts (elongate depressions bounded by faults) and subsequently backarc spreading centres. The trench axis of all subduction systems with active backarc basins migrates seawards. Stretching and splitting of the volcanic arc usually occurs along the central axis of the arc, where relatively higher heat flow weakens the crust. The initial rift basins subside along a zigzag pattern (in plan view) of border faults, many of which dip at low angles (20°-50°).

Transfer zones that link opposing master faults and/or rift flank uplifts further subdivide the rifts into segments along strike. Explosive, high-silica volcanism commonly reaches peak intensities during the initial rifting (as documented in the Japan, Izu-Bonin-Mariana, and Lau-Colville-New Zealand arcs). Nearby calderas shed voluminous pumiceous sediments into rapidly filled rift basins.

Magmas intrude along faults into the rifted arc crust of the basins, sometimes producing lineated magnetic anomalies. The magmas may be derived from the suprasubduction zone mantle arc source and/or from pressure-release partial melting of the shallow mantle: both arc-like and mid-ocean ridge basalt (MORB)-like compositions are observed temporally and are spatially juxtaposed.

As continued stretching widens the basins, the zone of greatest subsidence and intrusion migrates with the collapsing arc margin border faults. The result is an asymmetric basin in cross section. After development of a mature spreading centre, the backarc basins may reach 200 km in width. The seaward side of the rifted arc may remain active during the backarc spreading process; however, in many systems arc magmatic activity declines markedly at the start of the subsequent backarc spreading.

Backarc basins are loci of extensive hydrothermal activity. The hydrothermal deposits typically contain more zinc, barium, lead, cadmium, and arsenic than their mid-ocean ridge equivalents. Hydrothermal deposits discovered in backarc rifts such as the Okinawa Trough and Sumisu Rift are a modern analog of the Kuroko-type volcanic-hosted massive sulfide (VMS) deposits that formed in the Middle Miocene Hokuroku Basin during the last phase of Japan Sea opening. Like all sites of major VMS ore bodies, and unlike mid-ocean ridge deposits, they occur in association with subduction-related volcanism including silica-rich lavas as well as basalts.

6.2.2. Major steps in tectonic evolution of the Pontiac Subprovince

Stage 1 (~2700-2690 Ma): Backarc spreading and basin development

The ancestral Abitibi arc, now represented by the Northern Volcanic Zone, at this time starts to split into two subparallel masses (Fig. 6.7). The rifting model of Ludden *et al.* (1986) for superposition of the komatiites and large bimodal felsic volcanic complexes of the Southern Volcanic Zone over the emergent volcanic complexes of the Northern Volcanic Zone is favoured here. The model also accounts for the difference between mineral deposition style of these two parts of the Abitibi greenstone belt. Based on geochemical and petrogenetic study of

Fig. 6.7a. (Top) Abitibi arc system before rifting. Arc magmatism (1) at this time produced volcanic and plutonic assemblages that are now preserved as the Northern Volcanic Zone. The ancestral Cadillac-Larder Lake fault zone (ACLLFZ) initiated along the axis of the arc system with an offset that later evolved into a spreading centre. The solid arrow shows relative movement of the subducting plate.

Fig. 6.7b. (Bottom) Initiation of backarc spreading. Northern and southern segments of the Abitibi arc (NSA and SSA) are separated along the ACLLFZ to develop the Pontiac backarc basin. Backarc magmatism (2) produces volcanic and plutonic rocks of the Southern Volcanic Zone. Volcanogenic massive sulfide (VMS) deposits are emplaced within this volcanic zone. Arc magmatism (1) probably resumed in the southern segment of the rifted arc. Extension of the arc along the hot weakened axis results in development of the gneiss complexes (3), probably derived from sub-volcanic plutons, and preserved as Lac Opasatica, Lac de Quinze and other gneisses within the Pontiac Subprovince. The Pontiac backarc basin subsides along the normal faults parallel to the ACLLFZ.

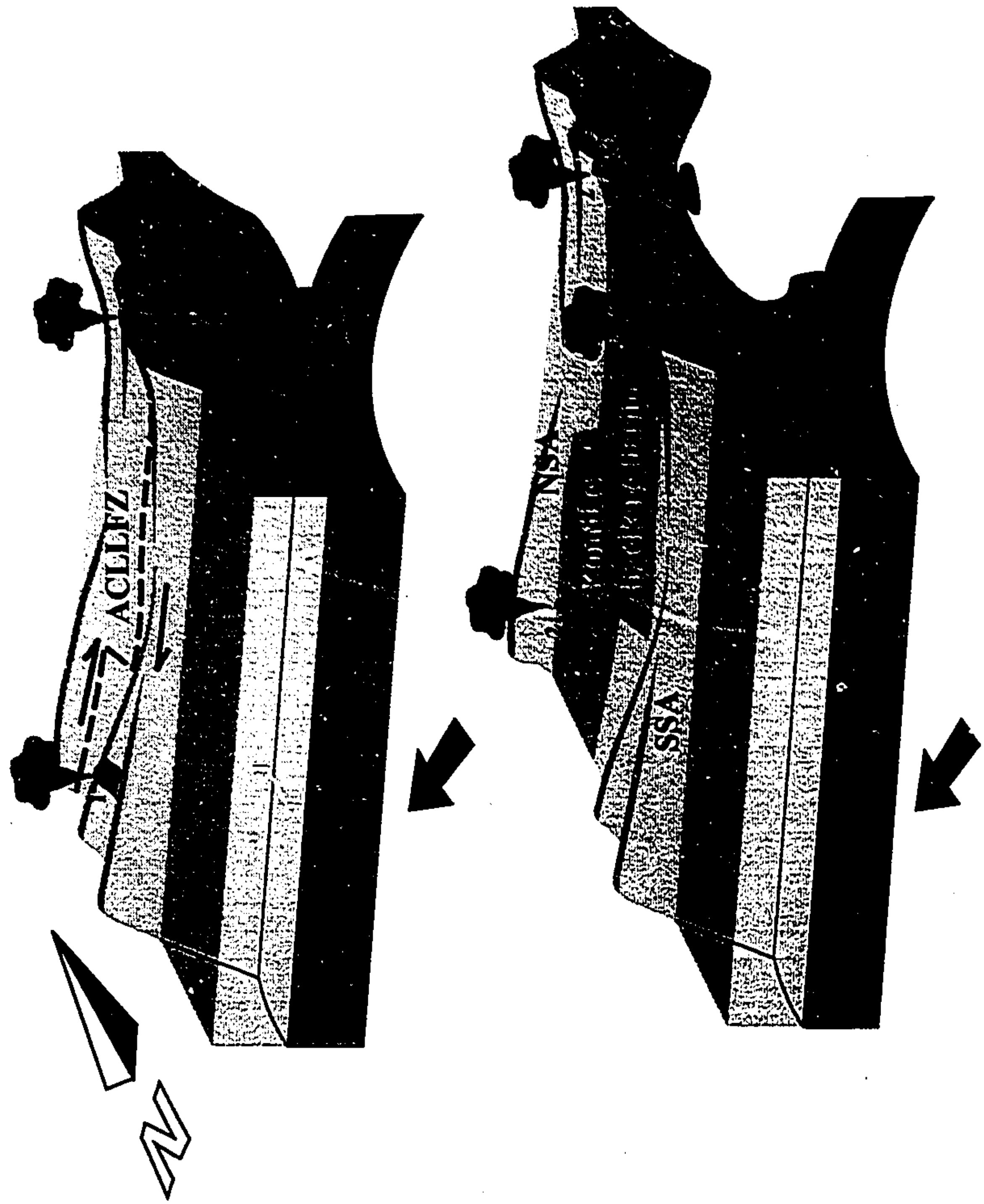
ACLLFZ
NSA
SSA
N

the volcanic rocks of the Blake River Group in the Southern Volcanic Zone of Abitibi, Laflèche *et al.* (1992) suggested that tholeiites from the lower part of this volcanic succession were produced by a high degree of partial melting of adiabatically rising diapirs below a rifted lithosphere. They further suggested that uncontaminated tholeiites from the upper part of the belt reflect a lower degree of partial melting, probably due to decreasing lithospheric stretching possibly related to closure of the rift-related basin at the beginning of Kenoran deformational events in the southern Abitibi.

Backarc extension behind a north-dipping subduction zone at the southern margin of the Abitibi arc system is in contrast to the model suggested by Ludden *et al.* (1986). In Phanerozoic backarc extension settings, volcanic arcs usually split along their central axis, and the trench side of the split arc continues the arc activity (Taylor 1995). No arc volcanic activity appears to have occurred in the Northern (or Southern) Volcanic Zone of the Abitibi Subprovince after rift magmatism in the Southern Volcanic Zone. It is therefore postulated that the (active) trench side segment of the arc was towards the south, implying a north-dipping subduction zone under the Abitibi arc system.

Sedimentary rocks within the Pontiac Subprovince most probably were deposited in a backarc basin rather than being deposited in an accretionary prism setting (as postulated by Card 1990, Dimroth *et al.* 1983b), because melange development and soft-sediment deformation, both diagnostic features of sedimentation in subduction zones (Williams *et al.* 1984), are not recorded in the Pontiac sedimentary sequence. Moreover, rapid deformation of sedimentary strata within accretionary wedges requires development of intraformational unconformities and large debris flows (resulting from the fast destabilization of underwater slopes), which also are not known in the area.

Splitting of the Northern Volcanic Zone is postulated therefore resulting in development of a backarc basin, hereafter referred to as the Pontiac backarc basin.

Gneissic structure of the Lac de Quinze gneiss (at *ca.* 2695 Ma) and probably other gneissic domains such as the Lac Opasatica and Baie des Lys orthogneisses, situated in western Pontiac Subprovince, developed during extension of the Abitibi arc, through high temperature deformation of I-type granitoid bodies that were earlier emplaced into the volcanic arc. The gneisses, therefore, appear to represent remnants of a sheared arc. Reasoning behind this idea includes: (1) dated gneissic plutons within the Pontiac Subprovince are older than the youngest dated detrital zircons from the Pontiac metasedimentary rocks, ruling out their intrusion into this sedimentary pile; (2) penetrative deformation of the gneisses is not concordant with deformation of the Pontiac Group rocks. For example, the Lac Opasatica gneiss shows an easterly mineral elongation lineation which is almost perpendicular to the regional elongation lineation of the Pontiac Group; (3) petrofabric study of the Lac Opasatica gneisses indicates that the gneissic fabric and the related elongation lineation probably developed at high temperatures in a pure shear or non-coaxial strain regime with the Z-axis of the strain ellipse being sub-vertical, which is in accord with extension of a still-hot (active) arc system composed of volcanic rocks intruded by granitoids.

Volcanic rocks of the Baby-Belleterre belt probably represent first eruptions within the backarc basin environment. These volcanic rocks, which have ages similar to the youngest volcanic rocks of the Blake River Group (but still older than the youngest detrital zircons within the Pontiac Group), thus may be considered as basement to sedimentary rocks of the Pontiac Group (Fig. 6.8). Sulfide mineralization in Noranda and Baby-Belleterre volcanic rocks represent hydrothermal activity during initial stages of development of the Pontiac backarc basin. Nickel-copper sulfide deposits in the Baby-Belleterre belt within the Pontiac Subprovince are associated with intrusion of synvolcanic gabbros. On the basis of geochemical study of nickel-copper sulfides from the Belleterre-Angliers belt of the Pontiac Subprovince, Barnes *et al.* (1993) suggested that associated synvolcanic gabbros of this volcanic belt have formed from a mantle plume which rifted the Belleterre-Angliers island arc in Late Archean time. However, it is here suggested that both the volcanic rocks of the Baby-Belleterre belt and the sulfide mineral deposits are the result of rifting of the Abitibi island arc. Ujike and

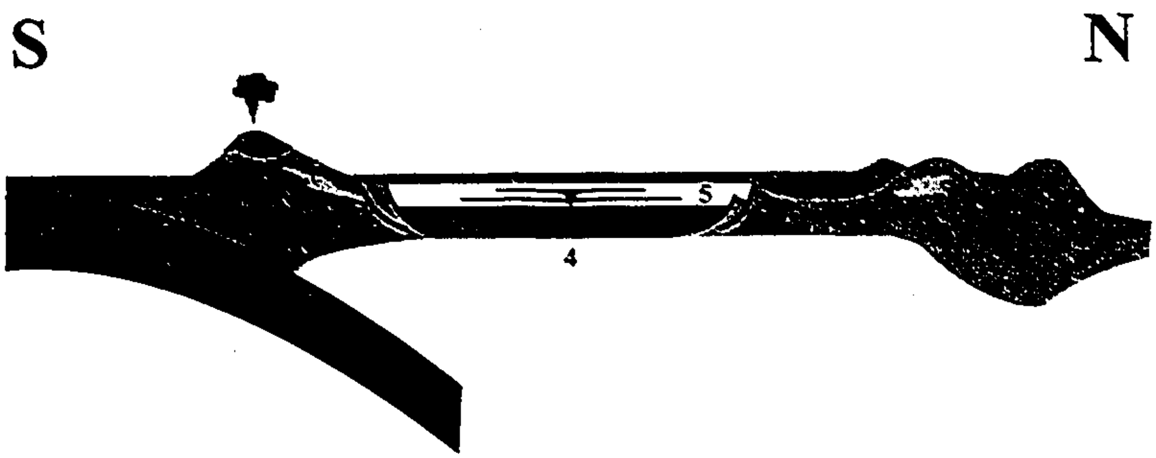

Fig. 6.8. Mature backarc spreading stage. Spreading centres (4) now established within the backarc basin produce komatiitic and basaltic flows within the graywacke sequence of the Pontiac Group (5).

Goodwin (1987) noted the similarity between the Noranda massive sulfide deposits and the Japanese Kuroko massive sulfide deposits which formed in a backarc spreading environment.

The komatiitic flows and mafic to intermediate volcanic rocks within the Pontiac Group sequence probably developed during the mature spreading-stage of the backarc basin over a hot mantle source.

Geometry and position of the Pontiac backarc basin

The Abitibi greenstone belt may be divided into two domains, similar in age and volcanic successions, that are separated along the Cadillac-Larder Lake fault zone. The lower parts of the volcanic succession in these two domains (Northern Volcanic Zone to the north, and tholeiite-komatiite assemblages to the south of the of Cadillac-Larder Lake fault zone in Ontario) represent two parts of the ancestral Late Archean Abitibi magmatic arc system that rifted apart during backarc spreading. The upper parts of these greenstones (Southern Volcanic Zone to the north, and ultramafic through felsic assemblages to the south of the Cadillac-Larder Lake fault zone, including the Bowman and Eldorado Groups, see Fig. 6.3), represent volcanism related to rifting of the arc. Later collision of these segments resulted in their re-unification along the fault zone (in Ontario).

The pattern of boundaries of the Pontiac metasedimentary subprovince and the Abitibi Subprovince to the north and west constrain the geometry of the postulated extensional basin. The northern boundary coincides with the steep east-west-trending Cadillac-Larder Lake fault zone, and on the basis of structural mapping, the western boundary appears to be a relatively shallow-dipping north-south-trending one. In the Val d'Or area, east of the present study area, the Cadillac-Larder Lake fault zone takes a sharp shift in orientation from east-trending to southeast-trending (see Fig. 2.1). Here it is proposed that separation and spreading of the Abitibi arc system at about 2700 Ma occurred along a jagged fault system ancestral to the Cadillac-Larder Lake fault zone (see Fig. 6.7). The north-trending western boundary of the Pontiac Subprovince, and the above mentioned southeast-trending boundary in the Val d'Or area, represent rifted margins of the Abitibi arc along a spreading centre that was highly oblique to orientation of the subduction zone (a high-angle spreading centre). East-trending mineral elongation lineation within the Lac Opasatica gneiss domain, and also in the Lac des Quinze domain was most probably produced during lateral extension along this north-trending spreading centre.

In this model, the east-trending part of the Cadillac-Larder Lake fault zone would be an ancestral transform fault against which the aforementioned spreading centre abutted. Separation occurred along this fault zone during the advanced opening stage of the backarc basin (see Fig. 6.7b). In this case, western and eastern continuation of the basin must have been narrower than the central part. The Pontiac basin must have subsided along normal faults that evolved parallel to the ancestral Cadillac-Larder Lake fault zone.

Deformation of the metasedimentary belts and arc terranes of the southern Superior Province in dextral transpressive regimes (Poulsen 1986, Borradaile *et al.* 1988, Hudleston *et al.* 1988) is widely documented as evidence for an oblique dextral component of plate convergence during accretion of these terranes (Card 1990, Hoffman 1991).

Geometry of this extensional basin may be compared in part to the Tertiary tectonic setting of backarc spreading in the Andaman Sea within the Indonesian arc system (Fig. 6.9). Because of curvature of the western part of this arc system, and northward movement of the Indian plate, convergence of the Indian and Eurasian plates in the northwestern segment of the Java subduction zone is highly oblique. Backarc spreading in this area occurs along oceanic ridges that are at a high-angle to the trend of the subduction zone, and a transform fault cuts the magmatic arc along its length.

A general investigation of orientations of spreading centres within recent backarc basins indicates that the axes of almost all spreading centres are normal or close to normal to the direction of relative movement of the subducting plate. This fact, along with an oblique-plate convergence framework for the southern Superior Province, supports the model here proposed

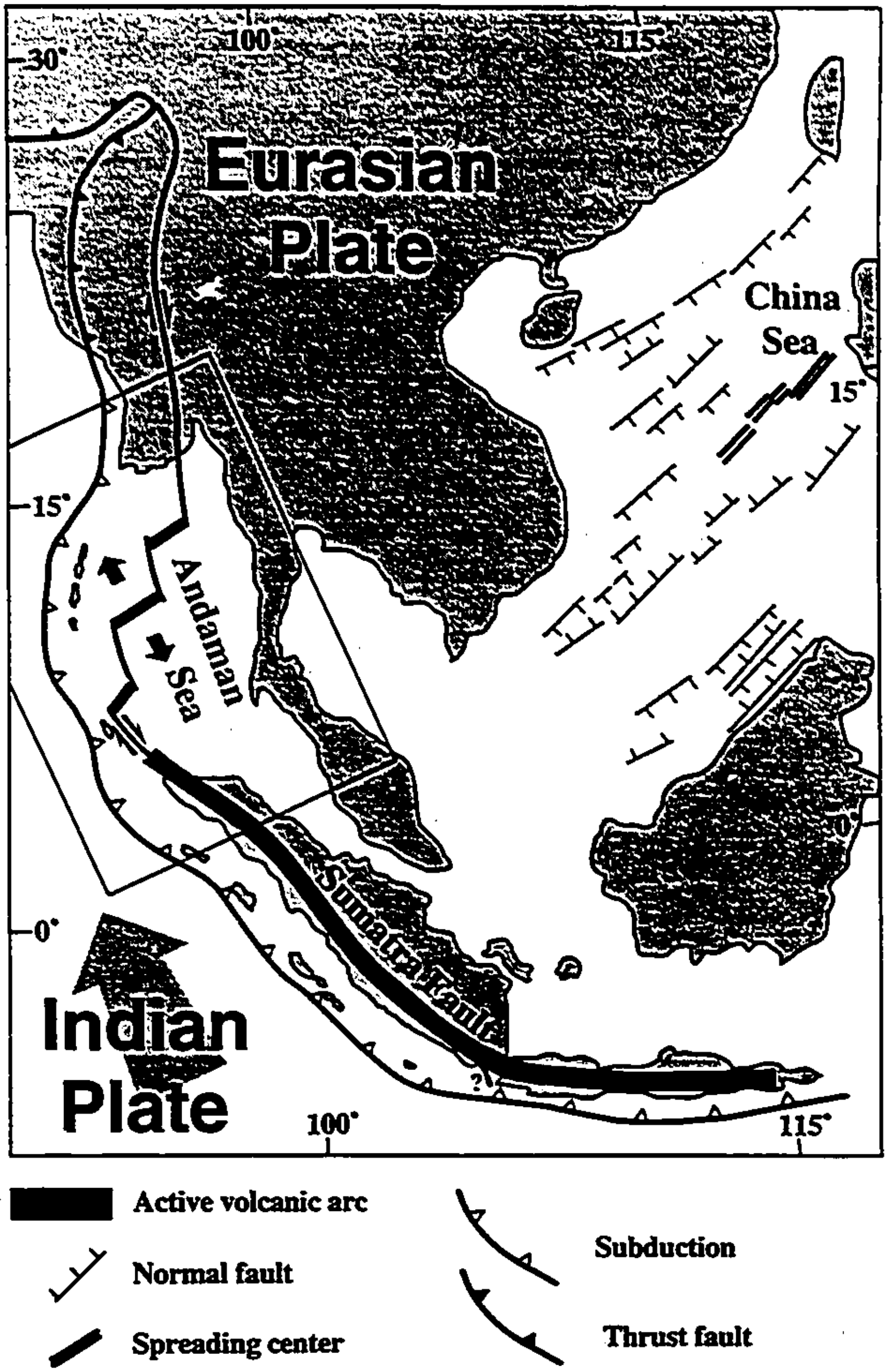

Fig. 6.9. Plate tectonic setting of the Indonesian region (modified after Hamilton 1988, and Peltzer and Tapponier 1988). The inset box represents the area that is compared to the tectonic setting of the Pontiac Subprovince in Late Archean. Note the high-angle position of the spreading centres within the Andaman sea and China Sea with respect to the boundary between the Indian and Eurasian plates. Arrows show direction of relative plate motions.

for high-angle configuration of the original spreading centre, and related transform faults with respect to the arc system and the subduction zone.

Assuming a north-dipping subduction zone, the southern segment of the Abitibi arc must have migrated southward, and may have resumed arc volcanism. The continued volcanic activity could have been a source of the relatively young detrital zircons within the Pontiac sedimentary rocks.

Stage 2 (~2680 Ma): Backarc basin inversion, collision, and crustal thickening

Sometime before *ca.* 2680 Ma, the Pontiac backarc basin started to close. Convergence of the two split parts of the Abitibi arc system at this stage resulted in closure of the backarc basin, deformation and emergence of turbiditic sedimentary rocks, and unconformable deposition of the overlying Timiskaming Group (Fig. 6.10). D_1 structures were produced during this contractional tectonic event. Plate convergence during this stage probably occurred in a dextral oblique fashion, similar to what has been suggested (Card 1990, Hoffman 1991) for other parts of the Superior Province .

The convergence of the two segments of the Abitibi magmatic arc may have occurred as a result of collision with a continental or arc terrane, or reorganization of the plates involved in the subduction system. The latter scenario may be compared with Cenozoic interaction of the north American plate with the Pacific plate, whereby reorganization of the Pacific and Farallon plates at about 30 Ma resulted in a change in state of stress within the western north American plate (Bohannon and Parsons 1995). Collision of the arc system with a continent, however, is more probable. Late Archean collision of the Wawa Subprovince of southwestern Superior Province with the Minnesota River Valley terrane along the Great Lakes tectonic zone (Fig. 1.1) is considered to be a major collisional event that marks amalgamation of the Superior Province with a continent to the south (Sims *et al.* 1980). Being obscured by the Grenvillian orogeny, eastward continuation of the Minnesota River Valley terrane can not be established unequivocally. However, considering the terrane to have a size similar to elongate arc terranes

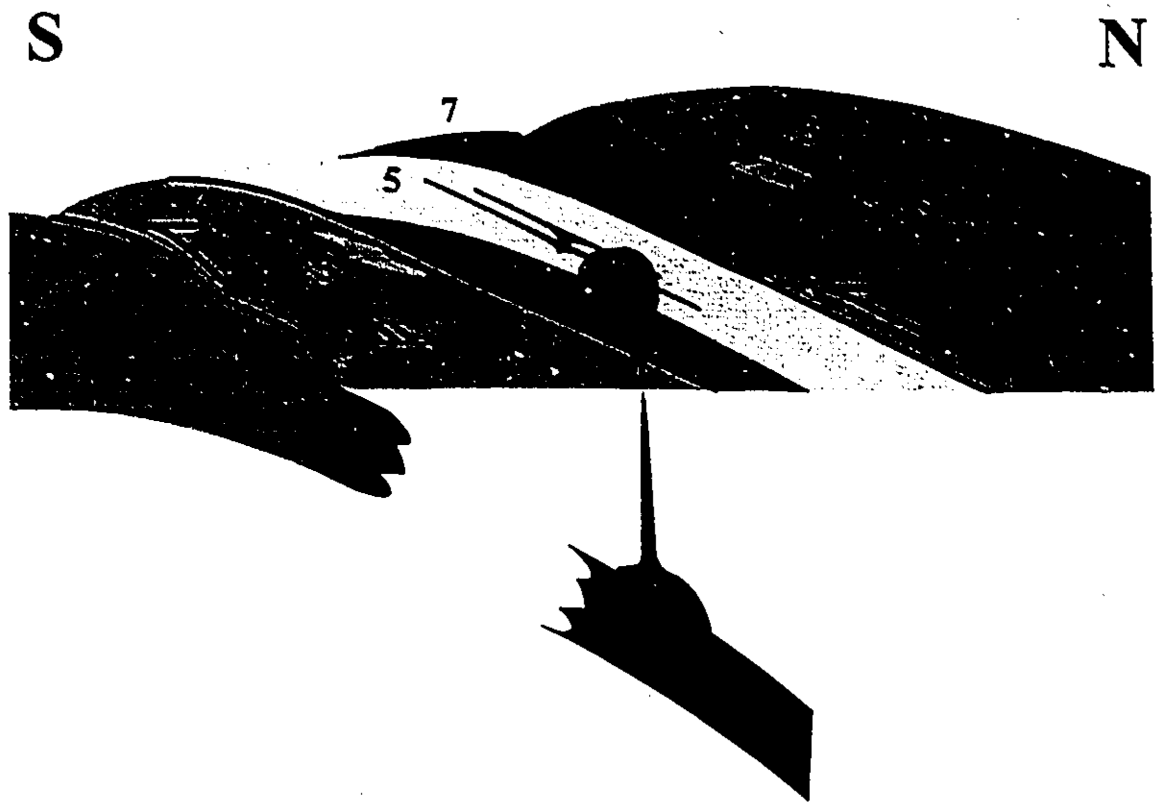

Fig. 6.10. Collision of a suspect terrane (Minnesota foreland) (6) with the Abitibi arc system, and the intervening Pontiac basin (5), results in inversion and closure of the Pontiac backarc basin, and thrusting of the NSA over the Pontiac sedimentary pile. The Pontiac in turn is thrust over the SSA. Timiskaming Group detritus rocks (7) are deposited in a foreland frontal to the thrust belt of NSA over Pontiac. Remnant of the subducted oceanic lithosphere (8) produces calc-alkaline I-type granitoids (9) that intrude both Pontiac and Abitibi Subprovinces after the collisional event.

within the Superior Province, a continuation of this terrane probably collided with the southern segment of the Abitibi arc system at a comparable time. This may also explain the presence of old (2.9-3.0 Ga) detrital zircons within the Pontiac and Timiskaming Groups, and in the Lacorne block. Collision of the Minnesota River Valley terrane with the southern segment of the Abitibi arc system before complete closure of the Pontiac backarc basin may have shed detritus into the basin.

Large-scale thrusting of the Abitibi Subprovince (northern segment of a dissected arc) over the Pontiac Subprovince must have occurred during and after deposition of the Timiskaming Group, and before attainment of peak metamorphic conditions. Meanwhile, Pontiac Group rocks along with intruded granitoid rocks were involved in folding and thrusting over the southern segment of the Abitibi arc system. The narrower western continuation of the backarc basin is postulated to be totally covered now by the overthrust Abitibi greenstones north of the Cadillac-Larder Lake fault zone. Jackson *et al.* (1990) in their interpretation of seismic profiles 12 and 12A from the western Abitibi Subprovince considered the probability that a layer of Pontiac metasedimentary rocks was thrust under the Abitibi greenstones.

The Timiskaming Group rocks, representing termination of sedimentation within the Pontiac backarc basin, were deposited in a foreland basin setting, in front of the south- or southwest-vergent thrust belt of the Abitibi greenstone belt. Clasts of the Pontiac sedimentary rocks constitute a small portion of the base of the Timiskaming Group south of the Cadillac-Larder Lake fault zone. Other parts of this succession, however, are essentially composed of clasts of volcanic and intrusive rocks that originated from the Abitibi greenstone belt. Outcrops of the Timiskaming Group in the study area are limited to south of the Cadillac Larder-Lake fault zone, where they lie with a sheared contact under volcanic rocks of the Abitibi Subprovince. This setting is similar to classic examples of foreland basins, where the thrust belt sheds coarse-grained sediments into its frontal basin, and it usually overthrusts the foreland's sediments at different stages of the thrusting event.

The I-type granites started and continued to intrude into sedimentary rocks of the Pontiac basin through this stage (*ca* 2680 Ma). Widespread intrusion of hot magma from great depths contributed to heating of the thickened crust. The presence of abundant metamorphosed Mg-rich calc-alkaline dykes was used by Camiré and Burg (1993) to suggest that subduction-related magmas intruded the sedimentary pile before it was strongly deformed and metamorphosed. These I-type magmas were probably related to remnants of the subducted lithospheric slab that survived a few million years after collision of the arc-backarc system with the Minnesota foreland (Fig. 6.10).

Stage 3 (~2670 Ma): Regional metamorphism and nappe-development within the thickened crust

Due to thickening of the crust, and intrusion of the I-type granites during stage 2, the collisional zone underwent regional amphibolite facies metamorphism. Softening of the heated crust during attainment of peak metamorphic conditions facilitated emplacement of high-grade nappes at this stage. Construction of P-T paths for the metasedimentary rocks of the study area indicates that the deformational event at this stage (D_2) was for the most part associated with a decrease in pressure and temperature. S-type granites, comparable to collision-related granites of the Himalayan orogen, were produced by melting of metasedimentary rocks, and started to intrude into shallower crustal levels; this phenomenon would have caused redistribution of heat throughout the crust.

Stage 4 (?between 2626 and 2529 Ma): Renewed north-south contraction of the Abitibi and Pontiac Subprovinces

Metasedimentary rocks of the Pontiac and Timiskaming Groups along with volcanic rocks of the Blake River Group in southern Abitibi were folded at this stage of tectonic activity. Large-scale east-trending upright to southerly inclined folds were developed both in Pontiac and Abitibi subprovinces. The tectonic setting for this event is not understood

Stage 5 (>2500 Ma): Extension of the crust, deposition of Cobalt Group

The Cobalt Group is the uppermost group within the Huronian Supergroup (see Chapter 2). Sedimentary rocks of this group lie unconformably on the Pontiac and Timiskaming Groups in the northwestern part of the study area, and provide an upper age limit for the first exposure of these metasedimentary rock.

The Huronian Supergroup, a southerly thickening passive margin sequence, was deposited during early Proterozoic crustal stretching along the southern margin of the Superior craton (Young 1983, Zolani et *al.* 1984). This extensional event must have had reduced the thickness of the (southern Superior) crust to a considerable extent before deposition of the Huronian Supergroup. Study of the stratigraphy and structure of the supergroup has indicated that down-to-the-basin (south) normal faulting was responsible for development of the sedimentary basin (Young 1983, Zolani et *al.* 1984).

The structural and tectonic importance of this extensional event has not been appreciated as well as its depositional aspects. The minimum age of this extensional event may be constrained by the maximum age of the Huronian Supergroup (Heaman 1988) at about 2500 Ma. The north-trending Matachewan dyke swarm, with a radiometric age of about 2454 (Heaman 1988), is suggested to be related to the ocean opening in which the Huronian Supergroup was deposited. The dyke swarm therefore may belong to a failed-arm setting related to the ocean that was spreading to the south of the Superior Province (Fahrig 1986). A relatively fast cooling rate between 2529 and 2517 Ma deduced from the $^{40}Ar/^{39}Ar$ dating of muscovites and biotites from the Pontiac metasedimentary rocks (see Chapter 5) may have been related to this event, resulting in a relatively fast exhumation of the rocks.

The only evidence for this major extensional event in the study area are structures documented close to the Cadillac-Larder Lake fault zone. Shallow late-formed crenulations and drag folds in this area indicate a top-to-the-north normal movement along the fault zone at this stage. Concentration of deformation related to this event along this major fault zone, along with restriction of the Cobalt Group rock outcrops to this fault zone, and to the western boundary of the Pontiac Subprovince with the Abitibi Subprovince south of the Cadillac-Larder Lake fault zone, may point to reactivation of old major faults as normal faults. A block diagram (Fig. 6.11) provides a tentative model for deformation before deposition of the Cobalt Group, and may explain the unique pattern of outcrops of this early Proterozoic sedimentary group. Branches of Cobalt Group rocks in southern Abitibi and Pontiac Subprovince appear to be deposited in relatively narrow half grabens that developed on old fault zones that were reactivated as normal faults, and/or new normal faults. The northeast-trending branches of the Cobalt Group in Abitibi Subprovince north of the Cadillac-Larder Lake fault zone (see Fig. 2.1) follow the northeast-trending normal faults mapped by Hubert *et al.* (1984).

Stage 6 (? 1.9-1.7 Ga): Late north-south contraction of the crust

Late brittle south-vergent thrust faults, northeast- and northwest-trending strike-slip faults, and kink bands within the study area were produced at this stage. Penokean orogeny (1.9-1.7 Ga., Barovich *et al.* 1989), resulting from a collisional event at the southern margin of the Superior Province, probably was responsible for this late deformational event that affected sedimentary rocks of the Cobalt Group within the study area.

6.3. Pontiac subprovince: similarities and differences with Phanerozoic metamorphic core complexes

Late extension after thickening of the crust in Phanerozoic orogenic belts is an almost integral part of the tectonic history of these belts (Dewey 1988, Malavieille 1993 and references therein). These late phases are usually syn- to post-peak regional metamorphism and result in thinning of the thickened crust. During this process, a considerable thickness of low grade rocks are tectonically stripped off from above higher grade rocks, resulting into development of core complexes. Metamorphic core complex development is considered to have been

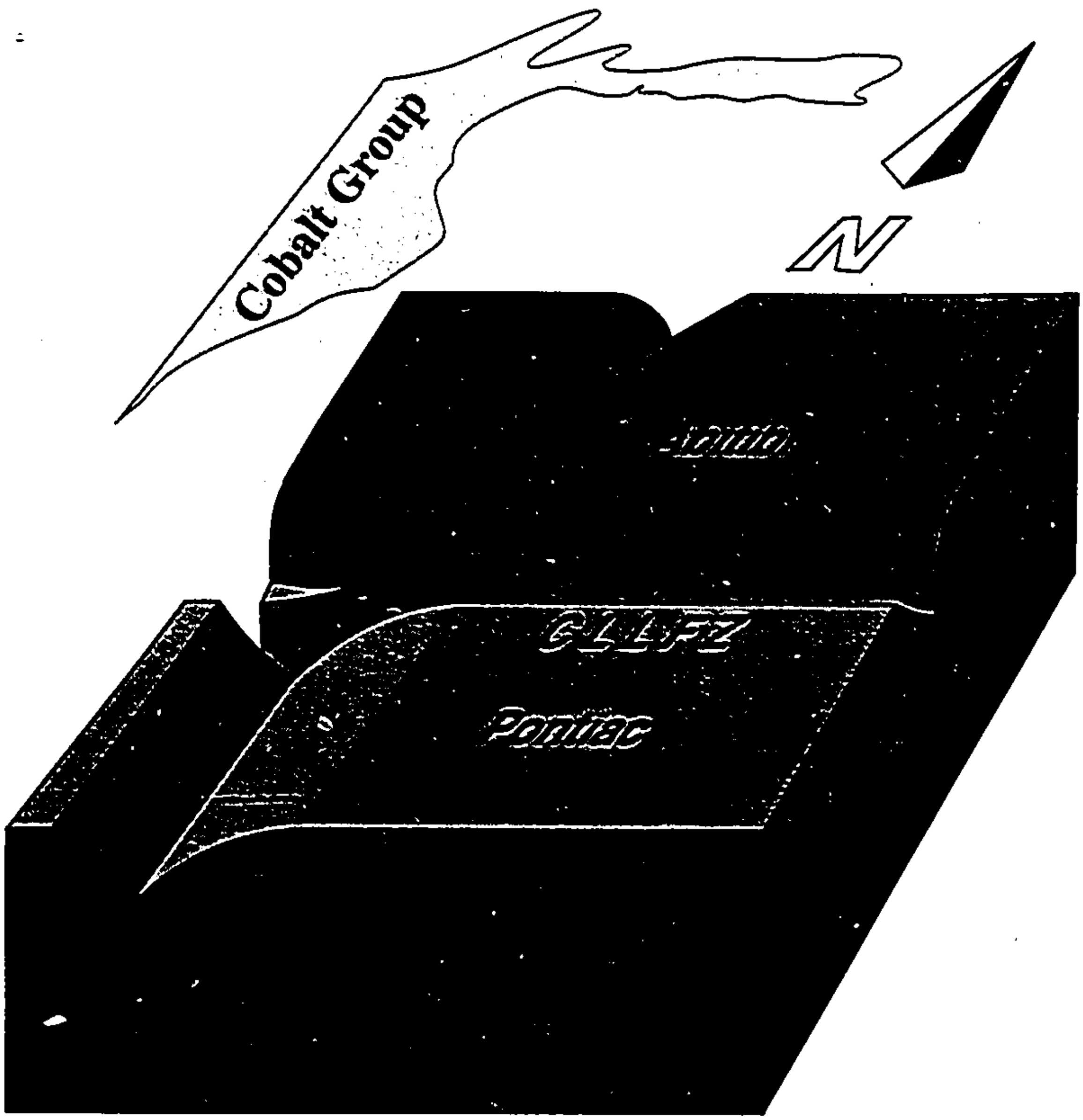

Fig. 6.11. Structural model for deposition of the Cobalt Group within the study area. Late Archean-Early Proterozoic extension related to development of a passive margin south of the Superior Province resulted in reactivation of old structures such as the Cadillac-Larder fault zone (CLLFZ). Some northeast-trending normal faults were also initiated at this stage within the Abitibi Subprovince. Normal movement along these faults produced small and large half grabens in which the Cobalt Group sedimentary rocks were deposited. The outcrop pattern of the Cobalt Group is shown for comparison with the trend of the reactivated structures.

responsible for juxtaposition of originally deep-seated higher grade rocks and shallow-seated lower grade rocks in the Archean terranes (cf. Kusky 1993).

Like other metasedimentary subprovinces of the Superior Province (Quetico and English river), the Pontiac Subprovince has a higher metamorphic grade than the surrounding greenstone belts. This difference in metamorphism, along with relatively more ductile deformation within the subprovince, suggest the possibility that the subprovince is an Archean metamorphic core complex. Based on their structural studies in western Pontiac Subprovince (south of the present study area), Sawyer and Barnes (1994) suggested a metamorphic core complex model for evolution of the Belleterre-Angliers belt of the Pontiac Subprovince. They suggested that the Belleterre-Angliers belt was emplaced as a south-vergent thrust sheet on the Pontiac Subprovince, and that extensional shear zones (and the metamorphic core complex) were later developed on the flanks of antiformal structures that formed by intraplating of monzodioritic, granodioritic, syenodyoritic and syenitic magmas in the middle crust of the Pontiac Subprovince.

A comparison is here made between features of the Pontiac Subprovince and the Phanerozoic metamorphic core complexes in order to consider the possibility of occurrence of a metamorphic core complex in this part of the Archean Superior Province. However, it must be noted that difficulties are always present in comparisons of this kind, usually because of complexity of the geology of Precambrian terranes that involve multiple tectonic and thermal events, and that usually have less well-preserved outcrops compared to what is accessible in the Phanerozoic terranes.

The term *metamorphic core complex* is used to describe metamorphic rocks that occur in relatively small to moderately sized outcrop areas, are often topographically high, and that are composed of igneous and metamorphic rocks that display anomalous deformation and metamorphism relative to the surrounding terrane. Original use of the term was to describe the over 25 complexes in the Cordillera of western North America, and is now used to describe any such occurrence (Spear 1993). Cordilleran metamorphic core complexes appear to be bodies from the middle crust that have been dragged out from beneath fracturing and extending upper crustal rocks, and exposed beneath shallow-dipping (normal-slip) faults of large areal extent (Lister and Davis 1989) known as detachment faults (Davis and Lister 1988). Features characterizing the metamorphic core complexes of the North American Cordillera as described by Armstrong (1982) include: location in the hinterland behind the foreland thrust and fold belt; a pre-extension history of crustal thickening; superimposed extensional crustal-scale shear zone(s) with a mylonitic footwall and ductile-brittle transition; and an uplifted and arched footwall that exposes the previously deeply buried crust.

The metamorphic facies of the Pontiac Group contrasts with the metamorphic facies in the southern Abitibi greenstone belt. However, this and other studies (Powell *et al.* 1993) indicate that only a small change in metamorphic grade is present across the tectonic border (the Cadillac-Larder Lake fault zone) between these two terranes. The Cadillac-Larder Lake fault zone, on the other hand, represents a major shear zone across which a change in rheology of deformation may be observed between the relatively ductile deformation within the Pontiac Subprovince and the relatively brittle deformation within the Abitibi Subprovince. The change may be viewed as a result of different deformational response of more competent, less-layered volcanic rocks of the Abitibi greenstone belt and more incompetent, layered sedimentary rocks of the Pontiac Subprovince. To this a general difference in temperature of deformation must be added.

A foreland fold and thrust belt setting, similar to that of metamorphic core complexes, may not be ruled out for the Pontiac Subprovince, because in the suggested tectonic model, it is postulated that the Subprovince was thrust over the southern segment of the Abitibi arc system. The Cadillac-Larder Lake fault zone may be considered a shear zone separating brittle deformation in the hanging wall from ductile deformation within the footwall (detachment fault). The difference in metamorphic facies between the Abitibi and Pontiac Subprovinces, and southward increase in metamorphic grade towards the south of the study area, with higher pressure metamorphism, may be interpreted as the Pontiac Subprovince being the previously deeply buried crust that has uplifted and arched to be exposed against the lower grade Abitibi Subprovince.

Dalziel and Brown (1989) suggested that inversion of a marginal basin during a compressional regime is one way of initiating a thickened crustal welt before development of metamorphic core complexes. Postulating the suggested tectonic history (of this study) for the Pontiac Subprovince, the suggestion of Dalziel and Brown may be considered another similarity between the Pontiac Subprovince and some Phanerozoic metamorphic core complexes.

Tectonic denudation of the thickened crust results in very fast cooling of the metamorphic core complexes. Minerals within these terranes usually record cooling rates of more than 20°C/Ma (see Fig. 12 in Kohn *et al.* 1995). Construction of cooling curves for the Pontiac Subprovince (this study and Powell *et al.* 1995b) indicates very slow cooling rates (about 2° to 8°C/Ma) for Pontiac metasedimentary rocks following peak metamorphic conditions in Late Archean time. This rules out rapid tectonic denudation of the Pontiac Subprovince after peak metamorphic conditions.

The metamorphic core complex development model for the Belleterre-Angliers belt of the Pontiac Subprovince suggested by Sawyer and Barnes (1994) is ruled out because the granitoid complexes documented by these authors to be responsible for the doming (Lac de Quinze and Lac Simard granitoids) have yielded ages that are older than age of peak metamorphic conditions, and even older than the youngest detrital zircons within the Pontiac metasedimentary rocks.

In conclusion, despite some basic similarities in structural, metamorphic and tectonic features between the Pontiac Subprovince and Phanerozoic metamorphic core complexes, some essential features of core complexes are not present in the Pontiac Subprovince, preventing this Late Archean metasedimentary terrane being unequivocally classified as a metamorphic core complex.

6.4. Advantages and disadvantages of the backarc basin model for tectonic evolution of the Pontiac Subprovince

The backarc basin model for evolution of the Pontiac Subprovince is favored because it can explain:

1) occurrence of the major break (Cadillac-Larder Lake fault zone) between the two very similar segments of the Abitibi greenstone belt.

2) irregular patterns of boundaries between the Pontiac and Abitibi Subprovinces.

3) presence of calc-alkaline I-type granitoid intrusions within the Pontiac Subprovince.

4) lack of melange and soft-sediment deformation within the metasedimentary pile, characteristics that are diagnostic of accretionary prism sedimentation.

The model can also indirectly explain the presence of extremely old and young detrital zircons within the Pontiac metasedimentary rocks.

Lack of evidence for analogous komatiitic rocks in Phanerozoic backarc basins may be considered as a disadvantage for the presented model. It must also be noted that the model presumes a plate tectonic context similar to those of the Phanerozoic time, and accepting a different tectonic regime with predominantly vertical movements does not allow for this or similar kinds of interpretations.

6.5. Implications for Late Archean tectonic processes

Applicability of the tectonic models quite similar to those of the Phanerozoic tectonic setting to the Late Archean Pontiac and Abitibi Subprovinces is another clue that plate tectonic processes were working in the same way then.

Estimated paleopressures and paleotemperatures for metasedimentary rocks of the Pontiac Subprovince (this study) indicate that, during the orogenic event, the continental thermal gradient within the study area was not different from those of the crusts that were involved in Phanerozoic orogens. The P-T path estimated through this study is similar to P-T paths estimated for Phanerozoic collisional belts. Timing of the P-T path (see Chapter 4) indicates that the orogen resulted from collision of the Abitibi arc system with a suspect terrane to the south, reaching its maximum thickness in a time span of about 10 Ma.

This study also suggests that for tectonic interpretations of the Archean cratons, generalizations such those of Card (1989) should be avoided (see section 6.1). If Phanerozoic tectonic settings are used as models for these interpretations, the possibility of alternative settings such as backarc basins may not be overlooked.

6.6. Summary and conclusions

The Late Archean tectonic setting of the Pontiac Subprovince within the southern Superior Province may be compared to Tertiary and Recent tectonic settings along the boundaries of the Indian and Eurasian lithospheric plates. A backarc basin tectonic model is proposed for the Late Archean evolution of this metasedimentary subprovince in which a backarc basin probably developed as a result of extension and dissection of the Abitibi arc system into a northern and a southern segment at about 2700-2690 Ma. Collision of a continental or oceanic arc terrane (probably the Minnesota Valley River terrane) with the southern segment resulted in convergence of the two arc segments (*ca.* 2680 Ma), closure of the Pontiac backarc basin, final amalgamation of the two segments, and thickening of the crust. The thickened crust underwent regional metamorphism and nappe development at about 2670 Ma. Collisional S-type granites were intruded into the crust at this time.

The tectonic setting of a north-south contractional event after the aforementioned event is not understood. However, it produced major east-trending structures both in the Abitibi and Pontiac Subprovinces. A major extensional event (before ca 2500 Ma), associated with development of a passive margin south of the Superior Province, affected parts of the Pontiac and Abitibi Subprovinces. Late Archean faults in these terranes were reactivated as normal faults, producing half grabens for deposition of the Cobalt Group sedimentary rocks. Late east-trending south-vergent thrust faults and some strike slip faults within the study area affecting the Early Proterozoic and underlying Archean basement rocks were probably the result of the Penokean orogeny at about 1.9-1.7 Ga.

7. Summary, conclusions and recommendation for further studies

The northwestern part of the Late Archean Pontiac Subprovince is composed of turbiditic graywackes, known as the Pontiac Group, that were deposited between about 2690-2680 Ma. These rocks are interlayered with volcanic rocks of komatiitic, basaltic and andesitic composition. Pillow structures within some of these volcanic rocks, and their interlayered relationship with the Pontiac Group, suggests that they developed by subaqueous syndepositional eruptions. Both rock types were intruded by voluminous I-type and S-type plutons and some lamprophyric dykes. Outcrops of gneisses known as Lac Opasatica gneiss are limited to the western part of the study area. These rocks appear to be bodies of granitoids that intruded volcanic rocks and were later deformed into a gneissic complex. Coarse-grained sedimentary rocks of the Timiskaming Group (*ca.* 2680 Ma) were deposited unconformably over the Pontiac Group rocks in the northern part of the study area. Outcrops of glaciomarine sedimentary rocks of the Early Proterozoic Cobalt Group are limited to the northwestern part of the study area. Different sets of early Proterozoic mafic dykes cut across the Pontiac and Timiskaming Group metasedimentary rocks.

Structural mapping and microstructural analysis of samples from the study area has revealed a complex and protracted history of deformation for the northwestern part of the Pontiac Subprovince. During Late Archean and Early Proterozoic time, different rock types within the study area have undergone six different deformational events, a brief description of which is given here.

D_1 microstructures record prograde conditions before attainment of peak metamorphic conditions. This event was the result of early crustal thickening within the Pontiac Subprovince. Large-scale thrusting of the Abitibi over Pontiac Subprovince occurred during the D_1 event. Timiskaming Group rocks also were affected by this deformational event. Microstructures of this event are preserved as relics within the D_2 microstructures.

D_2 produced recumbent east-trending folds, some brittle-ductile shear zones (the Montbeillard, Bellecombe and Saint Roch shear zones), and a penetrative discrete crenulation foliation associated with a prominent elongation lineation. These structures developed during and after peak metamorphic conditions, as demonstrated by relationships between these structures and peak metamorphic minerals, as well as their relationship with syn-peak metamorphic S-type granites. A major amount of deformation during this event appears to have occurred through south-southeast-directed nappe development along gently north-dipping sole thrusts, preserved as major shear zones.

D_3 represents a renewed north-south contractional event that superimposed east-trending (generally upright) folds on all older structures. These structures are comparable to similar east-trending structures within the Abitibi Subprovince.

D_4, which is confined to the vicinity of the Cadillac-Larder Lake fault zone, was an extensional event that resulted from normal faulting reactivation of this fault zone.

D_5 appears to be the most recent evident contractional event, and produced kink structures and brittle south-vergent thrusts which affected all older structures within the study area.

Gneissose structures in the Lac Opasatica gneisses and related mineral elongation lineation developed during a pre-D_1 event, not traceable into the Pontiac Group rocks.

Regional metamorphism to amphibolite facies (*ca.* 2670 Ma) is evident within sedimentary and volcanic rocks of the Pontiac and Timiskaming Groups. Metamorphic grade within the study area increases from the north, close to the Cadillac-Larder Lake fault zone, to the south, close to the outcrops of S-type granitic rocks. Four metamorphic isograds, +garnet, +staurolite, +kyanite and +sillimanite, are mappable in the area. Changes in metamorphic mineral assemblages of the Pontiac Group across these isograds are constrained through different possible metamorphic reactions. The S-type granites of Decelles batholith were produced by melting of the Pontiac Group or similar metasedimentary rocks during peak metamorphic conditions. Intrusion of voluminous I-type granites in the absence of a high heat-generating crust may have been responsible for a major part of heat contribution for regional metamorphism of the crustal rocks.

Geothermobarometry estimations for metasedimentary and metavolcanic samples from the study area indicate maximum paleo-temperature and paleo-pressures of about 620°C and 7.2, kbar respectively. The relationship between the estimated paleo-temperatures and paleo-pressures indicates that continental heat flow for this Late Archean terrane was not different from those of the crusts that were involved in Phanerozoic orogens. Microstructural, thermobarometric data from this study indicates that the rocks within the study area have followed a clockwise P-T path similar to those of Phanerozoic collisional belts.

$^{40}Ar/^{39}Ar$ cooling ages of muscovites and biotites from metamorphic rocks of the Pontiac Subprovince indicate that temperatures as high as 350°C and 280°C were persistent in crustal rocks of the area until *ca.* 150 Ma after attainment of the peak metamorphic conditions. Construction of a cooling curve for samples from the study area reveals a generally slow cooling rate that ranges from 2° to 6°C/Ma.

The tectonic history of the Pontiac Subprovince may be summarized in six sequential stages:

Stage 1 (~2700-2690 Ma): A backarc basin setting similar to that of Phanerozoic backarc basins is proposed for deposition of the Late Archean Pontiac sedimentary rocks. On the basis of this model, the Abitibi arc system was rifted along a jagged path that later evolved into the Cadillac-Larder Lake fault zone. The rifting occurred because of backarc spreading behind a north-dipping subduction zone under the Abitibi arc system.

Stage 2 (~2680 Ma): Collision of a continental or oceanic arc terrane (probably Minnesota Valley River terrane) with the southern segment of the dissected arc resulted in convergence of the two segments, closure (inversion) of the Pontiac backarc basin, final amalgamation of the two segments and the suspect terrane, and thickening of the crust. Intrusion of extensive I-type granites at this stage started to heat the thickened crust.

Stage 3 (~2670 Ma): Regional metamorphism and development of nappe structures within the thickened crust.

Stage 4 (? 2626-2529 Ma): Renewed north-south contraction of the crust.

Stage 5 (>2500 Ma): Major extension associated with development of a passive margin south of the Superior Province affected parts of the Pontiac and Abitibi Subprovinces. Late Archean faults in these terranes were reactivated as normal faults, producing half grabens in which the Cobalt Group sedimentary rocks were deposited.

Stage 6 (? 1.9-1.7 Ga): Late east-trending south-vergent thrust faults and some strike slip faults within the study area affecting the Early Proterozoic and underlying Archean basement rocks probably originated during the Penokean orogeny (1.9-1.7 Ga).

The present study provides a background for further geological studies within the Late Archean Pontiac metasedimentary Subprovince and the neighboring Abitibi Subprovince.

No detailed sedimentological study has yet been devoted to the Pontiac Subprovince. The presence of abundant and spectacular sedimentary structures despite amphibolite facies metamorphism invites sedimentologists into this area. Basin analysis studies may be useful for examination of the backarc basin or accretionary prism (or other) models to better assess the origin of the Pontiac sedimentary rocks. Further study of the Timiskaming Group is suggested for a better understanding of origin of this detrital sequence.

Geochronological, geochemical and structural study of the Lac Opasatica and other gneissic complexes within the Pontiac Subprovince should be used to investigate their relationship to the Pontiac and Abitibi Subprovinces. These gneisses may also be compared to gneisses within the Abitibi and Opatica Subprovinces as a basis for examining the model here suggested for development of the gneisses (see Chapter 6).

Structural studies should be carried in other parts of the Pontiac Subprovince, focused on the recognition (or dismissal) of the deformational events suggested by the present and other workers. Different aspects of the six deformational events suggested by this study are not yet well understood. The general trend of D_1 structures, regional continuity of D_2 nappes, and tectonic event(s) behind the D_3 structures must be investigated through more detailed and regional studies, to arrive at a solid level of understanding.

Metamorphic characteristics of the Pontiac has been established to a certain degree; however, geochronologic studies of metamorphic minerals such as garnet, kyanite and sillimanite will help to put more constraints on the timing of prograde and retrograde metamorphism of this metasedimentary terrane. Thermobarometry analyses parallel with geochronological studies of different dyke sets within the Pontiac Subprovince are also suggested. The resulting data may be used to acquire an understanding about rates of exhumation, uplift and erosion in this Late Archean terrane.

Further geochronologic study of detrital zircons from different parts of the Pontiac Subprovince, leading to the discovery of younger detrital zircons, will provide a better constraint for the minimum age of the Pontiac basin.

Regional study and comparison must be carried out to answer the following questions: Why do sedimentary subprovinces within the Superior Province show higher metamorphic grades (and hence more ductile deformation) relative to the greenstone belts? Why are metamorphic core complexes similar to those of Phanerozoic time, and blueschist metamorphic rocks, not common within these Archean terranes?

Similarities between the Pontiac Subprovince and other metasedimentary belts within the Superior Province invokes questions about the origin of these sedimentary subprovinces. Are all of these terranes, as suggested by previous workers, accretionary prisms deposited within a convergent setting? A glance at the tectonically active area of western Pacific, northern Indian ocean, and southeastern Asia indicates that, compared to the accretionary prisms, backarc basins cover vast areas of these regions. Any plate tectonic interpretation of the Archean cratons within a modern plate tectonic context must therefore take presence of backarc basin environments into consideration.

REFERENCES

Allmendinger, R. W., 1988, Stereonet: a plotting program for orientation data for Macintosh computer: Version 3.1 .

Anhaeusser, C. R., 1981, Geotectonic evolution of the Archean succession in the Barberton Mountainland, South Africa, *in* Kroner, A., ed., Precambrian plate tectonics: Amsterdam, The Netherlands, Elsevier, p. 137-160.

Archambault, G., 1985, Archean wrench fault tectonics and structural evolution of the Blake River Group, Abitibi Belt: Discussion: Can. J. Earth Sci., v. 22, p. 943-945.

Archibald, N. J., Bettenay, L. F., Binns, R. A., Groves, P. I., and Gunthorpe, R. J., 1978, The evolution of the Archean greenstone terrains, Eastern Goldfield Province, Western Australia: Precambrian Research, v. 9, p. 103-132.

Armstrong, R. L., 1982, Cordilleran metamorphic core complexes - From Arizona to southern Canada: Ann. Rev. Earth Planet Sci., v. 10, p. 129-154.

Baragar, W. R. A., and Mc.Glynn, J. C., 1976, Early Archean basement in the Canadian Shield: A review of evidence: Geological Survey of Canada paper No. 76-14.

Barnes, S.-J., Couture, J.-F., Sawyer, E. W., and Bouchaib, C., 1993, Nickle-copper occurences in the Belleterre-Angliers belt of the Pontiac Subprovince and the use of Cu-Pd ratios in interpreting platinum-group element distributions: Economic Geology, v. 88, p. 1402-1418.

Barovich, K. M., Patchett, P. J., Peterman, Z. E., and Sims, P. K., 1989, Nd isotopes and the origin of 1.9-1.7 Ga Penokean continental crust of the Lake Superior region: Geol. Soc. Am. Bul., v. 101, p. 333-338.

Benn, K., Sawyer, E. D., and Bouchez, J.-L., 1992, Orogen parallel and transverse shearing in the Opatica belt, Quebec: implications for the structure of the Abitibi Subprovince: Can. J. Earth Sci., v. 29, p. 2429-2444.

Benn, K., Miles, W., Gassemi, M. R., and Gillett, J., 1994, Crustal structure and kinematic framework of the northwestern Pontiac Subprovince, Quebec: An integrated structural and geophysical study: Can. J. Earth Sci., v. 31, p. 271-281.

Bennett, G., Dressler, B. O., and Robertson, J. A., 1991, The Huronian Supergroup and associated intrusive rocks, *in* Thurston, P. C., Williams, H. R., Sutcliffe, R. H., and Stott, G. M., eds., Geology of Ontario, Ontario Geological Survey, Special Volume 4, p. 549-591.

Berman, R. G., 1988, Internally-consistent thermodynamic data for minerals in the system Na_2O-K_2O-CaO-MgO-FeO-Fe_2O_3-Al_2O_3-SiO_2-TiO_2-H_2O-CO_2: J. Petrol., v. 29, p. 445-522.

Berman, R. G., 1990, Mixing properties of Ca-Mg-Fe-Mn garnets: Am. Mineral., v. 75, p. 328-344.

Berman, R. G., 1991, Thermobarometry using multi-equilibrium calculations: A new technique, with petrological applications: Canadian Mineralogist, v. 29, p. 833-855.

Bickle, M. J., 1978, Heat loss from the Earth: a constraint on Archean tectonics from the relation between geothermal gradient and the rate of plate production: Earth Planet. Sci. Lett., v. 40, p. 301-315.

Blacic, J., 1971, Hydrolytic weakening of quartz and olivine [Ph.D. thesis]: University of California, 205 p.

Blackburn, C. E., 1980, Towards a mobilist tectonic model for part of the Archean of northwestern Ontario: Geoscience Canada, v. 7, no. 2, p. 64-72.

Bohannon, R. G., and Parsons, T., 1995, Tectonic implications of post-30 Ma Pacific and North American relative plate motions: Geol. Soc. Am. Bul., v. 107, p. 937-959.

Borradaile, G., Sarvas, P., Dutka, R., Stewart, R., and Stubley, M., 1988, Transpression in slates along the margin of an Archean gneiss belt, northern Ontario-magnetic fabrics and petrofabrics: Can. J. Earth Sci., v. 25, p. 1069-1077.

Burke, K., and Kidd, W. S. F., 1978, Were Archean geothermal gradients much steeper than those of today?: Nature, v. 272, p. 240-241.

Burke, K., Dewey, J. F., and Kidd, W. J. F., 1978, Dominance of horizontal movements during the later permobile regime, *in* Windley, B. F., ed., The early history of the earth: London, England, Wiley, p. 113-130.

Camiré, G. E., 1992, Evolution tectono-métamorphique de la partie nord-ouest de la sous-province Archéenne de Pontiac, Bouclier canadien [Ph.D. thesis]: Univ. Montpellier.

Camiré, G. E., and Burg, J.-P., 1993, Late Archean thrusting in the northwestern Pontiac Subprovince, Canadian Shield: Precambrian Research, v. 61, p. 51-66.

Camiré, G. E., Lafleche, M. R., and Ludden, J. N., 1993, Archean metasedimentary rocks from the northwestern Pontiac Subprovince of the Canadian Shield: chemical characterization, weathering and modelling of the source areas: Precambrian Research, v. 62, p. 285-305.

Card, K. D., 1978, Geology of the Sudbury-Manitoulin area, Districts of Sudbury and Manitoulin: Ontario Geological Survey, Report No. 166.

Card, K. D., and Ciesielski, A., 1986, DNAG No. 1. Subdivisions of the Superior Province of the Canadian Shield: Geoscience Canada, v. 13, p. 5-13.

Card, K. D., 1990, A review of the Superior Province of the Canadian Shield, a product of Archean accretion: Precambrian Research, v. 48, p. 99-156.

Carignan, J., and Gariepy, C., 1991, The lead isotope geochemistry of volcanic rocks, gneisses, and granitoid intrusions from the Pontiac Subprovince, Proceedings of Geological Association of Canada Annual Meeting, Abstracts, Toronto.

Carignan, J., Machado, N., and Gariépy, C., 1992, U-Pb and Pb-Pb geochronology of the Baby-Belleterre greenstone belt and associated Pb-Cu-Ni deposits, Pontiac Subprovince, Proceedings of GAC MAC Annual Meeting, Wolfville.

Carmichael, D. M., 1969, On the mechanism of prograde metamorphic reactions in quartz-bearing pelitic rocks: Contr. Mineral. and Petrol., v. 20, p. 244-267.

Chatterjee, N. D., and Froese, E., 1975, A thermodynamic study of the pseudobinary join muscovite - paragonite in the system $KAlSi_3O_8$-$NaAlSi_3O_8$-Al_2O_3-SiO_2-H_2O: Am. Mineral., v. 60, p. 985-993.

Chown, E. H., Daigneault, R., Muller, W., and Mortensen, J. K., 1992, Tectonic evolution of the Northern Volcanic Zone, Abitibi belt, Quebec: Can. J. of Earth Sci., v. 29, p. 2211-2225.

Collins, W. H., 1917, Onaping map area, Geological Survey of Canada Memoir 5, 157 p.

Copeland, P., Parrish, R. R., and Harrison, T. M., 1988, Identification of inherited radiogenic Pb in monazite and implifications for U-Pb systematics: Nature, v. 333, p. 760-763.

Corfu, F., and Andrews, A. J., 1986, A U-Pb age for mineralized Nipissing diabase, Gowganda, Ontario: Can. J. Earth Sci., v. 23, p. 107-109.

Corfu, F., and Stott, G. M., 1986, U/Pb ages for late magmatism and regional deformation in the Shebandowan belt, Superior Province, Canada: Can. J. Earth Sci., v. 23, p. 1075-1082.

Corfu, F., Krogh, T. E., Kwok, Y. Y., and Jensen, L. S., 1989, U-Pb zircon geochronology in the southwestern Abitibi greenstone belt, Superior Province: Can. J. Earth Sci., v. 26, p. 1747-1763.

Corfu, F., 1993, The evolution of the Southern Abitibi Grenstone Belt in light of Precise U-Pb geochronology: Economic Geology, v. 88, p. 1323-1340.

Crawford, M. L., 1977, Calcium zonning in almandine garnet, Wissahickon Formation, Philadelphia, Pennsylvania: Can. Min., v. 15, p. 243-249.

Daigneault, R., St-Julien, P., and Allard, G. O., 1990, Tectonic evolution of the northeast portion of the Archean Abitibi greenstone belt, Chibougamau area, Quebec: Can. J. Earth Sci., v. 27, p. 1714-1736.

Dalrymple, G. B., Alexander, E. C. J., Lamphere, M. A., and Kraker, G. P., 1981, Irradiation of samples for $^{40}Ar/^{39}Ar$ dating using the Geological Survey TRIGA reactor: United States Geological Survey, Professional Paper, v. 1176, p. 1-55.

Dalziel, I. W. D., and Brown, R. L., 1989, Tectonic denudation of the Darwin metamorphic core complex in the Andes of Tierra del Fuego, southernmost Chile: Implications for Cordilleran orogenesis: Geology, v. 17, p. 699-703.

Davis, G. A., and Lister, G. S., 1988, Detachment faulting in continental extension: perspectives from the southwestern U.S. Cordillera, John Rogers symposium volume: Spec. Pap. Geol. Soc. Am., v. 218, p. 133-159.

Davis, D. W., Pezzutto, F., and Ojakangas, R. W., 1990, The age and provenance of metasedimentary rocks in the Quetico Subprovince, Ontario, from single zircon analyses: implications for Archean sedimentation and tectonics in the Superior Province: Earth and Planetary Sci. Letters, v. 99, p. 195-205.

Davis, D. W., 1991, Age constraints on deposition and provenance of Archean sediments in the southern Abitibi and Pontiac Subprovices from U-Pb analyses of detrital zrcons, Proceedings of Geological Association of Canada Annual Meeting, Toronto, p. A-29.

Davis, D. W., 1992, Age constraints on deposition and provenance of Archean sediments in the southern Abitibi and Pontiac Subprovices from U-Pb analyses of detrital zrcons, Litoprobe Abitibi-Grenville Transect , Report No. 25, p. 147-150.

Davis, W. J., Machado, N., Gariepy, C., Sawyer, E., and Benn, K., 1993, U-Pb geochronology of the Opatica metaplutonic-gneiss belt, Quebec and its relationship to the northern Abitibi, Proceedings of Geological Association of Canada Annual Meeting, Edmonton, p. A-22.

Davis, W. J., Gariepy, C., and Sawyer, E. W., 1994, Pre-2.8 Ga crust in the Opatica gneiss belt: A potential source of detrital zircons in the Abitibi and Pontiac Subprovinces, Superior Province, Canada: Geology, v. 22, p. 1111-1114.

Davis, W. J., Machado, N., Gariépy, C., sawyer, E. W., and Benn, K., 1995, U-Pb geochronology of the Opatica tonalite-gneiss belt and its relationship to the Abitibi greenstone belt, Superior Province, Quebec: Can. J. Earth Sci., v. 32, p. 113-127.

Dawson, K. R., 1966, A comprehensive study of Preissac-Lacorne batholith, Abitibi County, Quebec: Geol. Surv. Can. Bull., No. 142, p. 175.

Deer, W. A., Howie, R. A., and Zussman, J., 1992, An introduction to the rock-forming minerals: Hong Kong, Longman Scientific & Technical, 696 p.

Desrochers, J.-P., Hubert, C., Ludden, J. N., and Pilote, P., 1993, Accretion of Archean oceanic plateau fragments in the Abitibi greenstone belt Canada: Geology, v. 21, p. 451-454.

Dewey, J. F., 1988, Extensional collapse of orogens: Tectonics, v. 7, p. 1123-1139.

Dimroth, E., Imreh, L., Rocheleau, M., and Goulet, N., 1982, Evolution of the sout-central part of the Archean Abitibi Belt, Quebec. Part I: Stratigraphy and Paleogeographic model: Can. J. Earth Sci., v. 19, p. 1729-1758.

Dimroth, E., Imreh, L., Goulet, N., and Rocheleau, M., 1983, Evolution of the sout-central part of the Archean Abitibi Belt, Quebec. Part II: Tectonic evolution and geomechanical model: Can. J. Earth Sci., v. 20, p. 1355-1373.

Dimroth, E., Imreh, L., Goulet, N., and Rocheleau, M., 1983, Evolution of the sout-central part of the Archean Abitibi Belt, Quebec. Part III: Plutonic and metamorphic evolution and geotectonic model: Can. J. Earth Sci., v. 20, p. 1374-1388.

Dutrow, B. L., and Holdaway, M. J., 1989, Experimental determination of the upper thermal stability of Fe-staurolite + quartz at medium pressures: J. Petrology, v. 30, p. 229-248.

Engel, H. E. J., and Kulm, D. L., 1972, Pre-Precambrian global tectonics: a tectonic test: Geol. Soc. Am. Bul., v. 83, p. 2325-2340.

England, P. C., 1979, Continental geotherms during the Archean: Nature, v. 277, p. 556-558.

England, P. C., and Thompson, A. B., 1984, Pressure-Temperature-Time paths of regional metamorphism I. Heat transfer during the evolution of regions of thickened continental crust: J. Petrology, v. 25, p. 894-928.

Fahrig, W. F., 1987, The tectonic settings of continental mafic dyke swarms: failed arm and early passive margin, *in* Halls, H. C., and Fahrig, W. F., eds., Mafic dyke swarms, Geological Association of Canada Special Paper, p. 503.

Fairbairn, H. W., Hurley, P. M., Card, K. D., and Knight, C. J., 1969, Correlation of radiometric ages of Nipissing diabase and Huronian metasediments with Proterozoic orogenic events in Ontarion: Can. J. Earth Sci., v. 6, p. 489-497.

Feng, R., and Kerrich, R., 1990, Geobarometry, differential block movements, and crustal structure of the southwestern Abitibi greenstone belt, Canada: Geology, v. 18, p. 870-873.

Feng, R., and Kerrich, R., 1991, Single zircon age constranints on the tectonic juxtaposition of the Archean Abitibi greenstone belt and Pontiac Subprovince, Quebec, Canada: Geochimica et Cosmochimica Acta, v. 55, p. 3437-3441.

Feng, R., Kerrich, R., McBride, S., and Farrar, E., 1992, $^{40}Ar/^{39}Ar$ age constraints on the thermal history of the Archean Abitibi greenstone belt and the Pontiac Subprovince: implications for terrane collision, differential uplift, and overprinting of gold deposits: Can. J. Earth Sci., v. 29, p. 1389-1411.

Feng, R., and Kerrich, R., 1992, Geochemical evolution of granitoids from the Archean Abitibi Southern Volcanic zone and the Pontiac Subprovince, Superior Province, Canada: Implications for tectonic history and source regions: Chemical Geology, v. 98, p. 23-70.

Feng, R., Jianzhong, F., and Kerrich, R., 1993, Noble metal abundances and characteristics of six granitic magma series, Archean Abitibi belt, Pontiac Subprovince: Relationships to metallogeny and overprinting of mesothermal gold deposits: Economic Geology, v. 88, p. 1376-1401.

Feng, R., Kerrich, R., and Maas, R., 1993, Geochemical, oxygen, and neodymium isotope compositions of metasediments from the Abitibi greenstone belt and Pontiac Subprovince, Canada: Evidence for ancient crust and Archean terrane juxtaposition: Geochimica et Cosmochimica Acta, v. 57, p. 641-658.

Fuhrman, M. L., and Lindsley, D. H., 1988, Ternary-feldspar modeling and thermometry: Am. Mineral., v. 73, p. 201-215.

Ganguly, J., 1972, Staurolite stability and related paragenesis. Theory, experiments and applications: J. Petrology, v. 13, p. 335-365.

Gariepy, C., Allegre, C. J., and Lajoie, J., 1984, U-Pb systematics in single zircons from the Pontiac sediments, Abitibi greenstone belt: Can. J. Earth Sci., v. 21, no. 11, p. 1296-1304.

Gariépy, C., Verner, D., and Doig, R., 1990, Dating Archean metamorphic minerals southeast of the Grenville front, western Quebec, using Pb isotopes: Geology, v. 18, p. 1078-1081.

Gariépy, C., and Allègre, C. J., 1985, The lead isotope geochemistry and geochronology of late kinematic intrusives from the Abitibi greenstone belt, and the implications for Late Archean crustal evolution: Geochim. Cosmochim. Acta, v. 49, p. 2371-2384.

Ghent, E. D., 1976, Plagioclase-garnet-Al_2SiO_5-quartz: a potential geothermometer-geobarometer: Am. Mineralogist, v. 61, p. 710-714.

Ghent, E. D., and Stout, M. Z., 1981, Geobarometry and geothermometry of plagiocase-biotite-garnet-muscovite assemblages: Cont. Min. Petr., v. 76, p. 92-97.

Goldich, S. S., and Fischer, L. B., 1986, Air-abrasion experiments in U-Pb dating of zircon: Chemical Geology, v. 58, p. 195-215.

Goodwin, A. M., 1977, Archean basin-craton complexes and the growth of Precambrian shields: Can. J. Earth Sci., v. 14, p. 2737-2759.

Goodwin, A. M., 1982, Archean volcanoes in southwestern Abitibi Belt, Ontario and Quebec: form, composition, and development: Can. J. Earth Sci., v. 19, p. 1140-1155.

Goulet, N., 1978, Stratigraphic and structural relationships across the Cadillac-Larder Lake Fault, Rouyn-Beauchastel area, Quebec [Ph.D. Thesis thesis]: Queen's university, Kingston, Canada, 142 p.

Hames, W. E., Tracy, R. J., and Bondar, R. J., 1989, Post-metamorphic unroofing history deduced from petrology, fluid inclusions, thermochronometry and thermal modelling: an example from southwestern New England: Geology, v. 17, p. 727-730.

Hamilton, W. B., 1988, Plate tectonics and island arcs: Geol. Soc. Am. Bul., v. 100, p. 1503-1527.

Harker, A., 1932, Metamorphism: London,-Methuen.

Harrison, T. M., 1981, Diffusion of 40Ar in hornblende: Contrib. Mineral. Petrol., v. 78, p. 324-331.

Harrison, T. M., Duncan, I., and McDougall, I., 1985, Diffusion of ^{40}Ar in biotite: temperature, pressure and compositional effects: Geochim. Cosmochim. Acta, v. 49, p. 2461-2468.

Heaman, L. M., 1988, A precise U-Pb zircon age for a Hearst dyke, Proceedings of Geological Association of Canada Annual Meeting. 13:A53

Heaman, L., and Parrish, R. R., 1991, U-Pb geochronology of accessory minerals, Mineralogical Association of Canada, short course handbook on Applications of radiogenic isotope systems to problems in geology: Toronto, 498 p.

Hocq, M., 1989, Carte lithotectonique des sous-provinces de l'Abitibi et du Pontiac: Gouvernement du Québec, Ministére de l'Énergie et des Ressources (Mines), Direction de la recherche géologique, scale 1:500,000.

Hodges, K. V., and Crowley, P. D., 1985, Error estimation and empirical geothermobarometry for pelitic systems: Am. Min., v. 70, p. 702-709.

Hodgson, C. J., and Hamilton, J. V., 1989, Gold mineralization in the Abitibi greenstone belt: End stage result of Archean collisional tectonics?: Economic Geology, Monograph, v. 6, p. 86-100.

Hoffman, P. F., 1989, Precambrian geology and tectonic history of North America, Geology of North America-An overview: Boulder, Colorado, Geological Society of America, The Decade of North American Geology, p. 447-512.

Hoffman, P. F., 1991, On accretion of granite-greenstone terranes, Proceedings of Geological Association of Canada Annual Meeting, Mineral Deposits Division, St. John's, Newfoundland, p. 32-45.

Holdaway, M. J., 1971, Stability of andalusite and the aluminium silicate phase diagram: Am. J. Sci., v. 271, p. 97-131.

Hollister, L. S., Grissom, G. C., Peters, E. K., Stowell, H. H., and Sisson, V. B., 1987, Confirmation of the empirical correlation of Al in hornblende with pressure of solidification of calc-alkaline plutons: Am. Mineralogist, v. 72, p. 231-239.

Hoschek, G., 1969, The stability of staurolite and chloritoid and their significance in metamorphism of pelitic rocks: Contr. Mineral. and Petrol., v. 22, p. 208-232.

Hsu, L. C., 1968, Selected phase relationships in the system Al-Mn-Fe-Si-O-H: A model for garnet equilibria: J. of Petrology, v. 9, p. 40-83.

Huang, W. L., and Wyllie, P. J., 1973, Melting of muscovite-granite to 35 kbar as a model for fusion of metamorphosed subducted oceanic sediments: Contrib. Mineral. Petrol., v. 42, p. 1-14.

Hubard, M. S., 1989, Thermobarometric constraints on the thermal history of the Main Central Thrust Zone and Tibetan Slab, eastern Nepal Himalaya: Jour. Metamorphic Geol., v. 7, p. 19-30.

Hubert, C., Trudel, P., and Gelinas, L., 1984, Archean wrench fault tectonics and structural evolution of the Blake River Group, Abitibi Belt, Quebec: Can. J. Earth Sci., v. 21, p. 1024-1032.

Hubert, C., and Ludden, J. N., 1986, Archean wrench-fault tectonics in the Abitibi greenstone belt of Canada: *in* Workshop on tectonic evolution of greenstone belts, Edited by M. J. deWit and L. D. Ashwall, Lunar and Planetary Institute, Houston, LPI Technical Report No. 86-10, p. 121-123.

Hudleston, P. J., Schultz-Ela, D., and Southwick, D. L., 1988, Transpression in an Archean greenstone belt, northern Minnesota: Can. J. Earth Sci., v. 25, p. 1060-1068.

Hunter, R. D., 1974, Crustal development of the Kapvaal craton. I. The Archean: Precambrian Reasearch, v. 1, p. 259-294.

Imreh, L., 1973, Relations stratigraphique entre le Groupe de Pontiac et le sillon metavolcanique de Baby au Temiscamingue, Quebec: Can. J. Earth Sci., v. 10, p. 1350-1353.

Jackson, S. L., Sutcliffe, R. H., Ludden, J. N., Hubert, C., Green, A. G., Milkereit, B., Mayrand, L., West, G. F., and Verpaelst, P., 1990, Southern Abitibi greenstone belt: Archean crustal structure from seismic-reflection profiles: Geology, v. 18, p. 1086-1090.

Jackson, S. L., and Fyon, J. A., 1991, The Western Abitibi Subprovince in Ontario, in Thurston, P. C., Williams, H. R., Sutcliffe, R. H., and Stott, G. M., eds., Ontario Geological Survey special Volume 4, Part 1: Geology of Ontario, p. 405-482.

Jackson, S. L., Fyon, J. A., and Corfu, F., 1994, Review of Archean supracrustal assemblages of the southern Abitibi greenstone belt in Ontario, Canada: products of microplate interaction within a large-scale plate-tectonic setting: Precambrian Research, v. 65, p. 183-205.

Jackson, S. L., and Cruden, A. R., 1995, Formation of the Abitibi greenstone belt by arc-trench migration: Geology, v. 23, p. 471-474.

Jemielita, R. A., Davis, D. W., and Krogh, T. E., 1990, U-Pb evidence for Abitibi gold Mineralization: Nature, v. 346, p. 831-834.

Jolly, W. T., 1978, Metamorphic history of the Archean Abitibi belt, Metamorphism in the Canadian Shield, Geological Survey of Canada paper 78-10, P. 63-78.

Kalliokoski, J., 1987, The Pontiac problem, Quebec-Ontario, in light of gravity data: Can. J. Earth Sci., v. 24, p. 1916-1919.

Keating, P., 1992, Interpretation of the gravity anomaly field in the Noranda-Val d'Or region, Abitibi greenstone belt, Canadian Shield: Can. J. Earth Sci., v. 29, p. 962-971.

Kellett, R. L., Mareschal, M., and Kurtz, R. D., 1992, A model of lower crustal electrical anisotropy for the Pontiac Subprovince of the Canadian Shield: Geophysical Journal International, v. 111, p. 141-150.

Kerrich, R., and Feng, R., 1992, Archean geodynamics and the Abitibi-Pontiac collision: Implications for advection of fluids at transpressive collisional boundaries and the origin of giant quartz vein systems: Earth Sciences Reviews, v. 32, p. 33-60.

Kerrich, R., and Kyser, T. K., 1994, 100 Ma timing paradox of Archean gold, Abitibi greenstone belt, Canada: New evidence from U-Pb and Pb-Pb evaporation ages of hydrothermal zircons: Geology, v. 22, p. 1131-1134.

Kerrich, R., and Cassidy, K. F., 1994, Temporal relationships of lode gold mineralization to accretion, magmatism, metamorphism and deformation - Arhean to Present: A review: Ore Geology Reviews, v. 9, p. 263-310.

Kimura, G., Ludden, J. L., Desrochers, J.-P., and Hori, R., 1993, A model of ocean-crust accretion for the Superior Province, Canada: Lithos, v. 30, p. 337-355.

Kohn, M. J., and Spear, F. S., 1991, Error propagation for barometers: 1. Accuracy and precision of experimentally located end-member reactions: Am. Mineralogist, v. 76, p. 128-137.

Kohn, M. J., and Spear, F. S., 1991, Error propagation for barometers: 2. Applications to rocks: Am. Mineralogist, v. 76, p. 138-147.

Kohn, M. J., Spear, F. S., and Dalziel, I. W. D., 1993, Metamorphic P-T paths from Cordillera Darwin, a core complex in Tierra del Fuego, Chile: Jour. Petrology, v. 34, p. 519-542.

Kohn, M. J., Spear, F. S., Harrison, T. M., and Dalziel, I. W. D., 1995, $^{40}Ar/^{39}Ar$ geochronology and P-T-t paths from the Cordillera Darwin metamorphic complex, Tierra del Fuego, Chile: J. Metmorphic Geol., v. 13, p. 251-270.

Koziol, A. M., and Newton, R. C., 1988, Redetermination of the anorthite breakdown reaction and improvement of the plagioclase-garnet-Al2SiO5-quartz geobarometer: Am. Min., v. 73, p. 216-223.

Kretz, R., 1964, Analysis of equilibrium in garnet-biotite-sillimanite gneisses from Quebec: J. Petrology, v. 5, p. 1-20.

Kretz, R., 1983, Symbols for rock-forming minerals: Am. Mineral., v. 68, p. 277-279.

Kretz, R., 1994, Metamorphic crystallization: Toronto, John Wiley & Sons Ltd, 507 p.

Krogh, T. E., 1994, Precise U-Pb ages for Grenvillian and pre-Grenvillian thrusting of Proterozoic and Archean metamorphic assemblages in the Grenville Front tectonic zone, Canada: Tectonics, v. 13, p. 963-982.

Krogh, T. E., and Moser, D. E., 1994, U/Pb zircon and monazite ages from the Kapuskasing uplift: age constraints on deformation within the Ivanhoe Lake fault zone: Can. J. Earth Sci., v. 31, p. 1096-1103.

Kroner, A., 1981, Precambrian plate tectonics, *in* Kroner, A., ed., Precambrian plate tectonics: Amsterdam, The Netherlands, Elsevier, p. 57-90.

Kusky, T. M., 1993, Collapse of Archean orogens and the generation of late to postkinematic granitoids: Geology, v. 21, p. 925-928.

Laflèche, M. R., Dupuy, C., and Bougault, H., 1992, Geochemistry and petrogenesis of Archean mafic volcanic rocks of the southern Abitibi Belt, Québec: Precambrian Research, v. 57, p. 207-241.

Lajoie, J., and Ludden, J., 1984, Petrology of the Archean Pontiac and Kewagama sediments and implications for the stratigraphy of the southern Abitibi belt: Can. J. Earth Sci., v. 21, p. 1305-1314.

Legault, M., and Hattori, K., 1994, Late Archean geological development recorded in the Timiskaming Group sedimentary rocks, Kirkland Lake area, Abitibi greenstone belt, Canada: Precambrian Research, v. 68, p. 23-42.

Lewis, D. W., and McConchie, D. M., 1994, Analytical sedimentology: New York, Chapman & Hall, 197 p.

Lister, G. S., and Davis, G. A., 1989, The origin of metamorphic core complexes and detachment faults formed during Tertiary continental extension in the northern Colorado River region: J. Struc. Geol., v. 11, p. 65-94.

Lloyd, G. E., Law, R. D., Mainprice, D., and Wheeler, J., 1992, Microstructural and crystal fabric evolution during shear zone formation: J. Struc. Geol., v. 14, p. 1079-1100.

Ludden, J., Hubert, C., and Gariépy, C., 1986, The tectonic evolution of the Abitibi greenstone belt of Canada: Geological Magazine, v. 123, p. 153-166.

Ludden, J., and Hubert, C., 1986, Geologic evolution of the Late Archean Abitibi greenstone belt of Canada: Geology, v. 14, p. 707-711.

Machado, N., Gariépy, C., Philippe, S., and David, J., 1991a, Geochronologie U-Pb du territoire Quebecois: fosses du Labrador et du l'Ungava et Sous-province de Pontiac: Ministere de l'Energie et des Ressources du Quebec, Report No. MB 91-07.

Machado, N., Rive, M., Gariépy, C., and Simard, A., 1991b, U-Pb geochronology of granitoids from the Pontiac Subprovince: preleminary results, Proceedings of Geological Association of Canada Annual Meeting, Abstracts, p. A-78.

Malavieille, J., 1993, Late orogenic extension in mountain belts: insights from the Basin and Range and the Late Paleozoic Variscan Belt: Tectonics, v. 12, p. 1115-1130.

Mareschal, J. C., Pinet, C., Gariépy, C., Jaupart, C., Bienfait, G., Coletta, G. D., Jolivet, J., and Lapointe, R., 1989, New heat flow and radiogenic heat production data in the Canadian Shield and the Quebec Appalachians.: Can. J. Earth Sci., v. 26, p. 845-852.

Mäder, U. K., and Berman, R. G., 1992, Amphibole thermobarometry: a thermodynamic approach: *in* Current research, part E. Geological Survey of Canada, Paper 92-1E, p. 393-400.

McDougall, I., and Harrison, T. M., 1988, Geochronology and thermochronology by the $^{40}Ar/^{39}Ar$ method: Oxford, Oxford University Press, 272 p.

McMullin, D. W., Berman, R. G., and Greemwood, H. J., 1991, Calibration of the SGAM thermobarometer for pelitic rocks using data from phase-equilibrium experiments and natural assemblages: Can. Mineral., v. 29, p. 889-908.

Miller, W. G., 1913, The cobalt-nickel arsenides and silver deposits of Temiskaming (Cobalt and adjacent areas): Ontario Bureau of Mines, Annual Report, v. 19, part 2, 279p.

Morin, D., Jebrak, M., Bardoux, M., and Goulet, N., 1993, Pontiac metavolcanic rocks within the Cadillac tectonic zone, McWatters, Abitibi Belt, Quebec: Can. J. Earth Sci., v. 30, p. 1521-1531.

Morin, D., Jebrak, M., Beaufort, D., and Meunier, A., 1993, Metamorphic evolution of the Late Archean Cadillac tectonic zone, McWatters, Abitibi belt, Quebec: J. Metamorphic Geol., v. 11, p. 121-135.

Mortensen, J. K., and Card, K. D., 1993, U-Pb age constraints for the magmatic and tectonic evolution of the Pontiac Subprovince, Quebec: Can. J. Earth Sci., v. 30, p. 1970-1980.

Mortensen, J. K., 1993a, U-Pb geochronology of the eastern Abitibi Subprovince. Part 1: Chibougamau-Matagami-Joutel region: Can. J. Earth Sci., v. 30, p. 11-28.

Mortensen, J. K., 1993b, U-Pb geochronology of the eastern Abitibi Subprovince. Part 2: Noranda-Kirkland Lake area: Can. J. Earth Sci., v. 30, p. 29-41.

Moser, D. E., 1994, The geology and structure of the mid-crustal Wawa gneiss domain: a key to understanding tectonic variation with depth and time in the late Archean Abitibi-Wawa orogen: Can. J. Earth Sci., v. 31, p. 1064-1080.

Mueller, W., and Donaldson, J. A., 1992, Development of sedimentary basins in the Archean Abitibi belt, Canada: an overview: Can. J. Earth Sci., v. 29, p. 2249-2265.

Mustard, P. S., and Donaldson, J. A., 1987, Early-Proterozoic ice-proximal glaciomarine deposition: The lower Gowganda Formation at Cobalt, Ontario, Canada: Geol. Soc. Am. Bul., v. 98, p. 373-387.

Newton, R. C., Charlu, T. V., and Kleppa, O. J., 1980, Thermochemistry of high structural state plagioclases: Geochim. Cosmochim. Acta, v. 44, p. 933-941.

Newton, R. C., and Haselton, H. T., 1981, Thermodinamics of the garnet-plagioclase-Al_2SiO_5-quartz geobarometer: Adv. Phys. Geochem., v. 1, p. 131-147.

Nicolas, A., and Poirier, J. P., 1976, Crystalline plasticity and solid-state flow in metamorphic rocks: London, John Wiley & Sons.

Nisbet, E. G., and Walker, D., 1982, Komatiites and the structure of the Archean mantle: Earth Planet. Sci. Lett., v. 60, p. 105-113.

Nisbet, E. G., and Fowler, C. M. R., 1983, Model for Archean plate tectonics: Geology, v. 11, p. 376-379.

Oxburgh, E. R., and England, P. C., 1980, Heat flow and the metamorphic evolution of the Eastern Alps: Eclgae geol. Helv., v. 73, p. 379-398.

Parrish, R. R., 1990, Cooling rates from 700°-400°C in high grade rocks: applications of U-Pb geochronology, Proceedings of V. M. Goldschmidt Conference, Program and Abstracts, p. 72.

Peltzer, G., and Tapponier, P., 1988, Formation and evolution of strike-slip faults, rifts, and basins during the India-Asia collision: An experimental approach: J. of Geophys. Res., v. 93, p. 15085-15117.

Percival, J. A., and McGrath, P. H., 1986, Deep crustal structure and tectonic history of the northern Kapuskasing uplift of Ontario: an integrated petrological-geophysical study: Tectonics, v. 5, p. 553-572.

Percival, J., 1989, Archean tectonic settings in the Superior Province, Canada: A view from the bottom: *in* Granulites and crustal differentiation: Dordrecht, Kluver.

Percival, J. A., and Williams, H. R., 1989, The Late Archean Quetico accretionary complex, Superior Province, Canada: Geology, v. 17, p. 23-25.

Pettijohn, F. J., 1970, The Canadian Shield - A status report, *in* Symposium on basins and geosynclines of the Canadian Shield: Geol. Surv. Can. paper 70-40, p. 239-255.

Podolsky, T. M., 1950, Timiskaming-Pontiac relationship in Rouyn township, Quebec [M.Sc. thesis]: Queen's University, 97 p.

Poulsen, K. H., 1986, Rainy Lake wrench zone. In Workshop on the Tectonic evolution of greenstone belts: Lunar Planetary Institute, Report No. 86-10.

Powell, W. G., and Hodgson, C. J., 1992, Deformation of the Gowganda Formation, Matachewan area, Ontario, by post-Early Proterozoic reactivation of the Archean Larder

Lake - Cadillac break, with implications for gold exploration: Can. J. Earth Sci., v. 29, p. 1580-1589.

Powell, W. G., Charmichael, D. M., and Hodgson, C. J., 1993, Thermobarometry in a subgreenschist to greenschist transition in metabasites of the Abitibi greenstone belt, Superior Province, Canada: Jour. of Metamorphic Geology, v. 11, p. 165-178.

Powell, W. G., Carmichael, D. M., and Hodgson, C. J., 1995, Conditions and timing of metamorphism in the southern Abitibi greenstone belt, Quebec: Can. J. Earth Sci., v. 32, p. 787-805.

Powell, W. G., Hodgson, C. J., Hanes, J. A., Carmichael, D. M., McBride, S., and Farrar, E., 1995, $^{40}Ar/^{39}Ar$ geochronological evidence for multiple postmetamorphic hyrothermal events focused along faults in the southern Abitibi greenstone belt: Can. J. Earth Sci., v. 32, p. 768-786.

Pringle, C. J., 1989, A Fortran computer program to produce correcrted micoprobe analyses of minerals using an energy-dispersive X-ray spectrometer: Geological Survey of Canada, Report No. 2127.

Purdy, J. W., and Jager, E., 1976, K-Ar ages on rock-forming minerals from the Central Alps: Memoirs, Institute of Geology and Mineralogy, University of Padova, v. 30, p. 1-31.

Richardson, S. W., 1968, Staurolite stability in part of the system Fe-Al-Si-O-H: J. Petrology, v. 9, p. 467-488.

Rive, M., Melancon, M., and Savard, R., 1989, Carte de compilation geologique district de Rouyn-Noranda et de Ville Marie: Not Published, scale 1:125,000.

Rive, M., Pintson, H., and Ludden, J. N., 1990, Characteristics of late Archean plutonic rocks from the Abitibi and Pontiac Subprovinces, Superior province, Canada: *in* The northwestern Quebec polymetallic belt: a summary of 60 years of mining exploration, Canadian Institute of Mining Special Volume, p. 65-91.

Robert, F., 1989, Internal structure of the Cadillac tectonic zone southeast of Val d'Or, Abitibi greenstone belt, Quebec: Can. J. Earth sci., v. 26, p. 2661-2675.

Robertson, J. A., Card, K. D., and Frarey, M. J., 1969, The Federal-provincial Committe on Huronian Stratigraphy Progress Report: Ontario Department of Mines, Miscellaneous Paper, v. 31, 26p.

Robie, R. A., and Hemingway, B. S., 1984, Entropies of kyanite, andalusite, and sillimanite: additional constraints on the pressure and temperature of the Al2SiO5 triple point: Am. Miner., v. 69, p. 298-306.

Rocheleau, M., and Dimroth, E., 1985, Petrology of the Archean Pontiac and Kewagama sediments and implications for the southern Abitibi belt. Discussion: Can. J. Earth Sci., v. 22, p. 1374-1379.

Roddick, J. C., 1983, High-precision intercalibration of $^{40}Ar/^{39}Ar$ standards: Geochim. Cosmochim. Acta, v. 47, p. 887-898.

Sawyer, E. W., and Benn, K., 1993, Structure of the high-grade Opatica belt and the adjacent low-grade Abitibi Subprovince: An Archean mountain front: Jour. of Structural Geology, v. 15, p. 1443-1458.

Sawyer, E. D., and Barnes, S.-J., 1994, Thrusting, magmatic intraplating, and metamorphic core complex development in the Archean Belleterre-Angliers Greenstone Belt, Superior Province, Quebec, Canada: Precambrian Research, v. 68, p. 183-200.

Selverstone, J., Spear, F. S., Franz, G., and Morteani, G., 1984, High pressure metamorphism in the SW Tauern widow, Austria: P-T paths from hornblende-kyanite-staurolite schists: Jour. Petrology, v. 25, p. 501-531.

Selverstone, J., and Spear, F. S., 1985, Metamorphic P-T paths from pelitic schists and greenstones in the southwest Tauern window, Eastern Alps: Jour. Metamorphic Geol., v. 3, p. 439-465.

Sims, P. K., Card, K. D., Morey, G. B., and Peterman, Z. E., 1980, The Great Lakes tectonic zone - a major crustal structure in central north America: Geol. Soc. Am. Bul., v. 91, p. 690-698.

Sleep, N. H., 1979, Thermal history and degassing of the Earth: Some simple calculations: J. Geol., v. 87, p. 671-686.

Smith, J. P., Spooner, E. T. C., Broughton, D. W., and Ploeger, F. R., 1990, The Kerr Addison-Chesterville Archean gold-quartz vein system, Virginiatown: Time sequence and associated mafic "albitite" dyke swarm: Ontario Geological survey miscellaneous paper, v. 150, p. 175-199.

Spear, F. S., and Cheney, J. T., 1989, A petrogenetic grid for pelitic schists in the system SiO_2-Al_2O_3-FeO-MgO-K_2O-H_2O: Contrib. Mineral Petrol., v. 101, p. 149-164.

Spear, F. S., Kohn, M. J., Florence, F. P., and Menard, T., 1991, A model for garnet and plagioclase growth in pelitic schists: implications for thermobarometry and P-T path determinations: J. metamorphic Geol., v. 8, p. 683-696.

Spear, F. S., 1993, Metamorphic phase equilibria and pressure-temperature-time paths: Washington, Mineralogical Society of America Monograph, 799 p.

Steiger, R. H., and Wasserburg, G. J., 1969, Comparative U-Th-Pb systematics in 2.7 Ga plutons of different geological histories: Geochimica et Cosmochimica Acta, v. 33, p. 1213-1232.

Steiger, R. H., and Jäger, E., 1977, Subcommission on Geochronology: convention on the use of decay constants in geo- and cosmo-chronology: Earth and Planetary Sci. Letters, v. 36, p. 359-362.

Stesky, R. M., 1995, Spheristat, A software for analysis of structural data: Version 2.0 for Windows .

Taylor, S. R., and McLennan, S. M., 1981, The composition and evolution of the continental crust: rare earth element evidence from sedimentary rocks: Phil. Trans. Roy. Soc. Lon. series A, v. 301, p. 381-399.

Taylor, B., 1995, Backarc basins: Tectonics and magmatism: New York, Plenum Press, 524 p.

Thompson, A. B., 1976, Mineral reactions in pelitic rocks: I. Prediction of P-T-X (Fe-Mg) phase relations: Am. J. Sci., v. 276, p. 401-424.

Thompson, A. B., 1976, Mineral reactions in pelitic rocks: II. Calculation of some P-T-X (Fe-Mg) phase relations: Am. J. Sci., v. 276, p. 425-454.

Turcotte, D. L., and Schubert, G., 1982, Geodynamics applications of continuum physics to geological problems: New York, John Wiley & Sons, Inc., 450 p.

Ujike, O., 1984, Chemical composition of Archean Pontiac metasediments, southwestern Abitibi Belt, Superior province: Can. J. Earth Sci., v. 21, p. 727-731.

Ujike, O., and Goodwin, A. M., 1987, Geochemistry and origin of Archean felsic metavolcanic rocks, central Noranda area, Quebec, Canada: Can. J. Earth Sci., v. 24, p. 2551-2567.

Walle, M. v. d., 1978, Canton de Montbeillard: Ministere de l'Energie et de Ressources du Quebec, Report No. 188.

Williams, P. R., Pigram, C. J., and Dow, D. B., 1984, Melange production and importance of shale diapirism in accretionary terrains: Nature, v. 309, p. 145-146.

Williams, H. R., 1987, Structural studies in the Wabigoon and Quetico Subprovinces: Ontario Geological Survey, Report No. 5668.

Williams, H. R., 1990, Subprovince accretion tectonics in the south-central Superior Province: Can. J. Earth Sci., v. 27, p. 570-581.

Wilson, M. E., 1909, Larder Lake and eastward: Geological Survey of Canada Report .

Wilson, M. E., 1912, Geology and economic resources of the Larder Lake district, Ont. and adjoining portions of Pontiac county, Que.: Geological Survey of Canada, Memoire No. 17-E.

Wilson, M. E., 1962, Rouyn-Beauchastel map area: Geological Survey of Canada, Memoire No. 315.

Windley, B. F., and Smith, J. V., 1976, Archean High-grade complexes and modern continental margins: Nature, v. 260, p. 671-675.

Windley, B. F., 19?1, Precambrian rocks in the light of the plate tectonic concept, in Kroner, A., ed., Precambrian plate tectonics: Amsterdam, The Netherlands, Elsevier, p. 1-20.

Wood, J., 1980, Epiclastic sedimentation and stratigraphy in the North Spirit Lake and Rainy Lake areas: a comparison: Precambrian Res., v. 12, p. 227-255.

Wyman, D. A., and Kerrich, R., 1987, Archean lamprophyres I: Distribution and tectonic setting [abs], Proceedings of Geological Association of Canada Annual Metting, Program with Absracts, p. 102.

Yardley, B. W. D., 1977, An empirical study of diffusion in garnet: Am. Mineralogist, v. 62, p. 793-800.

Yardley, B. W. D., 1989, An introduction to metamorphic petrology: London, Longman.

Young, G. M., 1983, Tectono-sedimentary history of early Proterozoic rocks of the northern Great Lakes region, *in* Medaris, L. G., ed., Early Proterozoic geology of the Great Lakes region. Geological Society of America Memoir, p. 15-32.

Yuanming, P., and Fleet, M. E., 1994, Granulite-facies metamorphism in the Quetico Subprovince, north of Manitouwadge, Ontario: Can. J. Earth Sci., v. 31, p. 1427-1439.

Zolani, A. I., Price, R. A., and Helmstaedt, H., 1984, Regional cross section of the Southern Province adjacent to Lake Huron, Ontario: implications for the tectonic significance of the Murray Fault Zone: Can. J. Earth. Sci., v. 21, p. 447-456.

Appendices

Appendix A. A Matlab[TM] program for transformations of *c*-axis fabric data between two orthogonal thin-sections

```
%************************** Transect.m ******************************
% This file may be used for transforming all c-axis data in different
% thin-sections into a single thin-section with X pointing North,
% Y corresponding to the arrow on the thin-section pointing East, and
% Z pointing to the microscope and lower hemisphere (these are
% stereonet orientations and not necessarily geographic orientations).
%*********************************************************************
% First select a thin-section and define its coordinates as reference
% frame. This thin-section may be a conceptual profile in the Sample.
%*********************************************************************
% Before running this file do following steps in the command window:
% 1) type load #####.dat  (your raw data file name)
% 2) attribute the name "inputfile" to your data file by typing:
%     inputdat=##### in the command window.
%3) enter angles x'ox, x'oy, x'oz, y'ox, ... in degrees as a 3X3
%     matrix (A=[1,2,3;4,5,6;7,8,9]).
% After the end of running type "save filename.dat outputdat -ASCII"
% in the command window to save the transformed data.
%*********************************************************************
% Data files are in terms of Phi and Ro, which should be finally
% converted to azimuth (az) and plunge (pl) in the above-defined
% reference frame.
%************************ Dircos conversions ***********************
torad=pi/180;
todeg=180/pi;
a=A(1,1);
b=A(1,2);
c=A(1,3);
d=A(2,1);
e=A(2,2);
f=A(2,3);
g=A(3,1);
h=A(3,2);
i=A(3,3);
L1=cos(a.*torad);
M1=cos(b.*torad);
N1=cos(c.*torad);
L2=cos(d.*torad);
```

```
M2=cos(e.*torad);
N2=cos(f.*torad);
L3=cos(g.*torad);
M3=cos(h.*torad);
N3=cos(i.*torad);
%**************** Universal stage coordinates to polar coordinates *****
m=1;
phi=inputdat(m,1);
ro=inputdat(m,2);
while  phi>-99
phi=inputdat(m,1);
ro=inputdat(m,2);
if ro>0
      az=180-phi;
end
if ro<=0
      az=360-phi;
end
teta=abs(ro);
radteta=teta.*torad;
radaz=az.*torad;
%****************** Polar coordinates to Cartesian coordinates *********
x=sin(radteta).*cos(radaz);
y=sin(radteta).*sin(radaz);
z=cos(radteta);
%******************* Transformation into the reference frame ***********
X=L1.*x+M1.*y+N1.*z;
Y=L2.*x+M2.*y+N2.*z;
Z=L3.*x+M3.*y+N3.*z;
%*************************** Quadrant determination *******************
if X>0
      if Y>0
            q=1;
      end
      if Y<0
            q=4;
      end
      if Y==0
            q=41;
      end
end
if X<0
      if Y>0
```

```
            q=2;
        end
        if Y<0
            q=3;
        end
        if Y==0
            q=23;
        end
end
if X==0
        if Y>0
            q=12;
        end
        if Y<0
            q=34;
        end
        if Y==0
            q=0;
        end
end
%****************** Cartesian coordinates to polar coordinates *********
pphi=atan(Y/X);
pteta=acos(Z);
%****************** Polar coordinates to stereonet coordinates *********
azi=pphi.*todeg;
pl=((pi/2)-pteta).*todeg;
if q==1
        azim=azi;
end
if q==2
        azim=180-abs(azi);
end
if q==3
        azim=180+abs(azi);
end
if q==4
        azim=360-abs(azi);
end
if q==41
        azim=0;
end
if q==12
        azim=90;
```

```
end
if q==23
      azim=180;
end
if q==34
      azim=270;
end
if q==0
      azim=0;
end
m=m+1;
outputdat(m,1)=azim;
outputdat(m,2)=pl;
clear X;
clear Y;
clear x;
clear y;
clear q;
end
m
%*************************************************************************
outputdat(m,1)=-99;
outputdat(m,2)=0;
```

Appendix B. Calculated and expected values of Fe_2O_3 for standards used along with the natural samples in wet chemical analyses of biotite crystals from the study area

Standard sample ID	calculated Fe_2O_3 (%)	expected Fe_2O_3 (%)
mrg-1	20.86	17.93
sy-2	6.15	6.31
sy-2	5.92	6.31
Mica-Fe	25.52	25.65
Mica-FeC	26.01	25.65

Appendix C. XRF analysis of a Komatiitic sample from the study area

(Mark Shore, personal communications)

Oxide	Concentration
SiO_2	42.25 %
TiO_2	0.291 %
Al_2O_3	6.4 %
Fe_2O_3	10.44 %
MnO	0.155 %
MgO	27.31 %
CaO	5.45 %
Na_2O	0.247 %
K_2O	0.012 %
P_2O_5	0.0028 %
V	117 ppm
Cr	2240 ppm
Co	111 ppm
Ni	1592 ppm
Zn	69 ppm
Rb	0.6 ppm
Sr	49.7 ppm
Y	3.6 ppm
Zr	14 ppm
Ba	23 ppm
LOI	7.9 %
Total	101 %

LOI: loss of ignition

Appendix D. Crustal structure and kinematic framework of the northwestern Pontiac Subprovince, Québec: an integrated structural and geophysical study (publication in Canadian Journal of Earth Sciences)

The followings are contributions of the present author to this publication:

- Interpretations on microstructures and their relationships to metamorphism
- Interpreted pattern of metamorphic isograds within the study area (Fig. 2)
- Structural profile of the study area (Fig. 3)

Appendix E. Electron microprobe analyses of minerals in metasedimentary rocks of the northwestern Pontiac Subprovince.

Biotite

Sample No:	BT3	BT48	BT14	BT39	BT44	BT25
SiO_2	35.94	35.48	35.25	34.98	36.84	36.56
Al_2O_3	20.27	19.95	19.96	19.98	20.83	20.35
TiO_2	1.34	1.65	1.58	1.35	1.44	1.62
Cr_2O_3	0.08	0.02	0.11	0.00	0.04	0.12
FeO	18.27	17.80	18.90	17.62	16.48	17.16
MnO	0.12	0.14	0.20	0.00	0.04	0.09
MgO	10.53	11.03	11.18	11.39	12.11	10.83
CaO	0.10	0.08	0.00	0.10	0.14	0.05
K_2O	9.43	8.94	8.61	9.09	8.90	9.36
Na_2O	004	0.00	0.00	0.87	0.09	0.00
Cl	0.00	0.00	0.00	0.00	0.00	0.00
Total	96.21	95.09	95.79	95.38	96.91	96.14
Formula (basis 22 atoms of oxygen)						
Si	5.372	5.347	5.296	5.349	5.386	5.424
[4]Al	2.628	2.653	2.704	2.651	2.614	2.576
[6]Al	0.943	0.890	0.832	0.864	0.975	0.983
Ti	0.161	0.187	0.178	0.138	0.158	0.181
Cr	0.009	0.003	0.013	0.000	0.005	0.014
Fe	2.283	2.243	2.375	2.220	2.015	2.129
Mn	0.015	0.018	0.026	0.002	0.005	0.011
Mg	2.345	2.479	2.503	2.597	2.638	2.396
Ca	0.017	0.012	0.000	0.000	0.022	0.008
K	1.798	1.719	1.651	1.742	1.660	1.771
Na	0.012	0.000	0.000	0.127	0.025	0.000
Cl	0.000	0.000	0.000	0.000	0.000	0.000

Muscovite

Sample No:	MS41
SiO_2	46.18
Al_2O_3	37.05
TiO_2	0.42
Cr_2O_3	0.11
FeO	0.97
MnO	0.04
MgO	0.25
CaO	0.13
K_2O	9.04
BaO	0.12
Na_2O	1.35
Cl	0.00
Total	95.66
Formula (basis 22 atoms of oxygen)	
Si	6.079
[4]Al	1.921
[6]Al	3.828
Ti	0.042
Cr	0.012
Fe	0.107
Mn	0.004
Mg	0.049
Ca	0.019
K	1.519
Ba	0.006
Na	0.346
Cl	0.000

Fe denotes total iron as Fe^{2+}

Appendix E. Continued.

Garnet

Sample No:	GT48	GT39	GT25
SiO_2	37.52	36.37	37.64
Al_2O_3	21.06	20.66	21.40
TiO_2	0.05	0.00	0.03
FeO	30.27	26.83	29.24
MnO	7.38	14.69	8.27
MgO	2.79	1.00	2.89
CaO	1.98	0.64	1.83
Total	101.05	100.46	101.30
Formula (basis 24 atoms of oxygen)			
Si	5.996	5.956	5.987
$^{[4]}Al$	0.004	0.044	0.013
$^{[6]}Al$	3.962	3.943	3.999
Ti	0.006	0.000	0.003
Fe	4.045	3.674	3.889
Mn	0.999	2.075	1.115
Mg	0.664	0.244	0.686
Ca	0.339	0.112	0.312

Staurolite

Sample No:	ST39
SiO_2	27.81
Al_2O_3	54.09
TiO_2	0.54
FeO	12.29
MnO	0.16
MgO	2.02
ZnO	0.62
Total	97.53
Formula (basis 46 atoms of oxygen)	
Si	7.708
Al	17.673
Ti	0.112
Fe	2.850
Mn	0.038
Mg	0.836
Zn	0.128

Plagioclase

Sample No:	PL48	PL14	PL39	PL44	PL25
SiO_2	61.79	62.59	65.91	59.72	60.35
Al_2O_3	24.08	24.19	20.59	24.78	24.11
K_2O	0.11	0.06	0.09	0.03	0.15
CaO	5.67	5.04	1.32	6.96	5.90
Na_2O	8.26	8.58	11.22	7.54	8.14
FeO	0.16	0.13	0.17	0.15	0.13
Total	100.07	100.59	99.30	99.18	98.78
Formula (basis 20 atoms of oxygen)					
Si	5.479	5.508	5.835	5.363	5.433
Al	2.517	2.510	2.149	2.623	2.558
K	0.013	0.007	0.010	0.004	0.017
Ca	0.539	0.475	0.126	0.670	0.569
Na	1.419	1.464	1.926	1.312	1.421
Fe	0.005	0.009	0.013	0.011	0.010

Fe denotes total iron as Fe^{2+}

Appendix F. Electron Microprobe analysis of a garnet vein found within a syenitic intrusion close to the Cadillac-Larder Lake fault zone

Oxide	Percent
SiO_2	36.74
Al_2O_3	7.14
TiO_2	0.00
Cr_2O_3	0.00
Fe_2O_3	21.90
MgO	0.00
MnO	0.00
CaO	33.86
Total	99.64

Formula (basis 24 atoms of oxygen)	
Si	5.994
$^{[4]}Al$	0.006
$^{[6]}Al$	1.367
Ti	0.000
Cr	0.000
Fe^{+3}	2.689
Mg	0.000
Mn	0.000
Ca	5.920

Appendix G. Explanations proposed for observed discrepancy between paleo-pressure estimations of TWEEQU and conventional methods

Followings are explanations proposed for the discrepancy between paleo-pressure estimations of TWEEQU and conventional methods discussed in section 4.5.3.

Thermodynamic basis of the two barometers [equations (b) and (e)] are the same. The only difference between the two equations appears to be dependence of the conventional method on P° that represents the experimentally determined (Koziol and Newton 1988) equations [(f) and (g)] for boundary curves corresponding to anorthite breakdown reaction. In other words equations (f) and (g) are experimental approach to Clapeyron equation. The Clapeyron equation may be expressed as:

$$P=\left(\frac{\Delta S}{\Delta V}\right)T-\left(\frac{\Delta H}{\Delta V}\right)$$

where P is pressure in bars, T is temperature in kelvin, and ΔS, ΔH, and ΔV are entropy, enthalpy, and volume change of the reaction.

Equations (f) and (g) represent linear relationships between P and T, however it is known that S, H and V are, in turn, dependent on temperature and pressure; this implies that linear equations for the boundary curves are different at different pressures and temperatures. In order to assess the magnitude of this difference, ΔS, ΔH, and ΔV for anorthite breakdown reaction (involving kyanite as the aluminum-silicate mineral) were calculated (see Tables). It may be deduced from the results that values for both ΔS/ΔV and ΔH/ΔV increase towards higher pressure and higher temperature conditions.

Experiments, through which equations for the anorthite breakdown reactions were determined (Koziol and Newton 1988), were carried out at pressures between 18 and 28 kbar, and temperatures between 900°C and 1300°C. These conditions are much higher than those at which natural samples are metamorphosed. It is concluded that using experimentally detrmined high P° values in conventional barometry resulted in pressure estimates that are probably higher than pressures the samples have undergone. Moreover, there are some difference between activity models used in TWEEQU and conventional methods, that are possibly responsible for part of the discrepancies.

Tables

†P	†T	*ΔV
6650	298.15	-6.470
8920	400	-6.411
11150	500	-6.354
13380	600	-6.298
15610	700	-6.244
17840	800	-6.190
20070	900	-6.138
22300	1000	-6.086
24530	1100	-6.036
26760	1200	-5.987

T	‡ΔS
298.15	-133.42
400	-136.36
500	-136.12
600	-134.84
700	-133.49
800	-132.40
900	-131.72
1000	-132.27
1100	-133.03
1200	-133.82

T	‡ΔH
298.15	-50000
400	-50990
500	-50863
600	-50152
700	-49270
800	-48459
900	-47880
1000	-48407
1100	-49223
1200	-50135

P	T	ΔS /ΔV	ΔH /ΔV
6650	298.15	20.62	7728
8920	400	21.27	7954
11150	500	21.42	8005
13380	600	21.41	7963
15610	700	21.38	7891
17840	800	21.39	7828
20070	900	21.46	7801
22300	1000	21.73	7953
24530	1100	22.04	8155
26760	1200	22.35	8374

† Pressure and temperature ranges are chosen to be close to those at which experiments of Koziol and Newton (1988) were carried out

* Obtained by use of the thermodynamic database of Berman (1988) in the equation

$$V_{T,P} = V_{298,1}[1 + v_1(P-1) + v_2(P-1)^2 + v_3(T-298) + v_4(T-298)^2] \quad \text{(units: bars, K)}$$

‡ Calculated by use of the thermodynamic database of Robie *et al.* (1979)

Appendix H. Mathematical analysis of simple and superimposed symmetric and asymmetric fold series in two and three dimensions

Preliminary stages of the present study in the northwestern Pontiac Subprovince indicated that structure of the area is dominated by folds that were produced by different deformational events. The following appendix represents a method to produce fold interference patterns resulting from superposition of different fold sets. Interference patterns produced through this method were compared with regional map-scale structures of the study area to detect potential presence of complex fold interference patterns.

Mathematical analysis of simple and superimposed symmetric and asymmetric fold series in two and three dimensions

Abstract

The Fourier analysis approach to modeling fold series is first modified to produce simple symmetric and asymmetric fold series and then used to model and analyze folded surfaces produced by superposition of these fold series in two and three dimensions. Wavelength, amplitude, axial plane orientations, and relative sizes of the superimposed folds may be defined and changed through the modeling process. A combination of fold series with different geometrical patterns and orientations has been used to define a general classification for the interference patterns due to superimposed folding.

INTRODUCTION

The diversity in the geometries and scales of the folds in rocks, and the complexity of superimposed folded structures, have made the geometrical analysis of folded rocks a subject of prime interest to structural geologists. Interference patterns of superimposed folds are of particular interest since they are encountered in the internal zones of many orogenic belts of widely varying ages and tectonic settings. During the deformational histories of these belts, changes in metamorphic conditions associated with the burial and exhumation of the rocks may affect wavelengths and amplitudes of different generations of folds. Furthermore, multiple changes in orientation of the stress field and in strain rates, which are common in orogenic belts, can lead to the superposition of fold series with different characteristics, including different orientations, resulting in complex interference patterns.

Methods for the analysis of folds and their interference patterns may be grouped into three different categories: material modeling methods, statistical methods, and pure mathematical methods. Card decks and plastic material models are two well-known methods of the first category. Card decks have been used for modeling of folds and their interference patterns both in two (Carey 1962) and three dimensions (O'Driscoll 1962). Reynolds and Holms (1954), Skjernaa (1975), and Watkinson (1981) have used plastic material for the study of the superimposed folding. The work of Thiessen (1986) highlighted the efficiency of computer modeling in generating superimposed folds, and in analyzing the resulting wide variety of possible two-dimensional interference patterns. Statistical methods (Ramsay 1958, Weiss 1959) involve the projection of structural elements on the sphere, and while this is a good tool for the geometrical analysis of a folded terrane, it does not imply any aspect of scale, nor does it illustrate fold interference patterns. Mathematical analysis of the folds, when established, seems to be a convenient and universal method for elucidation of these structures.

The resemblance of fold profiles to sine waves has tempted structural geologists towards formulation of these structures as harmonic series known as Fourier analysis (Harbaugh & Preston 1965, Stabler 1968, Hudleston 1973). In this technique series of trigonometric functions are employed to express the shape of the fold profiles. The complexity arising from the general asymmetry of folds about their hinges and inflexions has lead to the selection of a small part of the complete fold series, a quarter wavelength, for this kind of approach. Field study of the folded terranes however involves analysis of the complete fold series in three dimensions. Though complete fold series defined by trigonometric functions may not be encountered in nature, this mathematical approach seems to be a good tool for regional analysis of folded terranes and interference patterns. It will be later noticed that modeling of the folds as complete series, despite its simplification, has its own complexities e.g. mathematical expression of asymmetric folds is easier when they are divided into quarter wavelength rather than when they are considered as a complete series.

In this paper some modifications to the Fourier series approach are proposed which allow the generation and analysis of symmetrical and asymmetrical folded surfaces, in two and three dimensions, and the generation and analysis of superimposed folded surfaces in three dimensions. A general classification of superimposed interference patterns, part of which not included in earlier classifications, is then suggested.

The mathematics are quite straightforward, and programming and production of graphical images can be done most efficiently by using a mathematics-graphics package such as MATLAB™ on a personal computer. Throughout the text the term 'simple' is used for folds which do not involve superposition by later folds.

TWO-DIMENSIONAL ANALYSIS OF SIMPLE SYMMETRIC AND ASYMMETRIC FOLD FORMS

The shapes of symmetric folds in two dimensions may be expressed using reduced form of the Fourier series (Stabler 1968, Ramsay & Huber 1983).

$$y = a_1 \sin x + a_3 \sin 3x + a_5 \sin 5x \qquad (1)$$

Selecting a quarter wavelength of a natural fold profile and dividing it into three equal parts, for which the values of y may be measured, makes it possible to calculate values for a_1, a_3 and a_5, and hence arrive at a mathematical description of a segment of a naturally occurring fold profile (Stabler 1968, Ramsay & Huber 1983). Modeling naturally occurring simple folds, on the other hand, would therefore require specific values for these variables, otherwise resulting forms would be either similar to polyharmonic folds or unrealistic curves. However, in many cases structural geologists are interested in prediction of the fold forms and their interference patterns rather than in their description. Hudleston (1973) reduced the harmonic components of the equation (1) into two, and by giving different values to a_1 and a_3 was able to define different shapes for fold forms. Asymmetric folds can be analyzed in this sector-wise method as well as symmetric folds. As mentioned above, this type of expression of the Fourier series is used for detailed description of a quarter wavelength from a complete fold series. Since complete fold series are the concern in this paper, and in order to avoid further complexities, the harmonic components are reduced into one,

$$y = a \sin bx \qquad (2)$$

where parameter 'a' is the amplitude, and 2π divided by 'b' equals the wavelength of the fold series. Because of the nature of the mathematical approach, the resulting folds are of shear fold character. Simplification is employed to avoid complexity, and in order to achieve an easily workable method of generating complicated fold forms and interference patterns. Comparison of the results with natural folding, to be discussed below, indicates that such simplification is justified. Symmetric sine wave series with different amplitudes and wavelengths may be defined in this way, however definition of asymmetric series would not be practicable. The mathematical expression of such series, which are frequently encountered in nature, involves attribution of more than one value of y to x. This would violate definition of y as a simple function of x, and not allow the series to be expressed in a simple equation.

A solution is proposed here for graphic projection of asymmetric fold series. This involves shearing of the simple sine waves at any desired angle (see Fig. 1a). After defining y as a sine function of the variable x, x' and y' are defined as functions of both x and y by applying the linear transformations below. The x is changed by the amount of '$y \tan\theta$'.

$$x' = x + y\tan\theta \tag{3}$$

$$y' = y \tag{4}$$

where θ denotes the angular shear or the complementary angle to the dip angle of the axial plane of the fold series. A plot of the x' against y' is then a representation of an asymmetric fold series (Fig. 1b). Amplitude, wavelength, and asymmetry of the series may be defined by giving different values to a and b in equation (2), and to θ in equation (3). It is important to note that no particular strain path is implied here; the superposition of a simple shear deformation on the symmetrical fold series is done in order to produce a particular fold geometry, which could of course be produced by any number of deformational histories. However, later in the sections on the analysis of superposition, it will be noticed that interference patterns resulting from superposition of a symmetric fold series on an asymmetric folds series are different from patterns produced by superposition of an asymmetric fold series on a symmetric folds series.

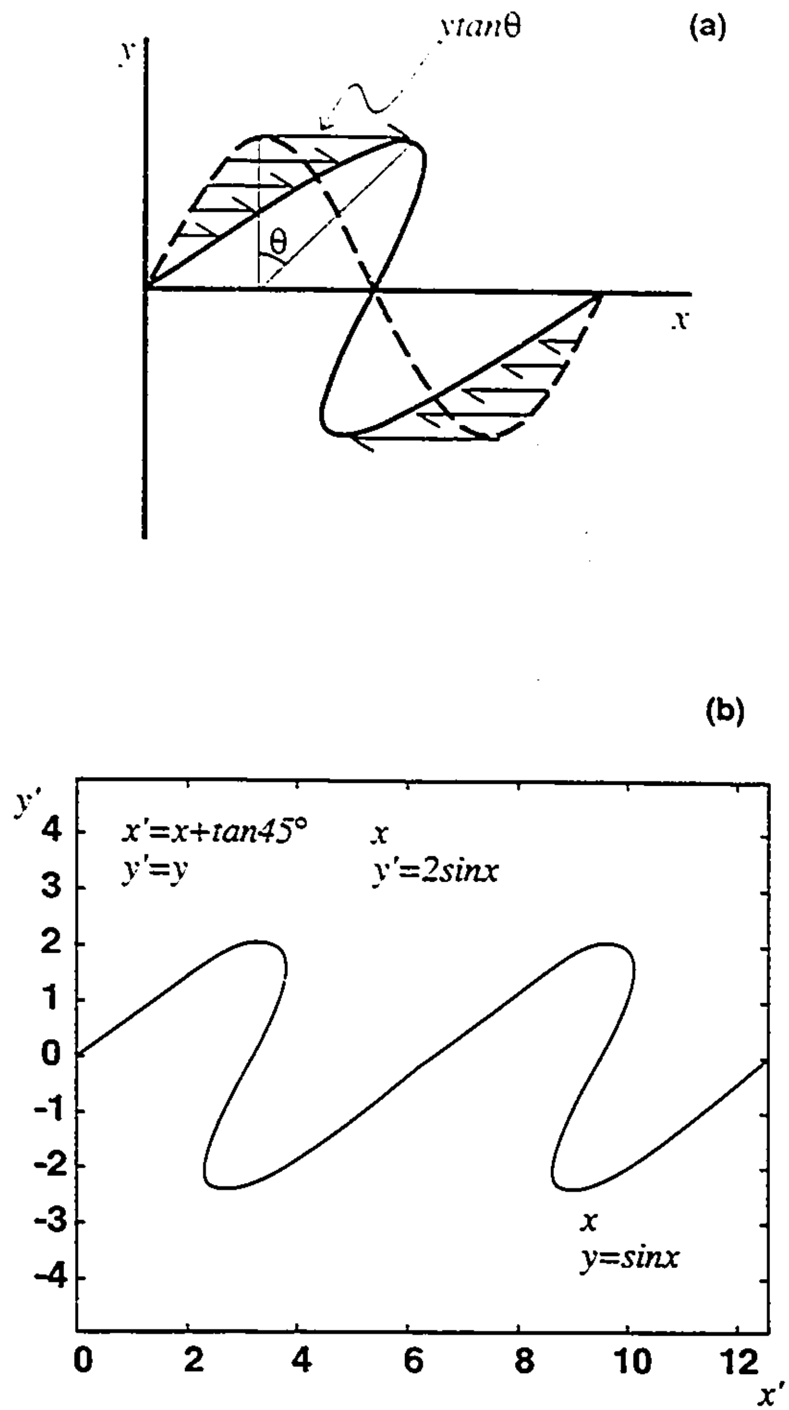

Fig. 1. (a) The symmetric fold series may be sheared to produce an asymmetric fold series; θ denotes the angular shear or the complementary angle to the dip of the axial plane of the fold series. (b) An asymmetric fold series defined through a 45° angular shear of a symmetric fold series.

TWO-DIMENSIONAL ANALYSIS OF SUPERIMPOSED SYMMETRIC AND ASYMMETRIC FOLD FORMS

Symmetric and asymmetric forms of the fold series in two dimensions can be subjected to repeated folding of parallel fold axis orientation. Symmetric folds of different amplitude and/or wavelengths can be superimposed by adding the related terms of equation (2),

$$y = a_1 \sin b_1 x + a_2 \sin b_2 x + \ldots + a_n \sin b_n x \qquad (5)$$

where parameters a_1, a_2, a_n and b_1, b_2, b_n respectively denote amplitudes and wavelengths of the different superimposed fold series. Equation (5) in many respects is similar to a Fourier series for the fold forms (see equation (1)), the difference is in the values which are given to a_1, a_2, a_n and b_1, b_2, b_n. Figure 2a shows three different fold series of different wavelengths and amplitudes which are superimposed on each other, and would represent a polyharmonic fold with three different fold orders. Adding a term of type '$y \tan\theta$' to x results in a form that illustrates shearing of the latest fold series (along with all older series) into asymmetric series, in other words superposition of an asymmetric transformation on symmetric fold series (Fig. 2b).

To produce an asymmetric series superimposed by a symmetric one (Fig. 2c), the term '$a' \sin b'x$' related to the symmetric fold series may be added to the y' defined through equations (4),

$$x'' = x' \qquad (6)$$

$$y'' = y' + a' \sin b'x' \qquad (7)$$

This expression in turn can be sheared using equations similar to equations (3) and (4) to produce an asymmetric transformation superimposed on another asymmetric one (see Fig. 2d),

$$x''' = x'' + y'' \tan\theta' \qquad (8)$$

$$y''' = y'' \qquad (9)$$

where θ' is the angular shear of the second transformation.

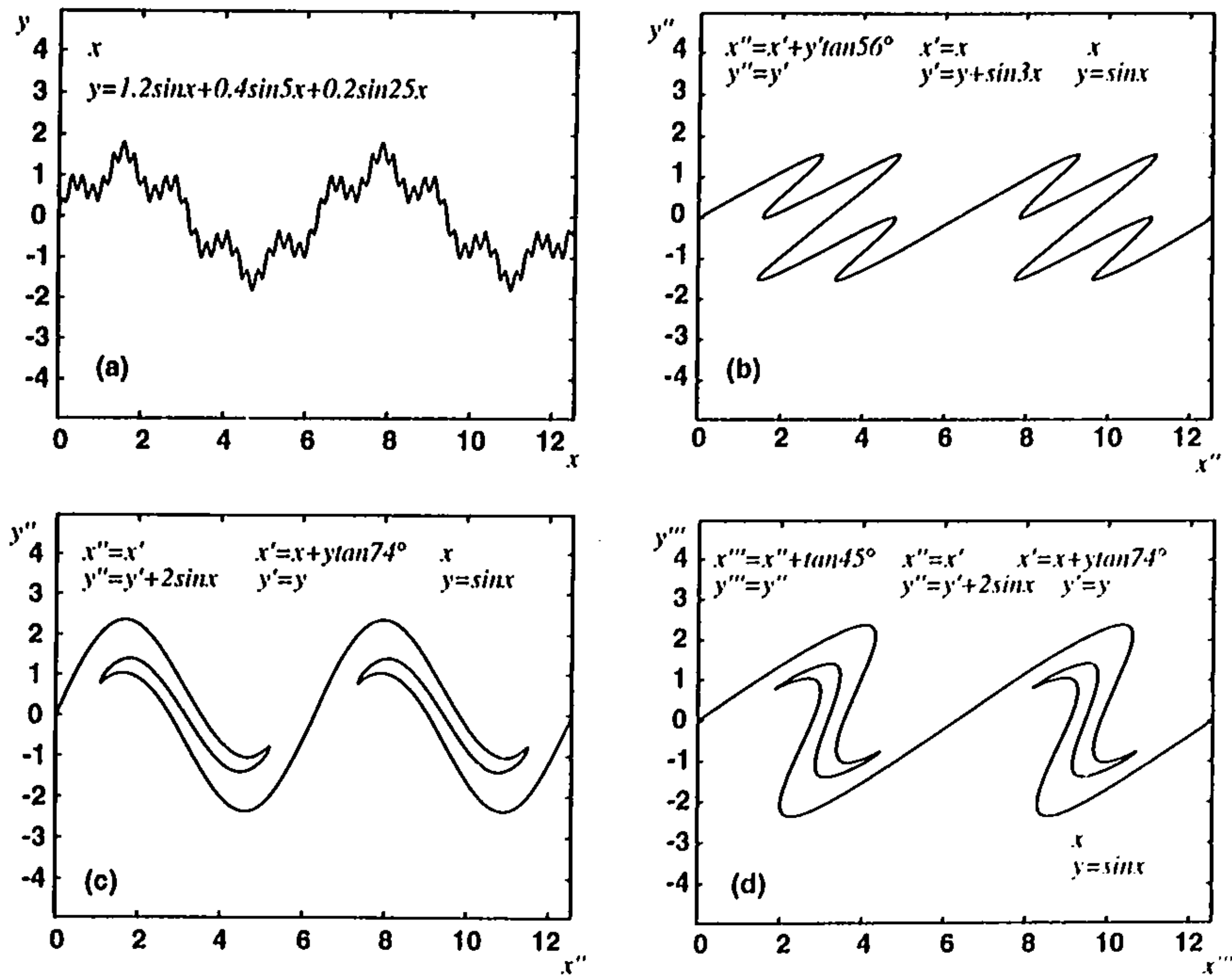

Fig. 2. (a) Three different fold orders with different wavelengths and amplitudes superposed on each other. Parameters *a* and *b* are denoted for each fold order.. (b) An asymmetric transformations superposed on a symmetric fold series. (c) A symmetric transformation superposed on an asymmetric fold series. (d) An asymmetric transformation superposed on an asymmetric fold series. Parameters *a* and *b* for each fold series and shear angle for the asymmetric fold series are quoted.

THREE DIMENSIONAL ANALYSIS OF THE SIMPLE SYMMETRIC AND ASYMMETRIC CYLINDRICAL FOLD FORMS

Three dimensional shape of simple cylindrical fold series may be expressed using equation (2) in a new form as,

$$z = a \sin bx \tag{10}$$

Equation (10) defines a fold series with axes parallel to the y-axis and axial plane parallel to the yz plane of the coordinate system (Fig. 3a). When defined, a symmetric fold series may be sheared into an asymmetric fold series applying equations (11), (12) and (13), and plotting the resultant surface defined by x', y' and z' (see Fig. 3b).

$$x' = x + z \tan \theta \tag{11}$$

$$y' = y \tag{12}$$

$$z' = z \tag{13}$$

Fold series with axes parallel to the xy plane but oblique to x- and y-axis of the coordinate system (Fig. 3c) may be first defined by equation (10) in a different coordinate system, and then coordinate transformation formulas will allow its definition in the reference coordinate system.

$$z = a \sin[b(x \sin \gamma - y \cos \gamma)] \tag{14}$$

where γ is the angle between x-axis in the reference coordinate system and the axes of the fold series (for more detail on the coordinate transformation see appendix).

THREE DIMENSIONAL ANALYSIS OF SUPERIMPOSED SYMMETRIC AND ASYMMETRIC FOLD SERIES AND RELATED INTERFERENCE PATTERNS

Three-dimensional interference patterns of two (or more) symmetrical fold series, when expressed in terms of equations (10) or (14), may be modeled by adding their terms. Equation (15) is an expression for superposition of two symmetric cylindrical fold series, α being the angle between their axes.

$$z = a \sin[b(x \sin \alpha - y \cos \alpha)] + (a' \sin b' y) \tag{15}$$

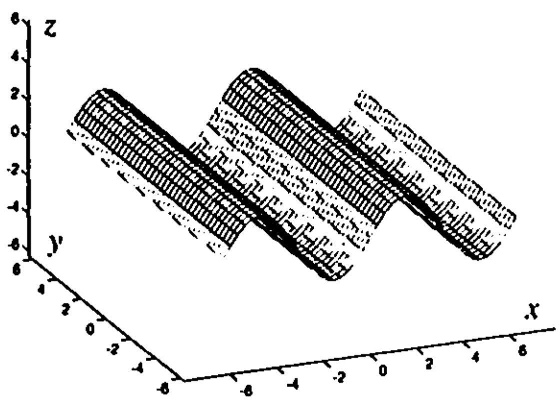

Fig. 3a

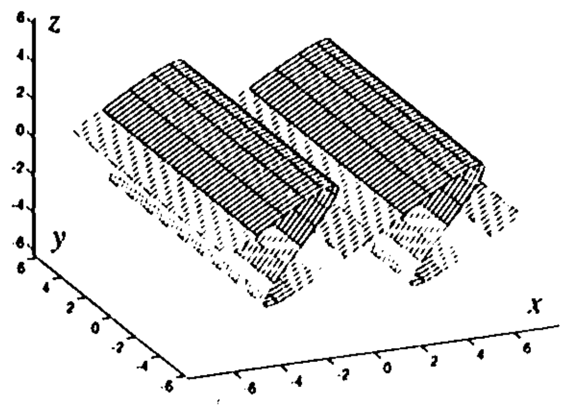

Fig. 3b

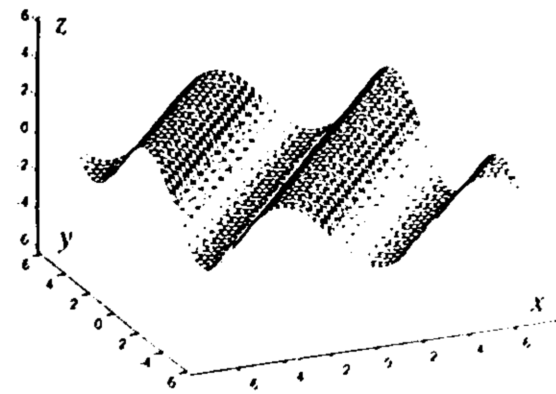

Fig. 3c

Fig. 3. Three-dimensional expression of a symmetric fold series through the equation $z = a \sin bx$ (a) and its shearing into an asymmetric fold series (b). (c) Equation (14) permits definition of a fold series with any desired angle between its axes and x- or y-axis of the coordinate system.

Interference patterns for two symmetrical fold series with axes that are orthogonal or at 45° are shown in Figures 4a and b respectively. Figure 4a is the 'egg carton pattern' similar to 'type 1' of interference patterns described by Ramsay (1967).

Superposition of an asymmetric transformation on a symmetric fold series may be modeled by shearing the surface resulting from equation (15) in a desired direction perpendicular to the axes of one of the fold series (+y direction for example), using equations similar to equations (11), (12) and (13).

To produce patterns resulting from superposition of a symmetric fold series on an asymmetric fold series, the asymmetric series should be first modeled through equations similar to equations (11), (12) and (13), and then equation of type equation (14) related to the symmetric series may be added to them. Taking another step and shearing the surface in another direction perpendicular to axis of the symmetric series produces a more complex interference form related to the superposition of two asymmetric fold series. Superposition of an asymmetric series on a symmetric one requires expression of two symmetric series first, and then shearing the resulting surface perpendicular to axes of desired fold series. The resultant superposition pattern, as may be seen in Fig. 5a, is different from the case where occurrence of the asymmetric series proceeds that of the symmetric series.

A CLASSIFICATION OF FOLD INTERFERENCE PATTERNS

Ramsay (1967, also see Ramsay & Huber 1983) proposed four main types of fold interference patterns. These are classified based on the angle between the first fold axial plane, $AxPl_1$, and a_2 direction of the second fold series, and the angle between the first fold axis, F_1, and the b_2 direction of the second fold series, where a_2 and b_2 represent the shear direction in the second axial planes and the direction normal to this in the axial planes (Table 22.2. in Ramsay & Huber 1983). Second fold series in this classification are always upright symmetric folds while natural cases in which an asymmetric fold series is superimposed on other fold series are not uncommon. The classification also supposes that the second fold series are all of

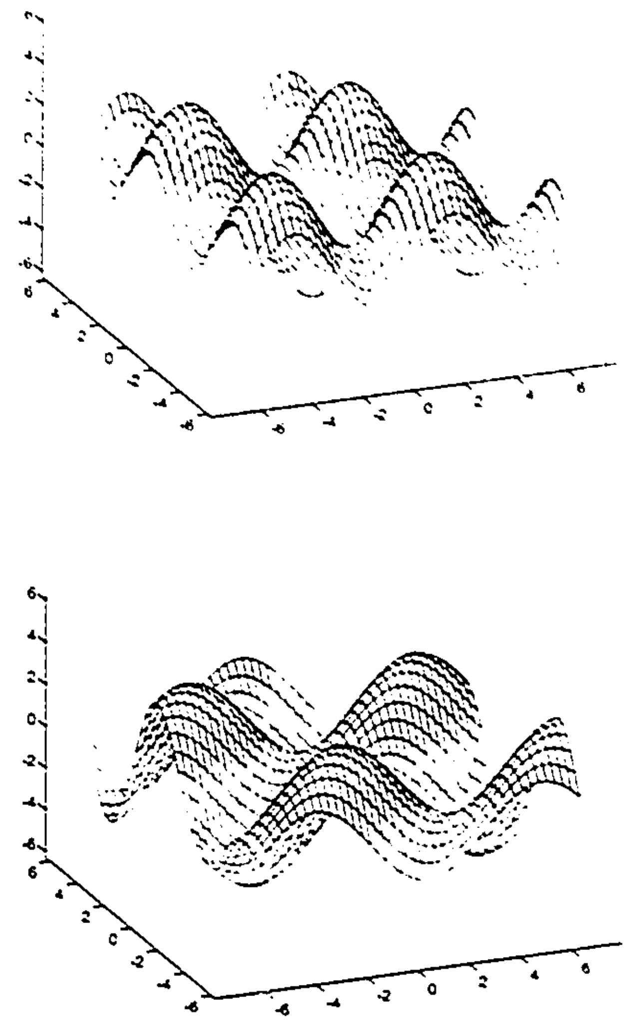

(a)

(b)

Fig. 4. Three-dimensional model of superposition of two symmetric fold series with axes making 90° (a), and 45° (b) angles.

the same wavelength and amplitude, which leads to the conclusion that in 'type zero' ,where angles between F_1 and b_2, and between $AxPl_1$ and a_2 are 'low', "the interaction of the two sets of folds produces none of the geometric features that are generally held to be characteristic of fold superposition, and the resulting three-dimensional geometry is practically identical to that of fold structures produced during a single phase of deformation". It will be shown further on that superposition of two fold series with parallel axial planes and with different wavelengths produces geometries which may be classified as fold interference patterns. Another ambiguity with Ramsay's classification appears in horizontal two-dimensional sections which he defines for types '0' and '3' of his classification (see Fig. 22.16 in Ramsay & Hubert 1983). These interference patterns would not form on a horizontal section unless the whole set of folds is folded by another folding event. The classification also ignores interference patterns which are produced by superposition of asymmetric folds on other asymmetric folds.

Thiessen and Means (1980), introducing three inter-axial angles, have modified and extended Ramsay's classification but they have retained the same terminology and notation. Their classification appreciates the possibility of production of interference patterns through superposition of two fold series with parallel axial planes. A large number of interference patterns are included in this classification, but the position of interference patterns which are produced by superposition of asymmetric folds on other asymmetric folds are not described in it.

An alternative classification for fold interference patterns is proposed here, which is as simple and general as possible and also avoids shortcomings and complexities that appear to be involved in the previous ones. In particular, it avoids associating particular interference patterns with any specific relationship of interaxial angles, which can be somewhat misleading in that, depending on the two-dimensional sections through the folded rocks, many different interference patterns may result (Thiessen and Means 1980, Thiessen 1986). This classification essentially uses the angular relationships between the axial planes of the involved fold series as well (see Table 1). Using the mathematical procedures described above makes it possible to

Group P

Axes of the fold series involved in the superposition are parallel

Type Pss	Type Psa	Type Pas	Type Paa
Involves two symmetric fold series	Involves an early symmetric and a late asymmetric fold series	Involves an early asymmetric and a late symmetric fold series	Involves two asymmetric fold series

Group N

Axes of the fold series involved in the superposition are not parallel

Type Nss	Type Nsa	Type Nas	Type Naa
Involves two symmetric fold series	Involves an early symmetric and a late asymmetric fold series	Involves an early asymmetric and a late symmetric fold series	Involves two asymmetric fold series

Table 1. Summary of fold interference pattern type classification.

produce and analyze a very large number of interference patterns of fold series with a wide range of wavelengths, amplitudes, dip of axial planes, and angles between axial planes. Clearly, not all of these can be discussed here, and in any case, it is not the goal of this paper to establish numerous templates of "type" interference patterns which would in any case be ambiguous when applied to the interpretation of folded terranes. The aim of the proposed classification is to establish a few broad groups of possible interference patterns, based on a small set of fundamental characteristics of superimposed folded surfaces. It is hoped that this will aid the structural geologist in proceeding to investigate the specific cases which may be of interest using the formulations presented in the earlier sections. The interference patterns are first classified into two major groups based on the parallelism (group 'P') or non-parallelism (group 'N') of the axes of the fold series involved in the superposition. Then based on the symmetry and asymmetry of the involved fold series, each major group is classified into four types, for the sake of convenience called 'ss', 'sa', 'as' and 'aa'. The final classification therefore would include eight types as 'Pss', 'Psa', 'Pas', 'Paa', 'Nss', 'Nsa', 'Nas' and 'Naa' (Table 1). Three-dimensional models of these eight major types, and corresponding horizontal sections are illustrated in Figures 5a and b respectively. In these figures the angle between the superimposed fold series of the group 'N' has been selected to be 90° ; it is obvious that a wide range of interpolations may be postulated between this end member of group 'N' and group 'P', which using the mathematical solutions described earlier can be produced and analyzed.

ANALYSIS OF THE INTERFERENCE PATTERNS OF SUPERIMPOSED FOLDS

As it may be seen in Fig. 5b, on the horizontal sections the trace of the axial surfaces of both early and late fold series in all types of group 'P' and two first types of group 'A' are straight lines. This is because either the axial surfaces in these types are not folded (in types

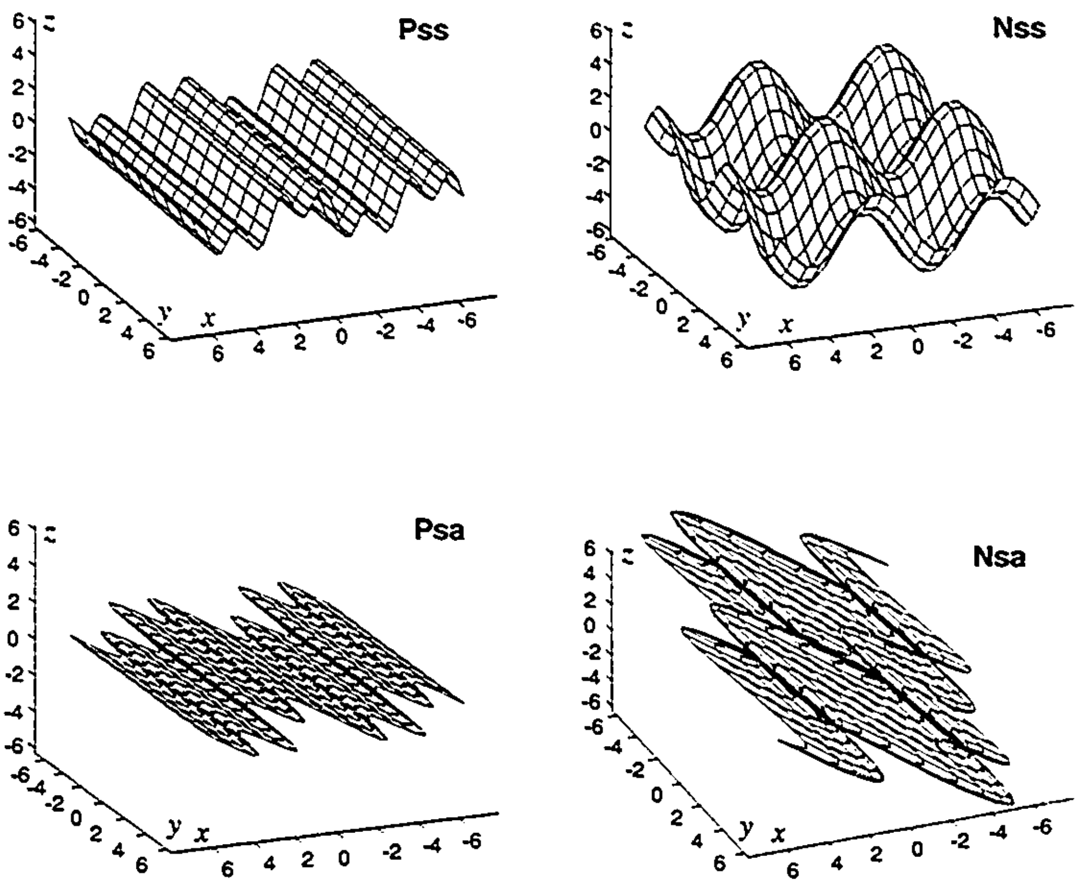

Fig. 5. Three-dimensional illustration of the six major types of superposition patterns modeled through the mathematical analysis (a), and related horizontal sections showing models for outcrop patterns of the folded strata and the axial surface trace of each fold series (b); dashed lines are traces of one of the axial surfaces from each fold series. Strike and dip of the earlier series before superposition of the second series are in bold.

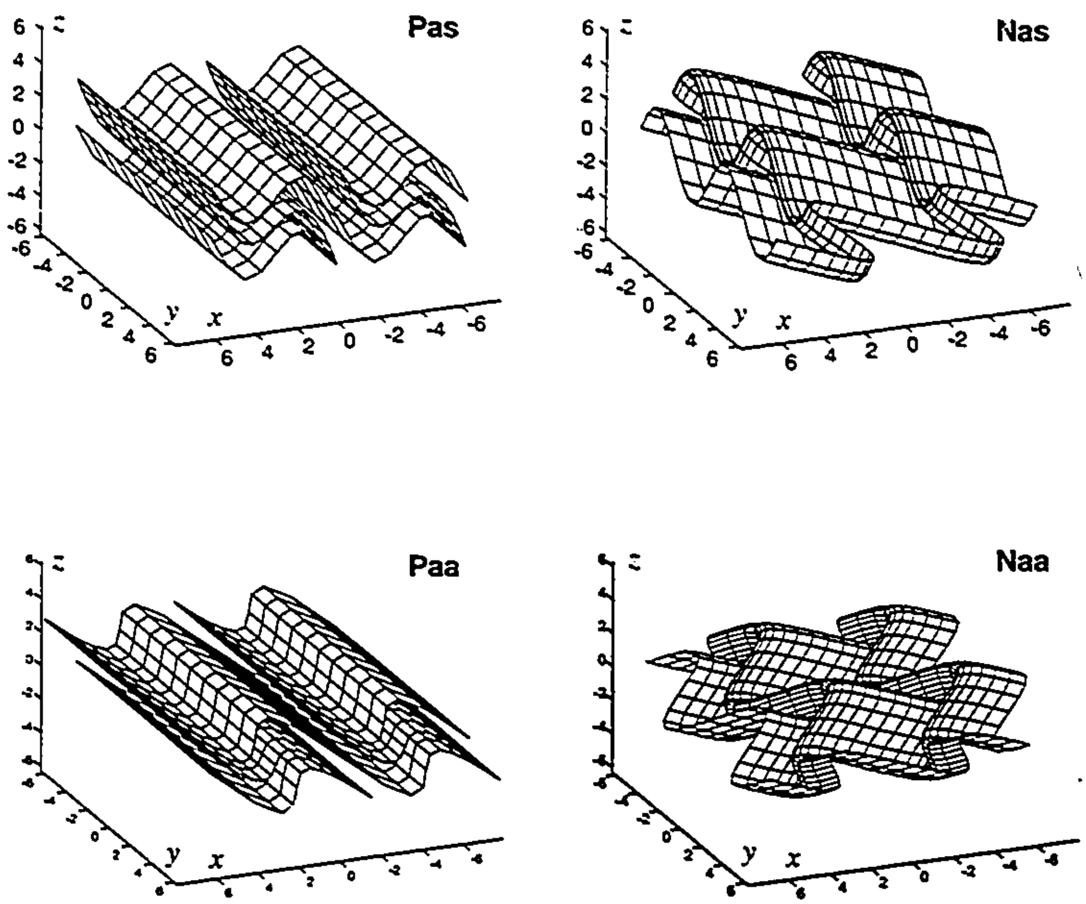

Fig. 5a. Continued.

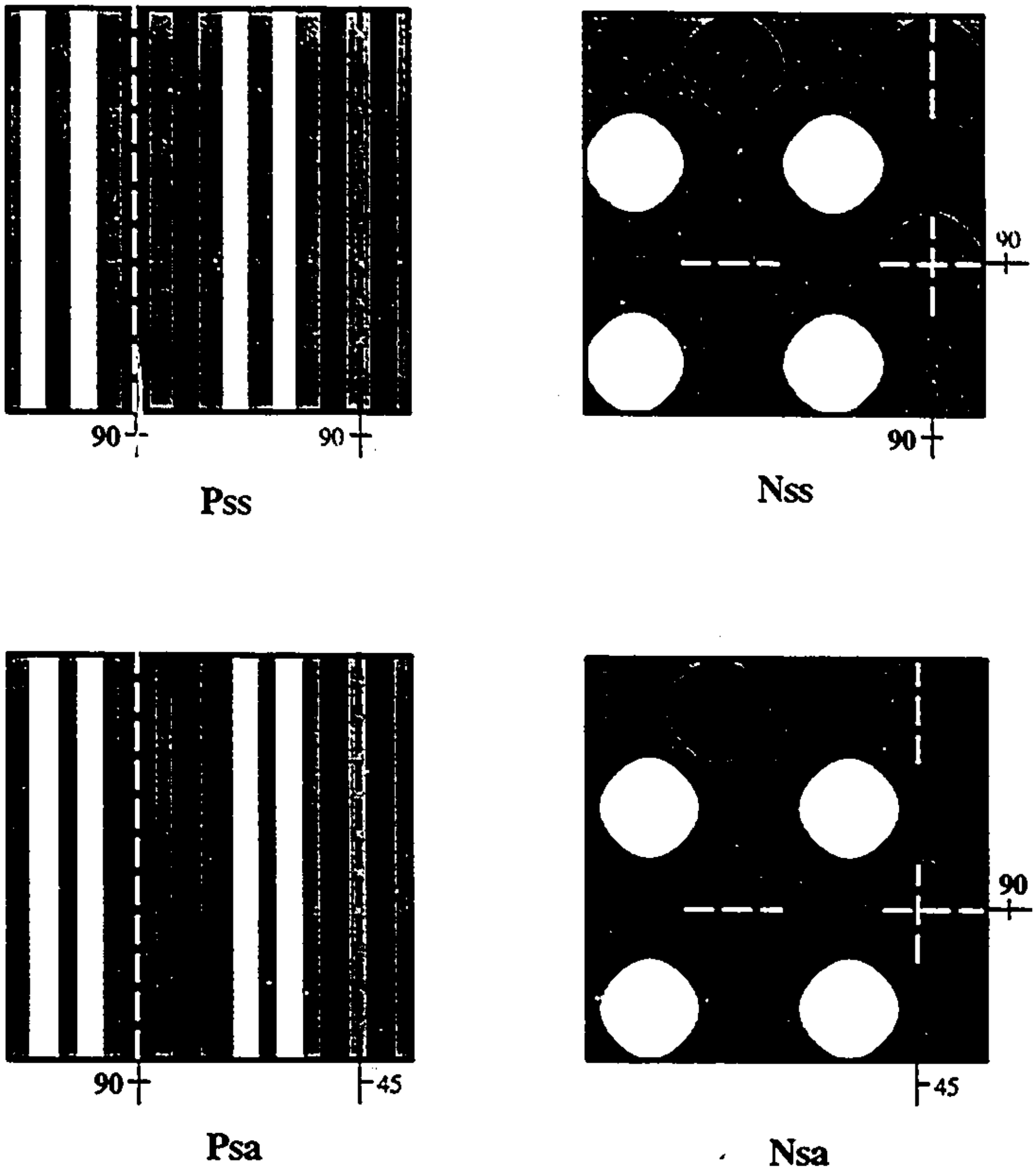

Fig. 5b.

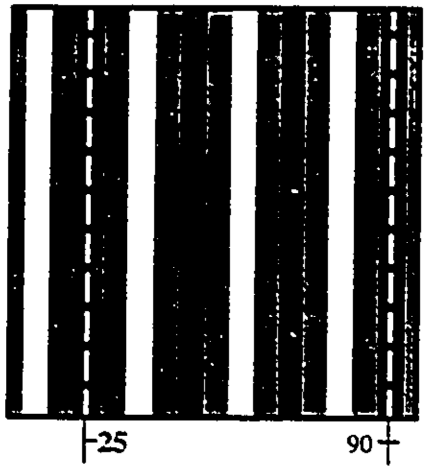

Pas

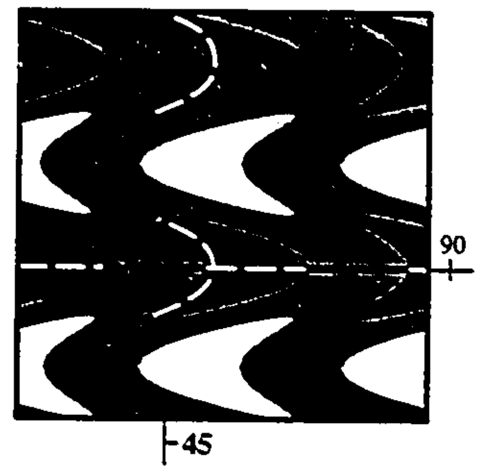

Nas

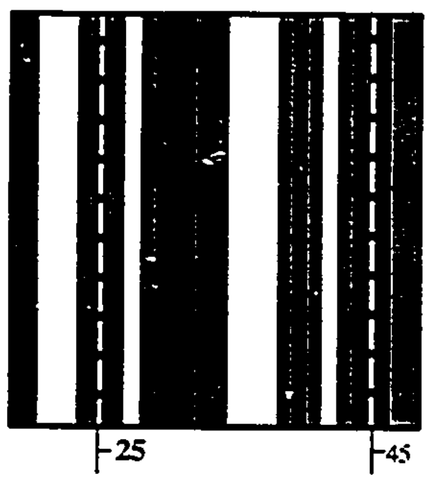

Paa

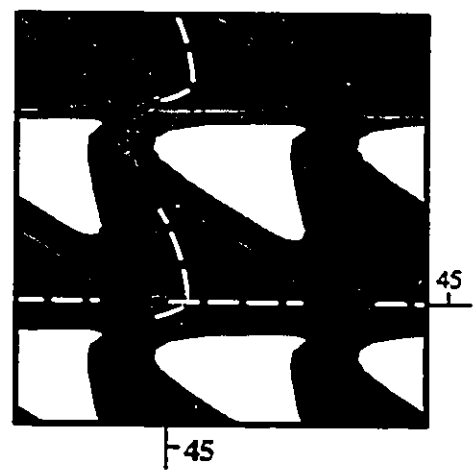

Naa

Fig. 5b. Continued.

'Pss', 'Psa', 'Nss' and 'Nsa'), or they are folded into folds with horizontal axes (in types 'Pas' and 'Paa').

Study of the fold interference patterns produced through mathematical modeling indicates that in map section (Fig. 5b) the outline patterns evolving from superposition of two fold series with parallel axes, group 'P', are not essentially different from the patterns produced by simple folding, however, repetition patterns of the strata are different. The real interference patterns are best demonstrated when these folded surfaces are viewed on the sections which make an angle with axes of the fold series. Traces of the axial surfaces for these types of superimposed folds on the horizontal sections are rectilinear (see Fig. 5b).

The interference patterns of group 'N' on the other hand are well recognizable both on horizontal and non-horizontal sections (Fig. 5b). Type Nss of the superimposed folds display 'dome and basin' or 'egg carton' interference patterns which are classified as 'type 1' under the classification by Ramsay (1967). Basin and dome pattern in type Nsa of the superimposed fold is essentially similar to type Nss; the difference appears in asymmetry of the outline patterns originating from asymmetry of the structure in three dimensions. Study of three-dimensional pattern in this type of superposition (Fig. 5a) indicates that the resultant conoidal shapes are very similar to sheath folds produced by simple shear . Deciding between this or that mechanism for the origin of sheath folds, therefore, should be carried out with caution. Traces of the axial surfaces of both fold series on the horizontal sections in these two types of superposition, unlike other two types of the group 'N', are rectilinear. Type Nas displays a 'mushroom' pattern which is classified as 'type 2' in Ramsay's classification. Traces of the axial surface of the first (asymmetric) fold series on the horizontal sections in this type of superposition is a symmetric sine wave. Type Naa, which involves two asymmetric fold series, displays a different interference pattern which may be called a 'triangular' pattern. Trace of the axial surface of the first (asymmetric) fold series on the horizontal sections in this type of superposition is asymmetrical. The types 'Pss', 'Pas', 'Nss' and 'Nas' may respectively be comparable with types '0', '3', '1' and '2' in Ramsay's classification, while the types 'Psa', 'Paa', 'Nsa', and 'Naa' have no counterpart in that classification.

CONCLUSIONS

Mathematical analyses introduced in this paper, which are modifications and extensions of the Fourier analysis approach to fold series, is proposed as a useful tool for the analysis of both symmetric and asymmetric fold series and interference patterns produced by their superposition both in two and three dimensions. Like any other mathematical approach, this method has limitations in reproducing natural geologic structures, for instance material properties are not accounted for, and only shear folding mechanisms are considered. However, the method does provide great ease of manipulation of the data, and can efficiently produce a wide variety of folds and interference patterns. Wavelengths and amplitudes of the folds involved in the superposition, as well as their axial plane orientation and their relative sizes may be easily defined and changed through the modeling process. The proposed alternative classification of fold interference patterns has been developed to be as simple and communicative as possible for the field geologists, and exclude the shortcomings that are involved in previous classifications. The patterns of trace of axial surface of the involved fold series also have been analyzed in this classification in order to be compared with corresponding patterns in the map scale.

APPENDIX

Transformation formula for rotation of a coordinate system on a plane perpendicular to the z axis are,

$$\begin{cases} x' = l_1 x + l_2 y \\ y' = m_1 x + m_2 y \\ z' = z \end{cases}$$

where l_1, l_2 and m_1, m_2 are the direction cosines of the angles between ox', oy' and ox, oy.

Expressing the first formula corresponding to x' in terms of γ, the angle between the axes of the folded series defined by $z = a\sin bx'$ and ox, will result in,

$$x' = x\sin\gamma - y\cos\gamma$$

and

$$z = a\sin[b(x\sin\gamma - y\cos\gamma)]$$

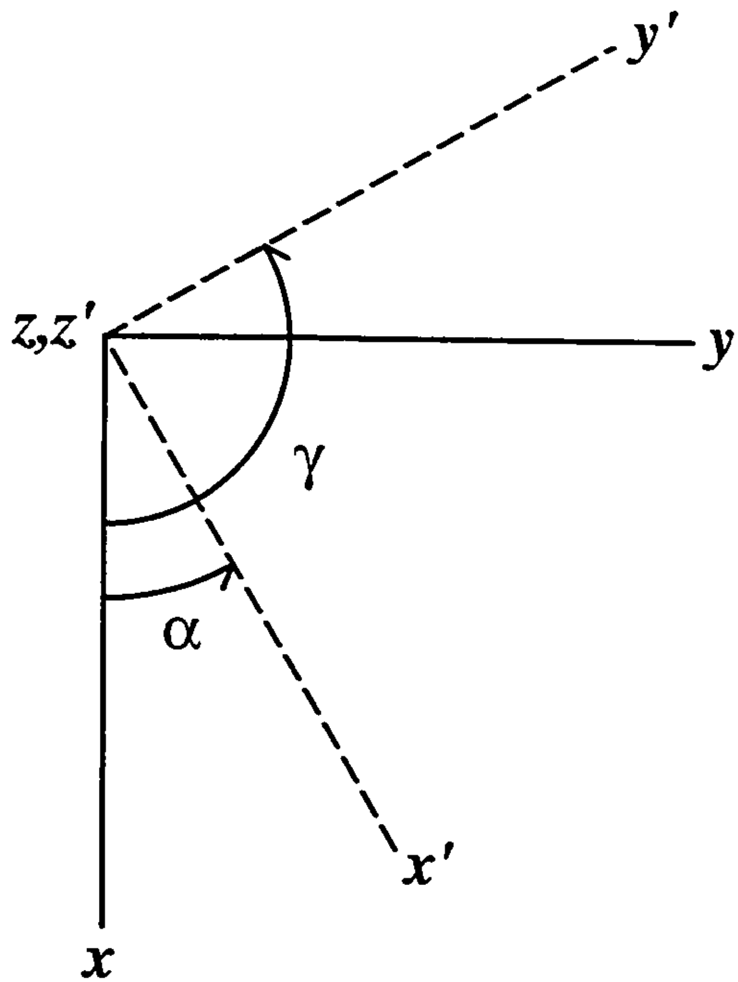

REFERENCES

Carey, S. W. 1962. Folding. J. Alberta Soc. Petrol. Geol. 10, 95-144.

Harbaugh, J. W. & Preston, F. W. 1965. Fourier series analysis in geology. In: 6th Symp. Computer Appl. Mineral Exploration, Tucson, Ariz., R1-R46.

Hudleston, P. J. 1973. Fold morphology and some geometrical implications of theories of fold development. Tectonophysics 16, 1-46.

O'Driscoll, E. S. 1962. Experimental patterns in superposed similar folding. j. Alberta Soc. Petrol. Geol. 10, 145-167.

Ramsay, J. G. 1958. Superimposed folding at Loch Monar, Inverness-Shire and Rose-Shire. Q. J. Geol. Soc. Lond. 113, 271-307.

Ramsay, J. G. 1967. Folding and fracturing of rocks. McGraw Hill, New York.

Ramsay, J. G. & Hubert, M. I. 1983. The techniques of modern structural geology. Academic Press, London.

Reynolds, D. L. & Holmes, A. 1954. The superposition of Caledonid folds on an olderfold-system in the Dalradians of Malin Head, Co. Donegal. Geol. Mag. 91, 417-444.

Skjernaa. 1975. Experiments on superimposed buckle folding. Tectonophysics 27, 255-270.

Stabler, C. L. 1968. Simplified Fourier analysis of fold shapes. Tectonophysics 6, 343-350.

Thiessen, R. L. & Means, W. D. 1980. Classification of fold interference patterns: a reexamination. J. Struct. Geol. 2, 311-316.

Thiessen, R. 1986. Two-dimensional refold interference patterns. J. Struct. Geol. 8, 563-573.

Watkinson, A. J. 1981. Patterns of fold interference: influence of early fold shapes. J.Struct. Geol. 3, 19-23.

Weiss, L. E. 1959. Geometry of superposed folding. Bul. geol. Soc. Am. 70, 91-106.

Wilson, G. 1967. The geometry of cylindrical and conical folds. Proc. Geol. Assoc. London 78, 179-210.